



UNIVERSIDADE ESTADUAL DE CAMPINAS
INSTITUTO DE BIOLOGIA

MARIANA RODRIGUES DA SILVA

DETERMINATION OF MICROPLASTIC-INDUCED SUBLETHAL
PHENOTYPIC CHANGES IN TWO HUMAN HEPATOCYTE
MODELS USING HIGH-CONTENT ANALYSIS

DETERMINAÇÃO DE ALTERAÇÕES FENOTÍPICAS
SUBLETAIS DESENCADEADAS POR MICROPLÁSTICOS EM
DOIS MODELOS DE HEPATÓCITOS HUMANOS ATRAVÉS DE
TRIAGEM CELULAR MULTIPARAMÉTRICA DE ALTO
CONTEÚDO

CAMPINAS

2025

MARIANA RODRIGUES DA SILVA

**DETERMINATION OF MICROPLASTIC-INDUCED SUBLETHAL
PHENOTYPIC CHANGES IN TWO HUMAN HEPATOCYTE MODELS
USING HIGH-CONTENT ANALYSIS**

**DETERMINAÇÃO DE ALTERAÇÕES FENOTÍPICAS SUBLETAIS
DESENCADEADAS POR MICROPLÁSTICOS EM DOIS MODELOS DE
HEPATÓCITOS HUMANOS ATRAVÉS DE TRIAGEM CELULAR
MULTIPARAMÉTRICA DE ALTO CONTEÚDO**

*Dissertação apresentada ao Instituto de
Biologia da Universidade Estadual de
Campinas como parte dos requisitos exigidos
para a obtenção do Título de Mestra em
Biologia Molecular e Morfofuncional na área
de Bioquímica*

*Dissertation presented to the Institute of
Biology of the University of Campinas in partial
fulfillment of the requirements for the degree of
Master in Molecular and Morphofunctional
Biology, in the area of Biochemistry*

Orientador: PROF. DR. MARCELO BISPO DE JESUS

ESTE ARQUIVO DIGITAL CORRESPONDE À
VERSÃO FINAL DA DISSERTAÇÃO
DEFENDIDA PELA ALUNA MARIANA
RODRIGUES DA SILVA E ORIENTADA PELO
PROF. DR. MARCELO BISPO DE JESUS

CAMPINAS

2025

FICHA CATALOGRÁFICA
Universidade Estadual de Campinas (UNICAMP)
Biblioteca do Instituto de Biologia
Mara Janaina de Oliveira - CRB 8/6972

D11d da Silva, Mariana Rodrigues, 1998-
Determination of microplastic-induced sublethal phenotypic changes in two human hepatocyte models using high-content analysis / Mariana Rodrigues da Silva. – Campinas, SP : [s.n.], 2025.

Orientador: Marcelo Bispo de Jesus.
Dissertação (mestrado) – Universidade Estadual de Campinas (UNICAMP), Instituto de Biologia.

1. Microplásticos. 2. Hepatotoxicologia. 3. Citotoxicidade. 4. Análise de imagem. 5. Hepatócitos. 6. Fenótipo. 7. Processamento de imagem assistida por computador. I. Jesus, Marcelo Bispo de, 1980-. II. Universidade Estadual de Campinas (UNICAMP). Instituto de Biologia. III. Título.

Informações complementares

Título em outro idioma: Determinação de alterações fenotípicas subletais desencadeadas por microplásticos em dois modelos de hepatócitos humanos através de triagem celular multiparamétrica de alto conteúdo.

Palavras-chave em inglês:

Mircoplastics
Hepatotoxicology
Citotoxicity
Image analysis
Liver cells
Phenotype
Image processing computer-assisted

Área de concentração: Bioquímica

Titulação: Mestra em Biologia Molecular e Morfofuncional

Banca examinadora:

Marcelo Bispo de Jesus [Orientador]

Nicolas Carlos Hoch

Alexandre Bruni Cardoso

Data de defesa: 11-03-2025

Programa de Pós-Graduação: Biologia Molecular e Morfofuncional

Objetivos de Desenvolvimento Sustentável (ODS)

Não se aplica

Identificação e informações acadêmicas do(a) aluno(a)

- ORCID do autor: <https://orcid.org/0000-0001-9233-6297>

- Currículo Lattes do autor: <http://lattes.cnpq.br/7950318299211126>

BANCA DA APROVAÇÃO

Prof. Dr. Marcelo Bispo de Jesus

Prof. Dr. Nicolas Carlos Hoch

Prof. Dr. Alexandre Bruni Cardoso

A Ata da defesa com as respectivas assinaturas dos membros encontra-se no SIGA/Sistema de Fluxo de **Dissertação** e na Secretaria do Programa de Pós Graduação em **Biologia Molecular e Morfofuncional** do Instituto de Biologia da Unicamp.

DEDICATÓRIA

*Dedico este trabalho à memória de minha
querida amiga e colega de graduação,
Mayara Roquette Valentim.*

*Mayara, seu apoio foi muito importante no início
deste projeto. Estávamos juntas na jornada de nos
tornarmos Mestras. Sua paixão pelo conhecimento
e sua generosidade sempre serão lembradas. Sua
ausência é sentida profundamente, mas sua
influência continuou a inspirar e guiar meu trabalho
ao longo destes dois anos.*

*Que esta dissertação sirva como um tributo ao
impacto duradouro que você teve em minha vida e à
vida dos colegas da turma da Bio 017D.*

Mayara é Luz!

AGRADECIMENTOS

Aos meus pais, Sueli e Alex, que sempre me incentivaram e apoiaram nos estudos, além de me proporcionarem toda a estrutura necessária para que eu pudesse estudar e realizar minha graduação e mestrado sem quaisquer outras preocupações. Sem vocês, eu jamais teria alcançado este momento.

Agradeço à minha mãe, professora e bióloga, por ser a grande responsável por cultivar em mim o amor pela Biologia desde a infância. Por me ensinar a amar e respeitar a natureza em seus mínimos detalhes, por instigar minha curiosidade e me fazer compreender desde cedo a importância da ciência, não apenas para os seres humanos, mas para o planeta como um todo.

Ao meu pai, professor e educador físico (e super pai!), cientista e engenheiro nato (mesmo sem ter título de mestre ou doutor), de uma inteligência admirável, por toda a dedicação que teve e tem comigo. Jamais esquecerei sua paciência para responder a todos os meus “por quês?”, me ajudar nos trabalhos escolares (de artes até física), e até parar por meses para estudar junto comigo, para que eu conseguisse passar no vestibulinho do Cotuca, que foi um divisor de águas na minha vida. Obrigada por sempre colocar a mim e ao meu irmão em primeiro lugar.

Ao meu irmão Guilherme, que também sempre me apoiou e que é meu companheiro das conversas mais bobas até as mais complexas e inteligentes, e quem eu admiro muito.

À minha avó Maria (*in memoriam*) por sempre ter torcido por mim, me colocado em suas orações e me apoiado incondicionalmente.

Aos nove gatos que fazem parte da minha família e que tiveram papel fundamental para a manutenção da minha saúde mental ao longo do meu mestrado: Matilda, Mimi, Maricota, Neguinha, Negona, Negão, Branquinha, Escaminha e Magrela. Já perdi as contas de quantas vezes eles foram minha plateia em ensaios de apresentações e palestras.

Ao meu orientador, Prof. Dr. Marcelo Bispo de Jesus, cuja orientação, paciência e dedicação foram indispensáveis ao desenvolvimento deste trabalho. Agradeço por disponibilizar o laboratório, os recursos necessários e um ambiente acolhedor e enriquecedor para aprendizado e pesquisa. Sua confiança e apoio me motivaram a enfrentar os desafios desta jornada.

Às minhas primeiras orientadoras, que foram essenciais no início da minha carreira acadêmica e sempre acreditaram e torceram por mim: Profa. Dra. Adriana Pavesi Ariseto Bragotto e Profa. Dra. Fabíola Málaga Barreto, que me orientaram no meu primeiro contato com

um laboratório de pesquisa e me inseriram na ciência mesmo antes da minha graduação; Profa. Dra. Talita Miguel Marin e Profa. Dra. Nathalia de Carvalho Indolfo, que me apresentaram o campo da cultura de células e da toxicologia *in vitro*, despertando minha paixão pelos métodos alternativos ao uso de animais. Agradeço do fundo do coração por todas as oportunidades que vocês me proporcionaram.

Aos queridos professores da minha banca de qualificação e de defesa, Prof. Dr. Mario Costa Cruz, Prof. Dr. Murilo de Carvalho, Profa. Dra. Talita Miguel Marin, Prof. Dr. Nicolas Carlos Hoch e Prof. Dr. Alexandre Bruni Cardoso pelas valiosas sugestões que enriqueceram este projeto.

Aos queridos amigos do grupo do laboratório NanoCell (da minha época): Tuanny, Rafaela, Giovana, Bruno e especialmente Fernanda, Thaís, André, Ju Mattoso e Luana.

À Fernanda, pela contribuição fundamental nas análises de dados com os softwares Cell pose, CellProfiler e Morpheus os quais foram utilizados para o processamento e análise dos dados deste projeto. Fer, te admiro muito!

À Thaís, por ter se tornado uma grande e amada amiga, companheira de ônibus, e de festas, e por sempre estar disponível para me socorrer com os erros de código dos meus Jupyter Notebooks devido à sua super habilidade em programação.

Ao André, pela linda amizade, e por ter se prontificado a me ajudar com as caracterizações físico-químicas das minhas micropartículas.

À Ju Mattoso, mais conhecida como nossa “mãe científica”, por todos os conselhos valiosos, por ouvir meus desabafos, por compartilhar suas histórias de vida, pelas caronas e por trazer muita paz ao ambiente de trabalho.

À Luana (a alegria do laboratório), por ter se tornado minha amiga irmã, que me acolheu de coração durante esses dois anos, com quem eu compartilhei todas as minhas dores e alegrias, momentos sérios de trabalho e momentos descontraídos de viagem e festas. Apreendi muitas coisas com você Lu, do nível técnico e científico à como levar a vida com um pouco mais de tranquilidade e felicidade. Te amo imensamente.

Às minhas amigas da graduação, e biólogas inspiradoras, que foram um suporte gigante durante esse processo: Elyara, Giuliana, Gabriela, Letícia, Lu Luchi, e Bruna. Vocês são luzes na minha vida! Agradeço por escutarem todos os meus desabafos, e compartilharem momentos tão especiais comigo. Às minhas amigas desde a época do Cotuca: Beatriz, Sabrina e Lara, por estarem comigo até hoje, e que sei que posso contar, mesmo de longe.

À Unicamp, por ter sido minha segunda casa durante 11 anos, que me abriu portas e proporcionou muito aprendizado, e por ter colocado pessoas maravilhosas em minha vida.

Por fim, agradeço ao **Conselho Nacional de Desenvolvimento Científico e Tecnológico (CNPq)** pelo financiamento de 3 meses deste projeto (**processo 157386/2022-8**), e à **Fundação de Amparo à Pesquisa do Estado de São Paulo (FAPESP)** pelo financiamento de 21 meses deste projeto (**processo 2022/07854-4**).

O presente trabalho foi realizado com apoio da Coordenação de Aperfeiçoamento de Pessoal de Nível Superior - Brasil (CAPES) - Código de Financiamento 001.

RESUMO

O acúmulo incontrollável de plásticos no meio ambiente constitui um problema global crescente. Microplásticos (MPs) e nanoplásticos (NPs), originados da degradação de resíduos plásticos e produzidos intencionalmente, são amplamente encontrados no ar, na água e em diversos alimentos, sendo o poliestireno (PS) um dos tipos mais comuns. Estima-se que ingerimos até 5 g dessas partículas semanalmente, o que gera preocupações devido à capacidade dos MPs, especialmente aqueles menores que 150 µm, e dos NPs de atravessar a barreira intestinal humana e se acumular em órgãos como o fígado, dada sua função de desintoxicação xenobiótica. Apesar dessas preocupações, ainda há uma escassez de estudos que avaliem o potencial hepatotóxico de MPs e NPs em concentrações ambientais e relevantes à exposição humana. Diante desse cenário, este estudo teve como objetivo investigar a hepatotoxicidade de MPs de PS (PS-MPs) em concentrações variando de 1 ng/L a 1 g/L, englobando valores relatados no ambiente (1 ng/L e 1 µg/L), estimativas de exposição humana diária (1 mg/L, considerando a soma da concentração ambiental, ingestão de frutos do mar, alimentos de embalagens plásticas, entre outros) e condições extremas (acima de 1 mg/L). Em vez de utilizar modelos animais, que apresentam limitações em termos de tempo, predição, custo e questões éticas, optamos por avaliar os efeitos tóxicos dos PS-MPs em duas linhagens de hepatócitos humanos, HepG2 e Huh7, empregando ensaios baseados em análise de imagens celulares (*High-Content Analysis*). Essas abordagens permitiram avaliar alterações em perfis celulares, incluindo alterações morfológicas e mecánísticas, por meio do uso de diversos marcadores celulares, visando resultados preditivos. Os resultados demonstraram que, embora os PS-MPs não tenham desencadeado efeitos hepatotóxicos em concentrações ambientais e relevantes para a exposição humana (1 ng/L a 1 mg/L), essas partículas se associaram à ambas as linhagens de hepatócitos nestas condições. Em concentrações elevadas (0,5 g/L e 1 g/L), os PS-MPs induziram alterações celulares significativas, que variaram entre as linhagens. Por exemplo, observou-se um aumento significativo de vesículas ácidas em Huh7 e desagregação celular em HepG2, ambos indicadores de estresse celular, além de uma redução na contagem de células mortas em ambas as linhagens, que pode estar relacionada à ativação de vias de sobrevivência celular. Esses resultados sugerem que, embora as concentrações ambientais de PS-MPs não causem hepatotoxicidade imediata, exposições a concentrações mais altas podem impactar significativamente os modelos de hepatócitos, revelando um potencial hepatotóxico. Apesar de concentrações elevadas representarem cenários extremos, é

importante considerar que a exposição humana aos MPs é cumulativa e diária. Ademais, projeta-se um aumento contínuo na presença desses resíduos no ambiente, o que pode levar as concentrações ambientais atuais a se aproximarem, ao longo do tempo, de níveis hoje considerados extremos. Nossos achados contribuem para uma compreensão mais aprofundada do potencial hepatotóxico dos PS-MPs em seres humanos e apontam elementos de vias de efeitos adversos (*Adverse Outcome Pathways*, AOPs) associados a diferentes concentrações de PS-MPs. Essas alterações celulares específicas poderão subsidiar a construção de AOPs de MPs em células hepáticas, oferecendo ferramentas úteis para a avaliação de riscos dessas partículas à saúde humana.

ABSTRACT

The uncontrolled accumulation of plastics in the environment constitutes a growing global problem. Microplastics (MPs) and nanoplastics (NPs), derived from the degradation of plastic waste and intentional production, are widely found in air, water, and various foods, with polystyrene (PS) being one of the most common types. It is estimated that humans ingest up to 5 g of these particles weekly, raising concerns due to the ability of MPs, especially those smaller than 150 μm , and NPs to cross the human intestinal barrier and accumulate in organs such as the liver, given its role in xenobiotic detoxification. Despite these concerns, there is still a lack of studies evaluating the hepatotoxic potential of MPs and NPs at environmentally relevant concentrations and levels reflective of human exposure. Given this scenario, this study aimed to investigate the hepatotoxicity of PS microplastics (PS-MPs) at concentrations ranging from 1 ng/L to 1 g/L, encompassing environmentally reported levels (1 ng/L and 1 $\mu\text{g/L}$), daily human exposure estimates (1 mg/L, considering the combined contribution of environmental concentrations, seafood ingestion, and consumption of food packaged in plastics), and extreme conditions (above 1 mg/L). Instead of using animal models, which have limitations in terms of time, prediction, cost, and ethical considerations, we chose to evaluate the toxic effects of PS-MPs in two human hepatocyte lineages, HepG2 and Huh7, employing assays based on cellular image analysis (High-Content Analysis). These approaches enabled the evaluation of changes in cellular profiles, including morphological and mechanistic alterations, through the use of various cellular markers, aiming for predictive results. The results demonstrated that, although PS-MPs did not trigger hepatotoxic effects at environmentally relevant concentrations (1 ng/L to 1 mg/L), these particles were associated with both hepatocyte lineages under these conditions. At elevated concentrations (0.5 g/L and 1 g/L), PS-MPs induced significant cellular changes, which varied between the lineages. For instance, a significant increase in acidic vesicles was observed in Huh7, while cellular disaggregation was noted in HepG2, both indicative of cellular stress. Additionally, a reduction in the number of dead cells was observed in both lineages, which may be related to the activation of cellular survival pathways. These findings suggest that, while environmental concentrations of PS-MPs do not cause immediate hepatotoxicity, exposure to higher concentrations can significantly impact hepatocyte models, revealing a hepatotoxic potential. Although elevated concentrations represent extreme scenarios, it is important to consider that human exposure to MPs is cumulative and occurs daily. Moreover, the continuous increase in the presence of these residues in the environment suggests that current environmental concentrations may rise over time, potentially approaching levels currently considered extreme. Our findings contribute to a deeper understanding of the hepatotoxic

potential of PS-MPs in humans and highlight elements of Adverse Outcome Pathways (AOPs) associated with different PS-MP concentrations. These specific cellular alterations may eventually support the construction of AOPs for MPs in hepatic cells, offering valuable tools for assessing the risks posed by these particles to human health.

LIST OF ABBREVIATIONS AND ACRONYMS

- 3-MA - 3-Methyladenine
- Akt - Protein Kinase B
- AO - Acridine Orange
- AOPs - Adverse Outcome Pathways
- APS - Ammonium Persulfate
- ATCC - American Type Culture Collection
- BAX - BCL2 Associated X Protein
- BCA - Bicinchoninic Acid
- BSA - Bovine Serum Albumin
- Calcein-AM - Calcein Acetoxymethyl Ester
- CD36 - Cluster of Differentiation 36
- COX-2 - Cyclooxygenase-2
- CYP - Cytochrome
- DMEM - Dulbecco's Modified Eagle Medium
- DMSO - Dimethyl Sulfoxide
- EFSA - European Food Safety Authority
- EU - European Union
- FABP1 - Fatty Acid-Binding Protein 1
- FBS - Fetal Bovine Serum
- FXR - Farnesoid X Receptor
- GSH - Glutathione (Reduced Form)
- HBSS - Hanks' Balanced Salt Solution
- HCA – High-Content Analysis
- IFN- γ - Interferon Gamma
- iNOS - Inducible Nitric Oxide Synthase
- IL - Interleukin
- JCRB - Japanese Collection of Research Bioresources Cell Bank Ki-67 - Proliferation Marker Protein
- LAMP-1 - Lysosome-Associated Membrane Protein 1
- LDPE - Low-Density Polyethylene
- MMP - Mitochondrial Membrane Potential
- MPs – Microplastics
- MRP2 - Multidrug Resistance-Associated Protein 2

- MTT - 3-(4,5-dimethylthiazol-2-yl)-2,5-diphenyltetrazolium bromide
- NPs - Nanoplastics
- NrF2 - Nuclear Factor Erythroid 2-Related Factor 2
- PBS - Phosphate Buffered Saline
- PE - Polyethylene
- Pen/Strep - Penicillin/Streptomycin
- PFA - Paraformaldehyde
- PI - Propidium Iodide
- PI3K - Phosphoinositide 3-Kinase
- PPAR α - Peroxisome proliferator-activated receptor alpha
- PPAR γ - Peroxisome proliferator-activated receptor gamma
- PS - Polystyrene
- PS-MPs - Polystyrene Microplastics
- PS-MPs-Fluor - Fluorescent Polystyrene Microplastics
- PVA - Polyvinyl Alcohol
- PVC - Polyvinyl Chloride
- SDS - Sodium Dodecyl Sulfate
- TEMED - N,N,N',N'-Tetramethylethylenediamine
- TMRM - Tetramethylrhodamine Methyl Ester
- TNF- α - Tumor Necrosis Factor Alpha
- ZO-1 - Zonula Occludens-1 Protein

SUMMARY

1. INTRODUCTION	18
1.1. Human Exposure to Micro and Nanoplastics: A Daily Issue.....	18
1.2. Need to Investigate the (Hepato)toxicity of Nano and Microplastics.....	21
1.3. Cell-Based Assays as Promising Alternatives for Assessing the Hepatotoxicity of MPs and NPs at Environmentally Relevant Concentrations.....	23
1.4. Obtaining Cellular Phenotypic Profiles and Elements of Adverse Outcome Pathways (AOPs) through High Content Analysis (HCA).....	24
1.5. HCA as a Predictive Approach for Hepatotoxicity Assessment of NPs and MPs <i>In Vitro</i>	27
1.5.1. HCA in Exploratory Approaches to Hepatotoxicity: Live Cell Painting and Cell Painting Assays	27
1.5.2. HCA in Targeted Approaches to Hepatotoxicity: Using Markers to Highlight Fundamental Parameters of <i>In Vitro</i> Hepatotoxicity (HepatotoxPath Assay)	29
1.6. Relevant <i>In Vitro</i> Models for Studying Hepatotoxicity	31
2. OBJECTIVES	34
3. TO BE PUBLISHED DOCUMENT	36
3.1. Material and Methods.....	36
3.1.1. Cell Culture and Plating	36
3.1.2. Preparation of Polystyrene Microplastics (PS-MPs) Suspensions.....	36
3.1.3. Cell Viability Assays	37
3.1.4. Total Cell Association of PS-MPs Over Time Assay	39
3.1.5. Live Cell Painting Assay.....	40
3.1.6. Statistical Analyses	43
3.1.7. Data and Analysis Availability	43
3.2. Results.....	43
3.2.1. High concentrations of PS-MPs showed a trend toward increased cell viability, as determined by MTT and Calcein-AM assay.....	43

3.2.2.	Treatment with PS-MPs at High Concentrations Induces Morphological Alterations and a Significant Decrease in the Number of Dead Cells.....	45
3.2.3.	Total Cell Association of PS-MPs Increases Over Time	48
3.2.4.	Treatment with PS-MPs at High Concentrations Increased the Amount of Acidic Vesicles in Huh7 Cells and Decreased Cell-Cell Adhesion in HepG2 Cells	51
3.3.	Supplementary Materials.....	63
3.3.1.	Supplementary Material 1: Characterization of Polystyrene Microplastics (PS-MPs)	63
3.3.2.	Supplementary Material 2: Stabilization Tests of PS-MPs in DMEM serum-free Medium.....	65
3.3.3.	Supplementary Material 3: Viability of Huh7 and HepG2 Cells Assessed by MTT and Calcein-AM Assays After Exposure to Triton X-100	68
3.3.4.	Supplementary Material 4: Full representative fluorescence microscopy images of Calcein-PI-Hoechst assay with Huh7 and HepG2 cells	69
3.3.5.	Supplementary Material 5: Cell Proliferation Assays in Huh7 and HepG2 Cells (after exposure to PS-MPs) Using EdU Assay and Ki-67 Protein Immunofluorescence	73
3.3.6.	Supplementary Material 6: Viability of Huh7 and HepG2 Cells Assessed by MTT Assay After Exposure to PS-MPs-Fluor.....	77
3.3.7.	Supplementary Material 7: Full representative fluorescence microscopy images of Total Cell Association of PS-MPs Over Time	78
3.3.8.	Supplementary Material 8: Confocal Microscopy Investigation of PS-MPs Internalization in Huh7 and HepG2 Cells.....	91
3.3.9.	Supplementary Material 9: Full representative fluorescence microscopy images of Live Cell Painting Assay with Huh7 and HepG2 cells.....	94
3.3.10.	Supplementary Material 10: Cell Painting Assay.....	100
4.	DISCUSSION.....	110
5.	CONCLUSION.....	114
6.	REFERENCES	115
7.	APPENDICES	129

7.1. APPENDIX 1: Preliminary Expression Assays of BAX- α and Akt Proteins in Huh7 and HepG2 cells (after PS-MPs exposure) via Western Blot.....	129
7.2. APPENDIX 2: Investigation of Autophagic Processes in Huh7 and HepG2 Cells Exposed to PS-MPs using MTT Assay.....	136
7.3. APPENDIX 3: Attempted Co-localization Assay of Autophagolysosome Proteins LC3 and LAMP-1.....	139
7.4. APPENDIX 4: Preliminary Expression Assays of Cell-Cell Junction Proteins β -Catenin and ZO-1 in HepG2 Cells.....	143
7.5. APPENDIX 5: HepatotoxPath Assay.....	147
7.6. APPENDIX 6: Steatosis Assay.....	165
8. ANNEX 1.....	173
9. ANNEX 2.....	174

1. INTRODUCTION

1.1. Human Exposure to Micro and Nanoplastics: A Daily Issue

The increasing global production and widespread use of plastics are resulting in the uncontrollable accumulation of these materials in the environment. In 2017 alone, 348 million tons of plastics were produced worldwide, with an annual growth rate of approximately 5% (Geyer et al., 2017; PEMRG, 2017). Projections suggest that plastic waste in the environment could reach 11 billion tons by 2050 (Brahney et al., 2020). A study warned that current plastic emission rates could lead to an irreversible tipping point in global plastic pollution (MacLeod et al., 2021).

Although plastics are not biodegradable, a significant portion of plastic waste undergoes progressive fragmentation in the environment due to various stressors, such as sunlight, temperature, wind, and rain. This fragmentation leads to the formation of secondary microplastics (100 nm to 5 mm) (Chatterjee & Sharma, 2019) and nanoplastics (<100 nm) (Gigault et al., 2018). In the European Union (EU), the unintentional release of secondary microplastics into the environment is estimated at approximately 1.8 million tons annually, equivalent to 600 Olympic-size swimming pools (ECHA, 2023).

In addition to secondary MPs, there are primary MPs and NPs intentionally produced within this size range to be added to various products, such as cosmetics, detergents, paints, fertilizers, agrochemicals, drug-delivery systems, and products used in the oil and gas industries. It is estimated that in the EU alone, about 145,000 tons of primary MPs are produced annually, of which approximately 42,000 tons are released into the environment (ECHA, 2023; Mitrano et al., 2021).

Due to the significant release of these particles into the environment, MPs and NPs are now found in the three major environmental compartments: terrestrial, aquatic, and atmospheric. This makes our exposure to these particles unavoidable and occurs daily through various routes, such as ingestion and inhalation. The environmental concentration of MPs today is considered to range from **ng/L to µg/L** (Lenz et al., 2016). Drinking water alone contributes to more than 80% of human exposure to MPs and NPs, as the aquatic environment is one of the most polluted. For instance, an estimated 14 million tons of MPs are accumulated on the ocean floor, transported mainly by rivers (Barrett et al., 2020). Additionally, wastewater treatment plants cannot effectively filter these small particles; only 25% of them are retained, with the remaining 75% being released into treated water (Carr et al., 2016; Napper et al., 2015; Rochman et al., 2015).

Studies have indicated that tap water may contain up to 260 MPs/L (Gambino et al., 2022), while bottled water may contain up to 240,000 MPs/L (Qian et al., 2024; Kosuth et al., 2018; Van Cauwenberghe et al., 2013). These concentrations, depending on the size and type of plastic particles, are estimated to range from **ng/L to µg/L**.

In addition to drinking water, MPs and NPs are now found in various foods, whether processed or not. Examples include shellfish, which can contain up to 12.8 MPs/g, and fish, which can contain up to 1.85 MPs/g (Alberghini et al., 2023; Akhbarizadeh et al., 2018; Barboza et al., 2020b); sea salt with up to 19.8 MPs/g (Renzi & Blašković, 2018); sugar with up to 0.39 MP/g and honey with up to 0.66 MP/g (Liebezeit & Liebezeit, 2013; FAO, 2022); lettuce (especially those from urban gardens fertilized with sewage sludge) with up to 1,000 MPs/g (Canha et al., 2023); meat with up to 18.7 MPs/kg (Kedzierski et al., 2020); milk with up to 14 MPs/L (Kutralam-Muniasam et al., 2020); beer with up to 80,000 MPs/L (Li et al., 2022); and plastic tea bags steeped at high temperatures, which can release approximately 11.6 billion MPs and 3.1 billion NPs per cup of tea (Hernandez et al., 2019). For processed foods, much of the contamination by MPs comes not only from the water used but also from plastic packaging and processing chains (Li et al., 2022; FAO, 2022). Furthermore, the quantification of MPs and NPs in foods is underestimated due to the limitations of current techniques for detecting such small particles (FAO, 2022). Moreover, as most studies report MP concentrations in terms of particle count, mass quantification often requires estimation (Koelmans et al., 2019).

Based on various studies quantifying MPs and NPs in water, food, and beverages, one study estimated the mass concentration of MPs ingested weekly by humans based on dietary exposure. Considering the standardized particle size reported in these studies (<1 mm), it was estimated that **humans ingest 0.1 to 5 g of MPs weekly**, i.e., 14 to 714 mg of MPs daily (Senathirajah et al., 2021). Considering that an adult human consumes 2 to 3 liters of liquids per day (including water, juices, and other beverages) and 1 to 2 kg (or L, considering the average density of solid foods as ~1 g/cm³) of solid foods daily, this results in a total daily intake of approximately 3 to 5 liters of combined liquid and solid foods. Based on these values, the average exposure concentration via liquids and foods ranges from 3 mg/L to 238 mg/L. Thus, the daily ingestion of MPs can reach the order of magnitude of **mg/L**.

The ingestion of MPs by humans is particularly concerning because all NPs and MPs up to 200 µm in size can cross the intestinal barrier of a healthy human (Lehr et al., 1991; Weir et al., 2012). Intestinal barriers with small lesions may also allow the passage of larger microparticles. Additionally, MPs larger than 200 µm may enter the systemic circulation during surgical procedures (Yang et al., 2023). Another route by which NPs and MPs can reach the

systemic circulation is via inhalation and subsequent translocation across the alveolar-capillary barrier, as air contains up to 100 MPs/m³ (ECHA, 2022; Prata et al., 2020; Dris et al., 2016), primarily originating from the fragmentation of clothing, paints, tires, masks, and other sources.

Once in the bloodstream, microplastics (MPs) can reach various organs where they may accumulate. The presence of MPs in the human body is now an established reality. Recent studies have detected MPs of various compositions and sizes in specific human organs, such as the intestine (colon) (MPs up to 1mm) (Ibrahim et al., 2020), placenta (MPs ranging from 5 to 10 µm) (Ragusa et al., 2021), lungs (MPs ranging from 20 to 200 µm) (Baeza-Martínez et al., 2022), heart (MPs ranging from 20 to 419 µm) (Yang et al., 2023), olfactory bulb of the brain (MPs ranging from 5 to 26 µm) (Amato-Lourenço et al., 2024), kidneys (Massardo et al., 2024), testis (Zhao et al., 2023), and liver (MPs ranging from 4 to 30 µm) (Horvatits et al., 2022). Furthermore, MPs have been detected and quantified in human blood at concentrations ranging from **184 to 465 µg/L** (Leonard et al., 2024), although these concentrations are **underestimated**, as the study highlights that the detection of MPs in human blood was limited by procedural blanks, incomplete digestion of organic material, and particle size detection constraints during analysis. These findings indicate that MPs and NPs are no longer only an environmental issue but also a growing concern for human health.

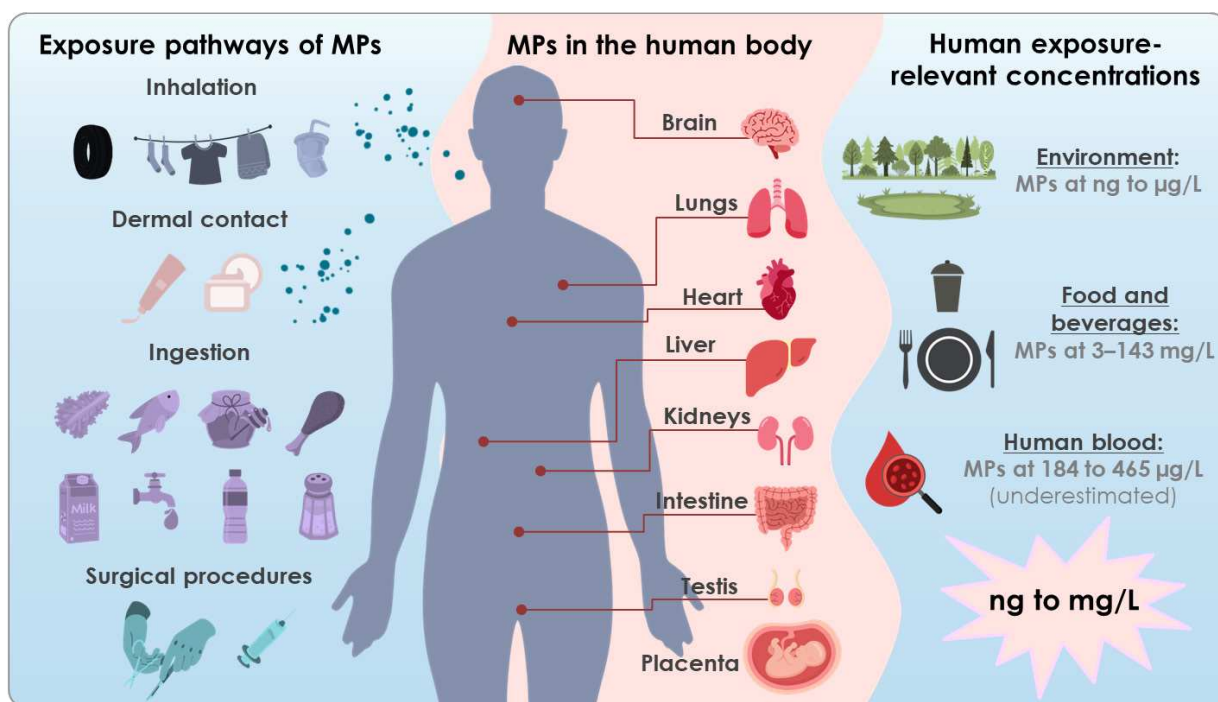


Fig. 1 - Exposure Pathways, Distribution in the Human Body, and Relevant Concentrations of Microplastics (MPs).

1.2. Need to Investigate the (Hepato)toxicity of Nano and Microplastics

According to the German Federal Institute for Risk Assessment (BfR: Bundesinstitut für Risikobewertung), data on the acute and chronic toxicity of NPs and MPs in humans are still insufficient (BfR, 2020), as the field of MPs toxicology is relatively new and lacks extensive results. Therefore, a reliable risk assessment of NPs and MPs cannot yet be conducted, making the investigation of their impacts on human health an urgent priority. The liver, due to its high xenobiotic detoxification activity, is considered one of the primary target organs for the accumulation of MPs and NPs (Hansjosten et al., 2018). Although MPs have already been detected in human liver samples (Horvatits et al., 2022), the hepatotoxic potential of these particles for humans remains poorly understood, as the scientific community is still in the early stages of investigating the hepatotoxicity of MPs and NPs in humans. Most of the *in vivo* and *in vitro* studies available in the literature regarding the hepatotoxicity of MPs and NPs have focused primarily on more obvious endpoints such as oxidative stress, changes in hepatic lipid metabolism, and hepatic inflammation.

As one of the most apparent endpoints, oxidative stress is often the primary focus of studies investigating the toxicity of MPs and NPs. *In vivo* oxidative stress studies in fish (Banaei et al., 2022; Capó et al., 2021; Dong et al., 2022; Umamaheswari et al., 2021) and mice (Djouina et al., 2023; Chen et al., 2022), as well as *in vitro* studies using AML12 cells (alpha mouse liver 12) (Chen et al., 2022), HepG2 cells (human hepatocellular carcinoma cells) (Goodman et al., 2022), and liver organoids derived from human pluripotent stem cells differentiated into hepatic lineage H1ES (Cheng et al., 2022), evaluated the activity of various redox system enzymes such as catalase, glutathione peroxidase, glutathione reductase, and glutathione S-transferase, as well as measured reduced glutathione content. These studies concluded that exposure to NPs and MPs of various compositions (e.g., polyethylene (PE), polystyrene (PS), low-density polyethylene (LDPE), and polyvinyl chloride (PVC)) and sizes (100 nm to 500 µm) in different *in vivo* and *in vitro* models led to oxidative stress, either by altering enzyme activity (increasing or decreasing their activity) or by changing the levels of reduced glutathione (which increased or decreased depending on the experiment). Studies conducted on mice (Luo et al., 2019) and human liver organoids (Cheng et al., 2022) indicated that oxidative stress triggered by MPs and NPs may lead to apoptosis through increased expression of pro-apoptotic proteins such as Bcl-2-associated X protein (BAX) and caspase-3, decreased expression of anti-apoptotic proteins in the phosphoinositide 3-kinase/protein kinase B (PI3K/Akt) pathway, and reduced expression of the cytoprotective nuclear factor erythroid 2-related factor (Nrf2).

Studies investigating alterations in hepatic lipid metabolism *in vivo* (in mice) (Zheng et al.,

2021; Luo et al., 2019) and *in vitro* (in HepG2 cells and human liver organoids H1ES) (Djouina et al., 2023; Cheng et al., 2022) showed that MPs ranging from 1 to 125 μm (PVC, PE, and PS) caused significant changes, resulting in hepatic steatosis. These studies demonstrated that MPs decreased the expression of peroxisome proliferator-activated receptor alpha (PPAR α), which promotes beta-oxidation and ketogenesis during fasting, leading to lipid accumulation in hepatic cells. Moreover, MPs induced overexpression of peroxisome proliferator-activated receptor gamma (PPAR γ), which enhances the transcription of genes related to lipid uptake, such as fatty acid translocase cluster of differentiation 36 (CD36) and liver fatty acid-binding protein 1 (FABP1), further contributing to hepatic steatosis.

Studies on hepatic inflammation induced by NPs and MPs *in vivo* (in mice and fish) (Cui et al., 2023; Choi et al., 2021) and *in vitro* (in HepG2 cells and human liver organoids H1ES) (Djouina et al., 2023; Cheng et al., 2022; Banerjee et al., 2022) demonstrated that NPs and MPs of PS and PVC (ranging from 50 nm to 8 μm) promote inflammation in hepatocytes and hepatic tissues by increasing the secretion of pro-inflammatory cytokines, such as interleukins 1- α , 1- β , 6, and 8 (IL-1 α , IL-1 β , IL-6, and IL-8), and elevating the expression of tumor necrosis factor alpha (TNF- α), interferon gamma (IFN- γ), and inflammatory response proteins such as inducible nitric oxide synthase (iNOS) and cyclooxygenase-2 (COX-2).

The induction of hepatic fibrosis by MPs and NPs has also been reported in both *in vivo* studies (in mice) (Djouina et al., 2023; Li et al., 2022) and *in vitro* studies (in human liver organoids H1ES and HepG2 cells) (Cheng et al., 2022; Banerjee et al., 2022) using MPs and NPs of PS and PVC ranging in size from 42 nm to 125 μm . Additionally, changes in the activity of cytochrome P450 enzymes related to xenobiotic metabolism were observed. A limited number of studies focused on subcellular effects in liver cells, but those that did reported decreased mitochondrial membrane potential (Pan et al., 2021) and DNA damage (Zheng et al., 2019). Based on the studies cited in this and previous paragraphs, it is evident that MPs and NPs have the potential to cause hepatic damage.

However, it is important to note that many studies on the potential toxicity of NPs and MPs to the liver and other organs have used exposure concentration ranges significantly higher than those to which humans are typically exposed, ranging from ng/L to mg/L, as described in the previous section (Section 1.1). Experimental exposure concentrations tend to be between two to seven orders of magnitude higher (Lenz et al., 2016). Therefore, there is an urgent need to assess the toxicity of NPs and MPs at environmentally relevant concentrations that align with human exposure levels. However, evaluating adverse effects caused by NPs and MPs at very low concentrations (ng/L to mg/L) remains challenging for existing toxicological methodologies,

as such concentrations are expected to produce sublethal or subtle changes.

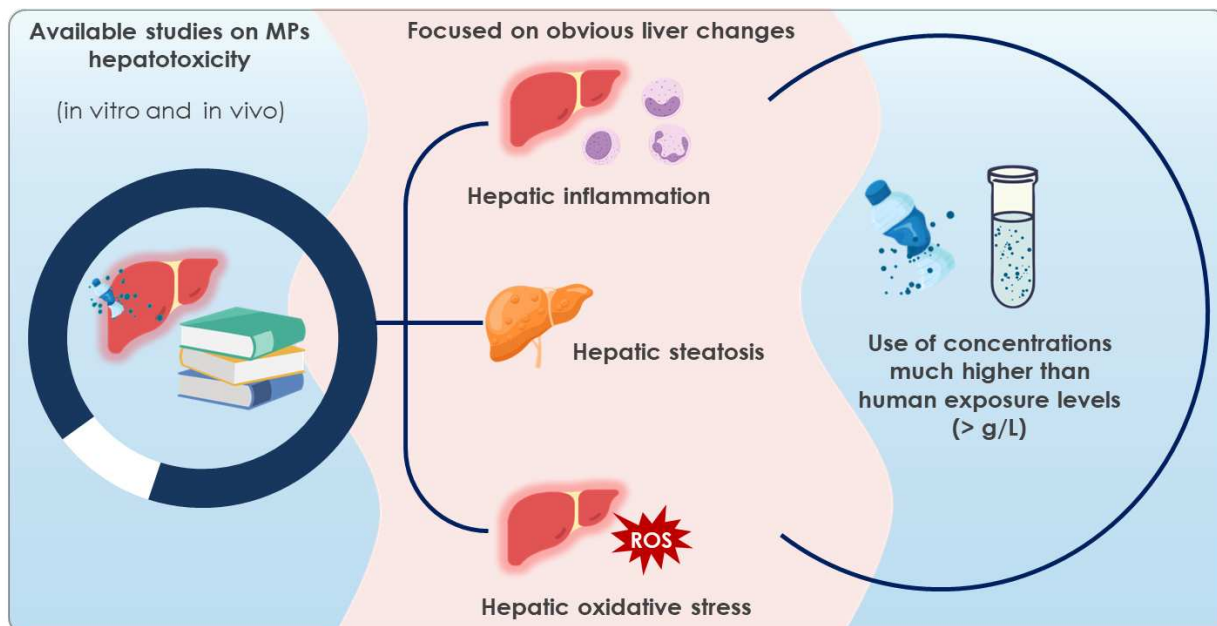


Fig. 2 - Overview of Available Studies on MPs' Hepatotoxicity, Key Findings, and Use of Concentrations Higher Than Human Exposure Levels.

1.3. Cell-Based Assays as Promising Alternatives for Assessing the Hepatotoxicity of MPs and NPs at Environmentally Relevant Concentrations

For hepatotoxicity assays, animal models, due to their phylogenetic differences from humans, can be questionable in terms of predictive capability and relevance for understanding the adverse effects of xenobiotics on human health. For example, routine preclinical species, such as rodents, show only about 50% concordance with drug-induced liver injuries in humans. Over 80% of drug withdrawals from the market occur due to cardiotoxicity and hepatotoxicity that were not accurately predicted in preclinical *in vivo* assays (O'Brien et al., 2014). This discrepancy arises because rodents typically exhibit sensitivity only to overtly hepatotoxic compounds, which can be identified through routine histopathology (Persson et al., 2014). However, more subtle or idiosyncratic adverse effects on the liver are rarely observed *in vivo*. Most unidentified toxicities *in vivo*, which eventually lead to drug withdrawals, involve off-target or non-pharmacological effects such as oxidative stress and mitochondrial inhibition, i.e., alterations in subcellular structures (O'Brien et al., 2014). These effects can be effectively identified using *in vitro* assays.

Cell-based assays are considered promising alternatives for addressing the challenges

of assessing human toxicity (O'Brien et al., 2014). In addition to being orders of magnitude cheaper and faster than *in vivo* assays (Chen et al., 2020), they are more ethical as they adhere to Russell & Burch's 3Rs principles (Reduction, Refinement, and Replacement of animals in testing) (Russell & Burch, 1959). Moreover, these assays circumvent interspecies differences by enabling the use of human cells in experiments, thereby generating toxicological results that are directly relevant to humans.

Furthermore, *in vitro* methods facilitate detailed investigations of cell-particle interactions and specific cellular and subcellular responses, which can reveal sublethal adverse effects (such as those expected to be triggered by MPs at environmentally relevant concentrations). In addition, cell-based assays can be designed to provide a mechanistic understanding of cellular events that cannot be achieved through animal studies (Fritsche et al., 2021; Halappanavar et al., 2021; Chen et al., 2020). These features make cell-based assays particularly valuable for identifying elements of Adverse Outcome Pathways (AOPs).

1.4. Obtaining Cellular Phenotypic Profiles and Elements of Adverse Outcome Pathways (AOPs) through High Content Analysis (HCA)

Among the numerous *in vitro* approaches, High Content Analysis (HCA) has emerged as a promising tool for measuring and quantifying a wide variety of cellular responses (Goodman et al., 2016; Giuliano et al., 2003). HCA enables effective and predictive cytotoxicity assays by combining bioimaging techniques, data analysis, and automated image acquisition and processing. It allows for the simultaneous monitoring of multiple cellular parameters using various fluorescent cell dyes (e.g., structural, organelle-specific, and protein-specific markers). This method facilitates both biochemical and morphological measurements at the single-cell level, enabling the collection of extensive data per cell and the identification of thousands of features that represent cellular responses to perturbations (Goodman et al., 2016). Once identified, these features can be further investigated. This characteristic of HCA is particularly valuable for exploratory assays, which are essential in emerging research fields such as the study of NPs and MPs toxicity. In this area, where data remain scarce, HCA can provide crucial initial insights and guide future investigations to clarify the mechanisms involved and the potential adverse effects of these particles.

Using HCA, large-scale multiparametric screening assays can be conducted, generating single-cell multiparametric data that can be used to define cellular phenotypes (Morris et al., 2019; Smith et al., 2018; O'Brien et al., 2014). Cellular phenotypes are complex and reflect the collective activity of various cellular pathways and observable characteristics (e.g., morphology,

functional and biochemical properties, among others) (Smith et al., 2018; Feng et al., 2009). A field of study known as "phenomics" utilizes large-scale phenotypic data to predict biological outcomes (Smith et al., 2018; Houle et al., 2010). These phenotypes can vary from cell to cell depending on perturbations such as exposure to NPs and MPs.

Phenotypic profiling has been employed to diagnose complex cellular phenotypes (Doan et al., 2018) and predict the biological activity of compounds (Simm et al., 2018), accelerating discoveries that traditionally rely solely on genetic profiling. However, the substantial potential of phenotypic profiling to investigate the cytotoxicity of NPs and MPs remains largely unexplored. Due to its high precision and sensitivity in distinguishing subtle differences between phenotypes (e.g., treated vs. untreated cells), HCA holds great promise for efficiently detecting sublethal toxicities, such as those expected from cellular perturbations caused by NPs and MPs at environmentally relevant and human exposure concentrations (1 ng to 1 mg/L).

Moreover, HCA enables comprehensive exploration and identification of AOPs, which are critical in toxicological investigations. AOPs have emerged as a valuable framework to integrate mechanistic evidence obtained from *in vitro* assays into pathways leading to adverse outcomes (Perkins et al., 2019). An AOP describes the sequence of mechanistic events leading to a specific toxicological effect, from the initial molecular trigger to the final adverse outcome. This provides crucial insights into the mechanisms by which NPs and MPs disrupt biological systems. For example, a hypothetical AOP involving MPs and hepatocytes could begin with a molecular initiating event (MIE), such as the cellular internalization of MPs, followed by physical disruption of organelles (Key Event (KE) 1). This disruption may lead to cellular responses, such as activation or inhibition of signaling pathways (KE 2), ultimately resulting in processes like apoptosis or autophagy (KE 3). These cellular events could then progress to tissue-level effects, ultimately leading to the adverse outcome (AO) of hepatic dysfunction (Fig. 4). Therefore, exploring AOPs in toxicological assays is crucial for obtaining a more comprehensive understanding of the toxic effects of NPs and MPs on human health, including sublethal cellular alterations. This understanding could significantly contribute to human health risk assessments.

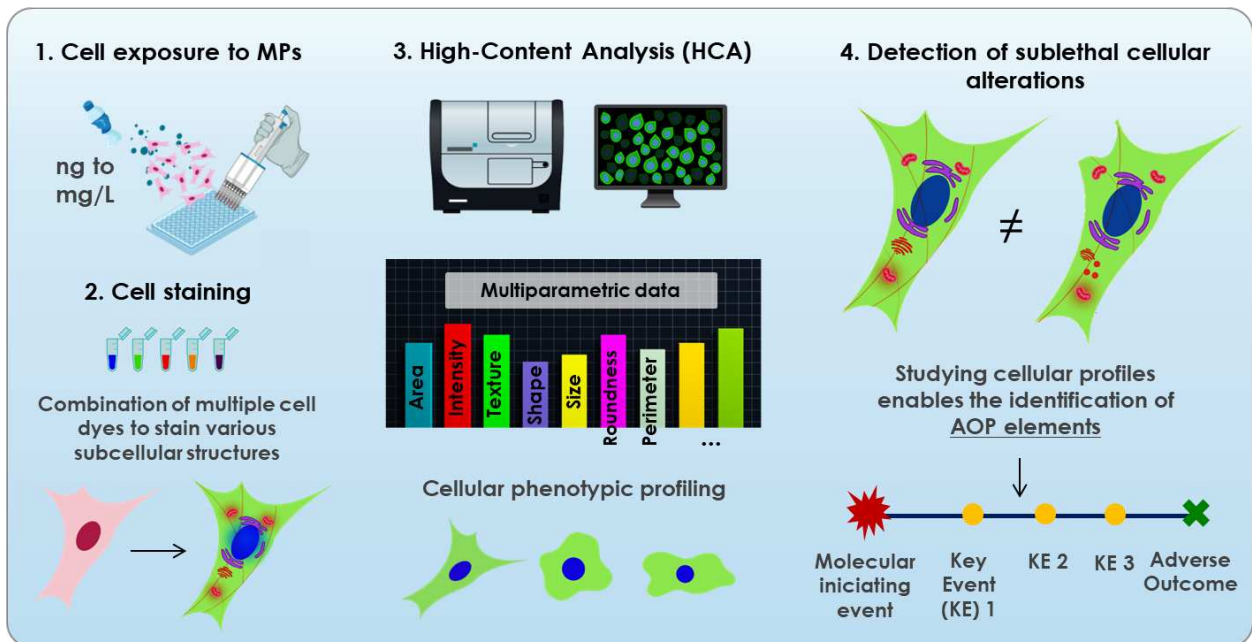


Fig. 3 - HCA as a promising tool for detecting subtle changes in cellular phenotypes and identifying elements of Adverse Outcome Pathways (AOPs).

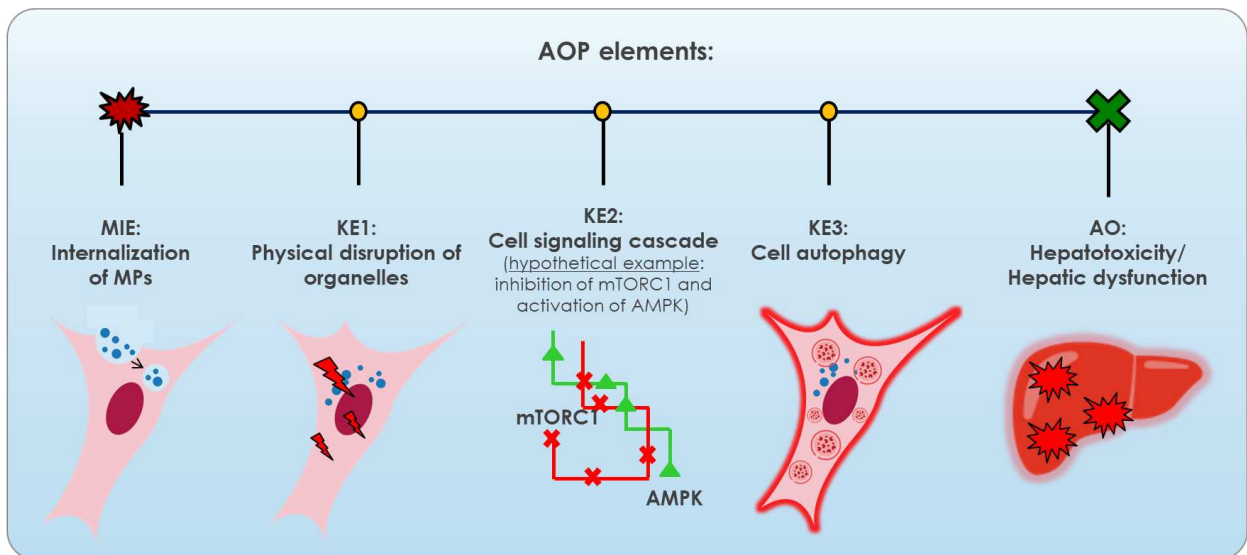


Fig. 4 - Hypothetical Adverse Outcome Pathway (AOP) Elements Associated with MPs and Hepatocyte Responses. MIE: Molecular Initiating Event (MIE); KE: Key Event; AO: Adverse Outcome.

1.5. HCA as a Predictive Approach for Hepatotoxicity Assessment of NPs and MPs *In Vitro*

HCA approaches facilitate the development of highly customizable assays, allowing endpoints to be tailored to detect general or specific mechanisms of toxicity, thereby offering flexibility and precision in toxicological investigations (Persson et al., 2014). This capability proves highly efficient for predictive toxicology, not only by enabling the selection of endpoints that align with parameters targeting specific toxicological outcomes and those describing toxicities not readily identified in preclinical animal models (Persson et al., 2014), but also by allowing for the selection of more general parameters. These broader parameters provide a comprehensive cellular overview, enabling the detection of subtle or non-obvious cellular alterations.

1.5.1. HCA in Exploratory Approaches to Hepatotoxicity: Live Cell Painting and Cell Painting Assays

A powerful strategy for exploratory cytotoxicity analysis and cellular phenotype acquisition involves assays that stain various cellular structures to provide a broader and more comprehensive view of cellular phenotypes. Two notable examples are Live Cell Painting (Garcia-Fossa et al., 2024) and Cell Painting (Bray et al., 2016).

Live Cell Painting is a novel assay developed by Dr. Fernanda Garcia Fossa and colleagues from the research group associated with this study, including the PhD candidate Thaís de Moraes Lacerda and the author of this dissertation, Mariana Rodrigues da Silva. This assay uses a single metachromatic dye, Acridine Orange, to stain live cells after exposure to substances of interest, such as MPs and NPs. Acridine Orange highlights acidic vesicles, the cytoplasm, the nucleus, and the nucleoli of live cells (Byvaltsev et al., 2019; Robbins et al., 1963). Additionally, this assay enables the detection of cellular phenotypic changes triggered by experimental treatments in live cells. Compared to Cell Painting, Live Cell Painting is faster and more cost-effective, making it an excellent choice for initial cytotoxicity investigations, which can later be complemented by more detailed analyses.

In contrast, the **Cell Painting assay** is a more complex approach that involves staining a broader range of subcellular structures, including the nucleus, plasma membrane, endoplasmic reticulum, F-actin cytoskeleton, Golgi complex, and mitochondria, among others, using multiple fluorescent stains (Bray et al., 2016). However, this assay requires fixing the cells, which limits real-time monitoring. Both assays can generate phenotypic cytotoxic signatures by comparing

cells exposed to known compounds with those treated with compounds of interest, such as MPs and NPs.

Using these assays in combination with tools like CellProfiler software (Carpenter et al., 2006), dozens of metrics can be extracted from cell images for each dye, which can then be combined to generate a detailed phenotypic profile. These metrics include staining intensities, texture patterns, size and shape of labeled cellular structures, correlations between markers/cellular dyes, and adjacency relationships between cells and intracellular structures. Evaluating phenotypic profiles using markers that are not biased towards a specific outcome allows for a more comprehensive and unbiased understanding of hepatotoxic effects induced by NPs and MPs (Bray et al., 2016).

It is important to highlight that phenotypic profiles obtained from Live Cell Painting and Cell Painting differ significantly from those generated by conventional screening assays. Traditional assays typically quantify selected characteristics specifically linked to the biology of interest. For example, they may investigate toxic effects through parameters such as DNA damage, reactive oxygen species production, hepatic steatosis biomarkers, or inflammation. In contrast, Live Cell Painting and Cell Painting provide a broader, unbiased view, avoiding the intensive customization often required for assays targeting specific issues.

The primary advantage of using unbiased approaches like Live Cell Painting and Cell Painting lies in the potential for unexpected toxicological discoveries. By not focusing exclusively on predefined endpoints, these assays allow for the identification of unanticipated cellular responses and mechanisms of toxicity (Bray et al., 2016). This capability is particularly valuable for exploratory studies in emerging research fields such as the toxicity of NPs and MPs, where there is still limited data and much to uncover about the mechanisms and effects of these particles.

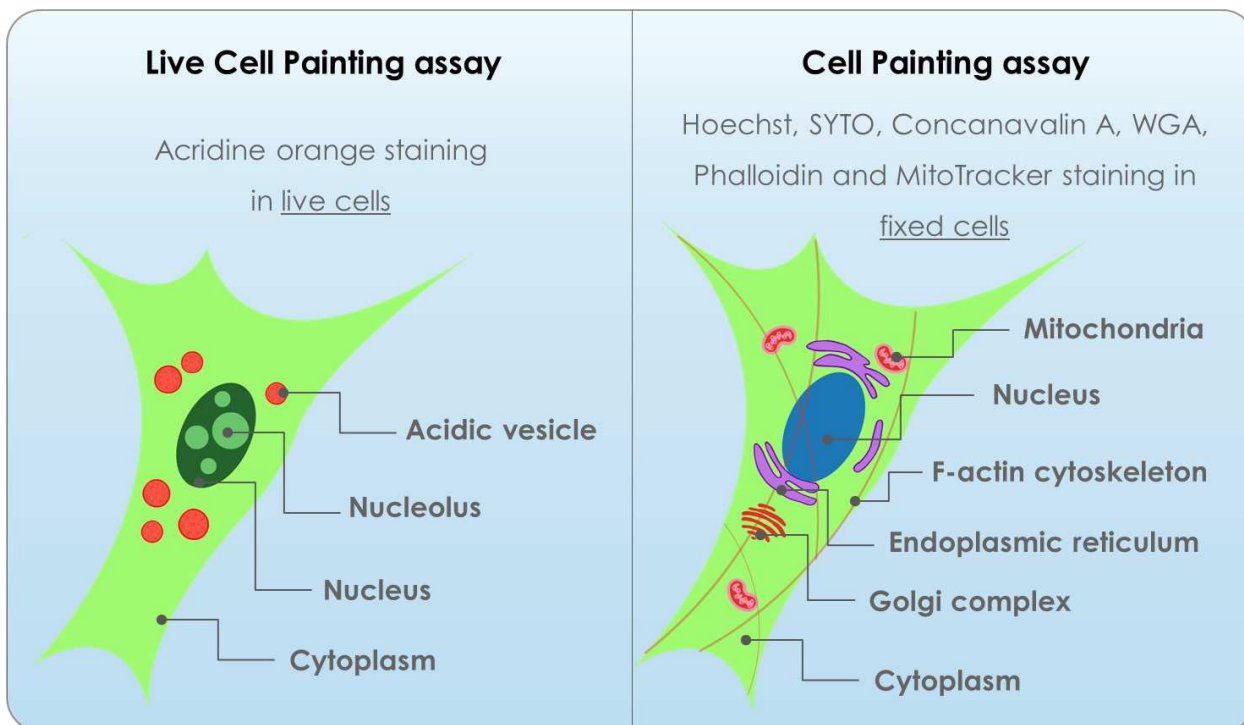


Fig. 5 - Overview of Cellular Structures Stained in Live Cell Painting and Cell Painting Assays.

1.5.2. HCA in Targeted Approaches to Hepatotoxicity: Using Markers to Highlight Fundamental Parameters of In Vitro Hepatotoxicity (HepatotoxPath Assay)

A targeted approach to hepatotoxicity can be achieved through the development of an HCA assay in which the selected parameters, or endpoints, reflect the key pathophysiological mechanisms commonly associated with hepatotoxicity observed *in vitro*. This enhances the predictive capability of the assay for detecting hepatotoxic effects (Persson et al., 2014). Among these parameters, mitochondrial toxicity is arguably one of the most sensitive indicators for predicting human liver damage (including idiosyncratic types) caused by xenobiotics, such as drugs, including moderately hepatotoxic ones (Persson et al., 2014; Dykens & Will, 2007).

For example, changes in mitochondrial membrane potential (MMP) induced by xenobiotics and detected in HCA assays are not readily identified in routine animal testing. However, alterations in MMP are highly predictive of human hepatotoxicity (Persson et al., 2014). Additionally, many hepatotoxic agents are metabolized into reactive intermediates that are detoxified through reactions with intracellular glutathione (GSH). This process often results in changes to GSH levels and disrupts the cellular redox system as a whole (Xu et al., 2008; Holt & Ju, 2006). Another common endpoint observed after treating cells with hepatotoxic compounds

is the disruption of calcium homeostasis (Xu et al., 2008; Holt & Ju, 2006).

In hepatocytes, the integrity and functionality of lysosomes are also critical for xenobiotic detoxification and cellular regeneration. Lysosomal alterations have been associated with conditions such as steatosis, inflammation, and the progression to hepatic fibrosis. Among the various mechanisms involved in the uptake and internalization of NPs and MPs into human cells, the **endocytosis pathway** stands out (Salvati et al., 2011; Zhao et al., 2011). Therefore, assessing hepatotoxicity induced by NPs and MPs must include investigations into potential alterations in the endosomal-lysosomal machinery, as this is part of the cell's initial interaction with these particles.

Thus, the **fundamental functional parameters** for predicting the *in vitro* hepatotoxicity of NPs and MPs include: alterations in mitochondrial membrane potential (MMP), disruptions in the redox system (e.g., changes in GSH levels), intracellular calcium level fluctuations, and changes in the endosomal-lysosomal machinery. In addition to these more sensitive endpoints for hepatotoxicity, conventional markers, such as those indicating hepatic steatosis, can also be combined. However, steatosis is not typically among the most sensitive endpoints for *in vitro* assays involving compounds that are not overtly hepatotoxic (Persson et al., 2014).

To assess these parameters in an HCA assay, appropriate cellular markers (fluorescent dyes or fluorophores) must be used. Examples include: Tetramethylrhodamine methyl ester (**TMRM**): To monitor changes in MMP (O'Brien et al., 2014; O'Brien et al., 2006). **ThiolTracker**: To evaluate intracellular glutathione levels (Mandavilli et al., 2010; Xu et al., 2008). **Fluo-4**: To measure intracellular calcium levels (O'Brien et al., 2014; O'Brien et al., 2006). **LysoTracker**: To analyze changes in the endosomal-lysosomal machinery (Anguissola et al., 2014). **LipidTOX**: To assess lipid metabolism changes (e.g., steatosis) (Grandl & Schmitz, 2010). By employing these fluorescent markers, HCA assays have the potential to detect hepatotoxic alterations triggered by NPs and MPs, even at low concentrations (ranging from ng/L to mg/L).

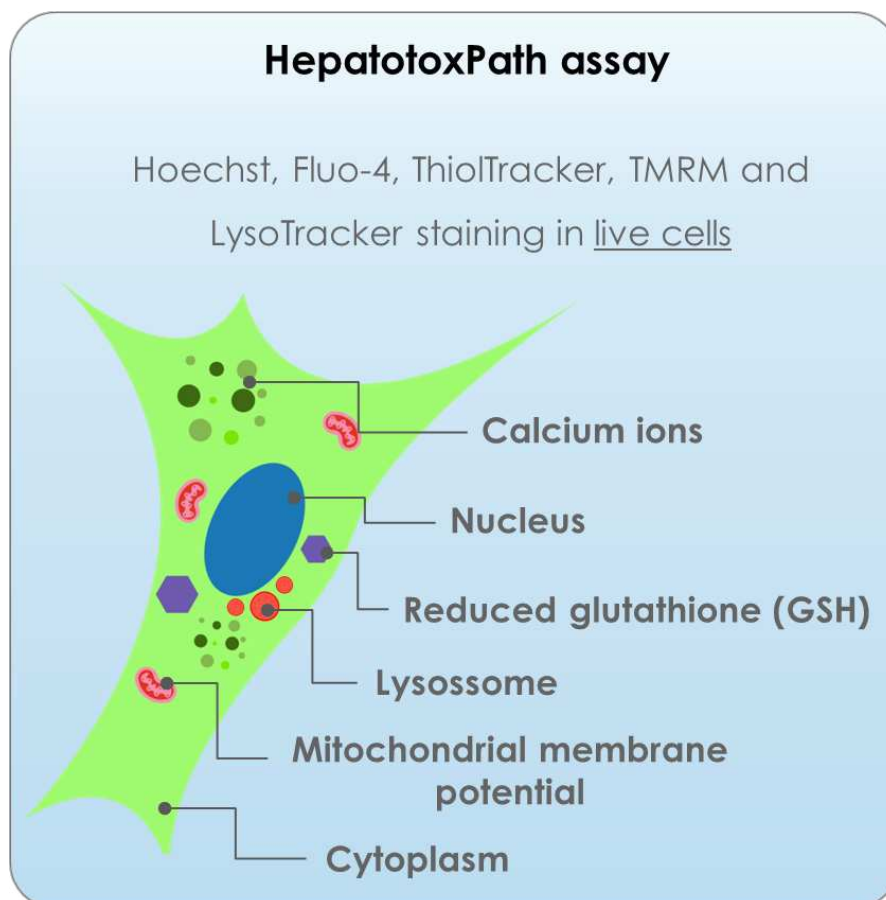


Fig. 6 – Example of Cellular Parameters that can be Stained and Assessed in a Hepatotoxicity-Targeted Assay

1.6. Relevant *In Vitro* Models for Studying Hepatotoxicity

All parameters that HCA enables exploration of are crucial for investigating cellular phenotypic profiles and elements of AOPs induced by NPs and MPs. By employing appropriate cell models, coupled with approaches sensitive enough to identify sublethal cellular changes and phenotypic alterations, it is possible to predict the human hepatotoxicity of NPs and MPs at environmentally relevant concentrations (O'Brien et al., 2009; Amit et al., 2005; Xu et al., 2004). Immortalized human hepatocyte models (cell lines) are particularly advantageous for predicting *in vitro* human hepatotoxicity due to their proliferative capacity, unlimited lifespan, ability to maintain differentiation over time during assays, and their human origin (O'Brien et al., 2014). Additionally, it is important to emphasize that ideal cell lines for this type of study are those that are well-characterized, well-understood, and widely reported in the scientific literature (O'Brien et al., 2014).

Hepatocytes are considered the primary cell type responsible for hepatic metabolism. They perform various functions, including carbohydrate, lipid, and protein metabolism, synthesis of serum proteins, activation of immune cells, and detoxification of xenobiotics (Ebrahimkhani et al., 2014). One human liver cell line that can differentiate into cells with functions and characteristics very similar to hepatocytes is the HepaRG cell line. However, there is a significant limitation in using these cells for *in vitro* assays, as they exhibit instability and tend to gradually lose their hepatic differentiation during culture. Instead, they acquire a mesenchymal phenotype with glycolysis-dependent energy metabolism (Adam et al., 2018; Laurent et al., 2013).

Although they exhibit less similarity to hepatocytes compared to HepaRG cells, the human hepatocellular carcinoma cell lines HepG2 and Huh7 are more stable and currently the most widely used for *in vitro* exploratory toxicity studies of drugs and compounds (Dogra et al., 2015; O'Brien et al., 2014; Bandi et al., 2014; Yu et al., 2014). Despite HepG2 cells having very low expression of cytochrome P450 proteins, they are well-established in predicting hepatotoxicity, including forecasting drug-induced liver injury potential (Weaver et al., 2020; Weaver et al., 2017), and have been shown to be among the best single-cell models for predicting human toxicity (O'Brien et al., 2014). On the other hand, while Huh7 cells show fewer similarities to hepatocytes in their gene expression profiles (Saran et al., 2022; Guo et al., 2011; Olsavsky et al., 2007), characterization of drug transporter expression in Huh7 cells revealed mRNA levels of the farnesoid X receptor (FXR), nuclear factor erythroid 2-related factor 2 (Nrf2), and multidrug resistance-associated protein 2 (MRP2) that are comparable or even superior to those found in human hepatocytes (Saran et al., 2022; Jouan et al., 2017). Confluent Huh7 cells also exhibit induction of important drug-metabolizing enzymes, including cytochrome P450 (CYP) 3A4 (Saran et al., 2022; Sivertsson et al., 2013), unlike HepG2 cells.

To overcome the metabolic limitations of individual cell lines and enhance the predictive power of hepatotoxicity assays, conducting studies using multiple cell models simultaneously, such as HepG2 and Huh7, can be highly advantageous. Each cell line can complement the metabolic shortcomings of the other—for instance, by expressing specific enzymes that the other lacks—thereby providing higher-quality responses for particular parameters evaluated. Additionally, comparing responses between cell lines allows for better correlation of cytotoxic mechanisms identified. Studies have demonstrated that using multiple cell lines in toxicological assessments enhances the predictive capacity of assays (Shaw et al., 2008). Thus, employing multiple hepatocyte models has the potential to significantly improve the predictive power and relevance of assays, producing more robust data regarding the hepatotoxicity of NPs and MPs.

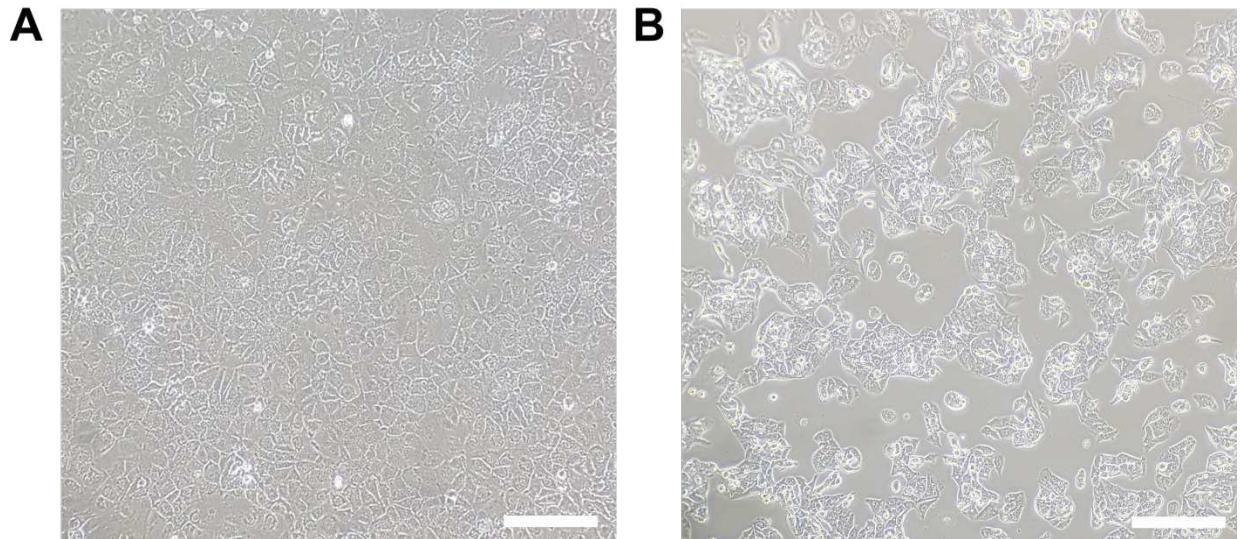


Fig. 7 - Light Microscopy Images of Huh7 and HepG2 Cells. Representative light microscopy images of human hepatocellular carcinoma cell lines used as *in vitro* models for hepatotoxicity studies: **(A)** Huh7 and **(B)** HepG2. Scale bar: 200 μm.

2. OBJECTIVES

General Objective: To investigate the sublethal phenotypic alterations and underlying mechanisms of hepatotoxicity induced by exposure to Polystyrene Microplastics (PS-MPs; 0.5 μm ; ng/L to g/L range) in two human hepatocyte models (Huh7 and HepG2), using High-Content Analysis (HCA) in both targeted and untargeted endpoints for hepatotoxicity outcomes.

Specific Objectives

- a) To determine whether PS-MPs induce cytotoxic or sublethal phenotypic changes in Huh7 and HepG2 cells after 24 h of exposure at a wide range of concentrations (1 ng/L to 1 g/L).
- b) To explore whether Live Cell Painting and Cell Painting assays can reveal novel and unpredicted phenotypic signatures associated with PS-MPs-induced hepatotoxicity.
- c) To evaluate specific phenotypic markers of hepatotoxicity, such as mitochondrial dysfunction, oxidative stress, lipid metabolism alterations, and calcium homeostasis disruption, through targeted HCA using the HepatotoxPath approach.
- d) To analyze and classify the cellular phenotypic profiles of Huh7 and HepG2 cells using image analysis and machine learning techniques, aiming to identify patterns associated with different PS-MPs concentrations and exposure conditions.
- e) To validate the main phenotypic alterations observed in HCA through molecular biology techniques (e.g., immunofluorescence, western blotting), aiming to confirm mechanistic pathways involved in PS-MPs-induced cellular stress and damage.
- f) To compare the phenotypic responses obtained by targeted vs. untargeted HCA approaches, and assess whether the cellular responses differ between the two hepatocyte models under identical exposure conditions.

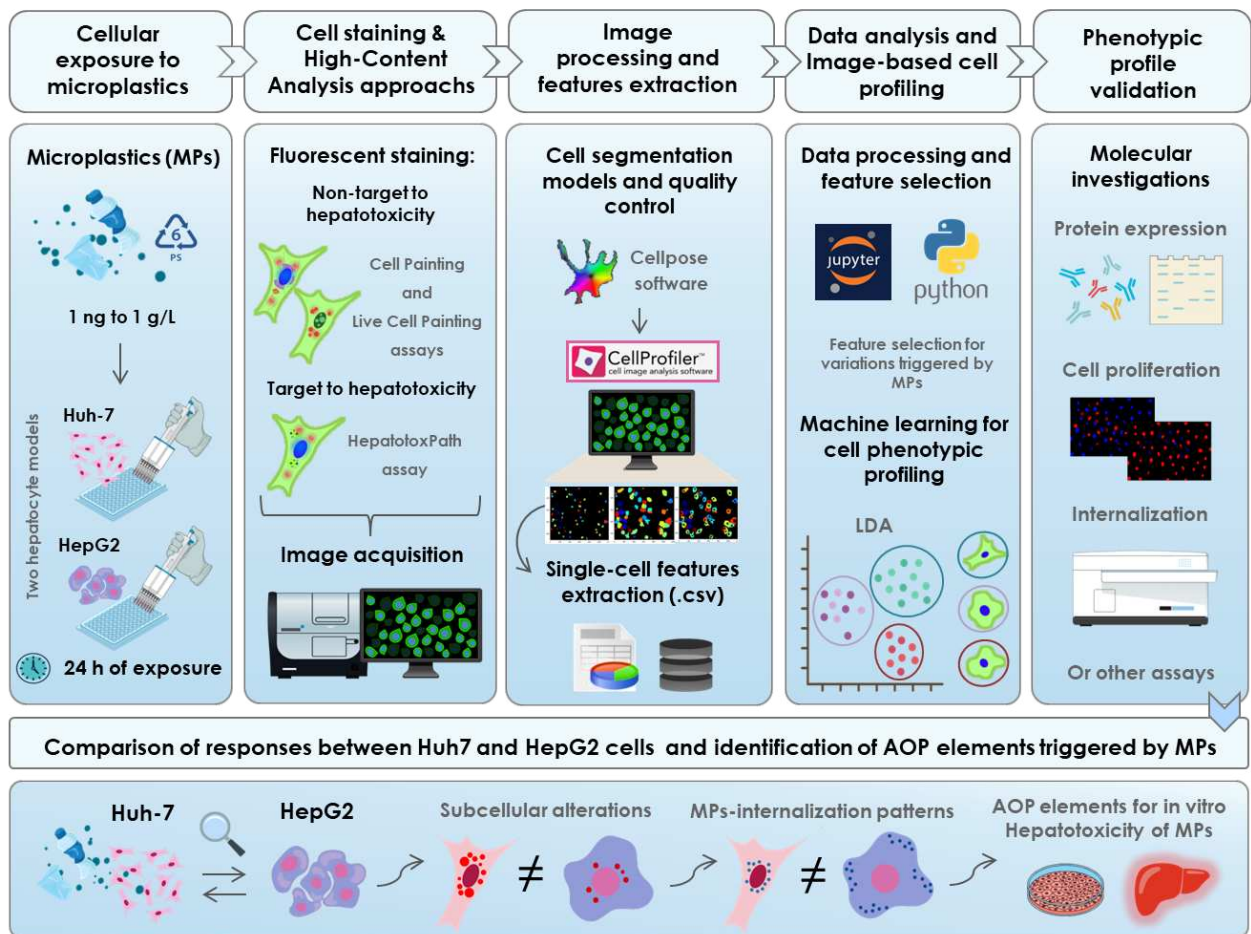


Fig. 7 - Graphical Abstract of the Project's Objectives: Investigating Cellular Responses and AOP Elements Induced by Microplastics in Hepatocyte Models.

3. TO BE PUBLISHED DOCUMENT

3.1. Material and Methods

3.1.1. *Cell Culture and Plating*

3.1.1.1. *Cell Culture*

Huh7 human hepatocellular carcinoma cells (JCRB0403) were obtained from the Japanese Collection of Research Bioresources Cell Bank (JCRB, Japan), and HepG2 human hepatocellular carcinoma cells (HB-8065) were obtained from the American Type Culture Collection (ATCC). Both cells were cultured in Dulbecco's Modified Eagle's Medium (DMEM; Life Technologies, Canada) supplemented with 10% Fetal Bovine Serum (FBS; Gibco, South America) and 1% antibiotics (Penicillin/Streptomycin; Pen/Strep) (Gibco, Grand Island - USA). For HepG2 cells, 1% (v/v) Non-Essential Amino Acids (Lonza, Switzerland) and 2 mM L-Glutamine (Gibco, Germany) to provide optimal growth conditions.

Cells were maintained in a controlled environment using a Panasonic incubator set at 37 °C, 95% relative humidity, and 5% CO₂. Subculturing was performed as needed to maintain cell confluence at approximately 80%. To ensure the integrity of the cell cultures, mycoplasma contamination was checked on cells cultured without antibiotics for three days using the direct DNA staining method with Hoechst 33342 (Invitrogen, USA), and then observed under fluorescence microscopy. Mycoplasma testing to certify the absence of contamination in the cultures was conducted every two weeks after thawing a vial of cells (no cell line was maintained in culture for more than two months). Only mycoplasma-free cultures were used in all experiments.

3.1.1.2. *Cell Plating*

For all exposure assays, Huh7 cells (7,500 cells/well) and HepG2 cells (22,000 cells/well) were plated in 96-well plates using supplemented DMEM medium and incubated at 37 °C and 95% for 24h.

3.1.2. *Preparation of Polystyrene Microplastics (PS-MPs) Suspensions*

The polystyrene microplastics (PS-MPs) used in this study (code: 'PP10-05-10') were sourced from SpheroTech Inc. (Illinois, USA). These particles have an approximate size of 0.5 µm and a negative surface charge. Physicochemical characterization assays of these PS-MPs were performed in antibiotic-and-serum-free DMEM (DMEM without Pen/Strep and FBS) and in

deionized water, as detailed in **Supplementary Material 1**.

PS-MPs suspensions were prepared in antibiotic-and-serum-free DMEM stabilized with 0.0025% (v/v) Tween 20 (Amresco, USA) (Banerjee et al., 2022). Prior to cell exposure, the suspensions were ultrasonicated for one hour and incubated at 37 °C for 24 hours to prevent MPs aggregation, as detailed in **Supplementary Material 2**.

3.1.3. Cell Viability Assays

3.1.3.1. Cell Exposure

After 24 hours, cells were exposed to PS-MPs (100 µL) at concentrations ranging from 1 ng/L to 1 g/L in sextuplicate for 24 hours at 37 °C. This range includes concentrations of microplastics considered environmentally relevant and realistic for human exposure (1 ng/L to 1 mg/L; Leonard et al., 2024; Senathirajah et al., 2021; Lenz et al., 2016), as well as higher concentrations (0.5 g/L and 1 g/L). Antibiotic-and-serum-free DMEM containing 0.0025% (v/v) Tween 20 (100 µL) was used as a negative control, while Triton X-100 (40 µM, 100 µL; Sigma-Aldrich, USA) was used as a positive control. Each experiment was conducted on at least three independent days, with a different plate layout (i.e., varying the position of treatments within the wells) used for each experimental run.

3.1.3.2. MTT Cell Viability Assay

MTT assay ([3-(4,5-dimethylthiazol-2-yl)-2,5-diphenyltetrazolium bromide]) was used to assess cytotoxicity by measuring the reduction of tetrazolium salts to formazan crystals, a process dependent on the activity of NADH-dependent dehydrogenase in metabolically active cells (Mosmann, 1983). After cell exposure, the treatment medium was replaced with MTT solution (100 µL; 0.5 mg/mL in antibiotic-and-antibiotic-and-serum-free DMEM; Invitrogen, USA) in three wells of each sextuplicate, while the remaining three wells received antibiotic-and-serum-free DMEM (100 µL) to serve as blanks. Following 2.5-hour incubation at 37°C, the MTT solution was replaced with Dimethyl sulfoxide (DMSO; (100 µL; Synth, Brazil) to dissolve the formazan crystals. Then, the plates were shaken for 15 minutes to ensure a homogeneous formazan solution. After homogenization, the absorbance of each well was measured at 570 nm using the Cytation 5 Hybrid Multidetector Reader (BioTek Instruments, Inc., Winooski, VT, USA), hereafter referred to as Cytation 5.

The absorbance data were processed by subtracting the blank values from those of the MTT-treated wells. These values were then normalized to the absorbance of the negative control, which was set at 100% cell viability. Finally, the percentage cell viability was plotted

against the concentration of PS-MPs using GraphPad Prism software (version 8.0.2, La Jolla, California, USA), to calculate the IC_{50} (the concentration of PS-MPs required to inhibit 50% of cell viability) by nonlinear regression (log(inhibitor) vs. response – variable slope, four parameters).

3.1.3.3. Calcein-AM Cell Viability Assay

The Calcein-AM assay evaluates cytotoxicity by measuring the intracellular conversion of Calcein acetoxymethyl ester (Calcein-AM), a non-fluorescent and cell-permeable molecule, into Calcein, a fluorescent and cell-impermeable molecule. This conversion depends on the activity of intracellular esterases in metabolically active cells (Bratosin et al., 2005). After cell exposure, the treatment medium was replaced with Calcein-AM solution (50 μ L; 0.05 μ M; Invitrogen, USA) diluted in FluoroBrite DMEM (Gibco, USA) in three wells of each sextuplicate, while the remaining three wells received FluoroBrite DMEM (50 μ L) to serve as blanks. The plates were then incubated for 30 minutes at 37°C, and the fluorescence of Calcein was measured at an emission wavelength of 528 nm and an excitation wavelength of 488 nm, using the Cytation 5.

The fluorescence data were processed by subtracting the values of the blanks from those of the wells that received Calcein-AM. These values were normalized to the fluorescence of the negative control, which was set at 100% cell viability. Finally, the percentage cell viability was plotted against the concentration of PS-MPs using GraphPad Prism software (version 8.0.2), to calculate the IC_{50} by nonlinear regression (log(inhibitor) vs. response – variable slope, four parameters).

3.1.3.4. Imaging Cell Viability Assay: Calcein-PI-Hoechst

Following cell exposure, the treatment medium was replaced with a staining solution (50 μ L) prepared in FluoroBrite DMEM containing Calcein-AM (0.05 μ M), Propidium Iodide (PI; 1.5 μ M; Invitrogen, USA), and Hoechst (1.6 μ M). Cells were incubated for 30 minutes at 37 °C, after which fluorescence images were acquired at 12 sites per well using a 10× objective on the Cytation 5, using the following filter cubes: GFP (green; excitation/emission = 445/510 nm) for Calcein, PI (red; excitation/emission = 531/647 nm) for PI, and DAPI (blue; excitation/emission = 377/447 nm) for Hoechst.

3.1.3.5. Imaging Cell Viability Image Analysis

To assist cell segmentation, nuclear (Hoechst, blue channel) and cytoplasmic (Calcein, green channel) images were combined into image stacks using Fiji software (version 2.7.0)

(Schindelin et al., 2012) via the following path: “Image > Stacks > Images to Stack”. At least five stacks were generated for each cell line. Although segmentation was performed on the green channel (Calcein), the nuclear images were used to guide and improve the accuracy of the segmentation process. The stacks were then loaded into Cellpose software (version 2.2.3) (Stringer et al., 2020), where a custom segmentation model was trained separately for each cell line.

The trained cell segmentation models were subsequently applied to segment cells using analysis pipelines developed in CellProfiler (version 4.2.5) software (Carpenter et al., 2006; Stirling et al., 2021), leveraging the ‘RunCellpose’ plugin (Weisbart et al., 2023). For each cell line, a pipeline was designed in CellProfiler to segment nuclei (blue channel), cells, and cytoplasm (green channel). These pipelines did not require the addition of illumination correction modules (i.e., adjustments for uneven background intensity commonly affecting microscopy images), as the Cytation 5 automatically performs this correction. After segmenting each object (nucleus, cell, and cytoplasm), single-cell object features were extracted into a database using CellProfiler modules. In summary, features related to the size and shape of objects, pixel intensity, and overlap between nuclei stained with Hoechst (blue channel) and PI (red channel) were obtained. Details of the features extracted by CellProfiler are provided in the CellProfiler documentation (https://cellprofiler-manual.s3.amazonaws.com/CellProfiler-4.2.5/help/output_measurements.html).

The numerical values of each feature were exported as ‘.csv’ files and analyzed in Jupyter Notebooks adapted from the Basic Protocol I described in Garcia-Fossa et al., 2023. The data were aggregated by calculating the median per well using Pycytominer’s *aggregate* function (Pycytominer version 0.2.0) (Serrano et al., 2023). The aggregated features were annotated with relevant information, such as cell type, the substance (PS-MPs or Controls) to which the cells were exposed, and its concentration. Normalization of the aggregated features was performed relative to the negative control of each experiment (considered as 100%), with normalization conducted separately for each independent assay plate.

3.1.4. Total Cell Association of PS-MPs Over Time Assay

3.1.4.1. Cell Exposure and Imaging Protocol

For this assay, fluorescent pink polystyrene microplastics (PS-MPs-Fluor; excitation/emission = 550/570 nm) sourced from SpheroTech Inc. (code: FP-0558-2) were primarily used in addition to non-fluorescent PS-MPs. Similar to PS-MPs, PS-MPs-Fluor have an approximate size of 0.5 μm and a negative surface charge.

After 24 hours, cells were exposed in duplicate to PS-MPs-Fluor (100 μ L) at concentrations of 1 mg/L, 0.01 g/L, and 0.1 g/L (that includes relevant human exposure concentration (1 mg/L) and higher concentrations (0.1 and 1 g/L)) in antibiotic-and-serum-free DMEM stabilized with 0.0025% (v/v) Tween 20. Concentrations higher than 0.1 g/L were avoided due to the saturated fluorescence signal emitted by PS-MPs-Fluor, which interfered with image acquisition. As controls, antibiotic-and-serum-free DMEM containing 0.0025% (v/v) Tween 20 (100 μ L) was used as the negative control, and non-fluorescent PS-MPs at 0.1 g/L (100 μ L) served as the fluorescence-negative control. Exposure times were set to 1 h, 3 h, 6 h, 8 h, 12 h, and 24 h at 37°C. Each experiment was conducted on at least three independent days.

Following cell exposure, the treatment medium was replaced with a staining solution (50 μ L) prepared in FluoroBrite DMEM containing Calcein-AM (0.05 μ M) and Hoechst (1.6 μ M) for cell visualization and subsequent segmentation. Cells were incubated for 30 minutes at 37 °C, after which fluorescence images were acquired at 12 sites per well using a 20 \times objective on the Cytation 5, using the following filter cubes: GFP (green; excitation/emission = 445/510 nm) for Calcein, PI (red; excitation/emission = 531/647 nm) for PS-MPs-Fluor, and DAPI (blue; excitation/emission = 377/447 nm) for Hoechst.

3.1.4.2. Total Cell Association Image Analysis

The cell segmentation models used for the set of images obtained in this assay were prepared as described in section 3.1.3.5. After cell segmentation, single-cell features were extracted into a database using CellProfiler modules. In summary, features related to pixel intensity in the PI channel (associated with PS-MPs-Fluor) within the cellular area defined by segmentation were obtained. The numerical values of these features were exported as '.csv' files and analyzed in Jupyter Notebooks. Unlike other analyses, the fluorescence intensity data were not normalized; instead, the raw data were used. This approach was necessary because the negative controls exhibited background fluorescence in the PI channel.

3.1.5. Live Cell Painting Assay

3.1.5.1. Cell Exposure and Imaging Protocol

After 24 hours of plating, cells were exposed in triplicate to PS-MPs (100 μ L) at concentrations ranging from 1 ng/L to 1 g/L (that includes environmental and relevant human exposure concentrations (1 ng/L, 1 μ g/L and 1 mg/L) and higher concentrations (0.01, 0.1, 0.5 and 1 g/L)) for 24 hours at 37 °C. As controls, antibiotic-and-serum-free DMEM containing 0.0025% (v/v) Tween 20 (100 μ L) was used as a negative control, while Bafilomycin A (100 μ L;

2 μM ; Cayman Chemical Company, USA) served as a positive control. Each experiment was conducted on at least three independent days, with a different plate layout used for each experimental run.

Following cell exposure, and as described in the original Live Cell Painting protocol (Garcia-Fossa et al., 2024), the treatment medium was replaced with staining solution (100 μL) prepared in antibiotic-and-serum-free DMEM containing Acridine Orange (AO; 20 μM ; Sigma-Aldrich, USA). For HepG2 cells, nuclear staining with Hoechst (1.6 μM) was performed to facilitate subsequent cell segmentation (as the nuclear images were combined into stacks with the cell images, enabling single-cell identification, which was not possible using only the cell/cytoplasm images for this cell line). After 10 minutes at 37 °C, the AO solution was replaced with FluoroBrite DMEM (100 μL). Fluorescence images were acquired at 12 sites per well using a 20 \times objective on the Cytation 5, with the following filter cubes: GFP (green; excitation/emission = 445/510 nm) and PI (red; excitation/emission = 531/647 nm) for AO, and DAPI (blue; excitation/emission = 377/447 nm) for Hoechst.

3.1.5.2. *Live Cell Painting Image Analysis*

To perform cell segmentation, stacks combining nuclear images (Hoechst; blue channel) and cellular images (AO; green channel) were created only for HepG2 cells, following the same protocol described in section 3.1.3.5. For Huh7 cells, the green AO channel alone was sufficient to train the cell segmentation model in Cellpose, as the AO staining in the green channel clearly delineated cellular compartments (nucleus and cytoplasm) for these cells. Since Hoechst staining was not used for Huh7 cells, a nuclear segmentation model in Cellpose was created using the green AO channel images to facilitate nuclear segmentation in CellProfiler.

For each cell line, a pipeline was developed in CellProfiler to segment nuclei (Hoechst, blue channel for HepG2, using the “IdentifyPrimaryObjects” module, and AO-green channel for Huh7, using the previously created nuclear segmentation model in Cellpose loaded into the ‘RunCellpose’ plugin), nucleoli (AO-green channel), cells (AO-green channel, using the previously trained cell segmentation model loaded into the ‘RunCellpose’ plugin for both cell lines), and cytoplasm (AO-green channel).

After segmenting each object (i.e., nucleus, nucleolus, cell, cytoplasm), single-cell object features were extracted into a database using CellProfiler modules. These features included the object size and shape, pixel intensity, texture, the overlap between the green and red AO channels, and the number of adjacent neighboring cells (the latter specific to HepG2). The numerical values for each feature were then exported as ‘.csv’ files for further analysis.

3.1.5.3. Phenotypic Profiling

The '.csv' files were processed in Jupyter Notebooks following the Basic Protocol I described in Garcia-Fossa et al., 2023. As described in section 3.1.3.5., data were aggregated by calculating the median per well using Pycytominer, and the aggregated features were annotated with relevant information. However, as outlined in the Basic Protocol I and differing from section 3.1.3.5., for profiling, the normalization of aggregated and annotated features relative to the negative control was performed using RobustMAD (Median Absolute Deviation), which is less sensitive to outliers compared to standard deviation. The normalized feature was calculated as: $RobustMAD = (x - median)/MAD$, where x is the feature value.

After normalization, feature selection was performed using Pycytominer's *feature_select* function (Pycytominer version 0.2.0), which excluded features with low variance, high correlation (greater than 90%), more than 5% missing data (Not Available, NA), and outliers (values exceeding 500) (Garcia-Fossa et al., 2023). A '.csv' file containing the hundreds of selected features was then generated.

To visualize and interpret profiles in a reduced-dimensional space, Linear Discriminant Analysis (LDA) with five components was applied to the selected features file using the *LinearDiscriminantAnalysis* function from the *sklearn.discriminant_analysis* package (scikit-learn version 1.1.2). Vectors were plotted for the top ten features contributing the most to the LDA (i.e., those with the highest variance in the data) and the top fifty features contributing the most to each of the five components, to assess features importance.

Next, to identify potential clusters among PS-MPs treatments and the negative control, the Elbow Method and Silhouette Method were applied to determine the optimal number of clusters, followed by clustering using K-means via the *KMeans* function from *sklearn.cluster* (scikit-learn version 1.1.2). The quality of clustering was evaluated using a confusion matrix generated with the *confusion_matrix* function from *sklearn.metrics* (scikit-learn version 1.1.2).

After identifying clusters, i.e., PS-MPs concentrations that differed from the negative control, an additional method was applied to identify important and biologically interpretable features, as most features extracted by CellProfiler are challenging to interpret biologically (e.g., Zernike shape features, Spatial Moment and Hu Moment features, among others). For this, the marker selection tool in the online software Morpheus (<https://software.broadinstitute.org/morpheus/>) (Broad Institute, 2024) was used to perform t-tests comparing the negative control with PS-MPs concentrations grouped into clusters distinct from the negative control.

Finally, the most important features selected through LDA and Morpheus were plotted as

boxplots using the *create_boxplot* function from the *Plotly Express library* (plotly version 5.24.0).

3.1.6. Statistical Analyses

Statistical analyses were performed to compare the negative control with PS-MPs concentrations and positive controls using the Kruskal-Wallis test. For the MTT and Calcein-AM viability assays (sections 3.1.3.2. and 3.1.3.3.), these analyses were carried out using GraphPad Prism software (version 8.0.2), with the Kruskal-Wallis test followed by Dunn's multiple comparisons test. For the remaining assays, statistical analyses were conducted using the *perform_kruskal_bonferroni* function, which integrates the *scipy.stats.kruskal* module (*scipy* version 1.8.1) and the *statsmodels.stats.multicomp.MultiComparison* module (*statsmodels* version 0.14.3), i.e. the Kruskal-Wallis test was followed by Bonferroni post hoc testing. Detailed information on each statistical test is provided in the corresponding figure captions. In general, p-values were considered significant when indicated by an asterisk (*: $p \leq 0.05$).

3.1.7. Data and Analysis Availability

The raw images, cell segmentation models trained using Cellpose (version 2.2.3), the image processing and feature extraction pipelines developed in CellProfiler (version 4.2.5), as well as the Jupyter Notebook (Python version 3.9.20) templates used for: normalization, aggregation, annotation, and feature selection; LDA, feature importance identification, clustering (Elbow Method, Silhouette Method, and K-means), and confusion matrix analysis; and performing Kruskal-Wallis statistical analysis with Bonferroni post hoc testing and plotting individual features as boxplots, have all been uploaded to the Research Data Repository of Unicamp (REDU), and are available at the following link: <https://doi.org/10.25824/redu/2BRSM6>.

3.2. Results

3.2.1. High concentrations of PS-MPs showed a trend toward increased cell viability, as determined by MTT and Calcein-AM assay

Initially, we sought to investigate the cytotoxic profile of PS-MPs in Huh7 and HepG2 hepatocellular carcinoma cells using orthogonal methods: MTT and Calcein-AM assays (Fig. 9). While the MTT assay measures cell viability based on the functional activity of mitochondrial dehydrogenases that convert MTT into formazan (a purple compound) (Mosmann, 1983), the Calcein-AM assay evaluates cell viability by assessing cytoplasmic esterase activity, which converts Calcein-AM into Calcein (a green fluorescent compound) (Bratosin et al., 2005). We

used exposure concentrations ranging from 1 ng/L to 1 g/L of PS-MPs, with a 24-hour exposure time. The resulting cell viabilities from our experiments are represented by non-linear regression models, plotted with five points corresponding to the five treatment concentrations using GraphPad Prism 8.0.2 software (Fig. 9). Both methods show that PS-MPs, at environmental or higher concentrations, did not reduce the viability of Huh7 or HepG2 cells. Triton X-100 (40 μ M) was used as a positive control significantly reducing cell viability in both cell lines (**Supplementary Material 3**). This finding was consistent across all tested treatment concentrations and assays (Fig. 9, items A and B). As a result, it was not possible to determine IC₅₀ values for these particles in these cell lines. Interestingly, we found a dose-dependent tendency towards increased viability in both cell lines and in both tests starting at a concentration of 0.5 g/L PS-MPs.

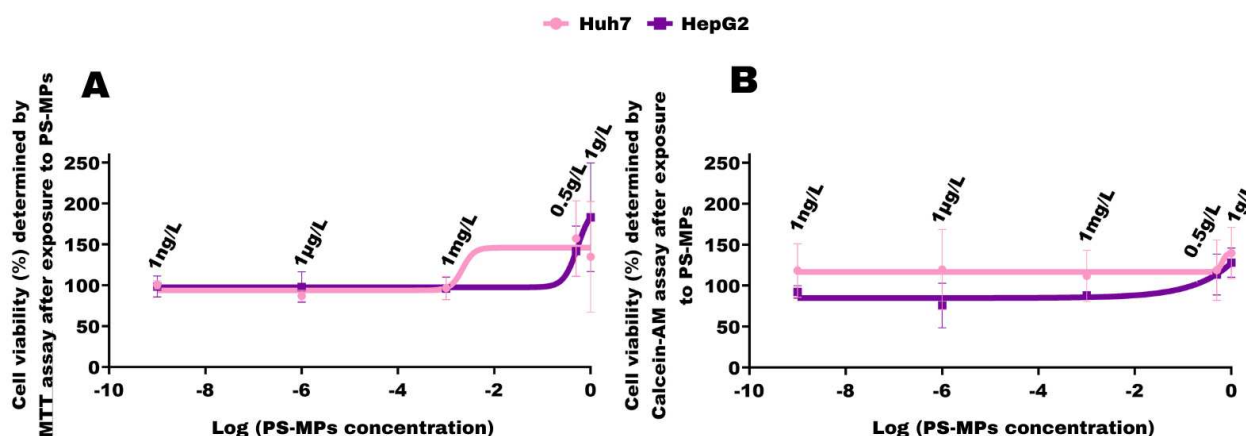


Fig. 9 – Cell viability curves by MTT and Calcein-AM assays of Huh7 and HepG2 cells after exposure to PS-MPs. Huh7 and HepG2 cells were plated at a density of 7,500 and 22,000 cells/well, respectively, in 96-well plates. After 24 hours, cells were treated in triplicate with PS-MPs (1 ng/L, 1 μ g/L, 1 mg/L, 0.5 g/L, and 1 g/L) for 24 hours. Then, cell viability was assessed by MTT or Calcein-AM assays. Cell viability was normalized relative to the non-treated cells. **(A)** Curves obtained by the MTT assay. **(B)** Curves obtained by the Calcein-AM assay. Each nonlinear regression represents triplicates from three independent experiments. Statistical analysis was performed using the Kruskal-Wallis test followed by Dunn's multiple comparisons test using GraphPad Prism software: * $p \leq 0.05$ indicates statistical significance compared to the non-treated group.

3.2.2. Treatment with PS-MPs at High Concentrations Induces Morphological Alterations and a Significant Decrease in the Number of Dead Cells

Because the cellular metabolic activity appeared unaffected by PS-MPs and the trend of increasing cell viability was intriguing, we assessed cell health with a more complex and imaging-based cell viability assay: the Calcein-PI-Hoechst assay. This assay enables the acquisition of fluorescence microscopy images of cells stained with three fluorescent dyes: Calcein, which stains the cytoplasm of viable cells green; Propidium Iodide (PI), which stains the nuclear DNA of dead cells or those with compromised plasma membrane integrity red (hereafter referred to as dead cells); and Hoechst, which stains the nuclear DNA of all cells blue, regardless of viability. This assay enables the visualization of cellular compartments, such as the nucleus and cytoplasm, and the identification of live and dead cells. Consequently, this method provides additional morphological information that cannot be captured by MTT or Calcein-AM assays.

Important features and representative images from the Calcein-PI-Hoechst assay are shown in Fig. 10, while complete panels of Huh7 and HepG2 cells treated with PS-MPs (1 ng/L, 1 µg/L, 1 mg/L, 0.5 g/L, and 1 g/L) are available in **Supplementary Material 4** (Figs. S4.1 and S4.2). Both Huh7 and HepG2 cells displayed a significant increase in the integrated fluorescence intensity of Hoechst in the nucleus (Fig. 10, A and G) and a marked reduction in the percentage of dead cells relative to total cells (Fig. 10, F and L) at the highest PS-MPs concentrations (0.5 and 1 g/L). Additionally, a trend toward increased total cell counts was noted at 0.5 g/L PS-MPs in both cell lines. Distinct differences were observed between the two cell lines. HepG2 cells treated with 1 g/L PS-MPs exhibited an increase in Calcein fluorescence intensity and nuclear area (Fig. 10, H and I), whereas these features remained unchanged in Huh7 cells (Fig. 10, B and C). Conversely, the cytoplasmic area decreased in Huh7 cells treated with 0.5 and 1 g/L PS-MPs (Fig. 10, D), while HepG2 cells showed a significant increase in cytoplasmic area at 1 g/L (Fig. 10, J). Notably, HepG2 cells exhibited morphological changes at 1 g/L PS-MPs, including elongation, increased intercellular spacing, and a loss of their typical clustered growth pattern (Fig. 10, N, row “PS-MPs 1 g/L”). These findings highlight concentration-dependent and cell-line-specific effects of PS-MPs on liver cells, suggesting significant alterations in cellular morphology and function at higher concentrations.

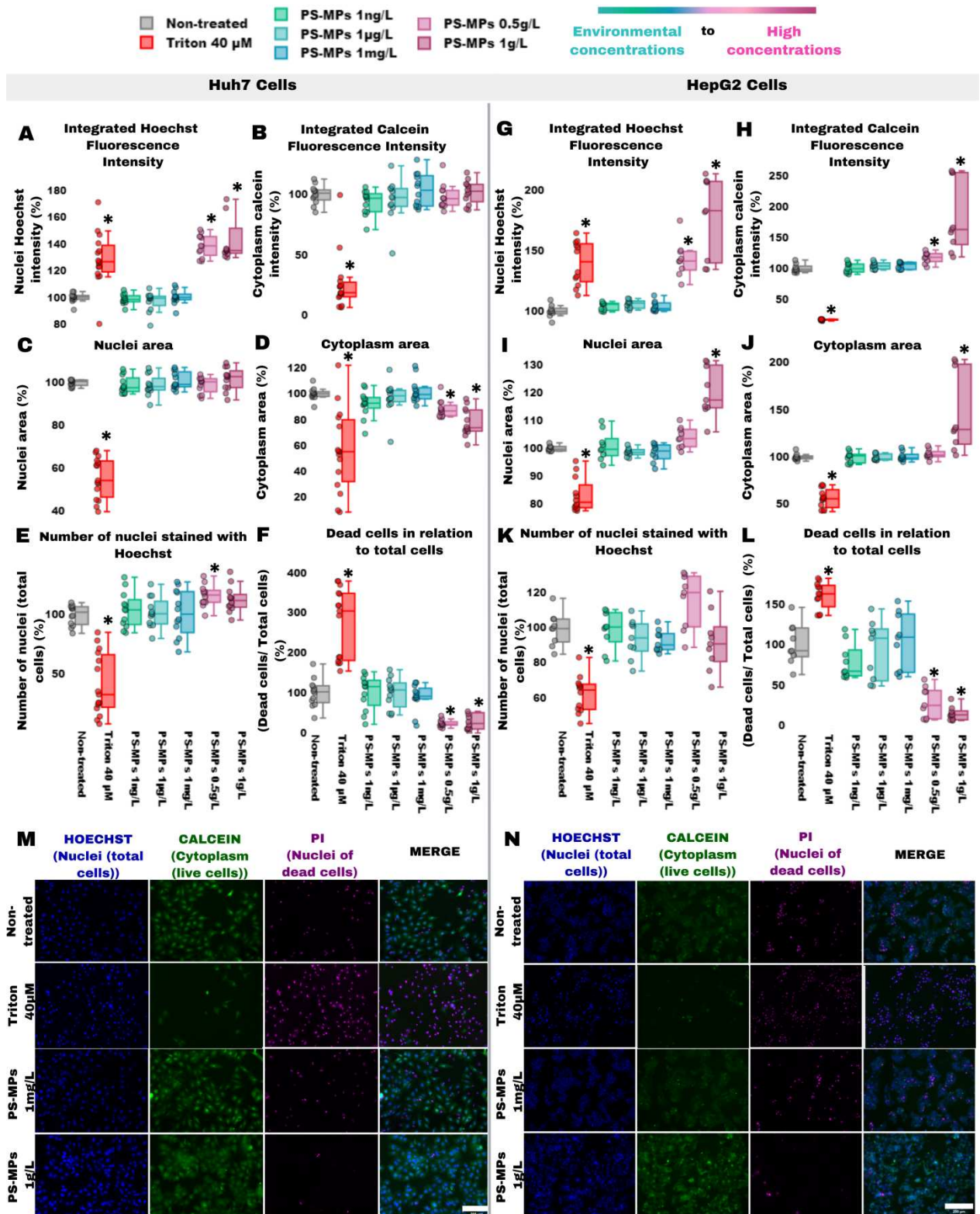


Fig. 10 – Features and fluorescence microscopy images from the Calcein-PI-Hoechst assay of Huh7 and HepG2 cells exposed to PS-MPs. Huh7 and HepG2 cells were plated at

densities of 7,500 and 22,000 cells per well, respectively, in 96-well plates. After 24 hours, cells were treated in triplicate with PS-MPs (1 ng/L, 1 µg/L, 1 mg/L, 0.5 g/L, and 1 g/L) and Triton X-100 (40 µM; positive control) for 24 hours. Images were acquired after staining with Calcein, PI, and Hoechst (Cytation 5, 10× objective). Calcein stains the cytoplasm of viable cells, Hoechst stains the nucleus (DNA) of total cells and PI stains the nucleus (DNA) of cells with compromised plasma membrane integrity (dead cells). The acquired images were analyzed in CellProfiler, where objects (cells, nuclei, and cytoplasm) were segmented, and their features extracted. These features were subsequently aggregated by well and normalized relative to the non-treated group, which was set at 100%. **(A–F)** Plots of fluorescence intensity, area, and object count features extracted from the nuclei and cytoplasm of Huh7 cells. **(G–L)** Plots of fluorescence intensity, area, and object count features extracted from the nuclei and cytoplasm of HepG2 cells. **(M, N)** Representative fluorescence microscopy images of Huh7 (M) and HepG2 (N) cells that were non-treated, treated with the positive control and with PS-MPs at concentrations of 1 mg/L and 1 g/L. The white scale bar in the lower right corner of the (M) and (N) images in fourth column indicates a scale of 200 µm. Experiments were performed in three independent replicates, and each point in the plots represents well-aggregated data. Statistical analysis was performed using the Kruskal-Wallis test followed by Bonferroni post hoc testing in Jupyter Notebook, utilizing the scipy and statsmodels libraries: * $p \leq 0.05$ indicates statistical significance compared to the non-treated group.

We wondered if the marked reduction in dead cells and the trend of increased total cell count observed following treatment with high PS-MPs concentrations (0.5 and 1 g/L) in both hepatocyte models might be due to enhanced cell proliferation. To test this hypothesis, we performed two proliferation assays: the EdU assay and immunofluorescence of the cell proliferation biomarker protein Ki-67 (**Supplementary Material 5**). The EdU assay revealed a statistically significant increase in proliferation for HepG2 cells at PS-MPs concentrations of 1 µg/L, 1 mg/L, and 0.5 g/L compared to the untreated group; however, no changes in proliferation were observed at 1 g/L (Fig. S5, item B). In contrast, EdU results showed no changes in proliferation for Huh7 cells treated with PS-MPs (Fig. S5, item A). Similarly, the Ki-67 immunofluorescence assay showed no significant differences in Ki-67 expression for either cell line at any PS-MPs concentration (Fig. S5, items D and E). Interestingly, despite the observed increase in EdU incorporation for HepG2 cells at intermediate concentrations, both assays suggest that PS-MPs (1 g/L) treatment does not consistently enhance cell proliferation across both hepatocyte models.

Additionally, to specifically investigate the pronounced reduction in dead cells following PS-MPs treatment in both cell lines, a preliminary study was conducted to assess the expression of BAX- α and Akt proteins via Western blot analysis (**Appendix 1**). This was based on reports suggesting that in hepatocyte and other cell types, death triggered by PS-MPs may occur through apoptosis (Lu et al., 2024; Wan et al., 2024; Chen et al., 2023; Yan et al., 2023). BAX- α is a pro-apoptotic protein that works with other BCL-2 family proteins to regulate apoptotic pathways critical for cellular homeostasis (Qian et al., 2022). Akt, on the other hand, is a key protein in cell survival pathways, regulating various processes such as inhibiting pro-apoptotic factors and promoting cell survival through the PI3K/Akt/mTOR signaling axis (Nitulescu et al., 2018). Meaning, both proteins are related in some way to apoptosis.

As we observed a reduction in cell death following treatment with high PS-MPs concentrations, we hypothesized that these conditions might modulate the expression of these proteins, potentially decreasing BAX- α expression to reduce apoptosis or increasing Akt expression to enhance cell survival. However, our preliminary study revealed no significant changes in BAX- α or Akt expression in Huh7 cells treated with PS-MPs (Fig. AP1, items A–H). In HepG2 cells, a trend toward decreased expression of both proteins was observed at PS-MPs concentrations of 0.01 g/L and 1 g/L (Fig. AP1, items I–P), although this was not statistically significant.

3.2.3. Total Cell Association of PS-MPs Increases Over Time

To better understand the effects of PS-MPs on Huh7 and HepG2 cells, we performed a total cell association of PS-MPs assay using epifluorescence microscopy to investigate the interaction dynamics of PS-MPs with these two hepatocyte models over time. This analysis is crucial to determining over time whether the morphological changes induced by PS-MPs are driven by extracellular or intracellular interactions. For this experiment, we incubate Huh7 and HepG2 cells with fluorescently labeled polystyrene microplastics (PS-MPs-Fluor), designed to match the physicochemical and biological properties of non-labeled PS-MPs (**Supplementary Material 6**). Cells were exposed to human-relevant concentration (1 mg/L) and higher concentrations (0.01 and 0.1 g/L). Additionally, non-fluorescent PS-MPs (0.1 g/L) served as a negative control to validate fluorescence signal. Exposure times included 1 h, 3 h, 6 h, 8 h, 12 h, and 24 h. The graphs of fluorescence intensity over time of PS-MPs-Fluor associated with the cells are presented in Fig. 11. Detailed panels of Huh7 and HepG2 cells incubated with PS-MPs across all exposure conditions is provided in **Supplementary Material 7 (Figs. S7.1–S7.12)**.

Both cell lines exhibited a time-dependent interaction with PS-MPs-Fluor at all tested concentrations. At higher concentrations (0.01 g/L and 0.1 g/L), significant accumulation of PS-MPs-Fluor in cells was already observed after 1 hour of incubation, progressively increasing up to 24 hours. Notably, Huh7 cells showed higher levels of interaction with PS-MPs-Fluor compared to HepG2 cells at all time points. This likely reflects the distinct growth patterns of the two cell lines: Huh7 cells grow as individual cells, resulting in a larger surface area for interaction with PS-MPs, whereas HepG2 cells grow in clusters, reducing the surface area available for interaction with dispersed PS-MPs in the medium. Additionally, the distribution of PS-MPs differed between the cell lines: Huh7 cells exhibited a typical perinuclear accumulation of PS-MPs, while HepG2 cells displayed a more peripheral localization, likely related to their islet-like growth pattern. To validate the data obtained by epifluorescence microscopy, confocal microscopy was performed and the results confirmed the observed internalization pattern and intracellular distribution in both cell lines (**Supplementary Material 8**). These findings suggest the presence of a concentration threshold required to trigger significant internalization of PS-MPs, which correlates with the observed differences in the Calcein-PI-Hoechst assay under similar experimental conditions, as cellular alterations were only observed at the highest PS-MPs concentrations (0.5 and 1 g/L; Fig.10).

Furthermore, confocal microscopy images of HepG2 cells revealed individual cells detached from the clusters, with the entire circumference of the plasma membrane densely occupied by PS-MPs-Fluor, as shown in the first row of the panel in Fig. S8. This observation suggests that the accumulation of PS-MPs-Fluor near the plasma membrane may impair cell-cell communication and junctions, causing cells located at the periphery of the clusters to detach over time as internalization increases.

Additionally, confirmation of the internalization of PS-MPs by Huh7 and HepG2 cells through confocal microscopy may explain the changes in cell size observed in the Calcein-PI-Hoechst assay (Fig. 10). Previous studies have demonstrated that mammalian cells can internalize MPs through endocytosis (Ding et al., 2021; Liu et al., 2021; Zhao et al., 2011), a process in which portions of the plasma membrane form endocytic vesicles. In Huh7 cells, the quantity of internalized PS-MPs at 0.1 g/L is higher than that observed in HepG2 cells, and this amount tends to increase at concentrations of 0.5 and 1 g/L (the concentrations used in the Calcein-PI-Hoechst assay), potentially explaining the morphological changes observed. As shown in Fig. 10, Huh7 cells decrease in size at these concentrations (0.5 and 1 g/L), likely due to the intense utilization of the plasma membrane by the endocytic mechanism, which may lead to cell shrinkage, even as PS-MPs occupy space within the cells. In contrast, HepG2 cells

exhibit an increase in size, which could result from a lower degree of particle internalization, meaning less plasma membrane is used for endocytosis. Consequently, the space occupied by PS-MPs at 0.5 and 1 g/L in HepG2 cells, as well as the observed cellular disaggregation, may contribute to the increase in HepG2 cell size.

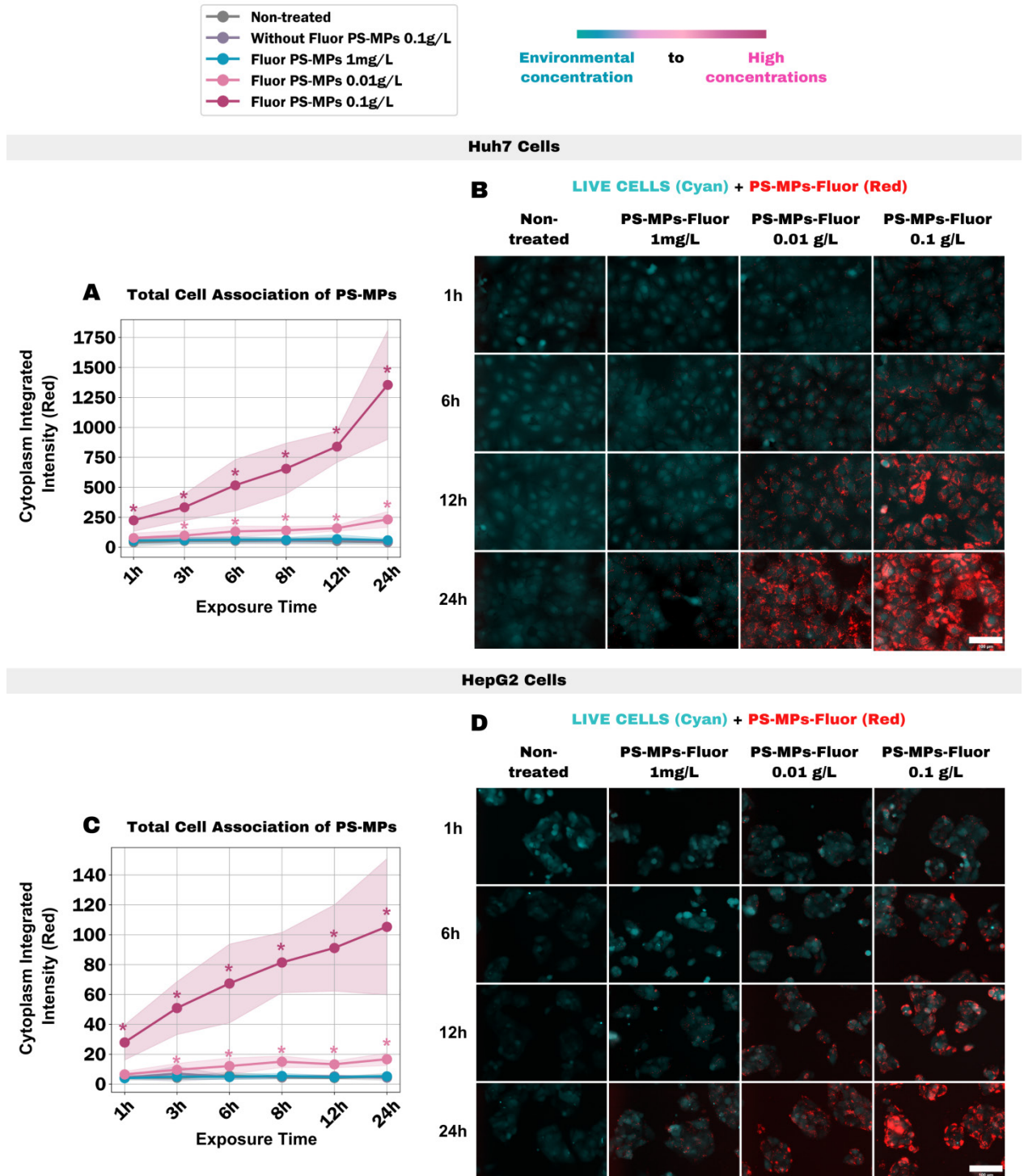


Fig. 11 – Total Cell Association (Huh7 and HepG2) of fluorescent PS-MPs (PS-MPs-Fluor).

Huh7 and HepG2 cells were plated at densities of 7,500 and 22,000 cells per well, respectively, in 96-well plates. After 24 hours, cells were treated in duplicate with PS-MPs-Fluor (1 mg/L, 0.01 g/L, and 0.1 g/L) and non-fluorescent PS-MPs (0.1 g/L) for 1, 3, 6, 8, 12, and 24 hours. Images were acquired following Calcein staining of live cells (Cytation 5, 20× objective) to visualize the entire cell area. The images were analyzed in CellProfiler, where the cytoplasm was segmented, and integrated red fluorescence intensity features (emitted by PS-MPs-Fluor) within the cytoplasmic region were extracted. These features were aggregated per well and plotted without normalization. **(A, C)** Curves of the integrated red fluorescence intensity (emitted by PS-MPs-Fluor) associated with Huh7 (A) and HepG2 (C) cells over time. **(B, D)** Representative fluorescence microscopy images of Huh7 (B) and HepG2 (D) cells that were non-treated and treated with PS-MPs-Fluor (1 mg/L, 0.01 g/L, and 0.1 g/L) for 1, 6, 12, and 24 hours. The white scale bar in the lower right corner of the (M) and (N) images in the fourth column indicates a scale of 100 μ m. Experiments were conducted in three independent replicates, and each point in the plots represents aggregated data per well. Statistical analysis was performed using the Kruskal-Wallis test followed by Bonferroni post hoc testing in Jupyter Notebook, utilizing the scipy and statsmodels libraries: * $p \leq 0.05$ indicates statistical significance compared to the non-treated group.

3.2.4. Treatment with PS-MPs at High Concentrations Increased the Amount of Acidic Vesicles in Huh7 Cells and Decreased Cell-Cell Adhesion in HepG2 Cells

Having established that PS-MPs are internalized by both Huh7 and HepG2 cells without affecting cell viability, we wanted to investigate their broader cellular effects. To address this issue, we used the Live Cell Painting assay (Garcia-Fossa et al., 2024), a phenotypic analysis to assess possible changes in cell morphology, function and behavior. Live Cell Painting particularly evaluates, among other things, the acidic vesicles involved in the endocytic pathway and intracellular processing of PS-MPs (Ding et al., 2021; Liu et al., 2021), also subcellular compartments such as nucleoli, nucleus and cytoplasm. Cells were treated with PS-MPs at a concentration range of 1 ng/L to 1 g/L (environmentally up to higher concentrations) for 24 hours. Representative images in larger size from the Live Cell Painting assay after treatment of Huh7 and HepG2 cells with all concentrations (1 ng/L, 1 μ g/L, 1 mg/L, 0.01 g/L, 0.1 g/L, 0.5 g/L, and 1 g/L) of PS-MPs can be found in **Supplementary Material 9 (Figs. S9.1 and S9.2)**.

In these images, we used Cellpose and CellProfiler to extract morphological features of single cells, such as fluorescence signal intensity, staining texture, number of objects,

neighboring objects, object size, etc. Following Basic Protocol I (Garcia-Fossa et al., 2023), we selected the features with the highest data variance and then performed dimensionality reduction analysis with LDA. LDA was applied to facilitate identifying cellular profiles generated by PS-MPs treatments (distinct from the non-treated group profile) and to visualizing the top 10 features contributing to data clustering, represented by ten vectors (Fig. 12 and Fig. 14, item A). The top ten features representing these vectors are plotted in **Supplementary Material 9 (Figs. S9.3 and S9.4)**.

We then performed clustering of these profile groups using K-means. Most of the high-variance features were biologically difficult to interpret (e.g., Zernike shape features, Spatial and Hu Moment features). Thus, LDA was used to list the fifty most important features for each of its five components. From this list, we selected features that are biologically clear and easier to interpret. Additionally, the online software Morpheus (Broad Institute, 2024) was used for this purpose, through which marker selection (t-test) was performed between the non-treated group and the groups treated with the highest PS-MPs concentrations (0.5 and 1 g/L), seeking features that varied compared to the non-treated group and were clearly biologically interpretable. As expected, we obtained distinct cellular phenotypic profiles between the non-treated groups and the high-concentration PS-MPs-treated groups, as well as differences between the two hepatocyte models.

For Huh7, two cellular phenotypic profiles were identified (Fig. 12, items A and B). Cluster 0 grouped non-treated cells (0 g/L PS-MPs) with cells treated with PS-MPs at 1 ng/L, 1 µg/L, 1 mg/L, 0.01 g/L, and 0.1 g/L, indicating no significant morphological changes at these concentrations compared to the non-treated group. Cluster 1 exclusively grouped cells treated with the highest PS-MPs concentrations (0.5 and 1 g/L), indicating similar morphological changes at these concentrations, distinct from the non-treated group. The primary change observed in Huh7 cells within Cluster 1 was a significant increase in the quantity and size of acidic vesicles, which is evident in Fig. 12, item E, and accompanied by increased AO fluorescence intensity in the red channel (AOPI) (Fig. 13, item D). This increase in acidic vesicles may be associated with the high internalization of PS-MPs at higher concentrations, as noted in Total Cell Association assay (Section 3.2.3.).

Additional changes in Huh7 cells grouped in Cluster 1 are shown in the plots in Fig. 13. These include a decrease in AO intensity in the green wavelength within the nucleus (Fig. 13, item A), which altered the correlation of green and red AO staining in this compartment (Fig. 13, item F). This AO staining pattern alteration may indicate cellular stress (Garcia-Fossa et al.,

2024). Changes in granularity and staining texture were also observed (Fig. 13, items E and G), potentially related to the physical impact of PS-MPs internalization.

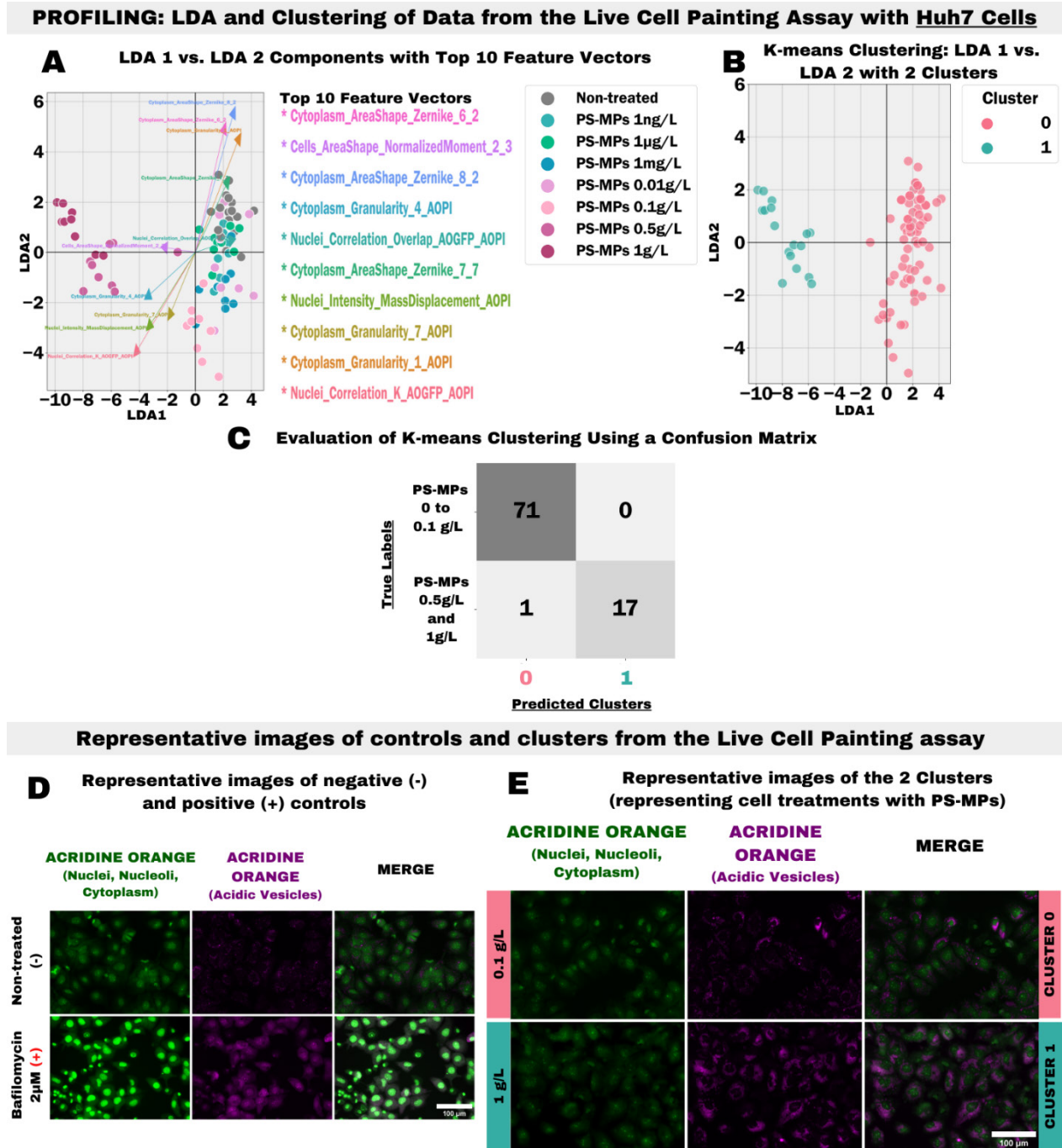


Fig. 12 – Phenotypic Profiling of Huh7 cells after treatment with PS-MPs using the Live Cell Painting assay. Huh7 cells were plated at a density of 7,500 cells per well in 96-well plates. After 24 hours, cells were treated in triplicate with PS-MPs (1 ng/L, 1 µg/L, 1 mg/L, 0.5 g/L, and 1 g/L) and Bafilomycin A1 (2 µM; positive control) for 24 hours. Images were acquired

after staining with Acridine Orange (AO) (Cytation 5, 20× objective). AO stains nuclear and cytoplasmic RNA in green, enabling visualization of the nucleus, nucleoli, and cytoplasm, while acidic vesicles are stained in red (in images, represented in magenta to a colorblind-friendly palette). The acquired images were analyzed using CellProfiler, where objects (cells, nuclei, nucleoli, and cytoplasm) were segmented, and their features extracted. These features were subsequently aggregated by well, normalized relative to the non-treated group, and selected using PyCytominer. **(A)** LDA was applied for dimensionality reduction and visualization, with vectors representing the 10 features contributing most to group separation plotted. **(B)** K-means clustering grouped treatments based on similar feature variances. **(C)** A confusion matrix validated the clusters obtained by K-means. **(D)** Representative fluorescence microscopy images of Huh7 cells that were non-treated (negative control) and treated with the positive control (Bafilomycin, 2 μ M). **(E)** Representative fluorescence microscopy images of each cluster obtained from the Huh7 phenotypic profiling, represented by treatments with PS-MPs at 0.1 g/L and 1 g/L. The white scale bar in the lower right corner of the (D) and (E) images in the third column indicates a scale of 100 μ m. Experiments were performed in three independent replicates, and each point in the plots represents well-aggregated data.

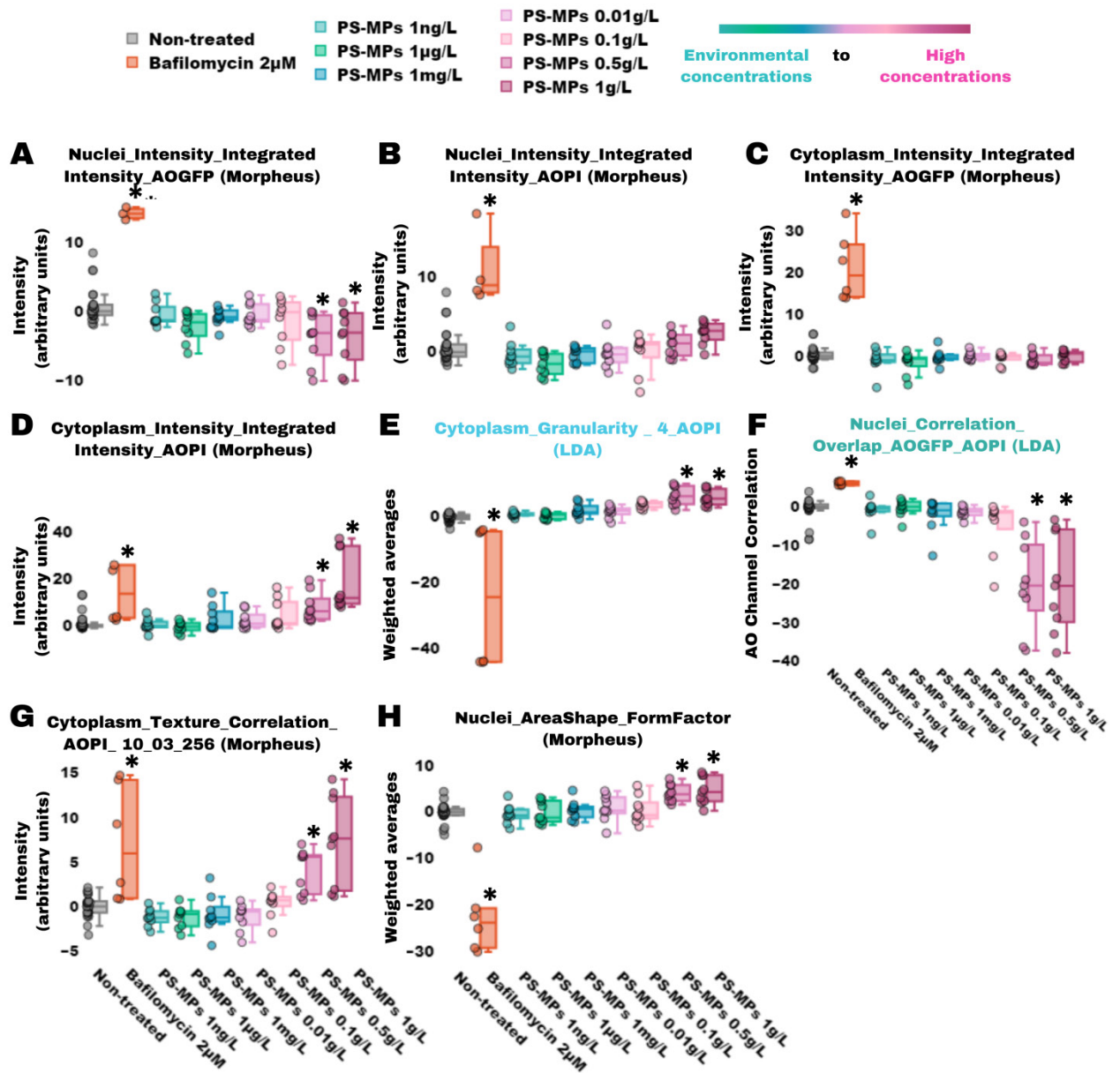


Fig. 13 – Biologically Interpretable Huh7 Cells Features from Live Cell Painting Assay Selected after LDA and Morpheus feature selection. Huh7 cells were plated at a density of 7,500 cells per well in 96-well plates. After 24 hours, cells were treated in triplicate with PS-MPs (1 ng/L, 1 μg/L, 1 mg/L, 0.5 g/L, and 1 g/L) and Bafilomycin A1 (2 μM; positive control) for 24 hours. Images were acquired after staining with Acridine Orange (AO) (Cytation 5, 20× objective). AO stains nuclear and cytoplasmic RNA in green, enabling visualization of the nucleus, nucleoli, and cytoplasm, while acidic vesicles are stained in red. The acquired images were analyzed using CellProfiler, where objects (cells, nuclei, nucleoli, and cytoplasm) were segmented, and their features extracted. These features were subsequently aggregated by well,

normalized relative to the non-treated group, and selected using PyCytominer. LDA analysis was used to list important features for each of the five components, enabling the selection of biologically interpretable features. Morpheus software was also used for this purpose, performing marker selection (t-test) between the non-treated group and groups treated with the highest concentrations of PS-MPs (0.5 and 1 g/L). **(A-H)** Plots of the features of Huh7 cells selected by LDA and Morpheus analysis that were considered clearly biologically interpretable: fluorescence intensity, granularity and texture patterns of AO staining, and nuclear form factor in Huh7 cells. Experiments were performed in three independent replicates, and each point in the plots represents well-aggregated data. Statistical analysis was performed using the Kruskal-Wallis test followed by Bonferroni post hoc testing in Jupyter Notebook, utilizing the `scipy` and `statsmodels` libraries: * $p \leq 0.05$ indicates statistical significance compared to the non-treated group.

Since incubation with PS-MPs led to an increase in acidic vesicles in Huh7 cells, we hypothesized that autophagy might be induced, particularly at higher concentrations, as this vesicle pattern is characteristic of cells undergoing autophagic processes (Volpe et al., 2023). Autophagy could serve as a mechanism for cells to manage internalized PS-MPs, potentially offering temporary protection and delaying cell death. This could explain the reduction in dead cells observed in Calcein-PI-Hoechst assay (Section 3.2.1) for Huh7 cells treated with PS-MPs at 0.5 and 1 g/L. To test this hypothesis, we performed MTT assays in the presence of autophagy inhibitors (3-Methyladenine [3-MA, 5 mM] and Bafilomycin A1 [2 μ M]) (**Appendix 2**). However, no statistically significant reduction in cell viability was observed in the presence of autophagy inhibitors and PS-MPs. Nevertheless, this result should be interpreted with caution, as the three independent assays exhibited significant standard deviations, rendering the findings inconclusive.

As a confirmation step, we performed preliminary immunofluorescence assays for Lysosome-Associated Membrane Protein 1 (LAMP-1) and LC3 (an autophagosome membrane protein) using confocal microscopy. These assays were conducted to investigate whether there was colocalization between these proteins, which would indicate the presence of autophagolysosomes (**Appendix 3**). However, the LC3 antibody displayed non-specific cytoplasmic distribution and was therefore unsuitable for colocalization analysis (Fig. AP3.1). The LAMP-1 antibody functioned properly, highlighting lysosomes and revealing an increase in their number at a PS-MPs concentration of 1 g/L (Fig. AP3.2), showing a pattern of lysosomal stress.

For HepG2, three cellular phenotypic profiles were identified (Fig. 14, items A and B). Cluster 0 grouped non-treated cells (0 g/L PS-MPs) with cells treated with PS-MPs at 1 ng/L, 1 µg/L, 1 mg/L, 0.01 g/L, and 0.1 g/L, similar to Huh7 phenotypic profiling. However, unlike Huh7, HepG2 cells treated at 0.5 and 1 g/L PS-MPs formed two distinct profiles in Clusters 1 and 2, presenting similar morphological changes, but with Cluster 1 showing slightly attenuated changes compared to Cluster 2, likely leading to the treatments being grouped into distinct clusters.

The primary change observed in HepG2 cells in Clusters 1 and 2 was evident cell disaggregation (Fig. 14, item E), as cells lost their characteristic clustered growth. This was further supported by a trend toward decreased adjacent cell contact percentage (Fig. 15, item H). As discussed in Total Cell Association assay (Section 3.2.3.), this disaggregation may result from PS-MPs accumulation near the plasma membrane (Fig. S8), potentially impairing cell–cell interactions. Preliminary investigations into the expression of two cell–cell junction proteins, β -Catenin and ZO-1, expressed in HepG2 cells (Arzumanian et al., 2021), were conducted using immunofluorescence and Western Blot assays (**Appendix 4**). These preliminary investigations revealed no statistically significant changes in the expression of these proteins in cells treated with PS-MPs at a concentration of 1 g/L, although ZO-1 showed a slight trend toward reduced expression in the Western Blot assay.

Additional changes in HepG2 cells grouped in Clusters 1 and 2 are shown in the plots in Fig. 15. Similar to Huh7 cells, HepG2 cells exhibited increased AO intensity in the red wavelength within the cytoplasm, suggesting an increase in acidic vesicles, although less pronounced than in Huh7. Furthermore, there was an increase in AO intensity in the red wavelength within the nucleus (Fig. 15, item B), which may indicate cellular stress (Garcia-Fossa et al., 2024). Changes in granularity and staining texture were also observed (Fig. 15, items E and F), potentially associated with PS-MPs internalization.

PROFILING: LDA and Clustering of Data from the Live Cell Painting Assay with HepG2 Cells

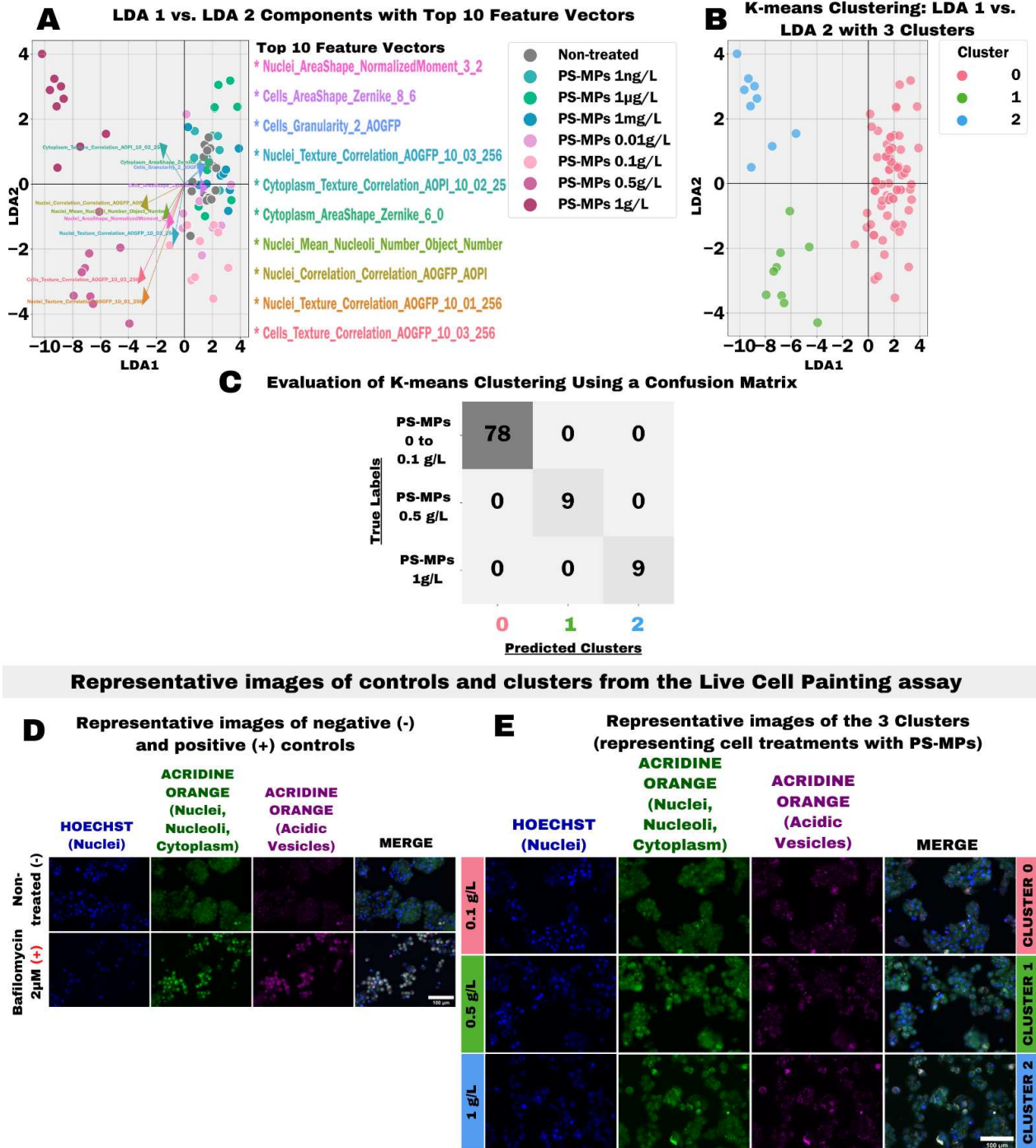


Fig. 14 – Phenotypic Profiling of HepG2 cells after treatment with PS-MPs using the Live Cell Painting assay. HepG2 cells were plated at a density of 22,000 cells per well in 96-well plates. After 24 hours, cells were treated in triplicate with PS-MPs (1 ng/L, 1 µg/L, 1 mg/L, 0.5 g/L, and 1 g/L) and Bafilomycin A1 (2 µM; positive control) for 24 hours. Images were acquired after staining with Acridine Orange (AO) (Cytation 5, 20× objective). AO stains nuclear

and cytoplasmic RNA in green, enabling visualization of the nucleus, nucleoli, and cytoplasm, while acidic vesicles are stained in red (in images, represented in magenta to a colorblind-friendly palette). The acquired images were analyzed using CellProfiler, where objects (cells, nuclei, nucleoli, and cytoplasm) were segmented, and their features extracted. These features were subsequently aggregated by well, normalized relative to the non-treated group, and selected using PyCytominer. **(A)** LDA was applied for dimensionality reduction and visualization, with vectors representing the 10 features contributing most to group separation plotted. **(B)** K-means clustering grouped treatments based on similar feature variances. **(C)** A confusion matrix validated the clusters obtained by K-means. **(D)** Representative fluorescence microscopy images of HepG2 cells that were non-treated (negative control) and treated with the positive control (Bafilomycin, 2 μ M). **(E)** Representative fluorescence microscopy images of each cluster obtained from the HepG2 phenotypic profiling, represented by treatments with PS-MPs at 0.1, 0.5 and 1 g/L. The white scale bar in the lower right corner of the (D) and (E) images in the fourth column indicates a scale of 100 μ m. Experiments were performed in three independent replicates, and each point in the plots represents well-aggregated data.

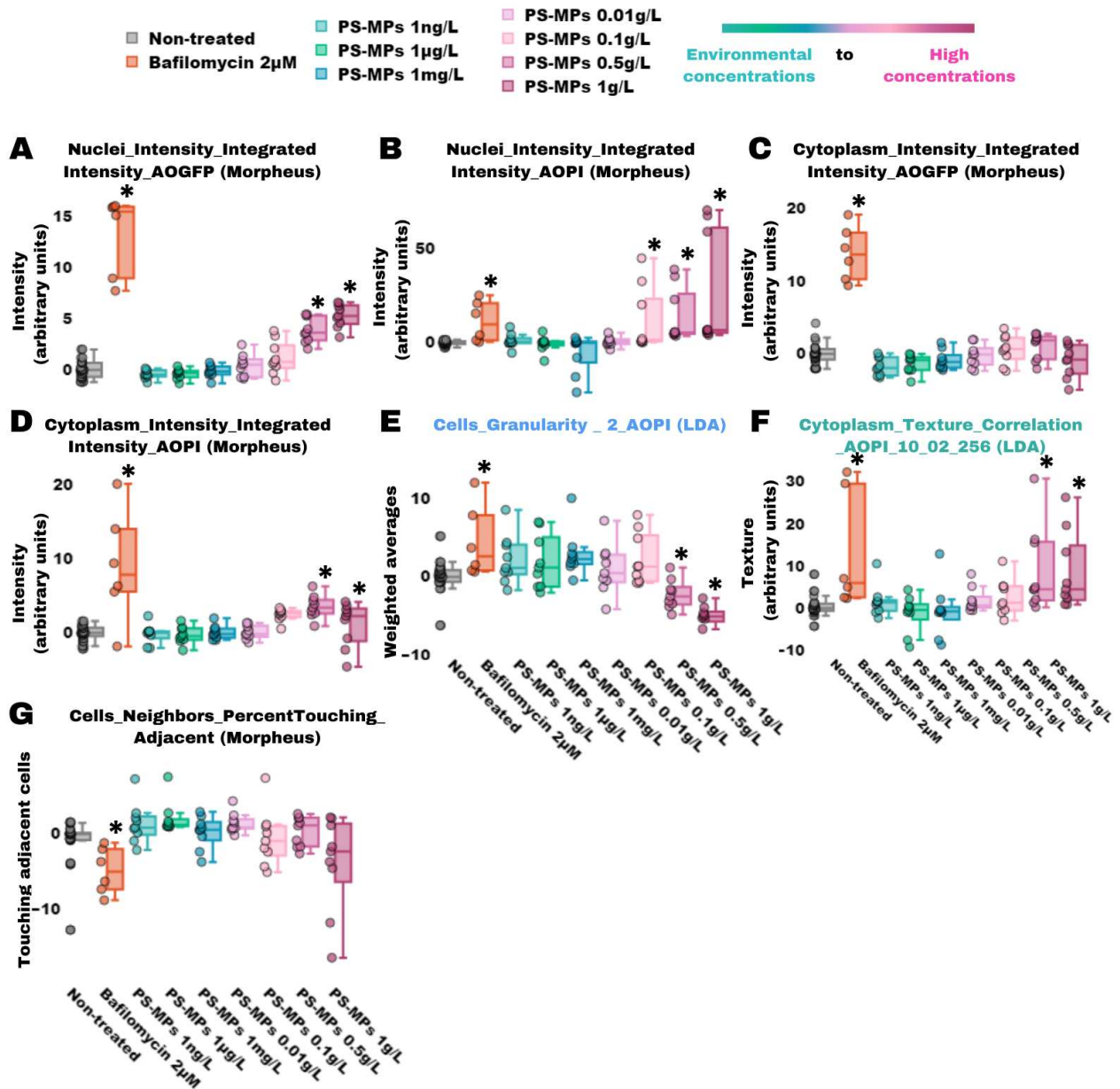


Fig. 15 – Biologically Interpretable HepG2 Cells Features from Live Cell Painting Assay Selected after LDA and Morpheus feature selection. HepG2 cells were plated at a density of 22,000 cells per well in 96-well plates. After 24 hours, cells were treated in triplicate with PS-MPs (1 ng/L, 1 μ g/L, 1 mg/L, 0.5 g/L, and 1 g/L) and Bafilomycin A1 (2 μ M; positive control) for 24 hours. Images were acquired after staining with Acridine Orange (AO) (Cytation 5, 20 \times objective). AO stains nuclear and cytoplasmic RNA in green, enabling visualization of the nucleus, nucleoli, and cytoplasm, while acidic vesicles are stained in red. The acquired images were analyzed using CellProfiler, where objects (cells, nuclei, nucleoli, and cytoplasm) were segmented, and their features extracted. These features were subsequently aggregated by well,

normalized relative to the non-treated group, and selected using PyCytominer. LDA analysis was used to list important features for each of the five components, enabling the selection of biologically interpretable features. Morpheus software was also used for this purpose, performing marker selection (t-test) between the non-treated group and groups treated with the highest concentrations of PS-MPs (0.5 and 1 g/L). **(A-G)** Plots of the features of HepG2 cells selected by LDA and Morpheus analysis that were considered clearly biologically interpretable: fluorescence intensity, granularity and texture patterns of AO staining, number of objects, and percentage of neighboring cells touching. Experiments were performed in three independent replicates, and each point in the plots represents well-aggregated data. Statistical analysis was performed using the Kruskal-Wallis test followed by Bonferroni post hoc testing in Jupyter Notebook, utilizing the scipy and statsmodels libraries: * $p \leq 0.05$ indicates statistical significance compared to the non-treated group.

To complement the Live Cell Painting data, we also performed the Cell Painting assay (which involves cell fixation) (Bray et al., 2016) on Huh7 and HepG2 cells (**Supplementary Material 10**). This assay allows for the visualization of the nucleus, cytoplasm, endoplasmic reticulum, Golgi apparatus, alpha-actin cytoskeleton, and mitochondria of the cells (Fig. S10.1). However, the set of fluorophores used in Cell Painting allowed for high-quality segmentation only in Huh7 cells, making data extraction from HepG2 cells infeasible (Fig. S10.2). The main finding from the Cell Painting assay in Huh7 cells was an increase in MitoTracker integrated fluorescence intensity in the cytoplasm of cells treated with 0.1 g/L PS-MPs (Fig. S10.4, item D), suggesting mitochondrial alterations. Additionally, MitoTracker fluorescence was observed in the nuclei of Huh7 cells treated with 0.1 and 1 g/L PS-MPs (Fig. S10.4, item F). This nuclear fluorescence may indicate mitochondrial integrity compromise, allowing tagged proteins to leak into other cellular compartments, including the nucleus; metabolic or transport alterations; or changes in cell or vesicular permeability due to increased endocytosis or related processes associated with PS-MPs internalization (Ding et al., 2021; Liu et al., 2021; Zhitomirsky et al., 2018).

After the investigations conducted in this study to obtain a broader understanding of the cellular phenotypic alterations triggered by PS-MPs, we performed mechanistic assays focused on detecting cellular changes associated with *in vitro* hepatotoxicity, in assays we designated as HepatotoxPath and Steatosis assays. We utilized a combination of fluorescent cellular dyes that allowed the visualization of parameters commonly affected in *in vitro* hepatotoxicity studies. For HepatotoxPath, the parameters included intracellular calcium ion levels (Holt et al., 2006;

O'Brien et al., 2004), mitochondrial membrane potential (MMP)—considered the most sensitive parameter for predicting human liver damage induced by xenobiotics (Persson et al., 2014; Dykens & Will, 2007)—and lysosomal integrity (Begriche et al., 2011), especially given that PS-MPs can enter cells via endocytosis (Ding et al., 2021; Liu et al., 2021) (**Appendix 5**). To complement the HepatotoxPath mechanistic assay, and considering studies that have reported changes in hepatic lipid metabolism induced by microplastics *in vivo* and *in vitro*, leading to hepatic steatosis (Djouina et al., 2023; Cheng et al., 2022; Zheng et al., 2021; Luo et al., 2019), we investigated whether PS-MPs at environmental or higher concentrations could alter intracellular lipid droplets in Huh7 and HepG2 cells using LipidTOX Stain (to label neutral lipid deposits, such as those found in lipid droplets in the cytoplasm) (**Appendix 6**).

However, probably due to the instability of PS-MPs, which tend to aggregate over time (Supplementary Material 1), and considering that the PS-MPs stock solution had been in use for over a year and a half by the time the HepatotoxPath and Steatosis assays were conducted, some precipitates of PS-MPs at 1 g/L were observed in the fluorescence microscopy images of Huh7 and HepG2 cells treated with PS-MPs at 1 g/L in the RFP channel, where TMRM is detected (MMP marker) in HepatotoxPath assay, and in the GFP channel, where LipidTOX is detected in Steatosis assay, compromising the interpretation of the results. Therefore, these data will not be included in the document to be published but can be viewed in the appendices of this dissertation.

3.3. Supplementary Materials

3.3.1. Supplementary Material 1: Characterization of Polystyrene Microplastics (PS-MPs)

3.3.1.1. Materials and Method

The characterization of PS-MPs was carried out using Dynamic Light Scattering (DLS) to determine their average hydrodynamic diameter and polydispersity index, employing a ZetaSizer Nano ZS 90 (Malvern, UK). Measurements were conducted at 25°C using 10 mm path length polystyrene cuvettes, with a fixed scattering angle of 90°. Zeta potential analysis was performed on the same device, utilizing capillary cells with a 10 mm optical path. The stock suspension (1 g/L) was diluted 1:10 in either ultrapure water or serum-and-antibiotics-free DMEM, and samples were immediately analyzed at a controlled temperature of 37°C. Following this, the same suspensions were incubated at 37°C in a 5% CO₂ atmosphere for 24 hours to assess their stability in both media. After incubation, new measurements were taken. All data were analyzed using GraphPad Prism software (version 7.00).

3.3.1.2. Results and Conclusions

Observing Fig. S1, item A, it is evident that the initial peak (0 h) of PS-MPs suspended in water is centered around 632 nm, and after 24 hours, this value slightly increases to 686.4 nm, a difference of 54 nm. This variation is relatively small, suggesting that PS-MPs are relatively stable in water over time at 37°C. In contrast, in DMEM antibiotic-and-serum-free (Fig. S1, item B), the main size distribution peak of the PS-MPs, initially centered at 1023 nm, shifts to 1620 nm after 24 hours of incubation at 37°C, representing an increase of approximately 600 nm. This increase in average size suggests that PS-MPs undergo an aggregation process over time in the medium. Furthermore, the curve after 24 hours becomes broader and more extended compared to the initial distribution, indicating greater heterogeneity in PS-MP size—a typical behavior of aggregation. The formation of larger aggregates may result from interactions between PS-MPs themselves or with components of the medium.

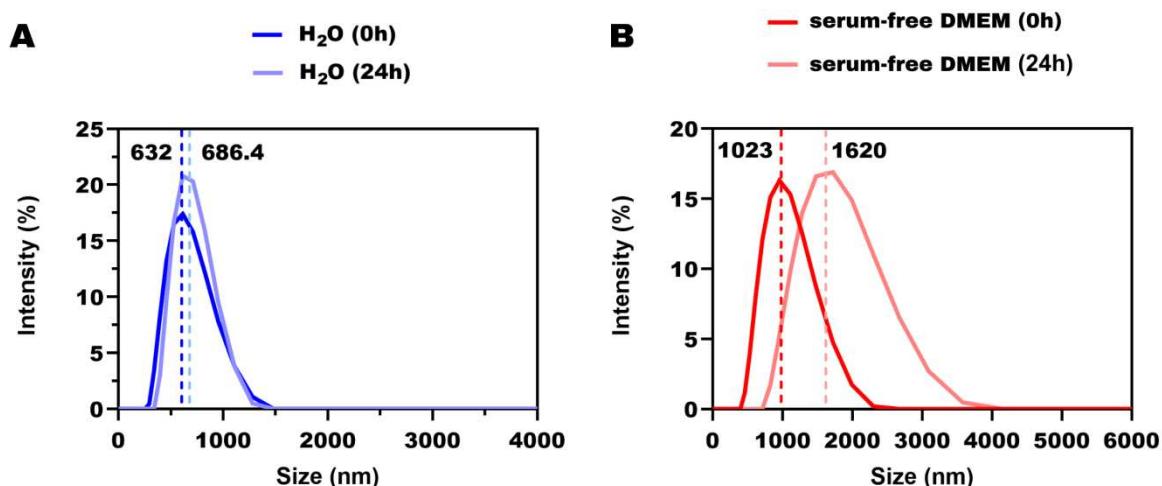


Fig. S1 – DLS analysis of PS-MPs size distribution in (A) ultrapure water (H₂O) and (B) antibiotic-and-serum-free DMEM culture medium at 0 and 24 hours of incubation at 37°C. The Z-average (hydrodynamic diameter) indicates the mean size of the particles.

The zeta potential of PS-MPs in water varied from -27.7 mV to -21.6 mV after 24 hours (Table S1), indicating a slight reduction in electrostatic repulsion, which suggests a tendency toward aggregation, although the suspension remains sufficiently stable, as seen in Fig. S1. In comparison, PS-MPs in DMEM serum-free exhibited a more negative zeta potential, with a smaller variation from -35.4 mV to -34 mV (Table S1). This behavior suggests that while PS-MPs in DMEM serum-free maintain a more stable surface charge, other factors, such as the composition of the medium, are promoting greater aggregation of PS-MPs despite the smaller change in zeta potential.

Table S1 - Hydrodynamic size (Z-average, d.nm), polydispersity index (PDI), and zeta potential values (\pm standard deviation, SD) of PS-MPs in ultrapure water (H₂O) and antibiotic-and-serum-free DMEM medium at 0 and 24 hours at 37°C.

Microparticle and Conditions	Z-average (d.nm) \pm SD	PDI \pm SD	Zeta Potential \pm SD
PS-MPs in H₂O (0 h)	632 \pm 12,7	0,20 \pm 0,05	-27,7 \pm 0,28
PS-MPs in H₂O (24 h)	686.4 \pm 24,88	0,20 \pm 0,03	-21,6 \pm 0,28
PS-MPs in DMEM (0 h)	1023 \pm 44,04	0,27 \pm 0,05	-35.4 \pm 0,78
PS-MPs in DMEM (24 h)	1620 \pm 56,44	0,25 \pm 0,02	-34 \pm 1,22

3.3.2. Supplementary Material 2: Stabilization Tests of PS-MPs in DMEM antibiotic-and-serum-free Medium

The PS-MPs suspensions used in this study has a cloudy/opaque white color (Fig. S2, item A), and as observed in the previous section (Fig. S1, item B), when diluted in antibiotic-and-serum-free DMEM, it becomes unstable, tending to aggregate (Fig. S2, item B), potentially interacting with cells as larger particles. Since the cytotoxicity of microparticles in general, including MPs, is often closely related to their size, it is crucial to maintain control over this parameter (Banerjee et al., 2022). Therefore, before conducting cell exposures, we performed several tests aimed at obtaining more stable PS-MPs dispersions in DMEM.

3.3.2.1. *Materials and Method*

Suspensions of PS-MPs at 0.01 g/L in antibiotic-and-serum-free DMEM were prepared under the following four conditions: **1.** With 0.1% of the surfactant Bovine Serum Albumin (BSA) and 1 hour of ultrasonication; **2.** With 0.1% BSA, 1 hour of ultrasonication, and incubated for 24 hours at 37°C; **3.** Without BSA and 1 hour of ultrasonication; **4.** Without BSA, 1 hour of ultrasonication, and incubated for 24 hours at 37°C. Subsequently, the dilutions were plated in 6-well plates and observed under a phase-contrast microscope (Cytation 5) using a 20× objective, and images were acquired.

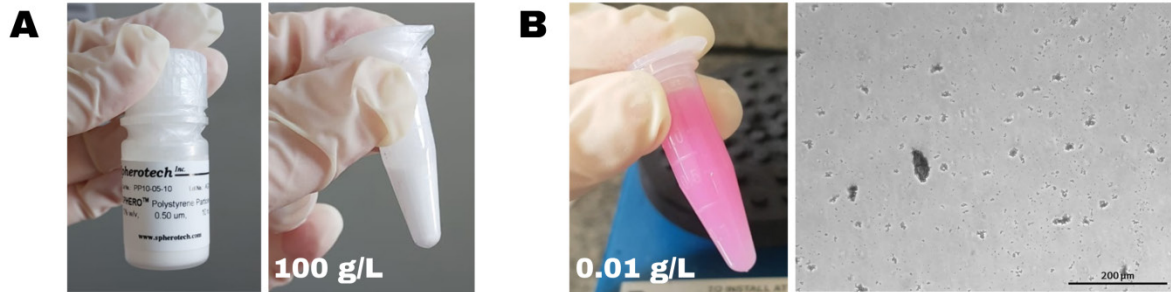
3.3.2.2. *Results and Conclusions*

Condition “1,” with 0.1% BSA and 1 hour of ultrasonication (Fig. S2, item C), resulted in a dispersion with fewer agglomerates compared to Fig. S2, item B, and the agglomerates were smaller in size. Condition “2”, with 0.1% BSA, 1 hour of ultrasonication, and incubation for 24 hours at 37°C (Fig. S2, item D), resulted in a dispersion with a significantly smaller number of agglomerates than condition 1, although some agglomerates were still present. Condition “3,” without BSA and with 1 hour of ultrasonication (Fig. S2, item E), showed the highest number of agglomerates. Finally, condition “4,” without BSA, with 1 hour of ultrasonication, and incubation for 24 hours at 37°C (Fig. S2, item F), was the most effective in preventing PS-MPs clustering.

Therefore, for the preparation of all PS-MPs dilutions used in cell exposures of this study, the procedure from **condition “4” was adopted**. Additionally, to ensure stability at higher concentrations, such as 1 g/L, Tween 20 at 0.0025% (v/v) was added to the DMEM medium (for all PS-MPs concentrations). The use of Tween 20 for stabilizing such particles in culture medium was proposed in the study by Banerjee et al. (2022), which evaluated the cytotoxicity of PS-MPs

in HepG2 cells at concentrations ranging from 0.1 to 100 g/L of PS-MPs without agglomeration issues.

Appearance of PS-MP suspension and agglomerate formation



Preparation of PS-MPs suspension (0.01 g/L) under different conditions in DMEM medium

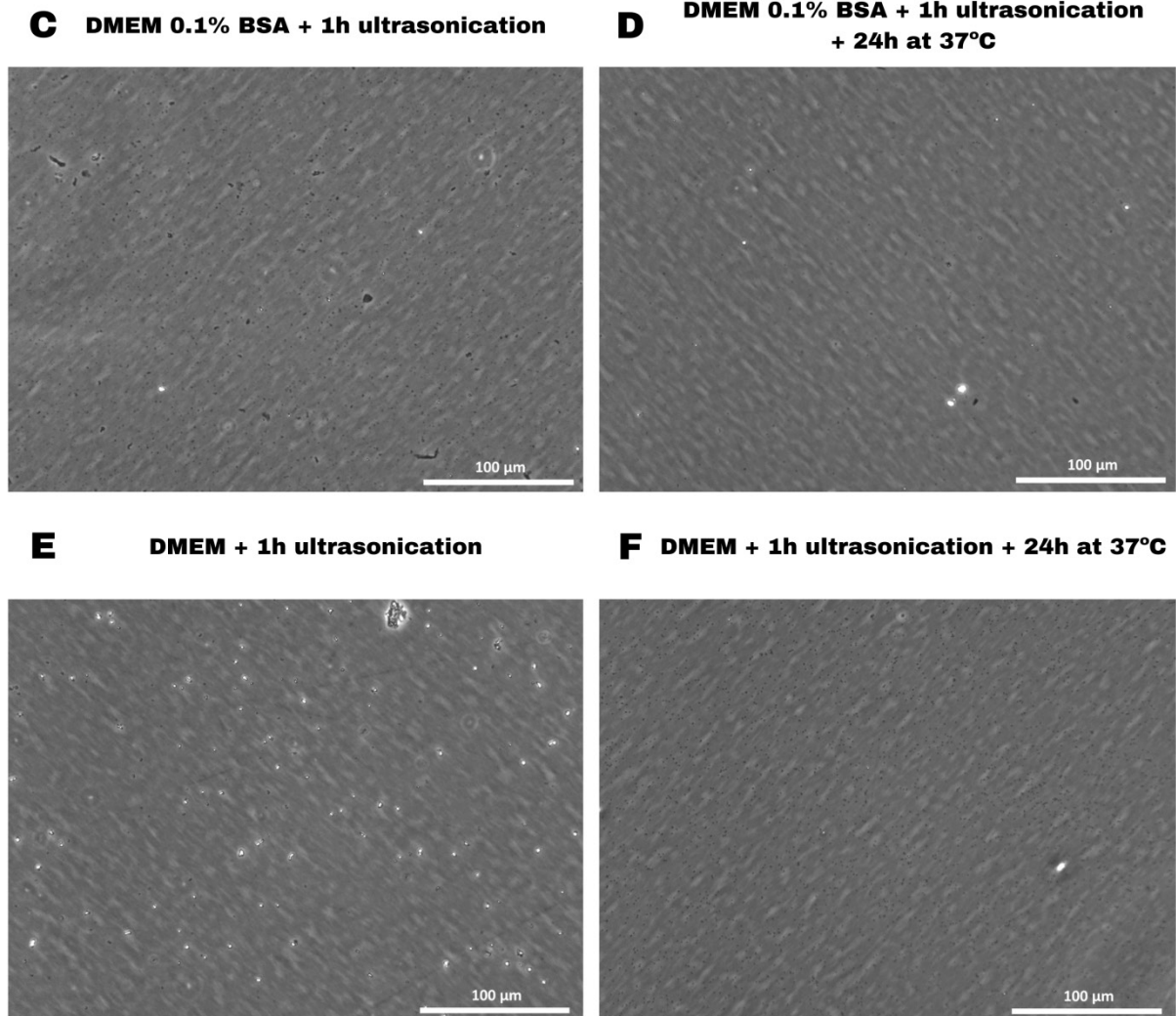


Fig. S2 - Appearance and Stabilization of PS-MP Suspensions in Antibiotic-and-serum-free DMEM Under Different Preparation Conditions.

(A) Appearance of the PS-MPs stock suspension from Spherotech Inc. (code: 'PP10-05-10'), 100 g/L. **(B)** Appearance of the PS-MPs suspension at 0.01 g/L diluted in antibiotic-and-serum-free DMEM, macro and microscopic views (phase contrast microscopy with a 10× objective, scale bar: 200 µm). **(C-F)** Phase contrast microscopy with a 20× objective of PS-MPs dispersions prepared under different conditions in antibiotic-and-serum-free DMEM: **(C)** With 0.1% BSA and 1 hour of ultrasonication; **(D)** With 0.1% BSA, 1 hour of ultrasonication and 24 hours of incubation at 37°C; **(E)** Without BSA and 1 hour of ultrasonication; **(F)** Without BSA, 1 hour of ultrasonication and 24 hours of incubation at 37°C.

3.3.3. ***Supplementary Material 3: Viability of Huh7 and HepG2 Cells Assessed by MTT and Calcein-AM Assays After Exposure to Triton X-100***

3.3.3.1. ***Materials and Method***

The same as described in Section 3.1.3.2, MTT Cell Viability Assay, and Section 3.1.3.3, Calcein-AM Cell Viability Assay, with cells being exposed to Triton X-100 (40 μ M, 100 μ L; Sigma-Aldrich, USA).

3.3.3.2. ***Results and Conclusions***

The exposure of Huh7 and HepG2 cells to the positive control for cellular damage, Triton X-100, as expected, resulted in a significant decrease in cell viability as measured by both the MTT assay (Fig. S3, items A and B) and the Calcein-AM assay (Fig. S3, items C and D). These results demonstrate that our hepatocyte models (Huh7 and HepG2) are responsive to compounds that induce cellular damage.

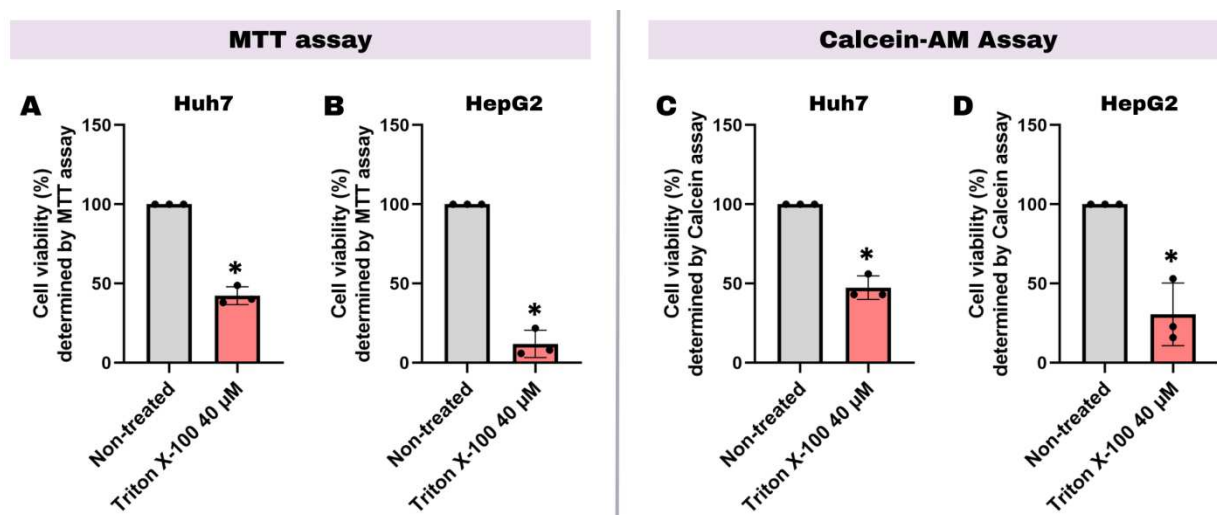


Fig. S3 – Viability of Huh7 and HepG2 Cells Assessed by MTT and Calcein-AM Assays After Exposure to Triton X-100. Huh7 and HepG2 cells were plated at a density of 7,500 and 22,000 cells/well, respectively, in 96-well plates. After 24 hours, cells were treated in triplicate with Triton X-100 (40 μ M) for 24 hours. Then, cell viability was assessed by MTT or Calcein-AM assays. Cell viabilities were calculated relative to the non-treated group, which was considered 100%. **(A)** Cell viabilities obtained by the MTT assay. **(B)** Cell viabilities obtained by the Calcein-AM assay. Statistical analysis was performed using the Kruskal-Wallis test followed by Dunn's

multiple comparisons test using GraphPad Prism software: * $p \leq 0.05$ indicates statistical significance compared to the non-treated group.

3.3.4. Supplementary Material 4: Full representative fluorescence microscopy images of Calcein-PI-Hoechst assay with Huh7 and HepG2 cells

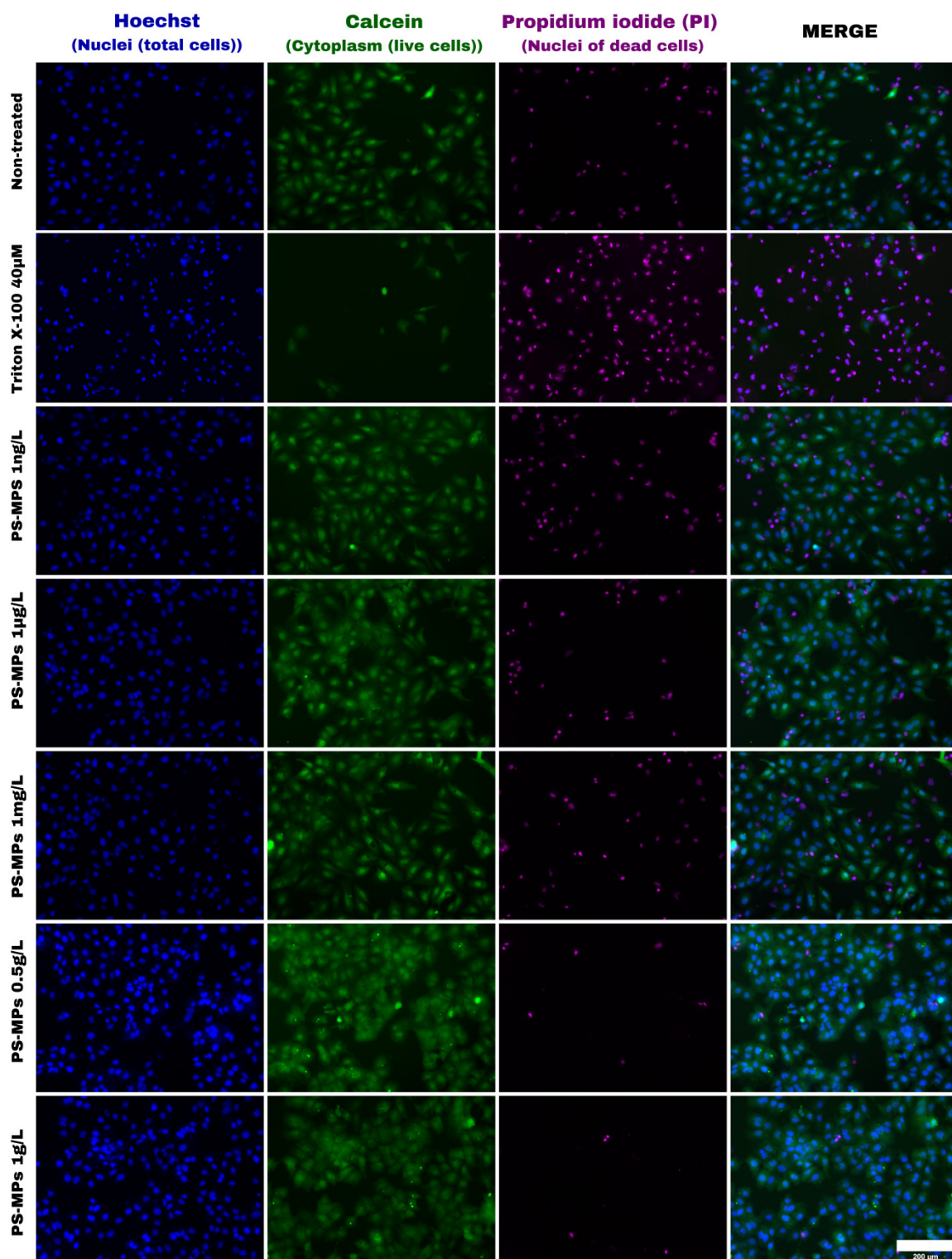


Fig. S4.1 – Representative Fluorescence Microscopy Images from the Calcein-PI-Hoechst Assay of Huh7 Cells Exposed to PS-MPs.

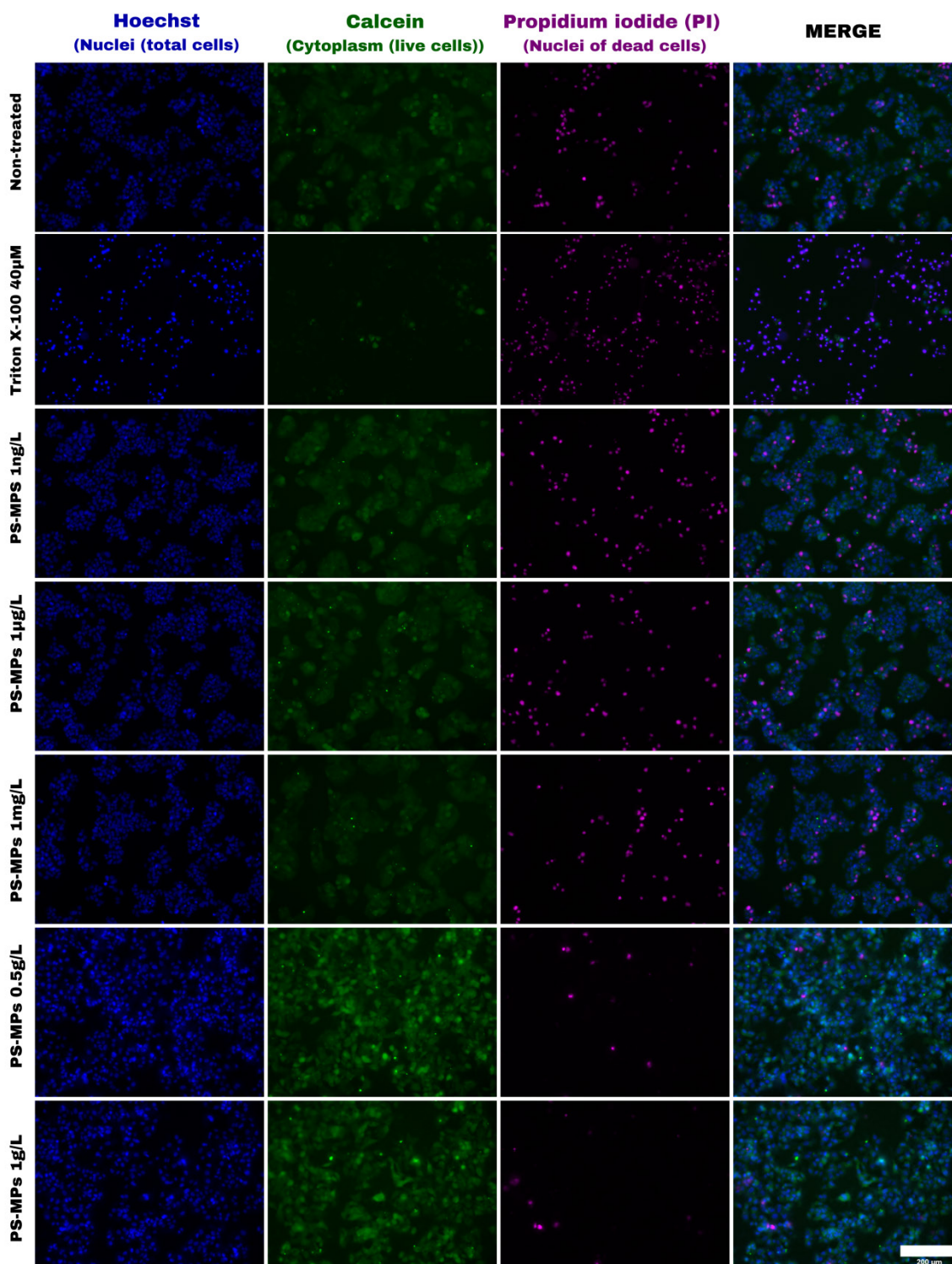


Fig. S4.2 - Representative Fluorescence Microscopy Images From the Calcein-PI-Hoechst Assay of HepG2 Cells Exposed to PS-MPs

Figs. S4.1 and S4.2 description: Huh7 and HepG2 cells were plated at densities of 7,500 and 22,000 cells per well, respectively, in 96-well plates. After 24 hours, cells were treated in

triplicate with PS-MPs (1 ng/L, 1 µg/L, 1 mg/L, 0.5 g/L, and 1 g/L) and Triton X-100 (40 µM; positive control) for 24 hours. Images were acquired after staining with Calcein, PI, and Hoechst (Cytation 5, 10× objective). Calcein stains the cytoplasm of viable cells, Hoechst stains the nucleus (DNA) of total cells and PI stains the nucleus (DNA) of cells with compromised plasma membrane integrity (dead cells). **(S4.1)** Representative fluorescence microscopy images of **Huh7 cells** that were non-treated, treated with the positive control, and treated with PS-MPs (1 ng/L, 1 µg/L, 1 mg/L, 0.5 g/L, and 1 g/L). **(S4.2)** Representative fluorescence microscopy images of **HepG2 cells** that were non-treated, treated with the positive control, and treated with PS-MPs (1 ng/L, 1 µg/L, 1 mg/L, 0.5 g/L, and 1 g/L). The white scale bar in the lower right corner of the images in the fourth column indicates a scale of 200 µm. Experiments were conducted in three independent replicates.

3.3.5. Supplementary Material 5: Cell Proliferation Assays in Huh7 and HepG2 Cells (after exposure to PS-MPs) Using EdU Assay and Ki-67 Protein Immunofluorescence

3.3.5.1. *Materials and Method*

3.3.5.1.1. *Cell Plating and Exposure*

Huh7 and HepG2 cells were plated in 96-well plates at 7,500 and 22,000 cells per well, respectively, and incubated for 24 hours. Next, the cells were exposed in triplicate to PS-MPs (100 μ L) at a concentration range of 1 μ g to 1 g/L. Each experimental replicate was performed on at least three different days.

3.3.5.1.2. *EdU Assay*

The EdU assay was performed using the Click-iT™ Plus EdU Cell Proliferation Kit for Imaging (Invitrogen, #C10420, USA). Immediately after adding PS-MPs to each wells, EdU (10 μ L; 100 μ M) was added. After 24 hours of cell exposure with PS-MPs in the presence of EdU, cells were fixed by replacing the treatment with PFA (100 μ L; 4% w/v). After 20 minutes, the cells were washed with 3% (w/v) BSA in PBS 1 \times , and permeabilized with a permeabilization solution (100 μ L; PBS 1 \times with 0.5% (v/v) Triton X-100) for 20 minutes. Cells were then washed with 3% (w/v) BSA, and stained using the Click-iT Plus detection cocktail (25 μ L; Reaction Buffer 1 \times , Copper Protectant, Alexa Fluor 647 picolyl azide, and Buffer Additive 1 \times) for 30 minutes. Next, cells were stained with Hoechst (50 μ L; 1.6 μ M) in PBS for 30 minutes. Fluorescence microscopy images were acquired on the Cytation 5 using the 10 \times objective and the following filter cubes: DAPI (blue; excitation/emission = 377/447 nm) for Hoechst and CY5 (deep red; excitation/emission = 628/685 nm) for Alexa Fluor 647 picolyl azide, which labels EdU incorporation into DNA.

3.3.5.1.3. *Detection of Ki-67 Protein Expression by Immunofluorescence*

After 24 hours of cell exposure, cells were fixed by replacing the treatment with PFA (100 μ L; 4% w/v). After 20 minutes, the wells were washed with PBS 1 \times (100 μ L), and the medium was replaced with a Blocking Buffer (100 μ L) containing PBS 1 \times with 5% (v/v) goat serum and 0.3% (v/v) Triton X-100. After 1 hour, the cells were washed with PBS 1 \times (100 μ L) and the cells were incubated at 37°C with the primary antibody solution Anti Ki-67 Mouse mAb (25 μ L; 5 μ L/mL; Cell Signaling #9449, USA) in PBS 1 \times . After 1 hour, cells were washed with PBS 1 \times (100 μ L) and stained with secondary antibody solution Alexa Fluor 647 goat anti-mouse IgG (25 μ L; 1 μ L/mL; Life Technologies, USA) in PBS 1 \times . After 1 hour at room temperature, the cells

were washed with PBS 1× (100 µL) and nuclear staining was performed with Hoechst (50 µL; 1.6 µM) in PBS. After 30 minutes of incubation at 37°C, fluorescence microscopy images were acquired on the Cytation 5 using the 10× objective and the following filter cubes: DAPI (blue; excitation/emission = 377/447 nm) for Hoechst and CY5 (deep red; excitation/emission = 628/685 nm) for Alexa Fluor 647 goat anti-mouse IgG, indicating Ki-67 expression.

3.3.5.1.4. *Image Analysis and Statistics*

Using Gen5 Software, Version 3.03 (BioTek Instruments, USA), nuclei segmentation was performed for EdU assay (Hoechst and Picolyl Azide Alexa Fluor 647) and for the Ki-67 assay (Hoechst and Alexa Fluor 647 goat anti-mouse IgG) to count the nuclei present in the image sets obtained from the Cytation 5. The ratio of the total nuclei (stained with Hoechst) to EdU-positive nuclei (Picolyl Azide Alexa Fluor 647-stained) was calculated, providing the percentage of EdU-positive nuclei. Similarly, the ratio of total nuclei to Ki-67-positive nuclei (Alexa Fluor 647 goat anti-mouse IgG-stained) was determined for the Ki-67 assay. Statistical analysis of both assay was conducted using GraphPad Prism software, employing Kruskal-Wallis followed by Dunn's multiple comparisons test, to compare the negative control with all concentrations of PS-MPs, p-values were considered significant when indicated by an asterisk (*: $p \leq 0.05$).

3.3.5.2. **Results and Conclusions**

To further understand the significant reduction in dead cells and the observed trend of increased total cell count following treatment with high concentrations of PS-MPs (0.5 and 1 g/L) in both hepatocyte models observed in Section 3.2.2., two proliferation assays were conducted: the EdU assay and immunofluorescence analysis of the cell proliferation biomarker protein Ki-67. The EdU assay revealed a statistically significant increase in proliferation for HepG2 cells treated with PS-MPs at concentrations of 1 µg/L, 1 mg/L, and 0.5 g/L compared to the non-treated group, with no changes observed at 1 g/L (Fig. S5, item B). In contrast, EdU results showed no changes in proliferation for Huh7 cells treated with PS-MPs (Fig. S5, item A). Similarly, the Ki-67 immunofluorescence assay revealed no changes in Ki-67 expression in either cell line treated with PS-MPs, suggesting no impact on cell proliferation (Fig. S5, items D and E).

As no increase in cell proliferation was observed in either of the two assays performed for both Huh7 and HepG2 cells treated with the highest concentration of PS-MPs (1 g/L)—the concentration at which the greatest reduction in dead cells was observed—we can conclude that this observed event is not related to increased cell proliferation.

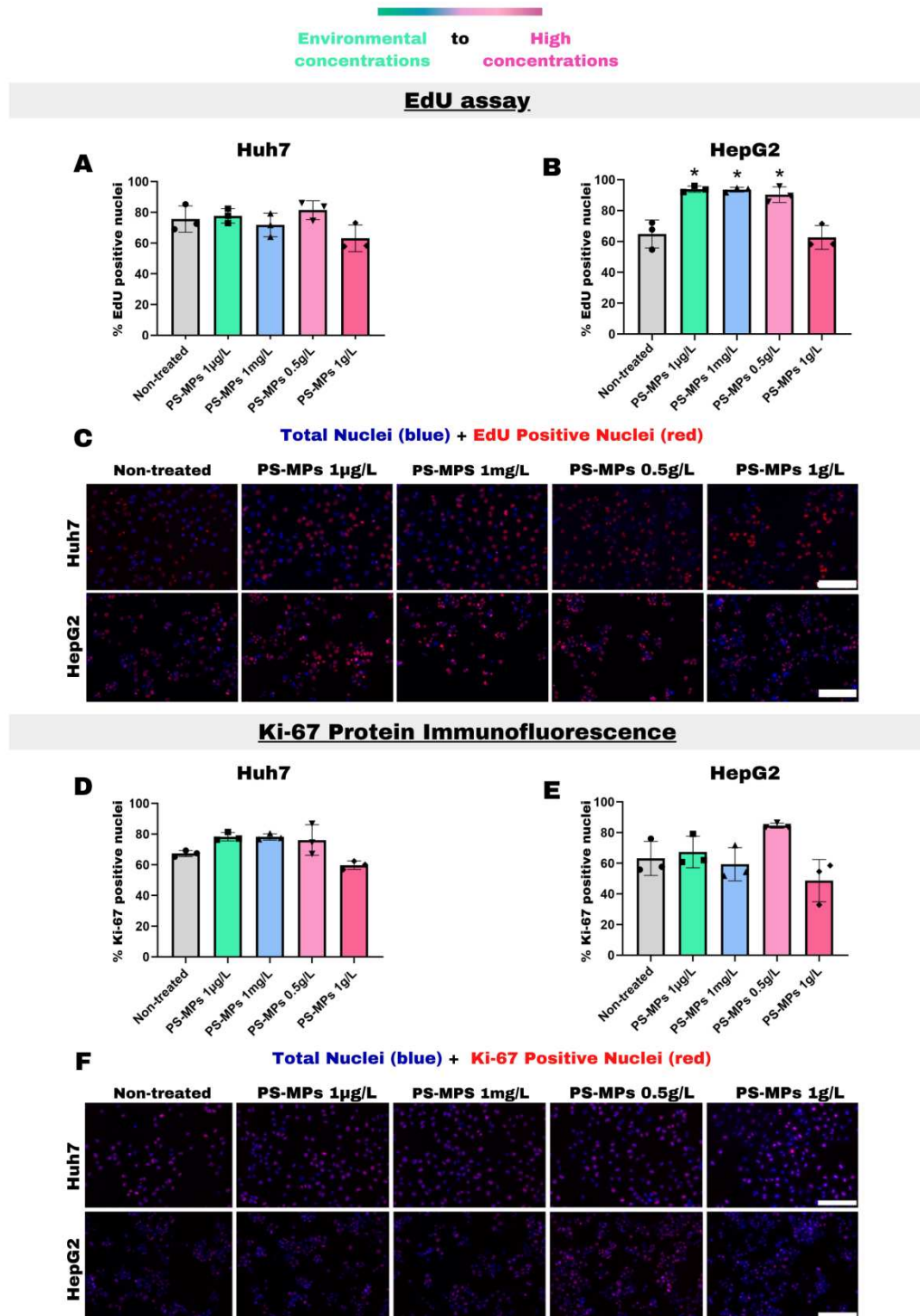


Fig. S5 – Representative Fluorescence Microscopy Images and Data obtained from the Edu Assay and the Ki-67 Assay in Huh7 and Hepg2 Cells Treated with PS-MPs. Huh7 and HepG2 cells were plated at densities of 7,500 and 22,000 cells per well, respectively, in 96-well plates. After 24 hours, cells were treated in triplicate with PS-MPs (1 µg/L, 1 mg/L, 0.5 g/L, and 1 g/L) for 24 hours. Images were acquired (Cytation 5; 10× objective) after Alexa Fluor 647

staining (for EdU or Ki-67 assay) with deep red (Alexa Fluor 647) and blue (Hoechst) fluorescence, which are merged in the images. Hoechst stains the nucleus (DNA) of all cells with fluorescent blue, while Alexa Fluor 647 stains EdU- or Ki-67-positive cells with fluorescent deep red (indicating cells in proliferation). The acquired images were analyzed in Gen5 Software, where nuclei were segmented and counted. The number of nuclei positive for EdU or Ki-67 was divided by the total number of nuclei in each image and multiplied by 100. These ratios were subsequently aggregated per plate. **(A,B)** Percentage of EdU-positive nuclei relative to total nuclei for Huh7 (A) and HepG2 (B). **(C)** Representative fluorescence microscopy images of Huh7 and HepG2 cells for the EdU assay. **(D,E)** Percentage of Ki-67-positive nuclei relative to total nuclei for Huh7 (D) and HepG2 (E). **(F)** Representative fluorescence microscopy images of Huh7 and HepG2 cells for the Ki-67 protein immunofluorescence assay. The white scale bar in the lower-right corner of the images represents 200 μm . Statistical analysis was performed using the Kruskal-Wallis test followed by Dunn's multiple comparisons test in GraphPad Prism: * $p \leq 0.05$ indicates statistical significance compared to the non-treated group.

3.3.6. ***Supplementary Material 6: Viability of Huh7 and HepG2 Cells Assessed by MTT Assay After Exposure to PS-MPs-Fluor***

3.3.6.1. ***Materials and Method***

The same as described in Section 3.1.3.2, MTT Cell Viability Assay, with cells being exposed to PS-MPs-Fluor (100 μ L; Spherotech Inc. code: FP-0558-2).

3.3.6.2. ***Results and Conclusions***

The exposure of Huh7 and HepG2 cells to PS-MPs-Fluor resulted in cell viabilities similar to those observed in treatments with non-fluorescent PS-MPs (Fig. S6 and Fig. 9). Thus, PS-MPs-Fluor tend to elicit cellular responses comparable to those triggered by non-fluorescent PS-MPs.

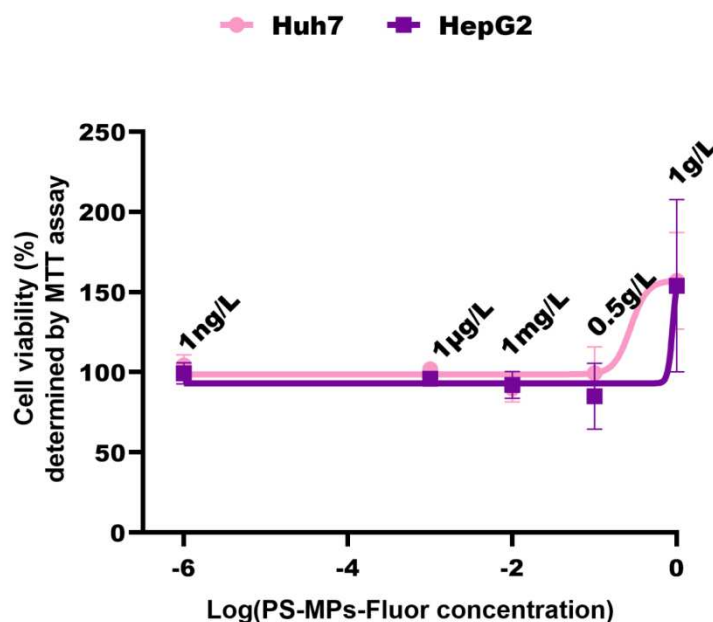


Fig. S6 – Cell viability curves by MTT assay of Huh7 and HepG2 cells after exposure to PS-MPs-Fluor. Huh7 and HepG2 cells were plated at a density of 7,500 and 22,000 cells/well, respectively, in 96-well plates. After 24 hours, cells were treated in triplicate with PS-MPs-Fluor (1 ng/L, 1 μ g/L, 1 mg/L, 0.5 g/L, and 1 g/L) for 24 hours. Then, cell viability was assessed by MTT assay. Cell viabilities were calculated relative to the non-treated group, which was considered 100%. Each nonlinear regression represents triplicates from three independent experiments. Statistical analysis was performed using the Kruskal-Wallis test followed by Dunn's multiple comparisons test using GraphPad Prism software: * $p \leq 0.05$ indicates statistical significance compared to the non-treated group.

3.3.7. *Supplementary Material 7: Full representative fluorescence microscopy images of Total Cell Association of PS-MPs Over Time*

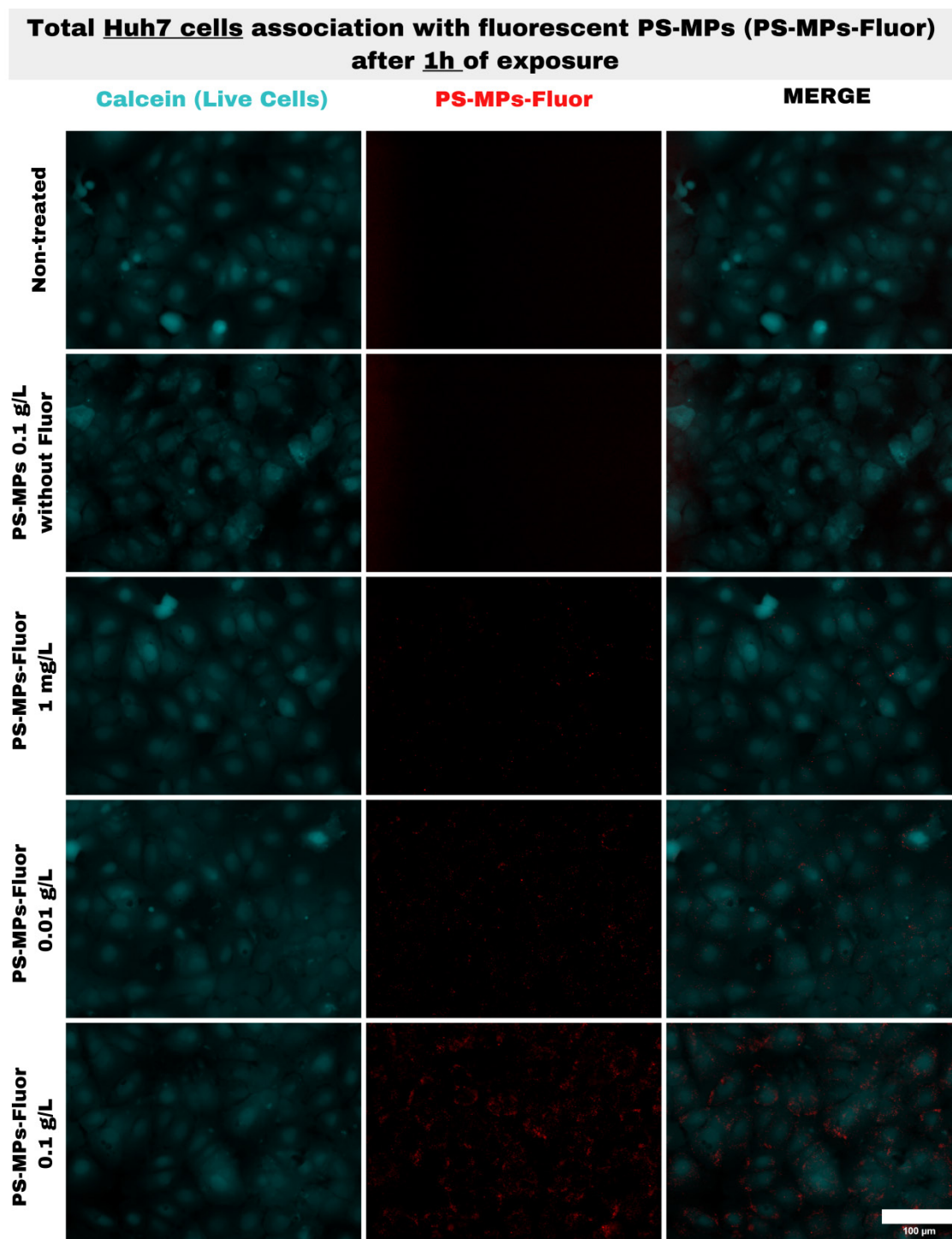


Fig. S7.1 - Total Huh7 Cell Association of PS-MPs-Fluor Over 1 Hour of Exposure.

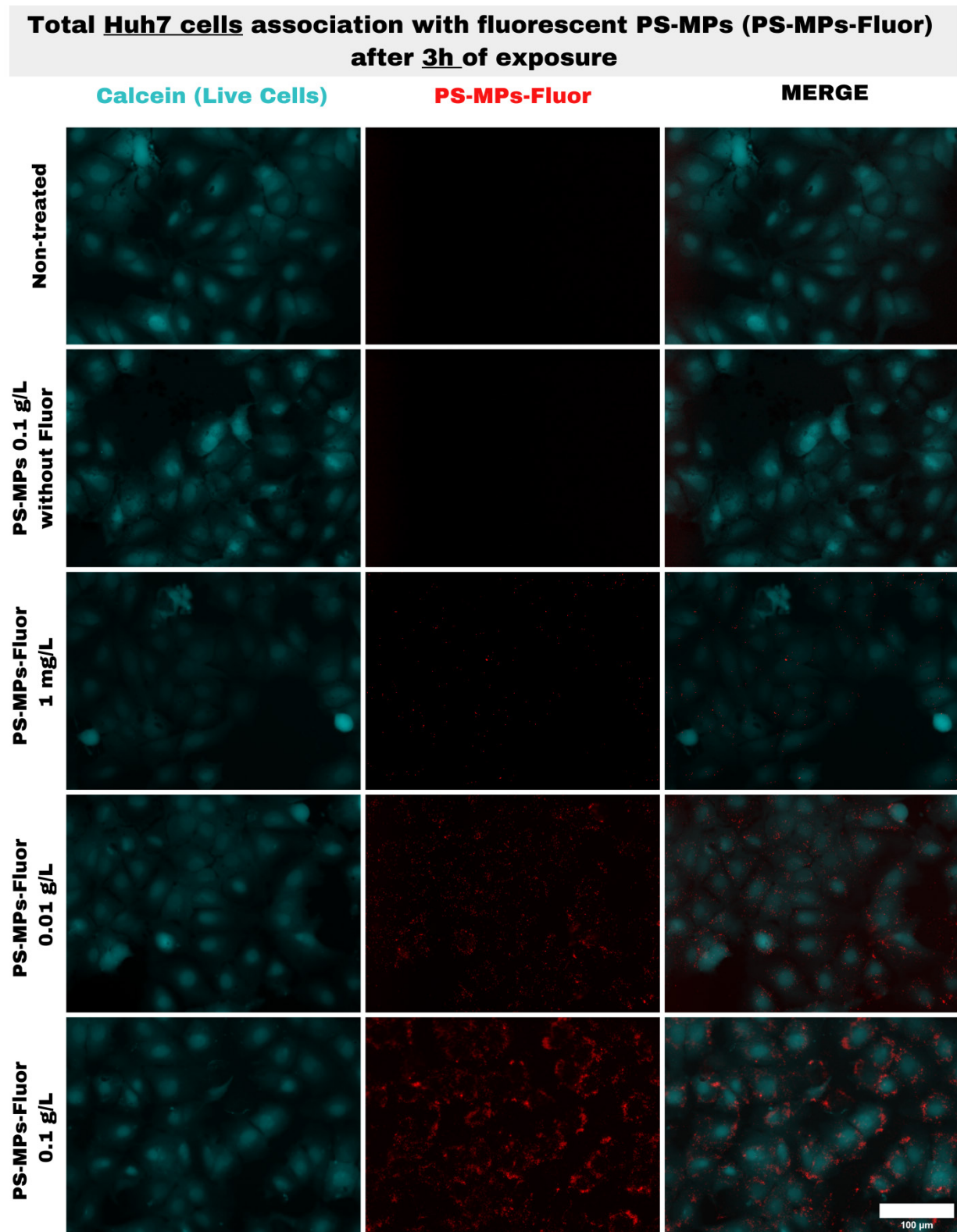


Fig. S7.2 - Total Huh7 Cell Association of PS-MPs-Fluor Over 3 Hours of Exposure.

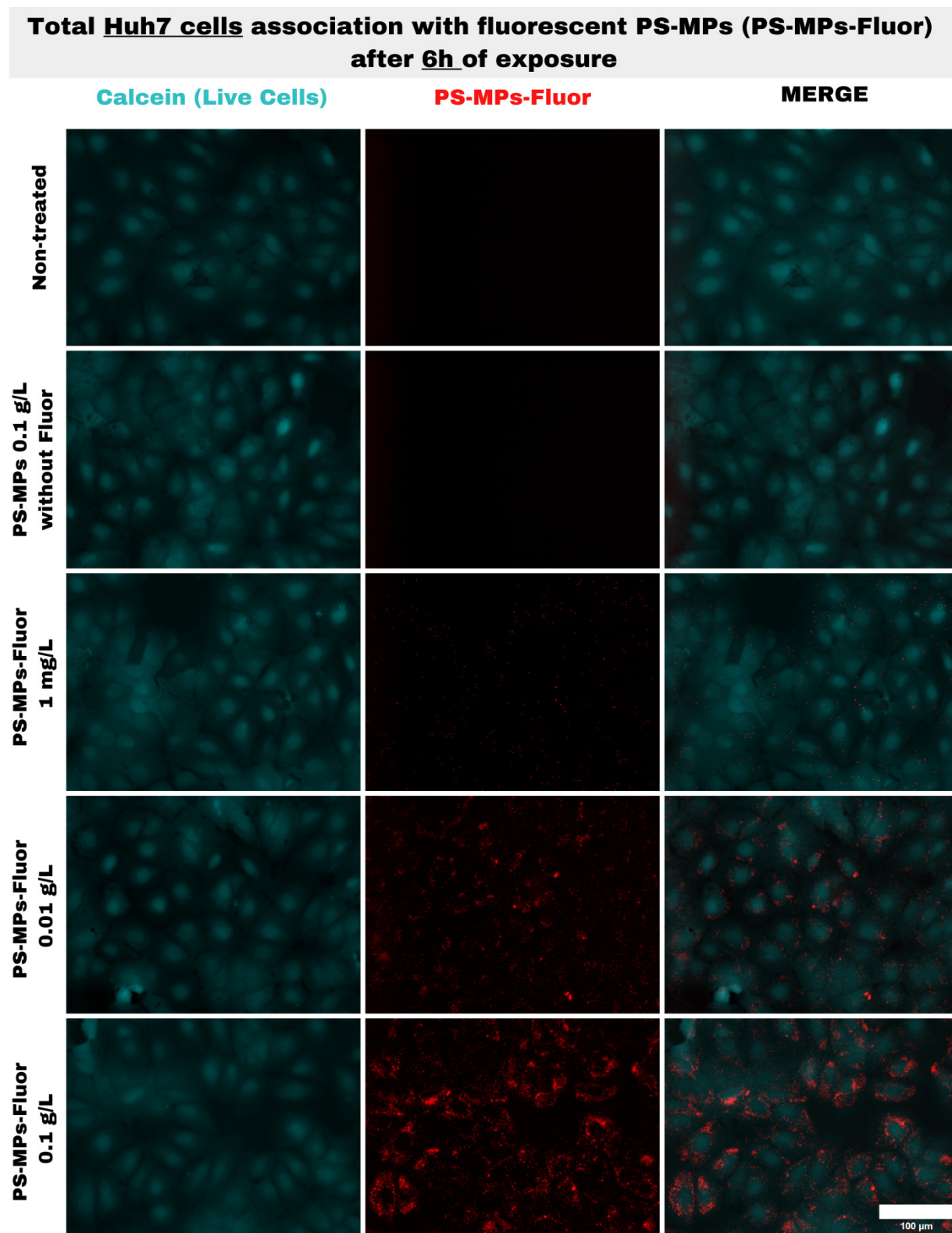


Fig. S7.3 - Total Huh7 Cell Association of PS-MPs-Fluor Over 6 Hours of Exposure.

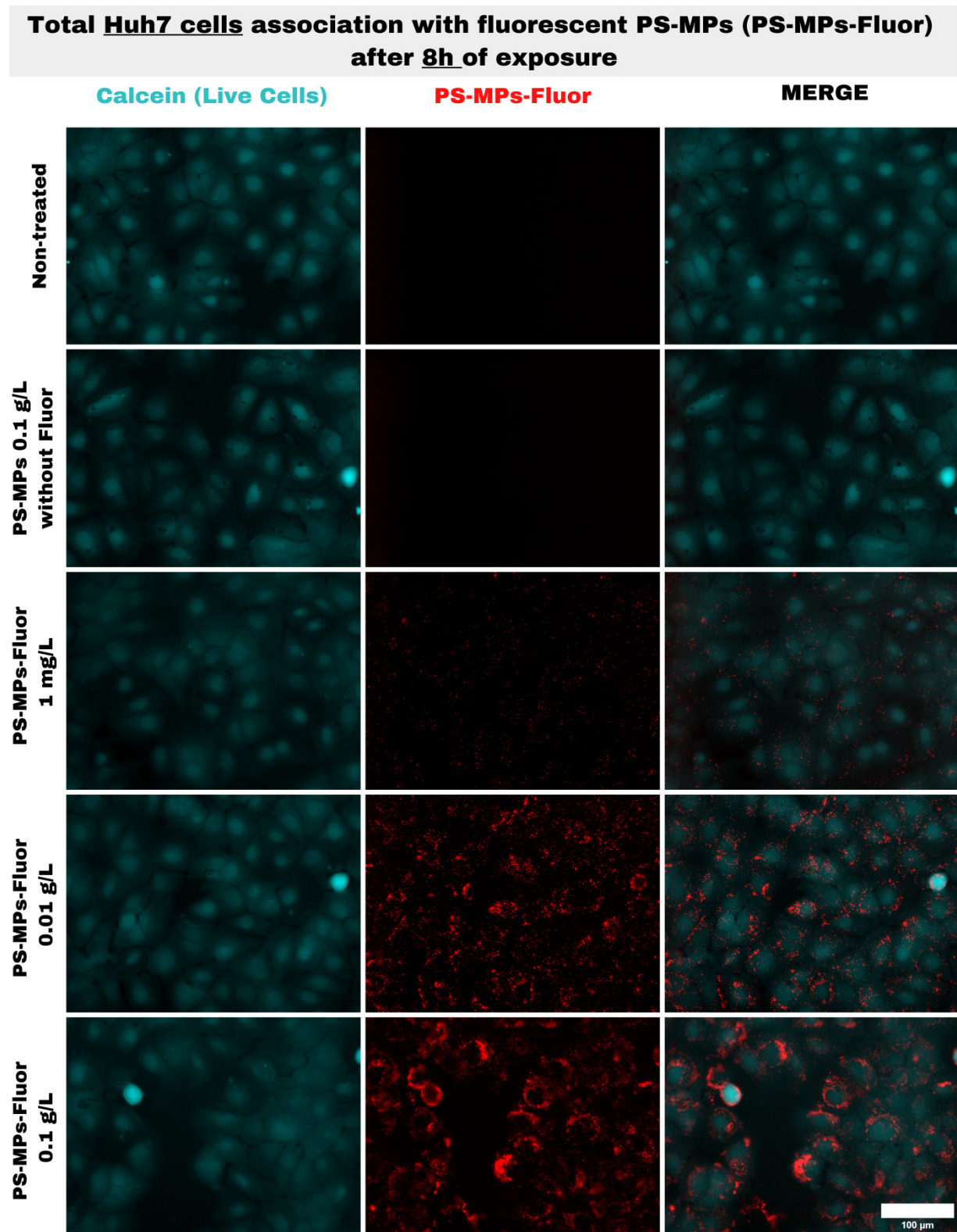


Fig. S7.4 - Total Huh7 Cell Association of PS-MPs-Fluor Over 8 Hours of Exposure.

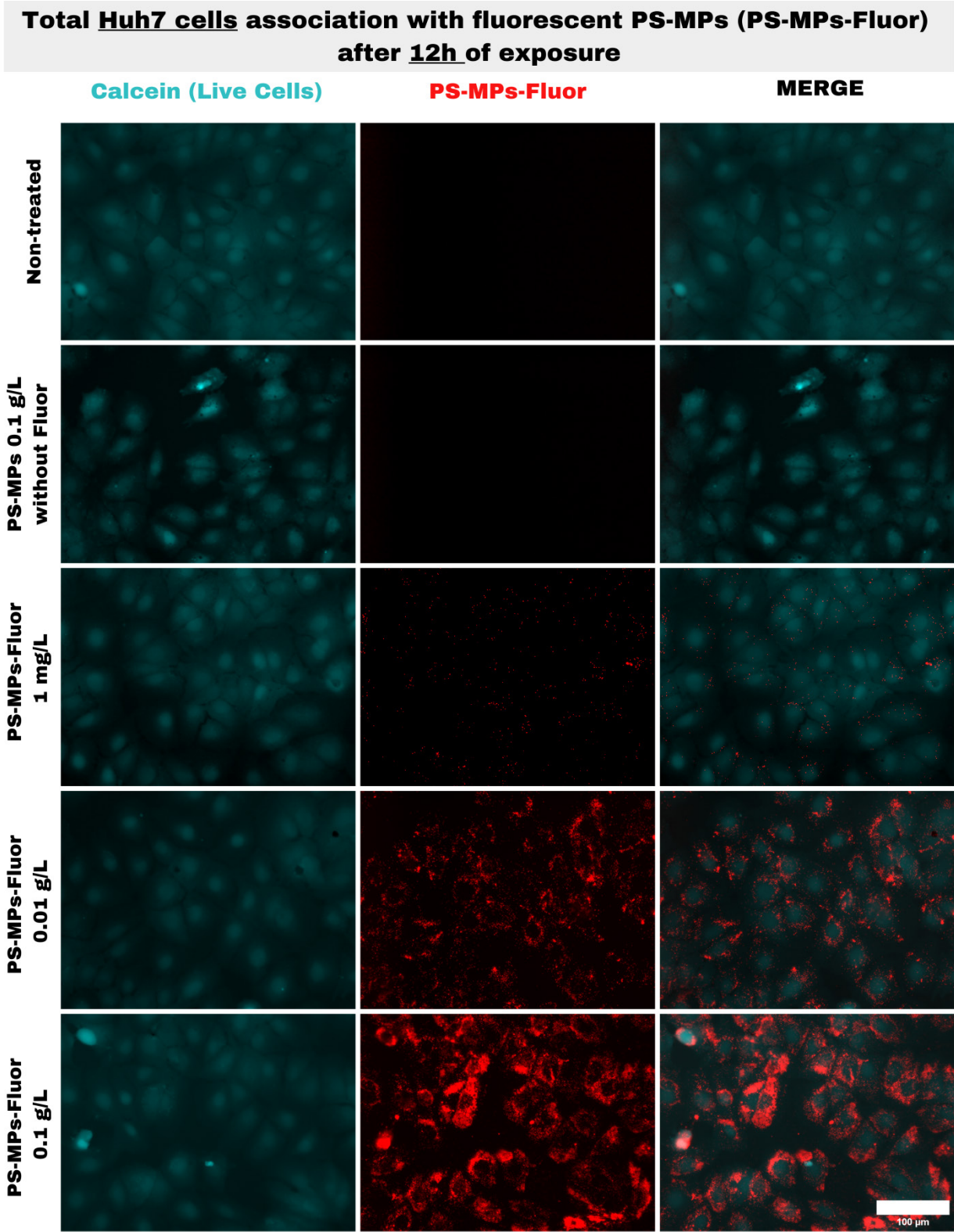


Fig. S7.5 - Total Huh7 Cell Association of PS-MPs-Fluor Over 12 Hours of Exposure.

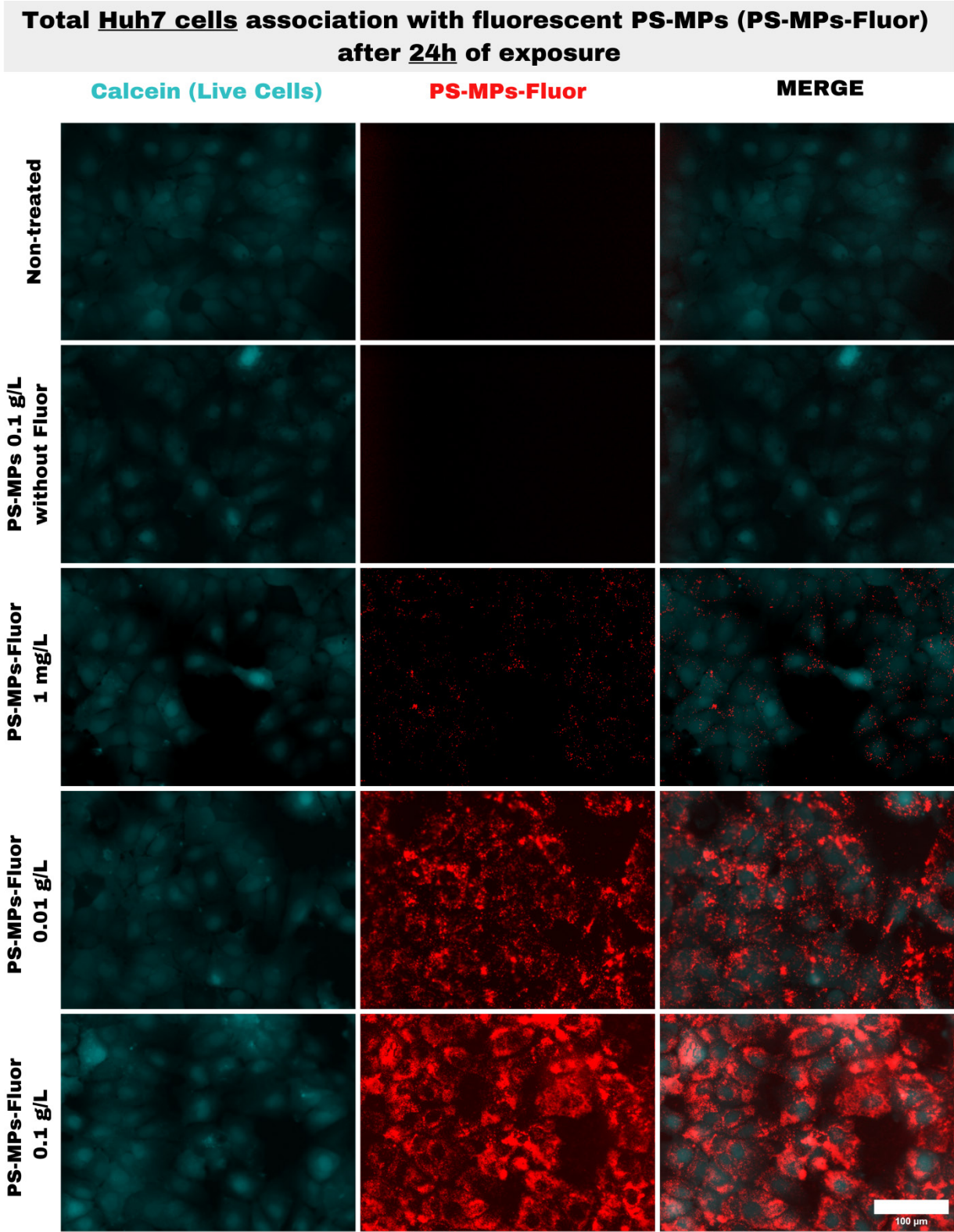


Fig. S7.6 - Total Huh7 Cell Association of PS-MPs-Fluor Over 24 Hours of Exposure.

Total HepG2 cells association with fluorescent PS-MPs (PS-MPs-Fluor) after 1h of exposure

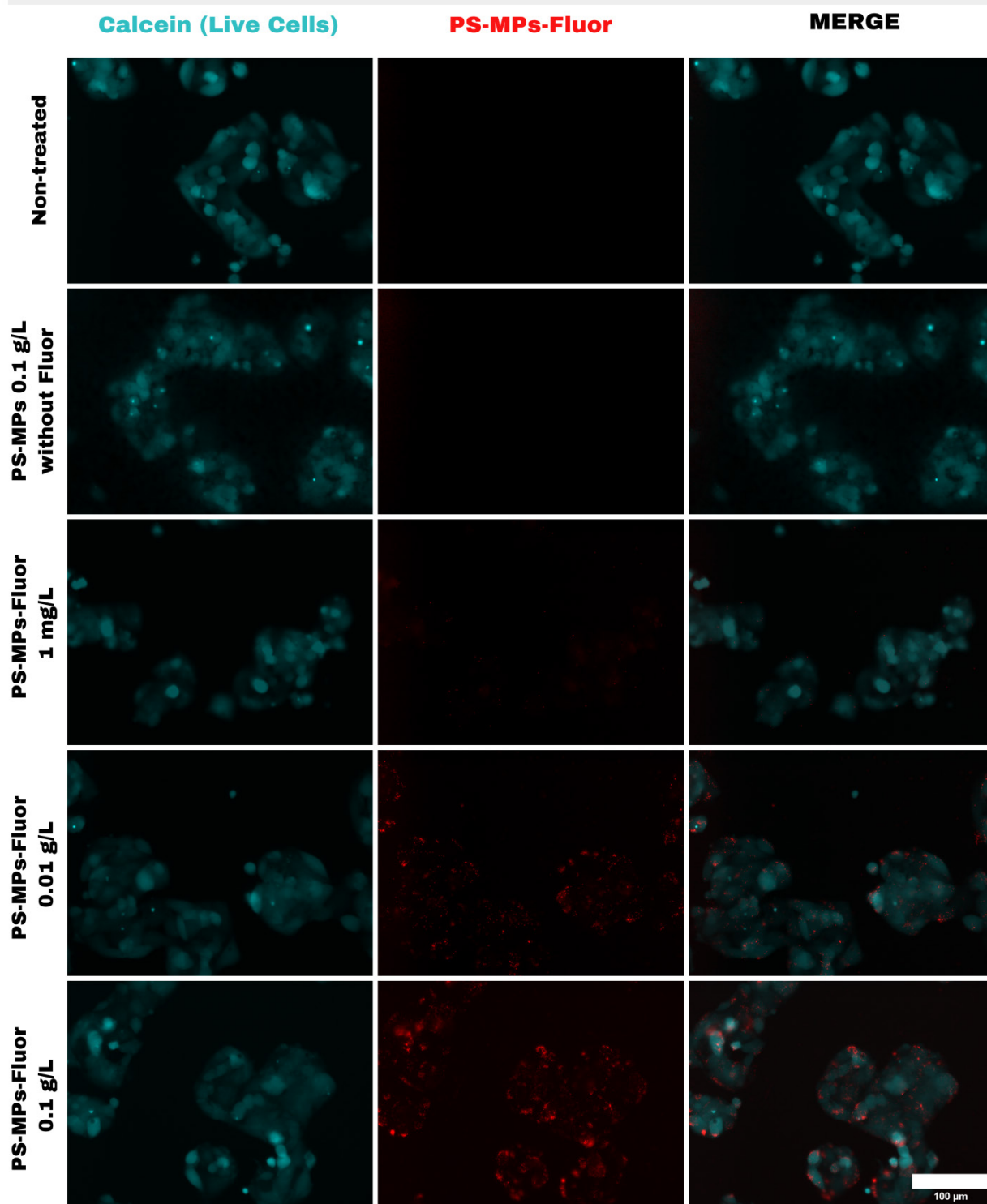


Fig. S7.7 - Total HepG2 Cell Association of PS-MPs-Fluor Over 1 Hour of Exposure.

Total HepG2 cells association with fluorescent PS-MPs (PS-MPs-Fluor) after 3h of exposure

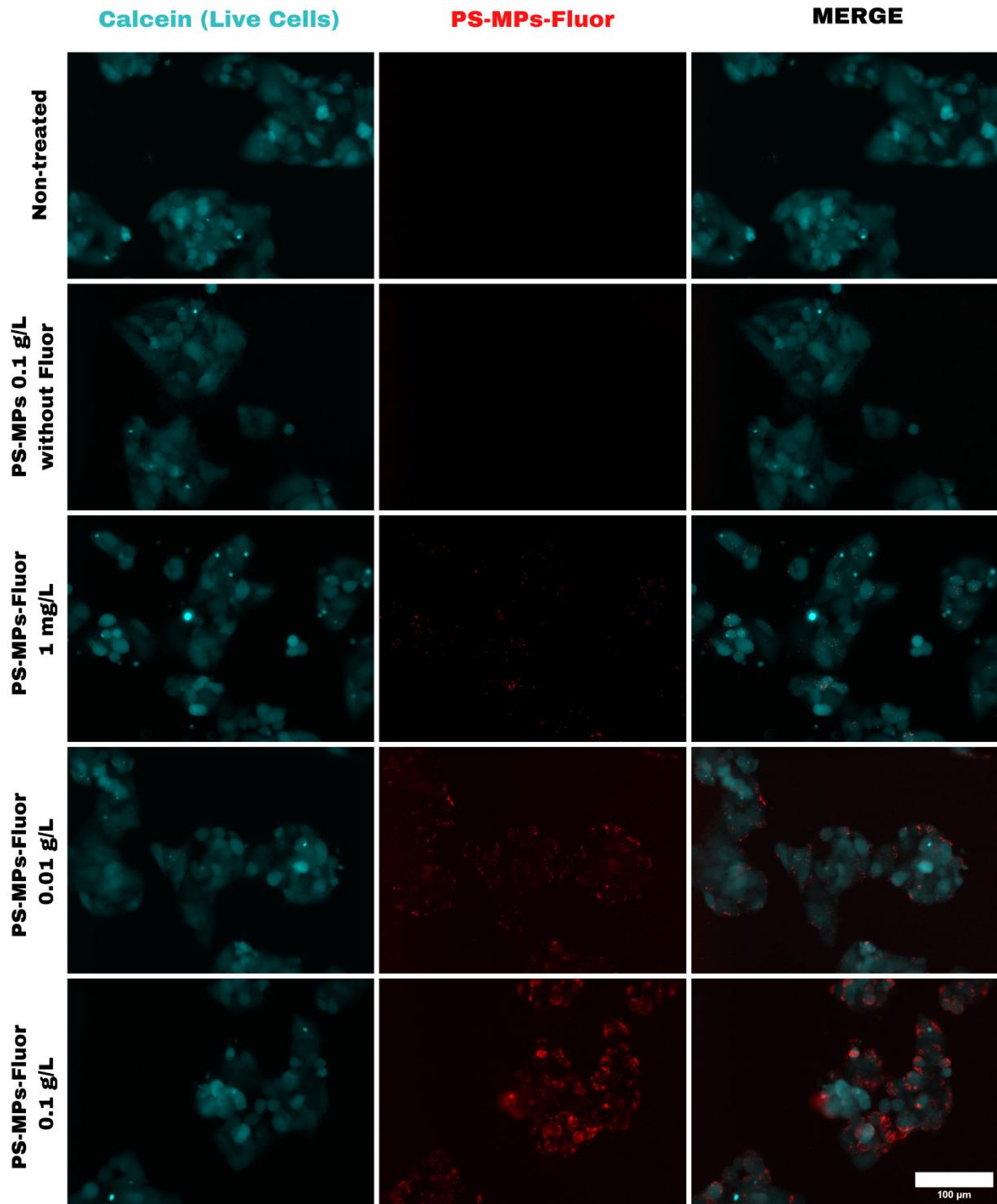


Fig. S7.8 - Total HepG2 Cell Association of PS-MPs-Fluor Over 3 Hours of Exposure.

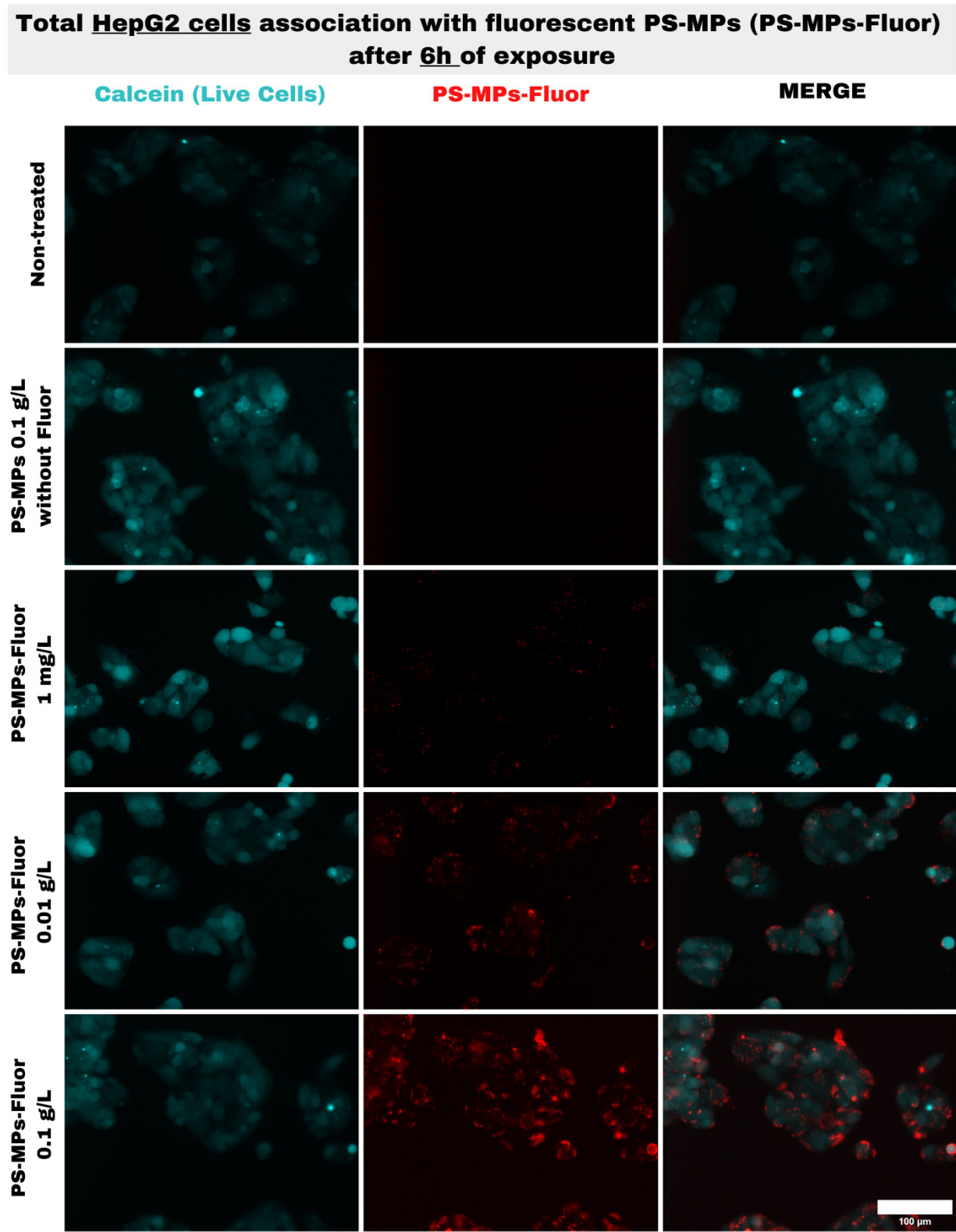


Fig. S7.9- Total HepG2 Cell Association of PS-MPs-Fluor Over 6 Hours of Exposure.

Total HepG2 cells association with fluorescent PS-MPs (PS-MPs-Fluor) after 8h of exposure

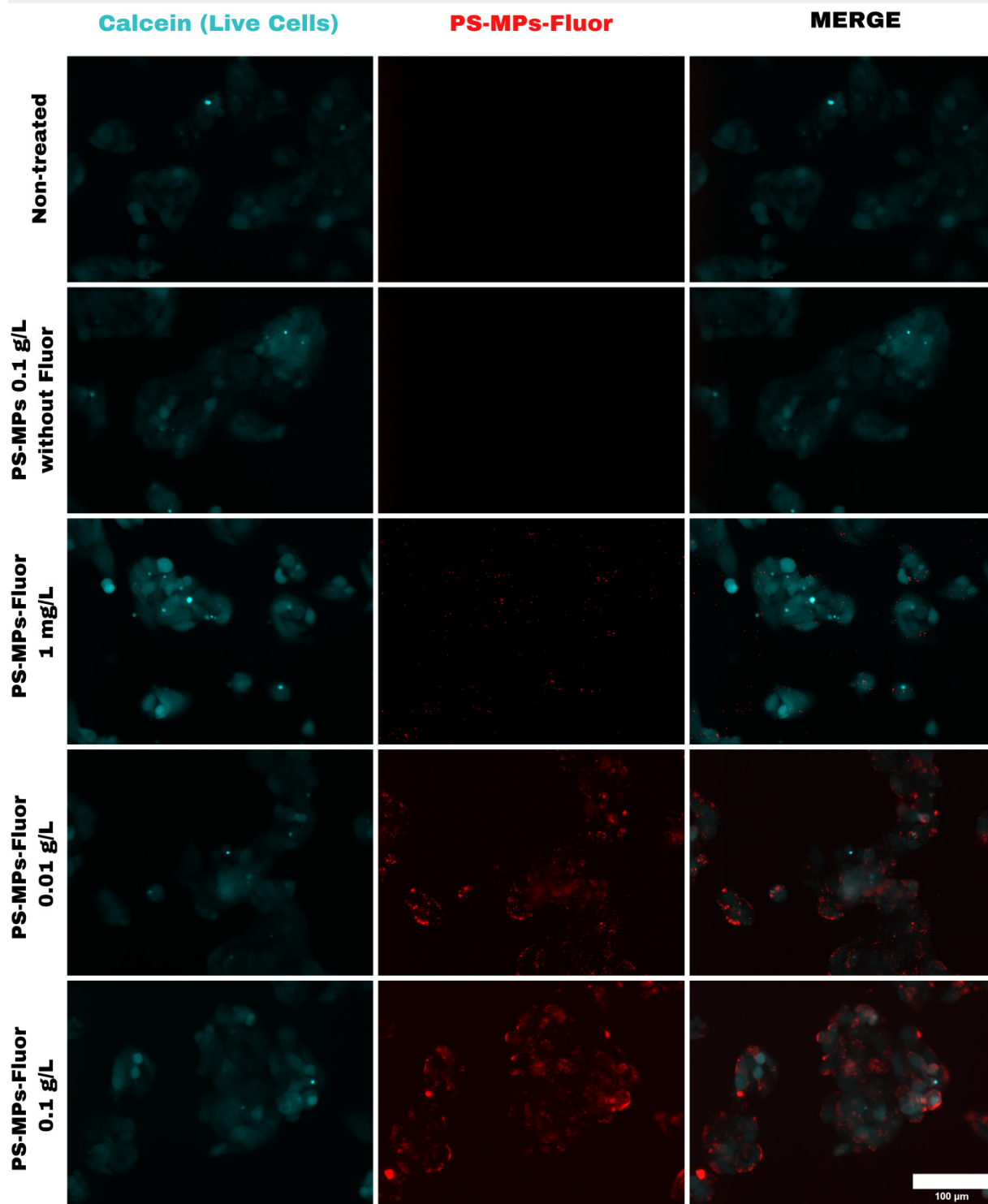


Fig. S7.10 - Total HepG2 Cell Association of PS-MPs-Fluor Over 8 Hours of Exposure.

Total HepG2 cells association with fluorescent PS-MPs (PS-MPs-Fluor) after 12h of exposure

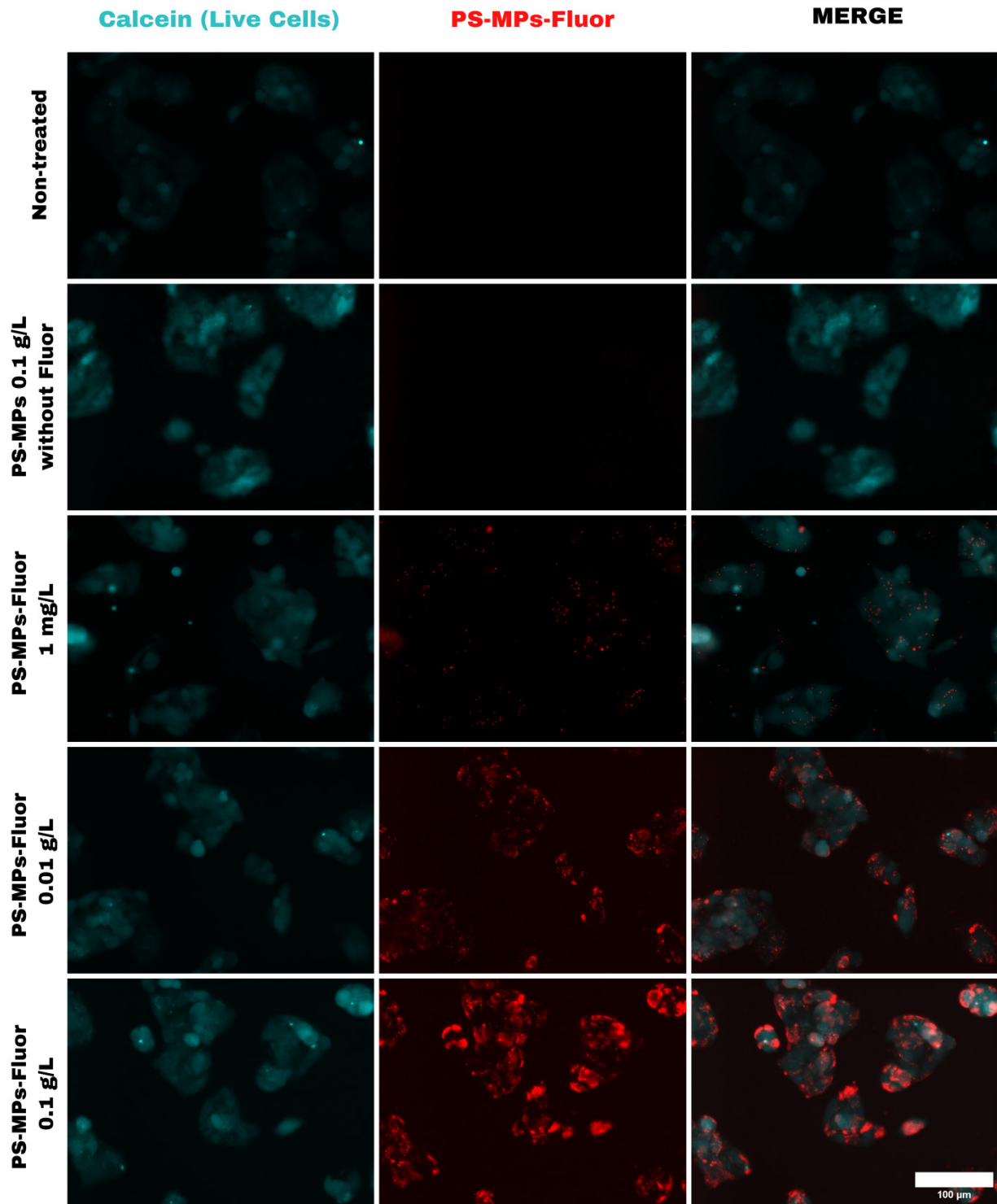


Fig. S7.11 - Total HepG2 Cell Association of PS-MPs-Fluor Over 12 Hours of Exposure.

Total HepG2 cells association with fluorescent PS-MPs (PS-MPs-Fluor) after 24h of exposure

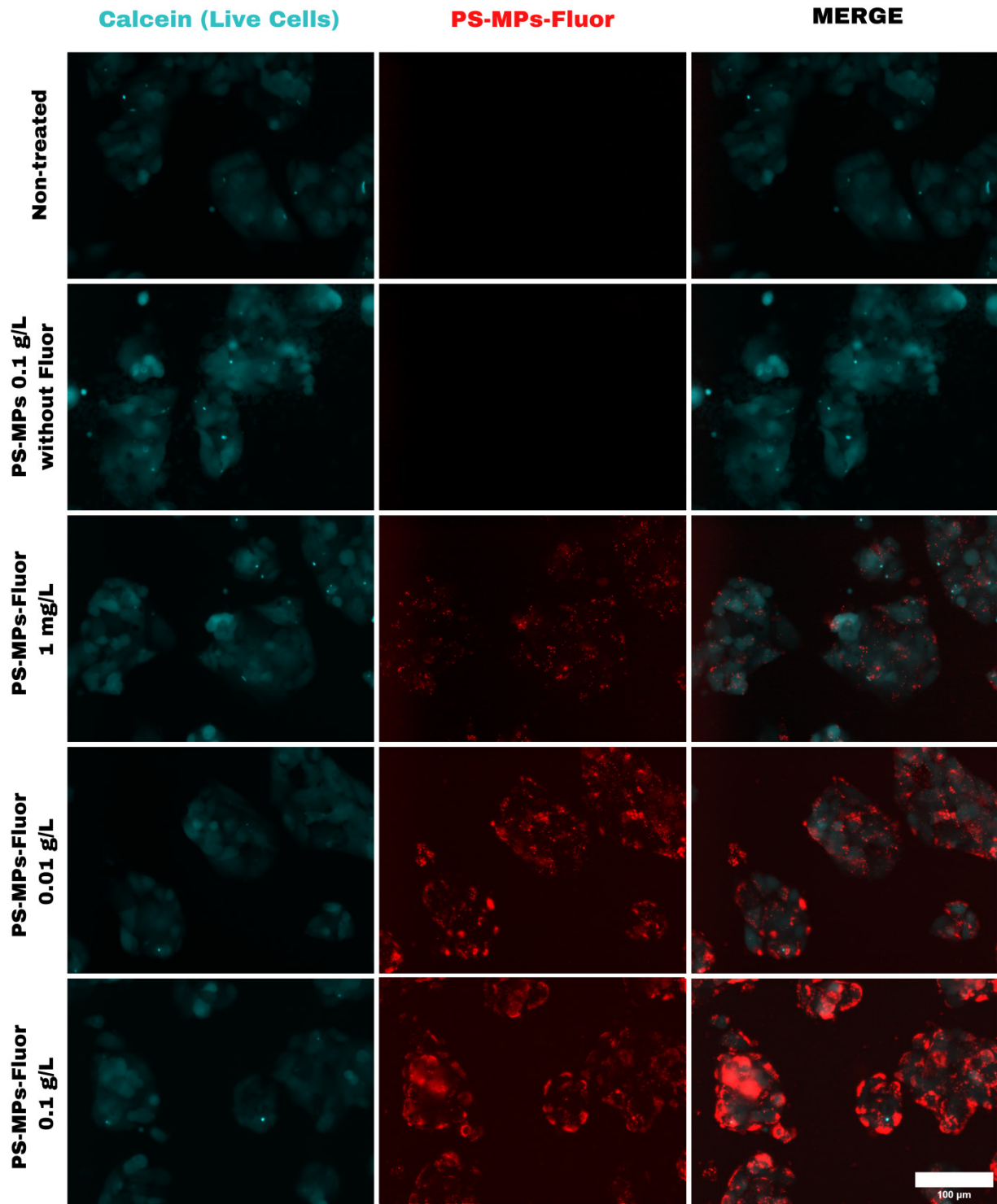


Fig. S7.12 - Total HepG2 Cell Association of PS-MPs-Fluor Over 24 Hours of Exposure.

Figs. S7.1 to S7.12 description: Huh7 and HepG2 cells were plated at densities of 7,500 and 22,000 cells per well, respectively, in 96-well plates. After 24 hours, cells were treated in duplicate with PS-MPs-Fluor (1 mg/L, 0.01 g/L, and 0.1 g/L) and non-fluorescent PS-MPs (0.1 g/L) for 1, 3, 6, 8, 12, and 24 hours. Images were acquired following Calcein staining of live cells (Cytation 5, 20× objective) to visualize the entire cell area. **(S7.1 to S7.6)** Representative fluorescence microscopy images of **Huh7** cells that were non-treated, treated with PS-MPs without fluorescence and PS-MPs-Fluor (1 mg/L, 0.01 g/L, and 0.1 g/L) for 1, 6, 12, and 24 hours. **(S7.1 to S7.6)** Representative fluorescence microscopy images of **HepG2** cells that were non-treated, treated with PS-MPs without fluorescence and PS-MPs-Fluor (1 mg/L, 0.01 g/L, and 0.1 g/L) for 1, 6, 12, and 24 hours. The white scale bar in the lower right corner of the images in the third column indicates a scale of 100 μm . Experiments were conducted in three independent replicates.

3.3.8. Supplementary Material 8: Confocal Microscopy Investigation of PS-MPs Internalization in Huh7 and HepG2 Cells

3.3.8.1. *Materials and Method*

3.3.8.1.1. *Cell Plating and Exposure*

Huh7 and HepG2 cells were plated in 96-well plates at 7,500 and 22,000 cells per well, respectively, and incubated for 24 hours. Next, the cells were exposed in duplicate to PS-MPs-Fluor (100 μ L; 0.1 g/L) for 24 hours.

3.3.8.1.2. *Imaging Protocol*

After 24 hours, the treatment in the wells was replaced with PFA (100 μ L; 4% w/v) for 20 minutes for cell fixation. Then, the cells were washed twice with PBS 1 \times (100 μ L) and incubated with a solution (25 μ L) of HCS CellMask™ Blue (60 μ M) and Hoechst (1.6 μ M), prepared in a permeabilization solution of 1% (w/v) BSA and 0.1% (v/v) Triton X-100 in PBS, for cell staining. After 30 minutes of incubation at 37°C, the cells were washed twice with PBS 1 \times (100 μ L). Next, PBS 1 \times (100 μ L) with 0.05% (w/v) sodium azide was added to the wells. Fluorescence images were acquired using a 40 \times objective (EC Plan-Neofluar 40 \times /1.3 Oil DIC M27) on the Zeiss LSM880 Airyscan Inverted Confocal Microscope (Carl Zeiss AG, Germany), using a 405 nm laser line (blue) for excitation of CellMask and Hoechst, and a 550 nm laser line (red) for excitation of PS-MPs-Fluor, both with the pinhole set to 1 AU.

3.3.8.2. *Results and Conclusions*

To confirm whether PS-MPs-Fluor were internalized by the cells, we conducted a confocal microscopy assay. In this assay, Huh7 and HepG2 cells were treated with PS-MPs-Fluor (0.1 g/L) for 24 h, fixed with PFA, and stained with the Hoechst and plasma membrane dye CellMask. Confocal microscopy images demonstrated that both hepatocyte models internalized PS-MPs-Fluor after 24 h exposure (Fig. S8). The interaction and spatial organization patterns of PS-MPs-Fluor in the cells observed were consistent with those identified in the Total Cell Association of PS-MPs assay (Section 3.2.3.). Huh7 cells internalized a greater number of PS-MPs-Fluor compared to HepG2 cells, with most particles localized in the perinuclear region. In HepG2 cells, most PS-MPs-Fluor were concentrated near the plasma membrane of cells at the periphery of the clusters, with little to no internalization observed in centrally located cells. Additionally, some confocal microscopy images of HepG2 cells revealed individual cells detached from the clusters, with the entire circumference of the plasma membrane densely

occupied by PS-MPs-Fluor, as shown in the first row of the panel in Fig. S8. This observation suggests that the accumulation of PS-MPs-Fluor near the plasma membrane may impair cell-cell communication and junctions, causing cells located at the periphery of the clusters to detach over time as internalization increases.

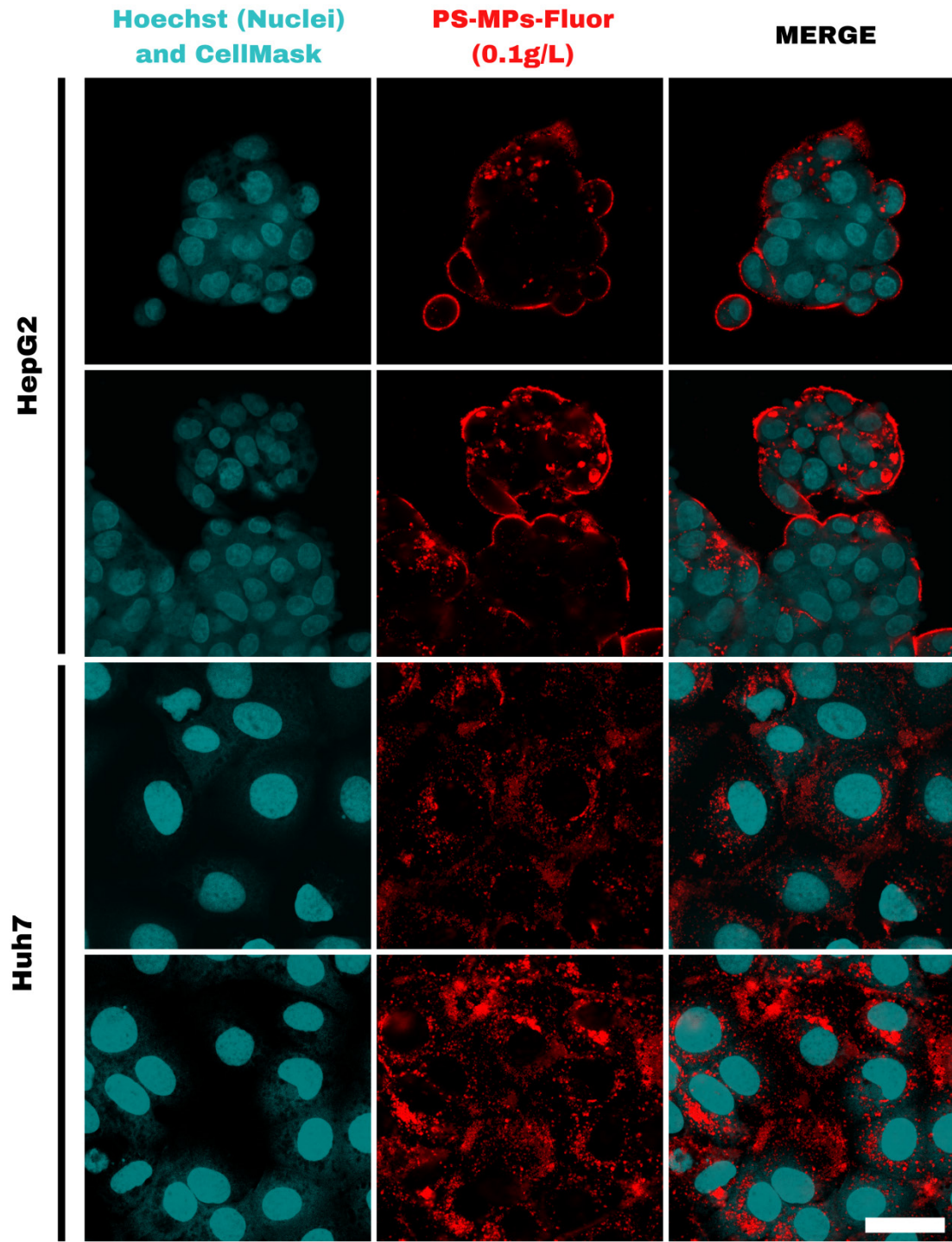


Fig. S8 – Representative Confocal Fluorescence Microscopy Images of Huh7 and HepG2 Cells Exposed to Fluorescent PS-MPs (PS-MPs-Fluor). Huh7 and HepG2 cells were plated at densities of 7,500 and 22,000 cells per well, respectively, in 96-well plates. After 24 hours, cells were treated in duplicate with PS-MPs-Fluor at 0.1 g/L for 24 hours. Images were acquired following cell fixation and Hoechst and CellMask staining (Zeiss LSM880 Airyscan Inverted Confocal Microscope, 40× objective) to visualize nucleus and the entire cell area. The white scale bar in the lower right corner of the images in the third column indicates a scale of 40 μm . This assay was conducted in a single independent replicate.

3.3.9. Supplementary Material 9: Full representative fluorescence microscopy images of Live Cell Painting Assay with Huh7 and HepG2 cells

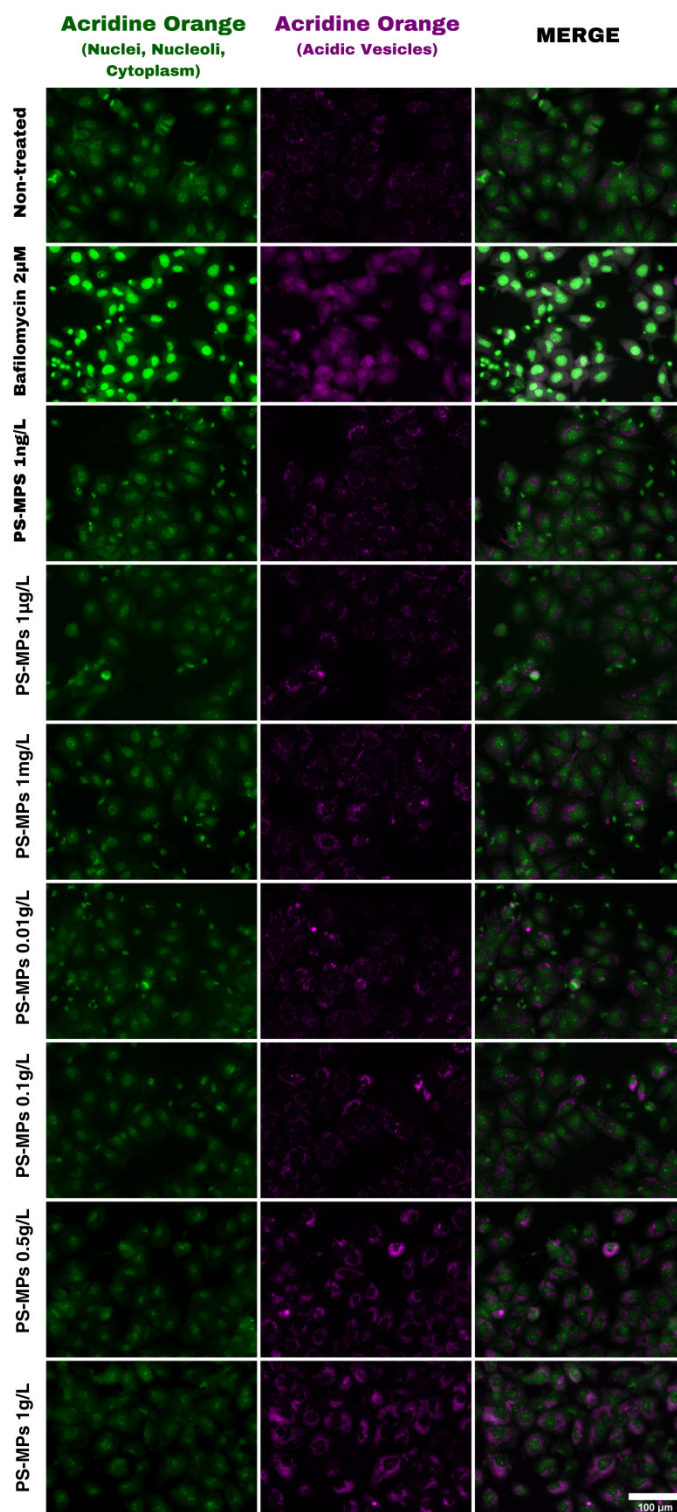


Fig. S9.1 – Representative Fluorescence Microscopy Images from the Live Cell Painting Assay with Huh7 Cells Exposed to PS-MPs.

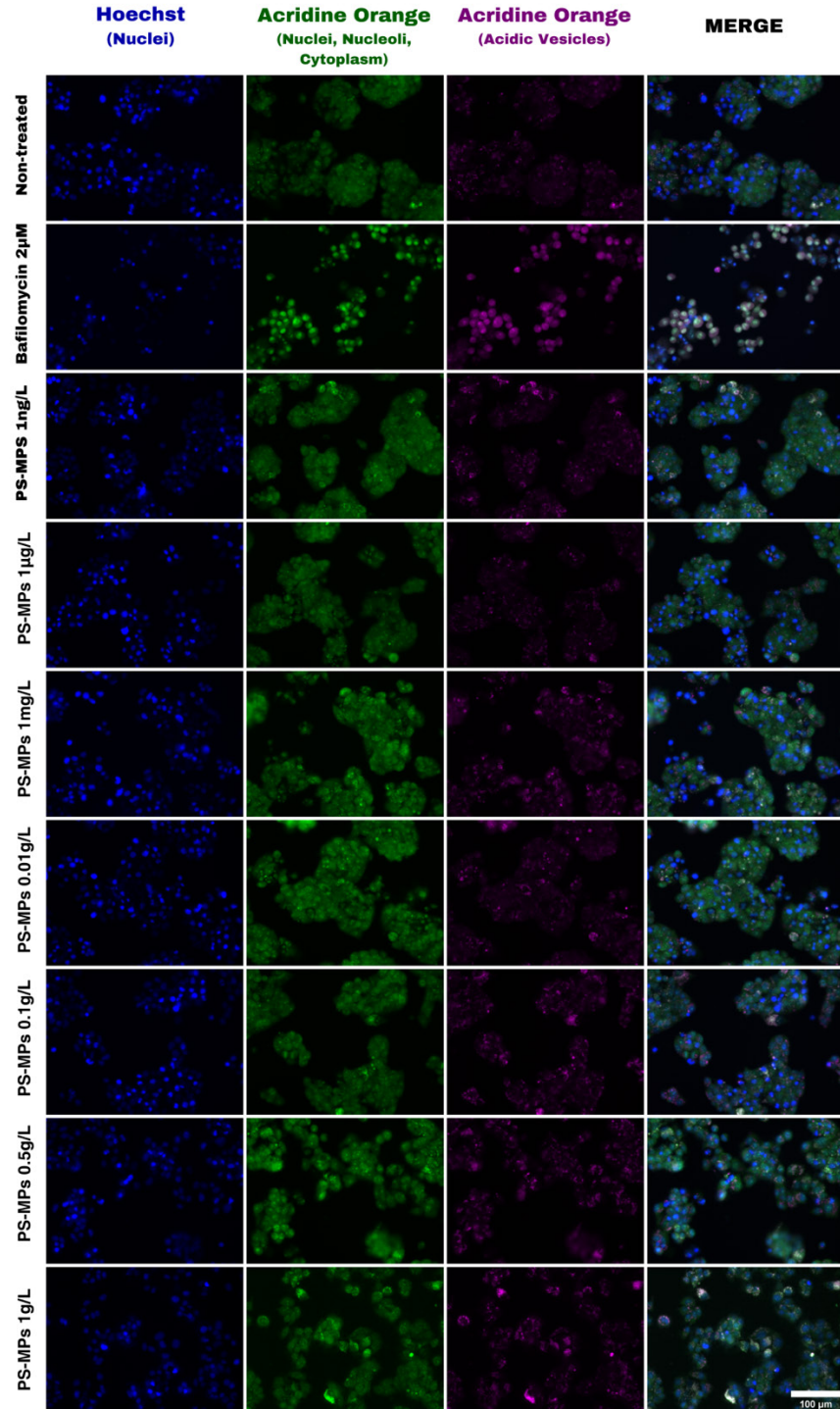


Fig. S9.2 – Representative Fluorescence Microscopy Images from the Live Cell Painting Assay with HepG2 Cells Exposed to PS-MPs.

Figs. S9.1 and S9.2 description: Huh7 and HepG2 cells were plated at densities of 7,500 and 22,000 cells per well, respectively, in 96-well plates. After 24 hours, cells were treated in

triplicate with PS-MPs (1 ng/L, 1 µg/L, 1 mg/L, 0.5 g/L, and 1 g/L) and Bafilomycin A1 (2 µM; positive control) for 24 hours. Images were acquired after staining with Acridine Orange (AO) (Cytation 5, 20× objective). AO stains nuclear and cytoplasmic RNA in green, enabling visualization of the nucleus, nucleoli, and cytoplasm, while acidic vesicles are stained in red (in images, represented in magenta to accessibility for individuals with colorblindness). **(S9.1)** Representative fluorescence microscopy images of **Huh7 cells** that were non-treated, treated with the positive control, and treated with PS-MPs (1 ng/L, 1 µg/L, 1 mg/L, 0.5 g/L, and 1 g/L). **(S9.2)** Representative fluorescence microscopy images of **HepG2 cells** that were non-treated, treated with the positive control, and treated with PS-MPs (1 ng/L, 1 µg/L, 1 mg/L, 0.5 g/L, and 1 g/L). The white scale bar in the lower right corner of the images in the fourth column indicates a scale of 100 µm. Experiments were conducted in three independent replicates.

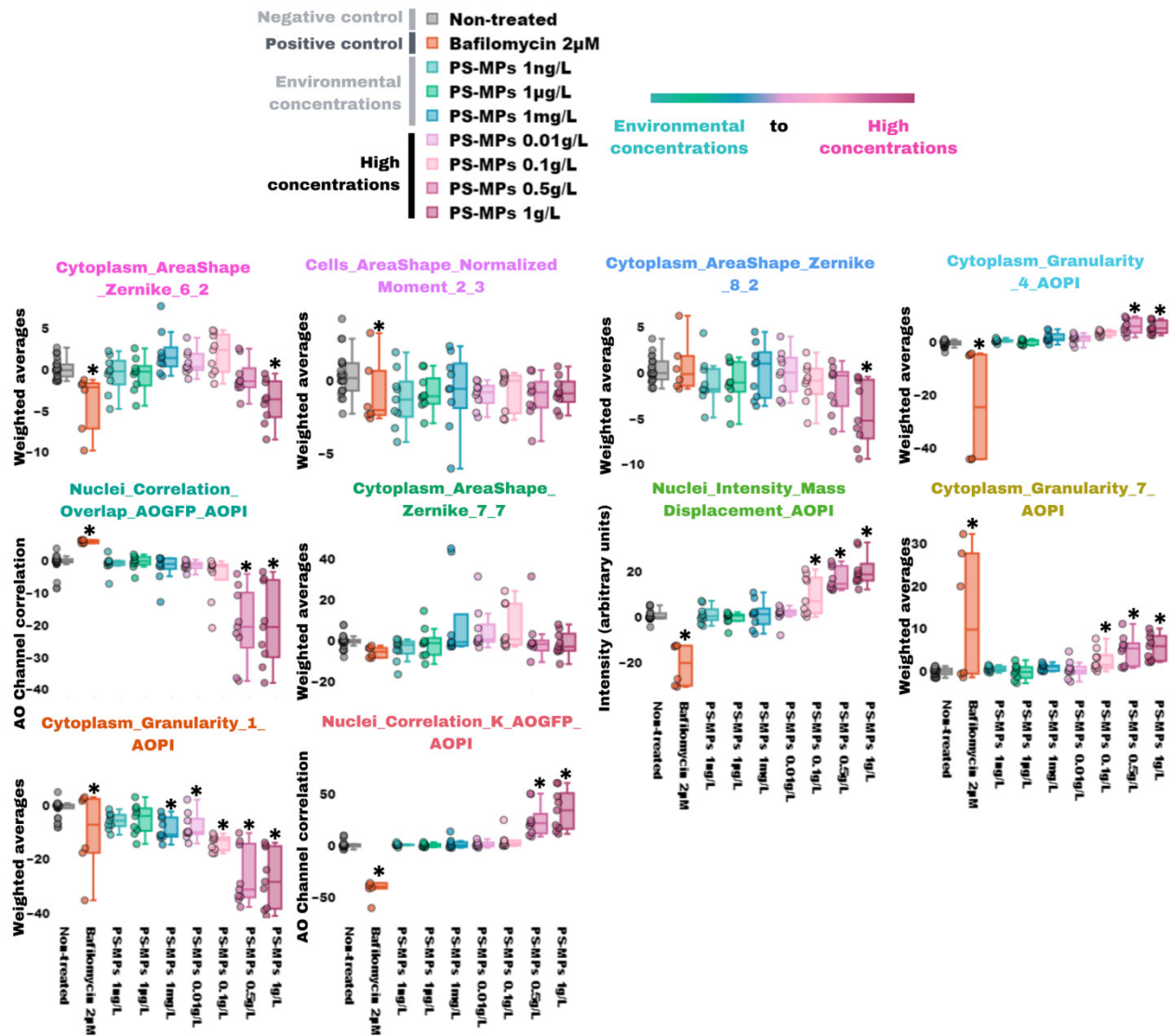


Fig. S9.3 – Top 10 Feature Vectors from LDA Analysis of Data from the Live Cell Painting Assay with Huh7 Cells.

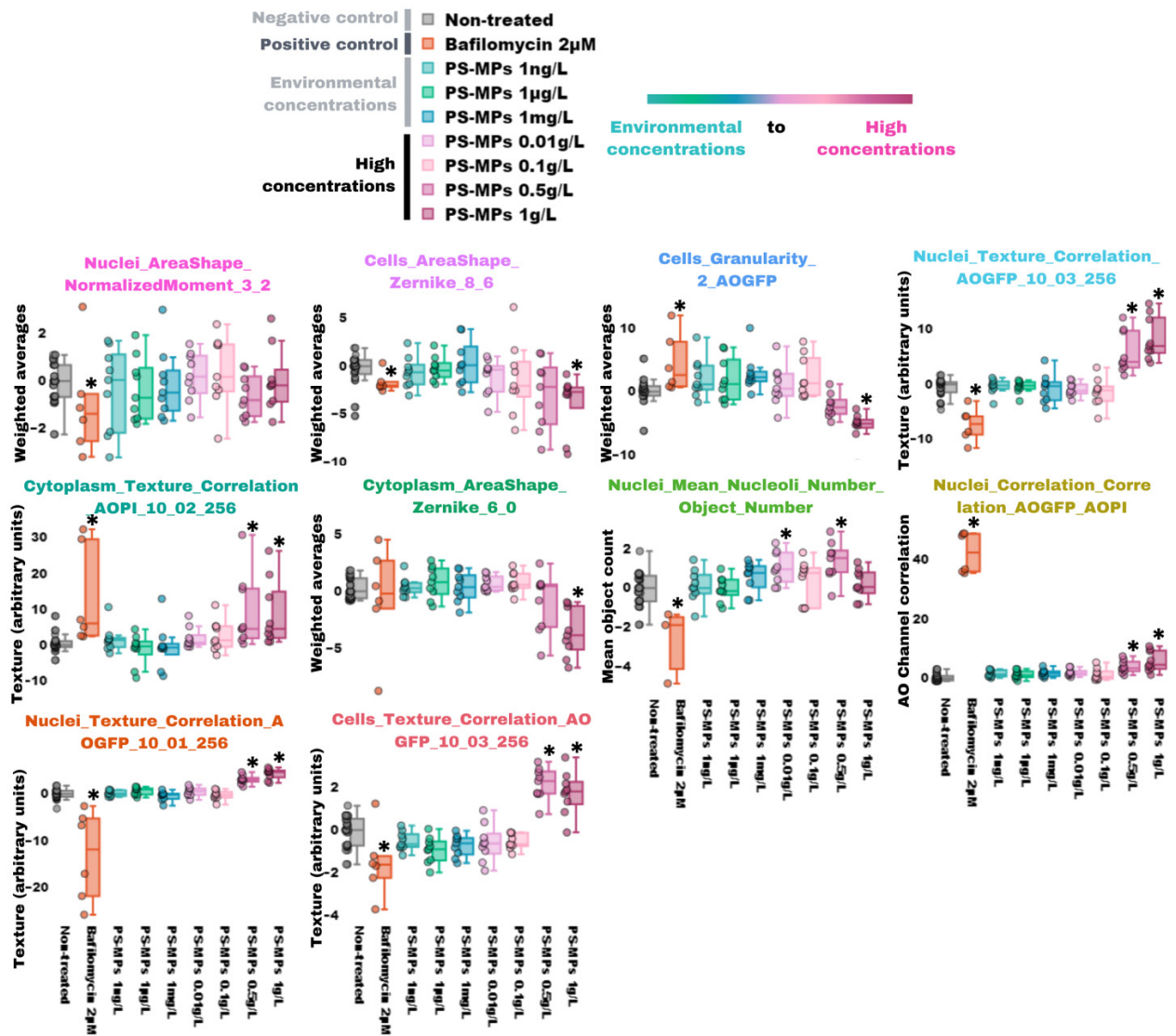


Fig. S9.4 – Top 10 Feature Vectors from LDA Analysis of Data from the Live Cell Painting Assay with HepG2 Cells.

Figs. S9.3 and S9.4 description: The acquired images from the Live Cell Painting Assay were analyzed using CellProfiler, where objects (cells, nuclei, nucleoli, and cytoplasm) were segmented, and their features extracted. These features were subsequently aggregated by well, normalized relative to the non-treated group, and selected using PyCytominer. LDA was applied for dimensionality reduction and visualization, with vectors representing the 10 features contributing the most to group separation and cell phenotypic profiling. These top 10 features are plotted in the images **(S9.3) for Huh7** and **(S9.4) for HepG2**. Experiments were performed in three independent replicates, and each point in the plots represents well-aggregated data. Statistical analysis was performed using the Kruskal-Wallis test followed by Bonferroni post hoc testing in Jupyter Notebook, utilizing the scipy and statsmodels libraries: * $p \leq 0.05$ indicates statistical significance compared to the non-treated group.

3.3.10. Supplementary Material 10: Cell Painting Assay

3.3.10.1. Materials and Method

3.3.10.1.1. Cell Plating and Exposure

Huh7 and HepG2 cells were plated in 96-well plates at 7,500 and 22,000 cells per well, respectively, and incubated for 24 hours. Next, the cells were exposed in triplicate with PS-MPs (100 μ L) in a concentration range of 1 μ g/L to 1 g/L, with Lactose (10 μ M; Merck, USA) as negative control, and with Amiodarone (10 μ M; Chem-Impex, USA) as the positive control.

3.3.10.1.2. Imaging Protocol

After 24 hours of exposure, the treatment was replaced with MitoTracker™ Deep Red (30 μ L; 0.5 μ M; Invitrogen, USA) solution in FluoroBrite for mitochondrial staining. After 30 minutes of incubation at 37°C, the cells were fixed PFA (100 μ L; 4% w/v) for 20 minutes. Following fixation, the cells were washed twice with 1 \times PBS (100 μ L). Subsequently, the cells were treated with a staining solution (30 μ L) containing Concanavalin A (Con A; 5 μ M), Phalloidin Alexa Fluor 568 (8.25 nM), Wheat Germ Agglutinin Alexa Fluor 555 Conjugate (WGA; 41.7 nM); HCS CellMask™ Blue*¹ (60 μ M), and Hoechst (1.6 μ M) (all from Invitrogen, USA), prepared in a permeabilization solution of 1% (w/v) BSA and 0.1% (v/v) Triton X-100 in 1 \times Hank's Balanced Salt Solution (HBSS, Gibco, USA) for cellular staining. After 30 minutes of incubation at 37°C, the cells were washed twice with 1 \times PBS (100 μ L). Finally, 1 \times PBS with 0.05% (w/v) sodium azide (100 μ L) was added to the wells.

Subsequent fluorescence microscopy images were acquired using a 20 \times objective on the Cytation 5 with the following filter cubes: GFP (green; excitation/emission = 445/510 nm) for Con A, PI (red; excitation/emission = 531/647 nm) for Phalloidin and WGA, CY5 (deep red; excitation/emission = 628/685 nm) for MitoTracker, and DAPI (blue; excitation/emission = 377/447 nm) for CellMask and Hoechst. The detailed steps of image analysis performed in this assay, as well as **Cellular Phenotypic Profiling**, are described in this study under Section 3.1.5.3.

*¹ The SYTO™ Green Fluorescent Nucleic Acid Stain is part of the original Cell Painting protocol (Bray et al., 2016); however, it was excluded from our protocol. SYTO would typically be captured by the GFP filter cube on the Cytation 5, but due to its broad spectral range, it also appears in the PI channel, interfering with the visibility of images intended for the PI channel. To address this limitation, SYTO was replaced with HCS CellMask™ Blue, a plasma membrane marker, to adapt the protocol to our equipment's capabilities.

3.3.10.2. Results and Conclusions

To complement the Live Cell Painting data, we also performed the Cell Painting assay (which involves cell fixation) (Bray et al., 2016) on Huh7 and HepG2 cells. This assay allows for the visualization of the nucleus, cytoplasm, endoplasmic reticulum, Golgi apparatus, alpha-actin cytoskeleton, and mitochondria of the cells (Fig. S10.1). However, the set of fluorophores used in Cell Painting allowed for high-quality segmentation only in Huh7 cells, making data extraction from HepG2 cells infeasible (Fig. S10.2). The main finding from the Cell Painting assay in Huh7 cells was an increase in MitoTracker integrated fluorescence intensity in the cytoplasm of cells treated with 0.1 g/L PS-MPs (Fig. S10.3, item D), suggesting mitochondrial alterations. Additionally, MitoTracker fluorescence was observed in the nuclei of Huh7 cells treated with 0.1 and 1 g/L PS-MPs (Fig. S10.3, item F). This nuclear fluorescence may indicate mitochondrial integrity compromise, allowing tagged proteins to leak into other cellular compartments, including the nucleus; metabolic or transport alterations; or changes in cell or vesicular permeability due to increased endocytosis or related processes associated with PS-MPs internalization (Ding et al., 2021; Liu et al., 2021; Zhitomirsky et al., 2018).

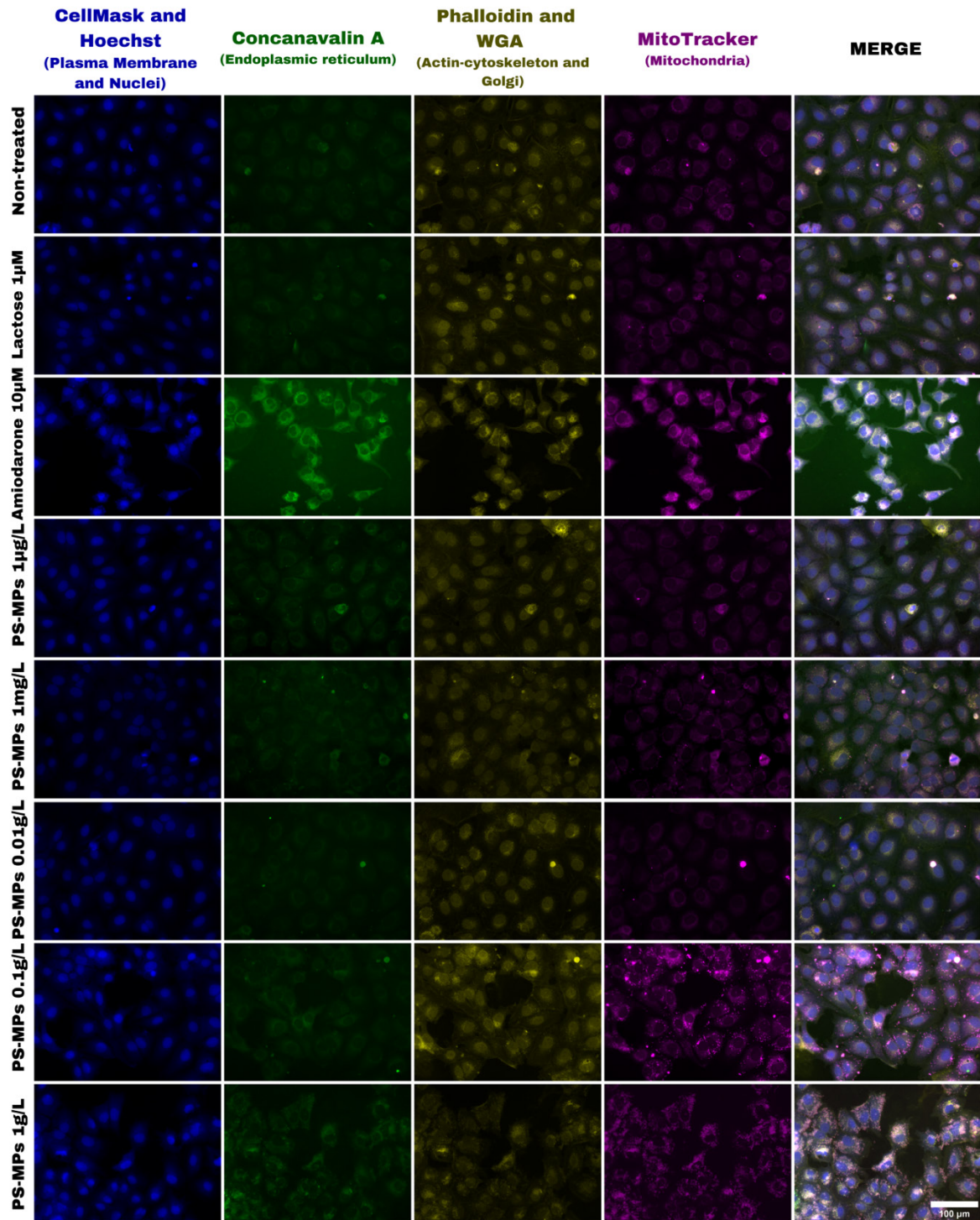


Fig. S10.1 – Representative Fluorescence Microscopy Images from Cell Painting Assay of Huh7 Cells Exposed to PS-MPs. Huh7 cells were plated at density of 7,500 cells per well, in 96-well plate. After 24 hours, cells were treated in triplicate with PS-MPs (1 μg/L, 1 mg/L, 0.01 g/L, 0.1g/L and 1 g/L), with Lactose (1 μM; negative control) and Amiodarone (10 μM; positive

control) for 24 hours. Images were acquired (Cytation 5, 20× objective) after cell fixation and staining with Hoechst (nuclei blue stain), CellMask Blue (plasma membrane blue stain), Concanavalin A (endoplasmic reticulum green stain), Phalloidin and WGA (Actin-cytoskeleton and Golgi red stains, but represented in yellow in images) and MitoTracker Deep Red (mitochondria deep red stain, but represented in magenta in images). The white scale bar in the lower right corner of the images in the fourth column indicates a scale of 100 μm . Experiments were conducted in three independent replicates.

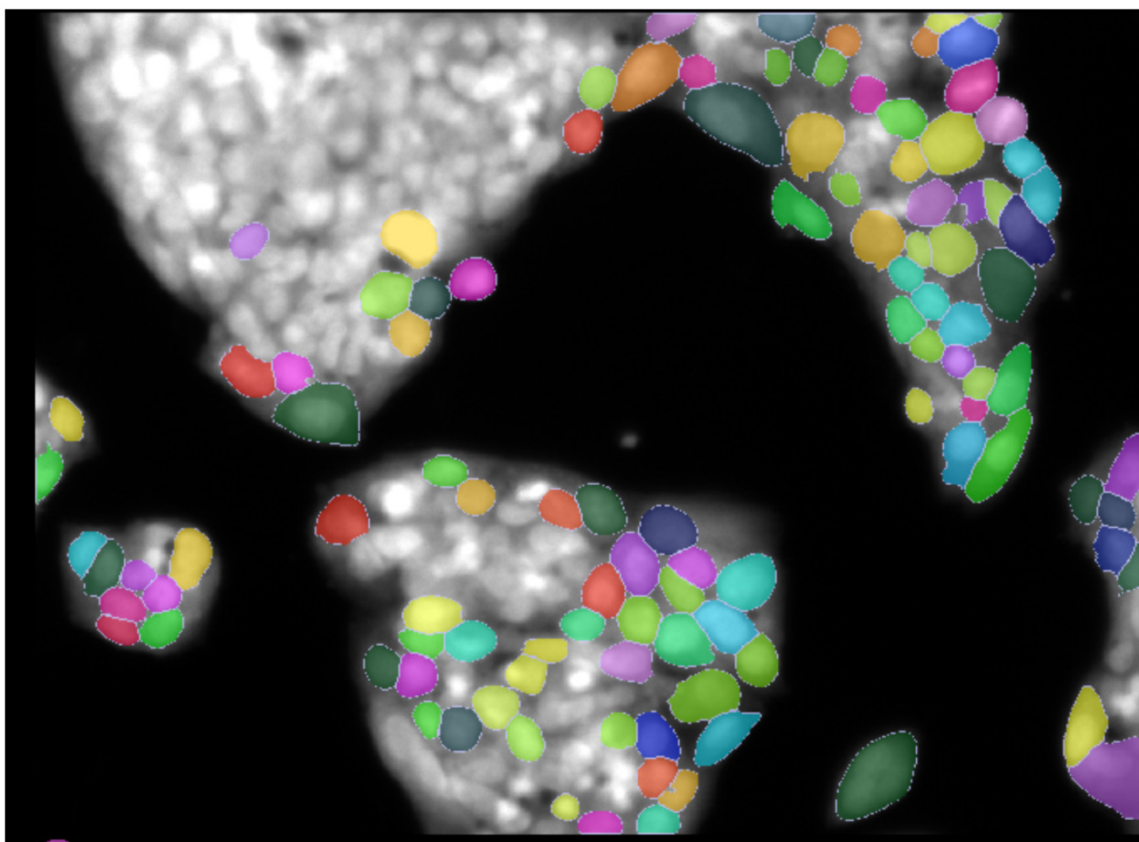


Fig. S10.2 – Cell Segmentation of CellMask and Hoechst Staining in HepG2 Cells Using Cellpose Software. The combination of dyes used in the Cell Painting assay for HepG2 did not allow for proper cell segmentation (represented by the colored areas); therefore, no data were extracted from the Cell Painting assay with HepG2.

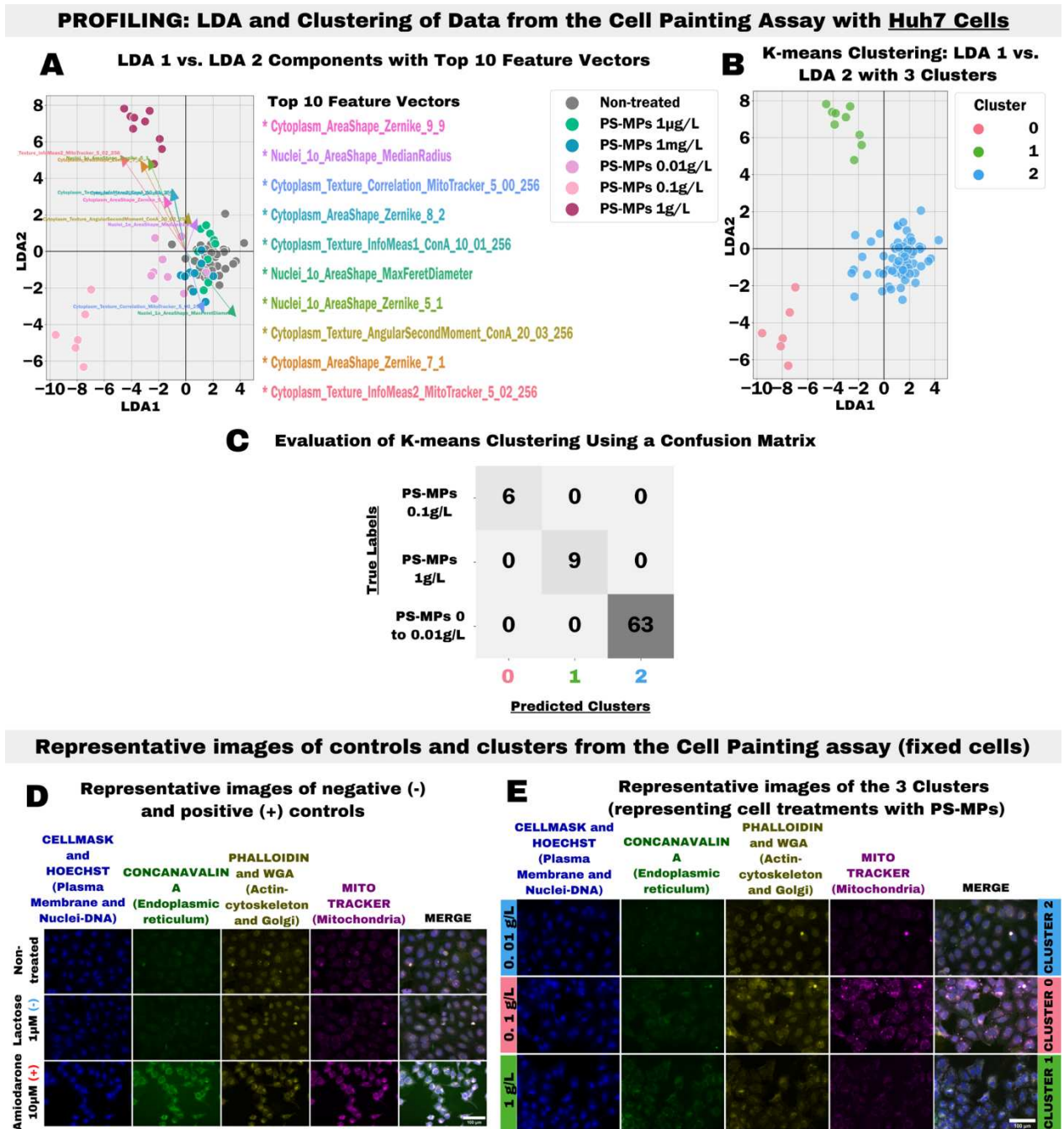


Fig. S10.3 – Cell Phenotypic Profiling of Huh7 Cells after treatment with PS-MPs using the Cell Painting assay. Huh7 cells were plated at a density of 7,500 cells per well in 96-well plates. After 24 hours, cells were treated in triplicate with PS-MPs (1 µg/L, 1 mg/L, 0.01 g/L, 0.1 g/L, and 1 g/L), with Amiodarone (10 µM) as a positive control and Lactose (1 µM) as a negative control. The exposure time was 24 hours. After exposure, cells were fixed and stained with Hoechst (nuclei blue stain), CellMask Blue (plasma membrane blue stain), Concanavalin A (endoplasmic reticulum green stain), Phalloidin and WGA (Actin-cytoskeleton and Golgi red

stains, but represented in yellow in images) and MitoTracker Deep Red (mitochondria deep red stain, but represented in magenta in images). Images were acquired using a Cytation 5 (20× objective), and the images were analyzed using CellProfiler, where objects (cells, nuclei, and cytoplasm) were segmented, and their features extracted. These features were subsequently aggregated by well, normalized relative to the non-treated group, and selected using PyCytominer. **(A)** LDA was applied for dimensionality reduction and visualization, with vectors representing the 10 features contributing most to group separation plotted. **(B)** K-means clustering grouped treatments based on similar feature variances. **(C)** A confusion matrix validated the clusters obtained by K-means. **(D)** Representative fluorescence microscopy images of Huh7 cells that were non-treated (negative control), treated with the positive control (Amiodarone (10 μ M)) and the negative control (Lactose (1 μ M)). **(E)** Representative fluorescence microscopy images of each cluster obtained from the Huh7 phenotypic profiling, represented by treatments with PS-MPs at 0.01 g/L, 0.1 g/L, and 1 g/L. The white scale bar in the lower right corner of the (D) and (E) images in the fifth column indicates a scale of 100 μ m. Experiments were performed in three independent replicates, and each point in the plots represents well-aggregated data.

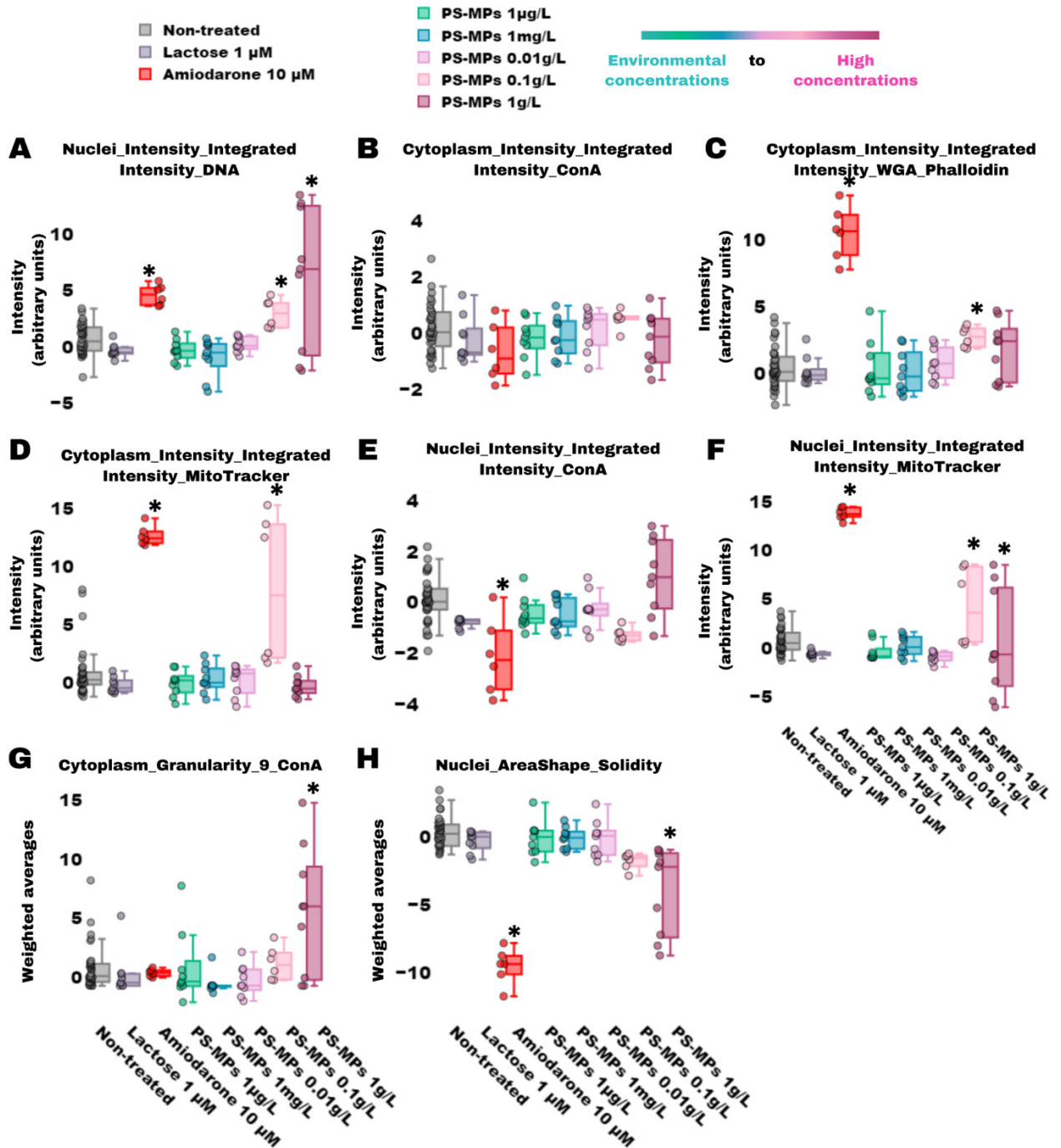


Fig. S10.4 – Biologically Interpretable Huh7 Cells Features from CellPainting Assay Selected after LDA and Morpheus feature selection. Huh7 cells were plated at a density of 7,500 cells per well in 96-well plates. After 24 hours, cells were treated in triplicate with PS-MPs (1 μ g/L, 1 mg/L, 0.01 g/L, 0.1 g/L, and 1 g/L), with Amiodarone (10 μ M) as a positive control and Lactose (1 μ M) as a negative control. The exposure time was 24 hours. After exposure, cells were fixed and stained with Hoechst (nuclei stain), CellMask Blue (plasma membrane stain),

Concanavalin A (endoplasmic reticulum stain), Phalloidin and WGA (Actin-cytoskeleton and Golgi stains) and MitoTracker Deep Red (mitochondria stain). Images were acquired using a Cytation 5 (20× objective), and the images were analyzed using CellProfiler, where objects (cells, nuclei, and cytoplasm) were segmented, and their features extracted. These features were subsequently aggregated by well, normalized relative to the non-treated group, and selected using PyCytominer. LDA analysis was used to list important features for each of the five components, enabling the selection of biologically interpretable features. Morpheus software was also used for this purpose, performing marker selection (t-test) between the non-treated group and groups treated with the highest concentrations of PS-MPs (0.1 and 1 g/L). **(A-H)** Plots of the features of Huh7 cells selected by LDA and Morpheus analysis that were considered clearly biologically interpretable. Experiments were performed in three independent replicates, and each point in the plots represents well-aggregated data. Statistical analysis was performed using the Kruskal-Wallis test followed by Bonferroni post hoc testing in Jupyter Notebook, utilizing the scipy and statsmodels libraries: * $p \leq 0.05$ indicates statistical significance compared to the non-treated group.

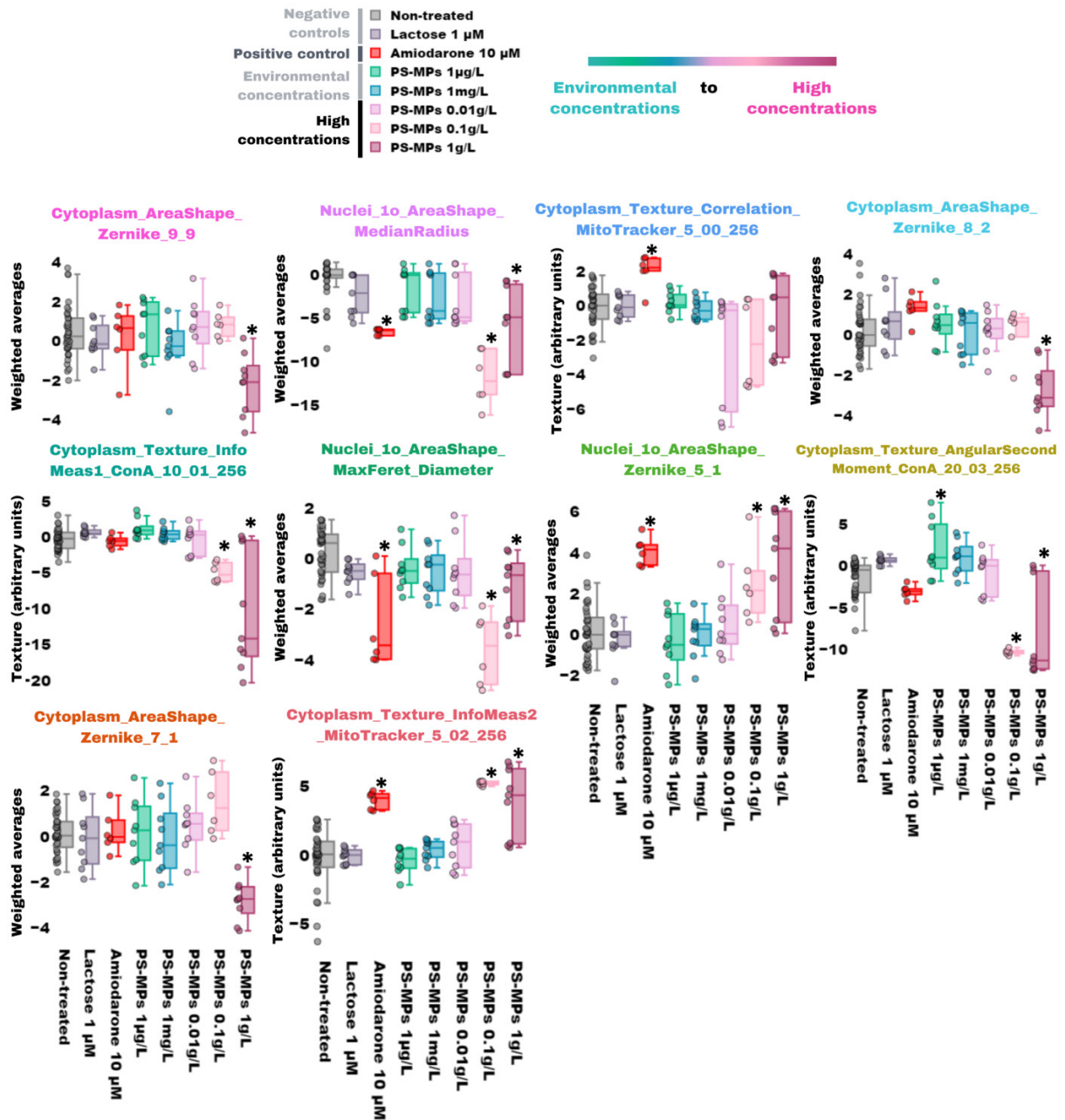


Fig. S10.5 – Top 10 Feature Vectors from LDA Analysis of Data from the Live Cell Painting Assay with Huh7 Cells. The acquired images from the Cell Painting Assay were analyzed using CellProfiler, where objects (cells, nuclei, nucleoli, and cytoplasm) were segmented, and their features extracted. These features were subsequently aggregated by well, normalized relative to the non-treated group, and selected using PyCytominer. LDA was applied for dimensionality reduction and visualization, with vectors representing the 10 features contributing the most to group separation and cell phenotypic profiling. These top 10 features are plotted in the images. Experiments were performed in three independent replicates, and

each point in the plots represents well-aggregated data. Statistical analysis was performed using the Kruskal-Wallis test followed by Bonferroni post hoc testing in Jupyter Notebook, utilizing the `scipy` and `statsmodels` libraries: * $p \leq 0.05$ indicates statistical significance compared to the non-treated group.

4. DISCUSSION

In this study, we aimed to investigate the phenotypic alterations triggered by PS-MPs in two human hepatocyte models (Huh7 and HepG2), using 24-hour exposures at environmentally relevant concentrations (ng to mg/L) and higher concentrations (up to 0.01 g/L). We determined that PS-MPs can be internalized by both Huh7 and HepG2 cells, leading to distinct phenotypic alterations, particularly at higher concentrations. The various HCA assays in this study used different cell dyes to visualize subcellular structures including the nucleus, nucleolus, cytoplasm, lysosomes, acidic vesicles, mitochondria, endoplasmic reticulum, Golgi complex, and alpha-actin cytoskeleton. This approach provided a comprehensive view of the cell as a whole (Calcein-PI-Hoechst, Live Cell Painting, and Cell Painting assays). Furthermore, we applied complex image processing and analysis techniques using CellProfiler and Cellpose softwares to capture the largest number of cellular features potentially altered by PS-MPs exposure. The data from thousands of images were processed using programming to construct phenotypic profiles of cells exposed to PS-MPs. As indicated by our results, our findings will significantly contribute to addressing existing gaps in the literature regarding the toxicological effects of MPs on human hepatocytes.

One of our main findings, which was consistent across both cell lines, was the increased viability and reduced cell death in Huh7 and HepG2 cells following treatment with PS-MPs at concentrations higher than environmental levels (i.e., 0.5 and 1 g/L). The pattern of increased cell viability was also observed in other studies that used the MTT assay to investigate the cytotoxicity of MPs in other cellular models, such as AGS (human gastric cancer), MDCK (canine kidney), L929 (murine fibroblast) and HUVEC (vascular endothelial cells), which showed a dose-dependent increase in viability (concentrations of 1 to 20 g/L of PS and PE MPs) (Rafazi et al., 2024; Palaniappan et al., 2022; Lu et al., 2023). However, we did not find reports in the literature showing an increase in cell viability accompanied by a reduction in dead cells, yet without a concurrent increase in cell proliferation, as observed in our study. This finding may suggest that exposure of Huh7 and HepG2 cells to PS-MPs (0.5 μm and negative surface charge) could induce adaptive responses in these cell lines by activating cell survival pathways.

It is important to highlight that Huh7 and HepG2 cells are carcinoma-derived cell lines. Notably, previous studies have demonstrated that certain cancer-derived cell lines frequently exhibit dysregulated survival signaling pathways, such as the PI3K/Akt pathway. This pathway can be activated by stress factors, including microplastics (Koundouros & Poulogiannis, 2018), potentially contributing to the prevention of cell death and the promotion of stress resistance. In Western blot experiment, which we performed only once, we did not observe significant

differences in Akt expression between treated cells and the control. This may suggest that the activation of these cell survival pathways, if it occurs, may require a larger number of experimental repetitions to reveal significant differences or may involve other types of proteins in these pathways. Therefore, our results suggest that PS-MPs, by decreasing the number of dead cells, may be altering cell survival pathways in HepG2 and Huh7 cell lines suggesting a potential protective effect against cell death under conditions of exposure to high concentrations of PS-MPs (0.5 and 1 g/L). However, only future studies investigating these specific pathways will be able to better clarify the underlying mechanisms of the observed cellular response, and necessarily should be repeated on at least three independent days to ensure reliable conclusions.

Another interesting result from our study was the pronounced increase in acidic vesicles in Huh7 cells exposed to high concentrations of PS-MPs (0.5 and 1 g/L). To date, no other study in the literature has reported such a marked increase in acidic vesicles triggered by PS-MPs. One hypothesis is that the increase in acidic vesicles could be related to the endocytic machinery involved in PS-MPs internalization. This is supported by the fact that Huh7 cells internalized a greater amount of PS-MPs at the same concentration and time point compared to HepG2 cells (Fig. S8), and only Huh7 cells exhibited a significant increase in acidic vesicles. This difference in the rate of PS-MPs internalization is likely attributable to the distinct growth patterns of these cell lines: Huh7 cells grow as single cells, unlike HepG2 cells, which form clusters. This provides Huh7 cells with a larger surface area to interact with the medium in which PS-MPs are dispersed. Another hypothesis for the increase in acidic vesicles in Huh7 cells is cellular autophagy or senescence, as cells undergoing these processes often exhibit an increase in acidic vesicles and delayed cell death due to their resistance to apoptosis and prolonged survival under stress (Volpe et al., 2023; Tanaka & Takahashi, 2020). However, to confirm the cellular events responsible for the increase in acidic vesicles in Huh7 cells, further detailed molecular studies are required.

Furthermore, we demonstrated that HepG2 cells exposed to high concentrations of PS-MPs (0.5 and 1 g/L) exhibited cellular disaggregation. This finding is supported by other studies, which have reported similar disaggregation in HepG2, A549 (human alveolar), and HT-29 (human intestinal) cells treated with 5 to 100 g/L of PS-MPs (Goodman et al., 2022; Goodman et al., 2021; Visalli et al., 2021). However, none of these studies investigated the specific localization of PS-MPs within the cells or whether the cells internalized these particles, which we addressed in our study. Using confocal microscopy, we demonstrated that HepG2 cells internalize PS-MPs, particularly those located at the periphery of cellular clusters (i.e., more

exposed to the medium). Once internalized, PS-MPs in HepG2 cells, unlike in Huh7 cells, tend to concentrate near the plasma membrane after 24 hours. Additionally, some confocal microscopy images of HepG2 cells revealed individual cells detached from the clusters, with the entire circumference of the plasma membrane densely occupied by PS-MPs (Fig. S8). This observation suggests that the accumulation of PS-MPs near the plasma membrane may impair cell–cell communication and junctions. Over time, this could lead to the detachment of cells at the periphery of the clusters as internalization increases, ultimately causing cellular cluster disaggregation. To explore whether PS-MPs influence the expression of cell junction proteins in HepG2 cells, such as ZO-1 and β -Catenin, we conducted a preliminary immunofluorescence and Western blot assay. However, no statistically significant differences were observed. Additional replicates will be necessary to draw definitive conclusions regarding the impact of PS-MPs on the expression of these proteins.

Finally, a clear difference in responses was observed within each cell line, Huh7 and HepG2, depending on the concentration of PS-MPs: environmental concentrations (1 ng/L to 1 mg/L) versus higher concentrations (0.01 to 1 g/L). While environmental concentrations did not induce significant changes in most of the parameters assessed in this study, higher concentrations triggered several phenotypic alterations in both cell lines, as outlined earlier. These findings align with previous studies that also compared environmental and higher concentration ranges (Cheng et al., 2022; Hwang et al., 2020). This pattern is further supported by the Total Cell Association of Fluorescent PS-MPs assay (Section 3.2.3), which demonstrated that at concentration of 1 mg/L, even after 24 hours, the amount of PS-MPs associated with cells was significantly lower compared to higher concentrations. Consequently, cellular alterations at environmental concentrations were statistically insignificant.

Although this study demonstrated that MPs at current human exposure concentrations do not induce cellular alterations associated with *in vitro* hepatotoxicity, it is crucial to avoid limiting conclusions about the potential risks of MPs to human health solely to these concentrations. Human exposure to MPs is continuous, primarily through food, water, and air, with reported exposure levels ranging from ng/L to μ g/L (as quantified in human blood; Leonard et al., 2024) and up to mg/L (via dietary intake; Senathirajah et al., 2021). However, human cells are capable of internalizing these particles, which may accumulate within the cellular microenvironment over time, potentially leading to local concentrations exceeding mg/L. Furthermore, environmental concentrations of MPs are expected to rise due to the ongoing fragmentation of existing plastic waste and the alarming increase in global plastic production and plastic waste release into the environment. As a result, the magnitude of environmental MPs concentrations could significantly

increase in the coming decades. Evaluating MPs at concentrations exceeding current environmental levels is therefore critical, as it allows for the simulation of future exposure scenarios and provides a broader understanding of their potential impacts on human health.

Although our study produced results consistent with existing literature and introduced novel findings, certain limitations must be acknowledged. First, the 24-hour exposure period may not fully capture the long-term effects of MPs on Huh7 and HepG2 cells. Prolonged exposure studies could provide more comprehensive insights into the chronic impacts of these particles, which is particularly relevant given the continuous human exposure to MPs. Additionally, the potential interference from PS-MPs precipitates at higher concentrations should be considered in certain assays, particularly in the HepatotoxPath and Steatosis assays (**Appendices 5 and 6**), where artifacts might influence quantitative fluorescence analyses due to the instability and aggregation (with autofluorescence) tendency of Spherotec PS-MPs. Another limitation is the exclusive use of cancer-derived cell lines (Huh7 and HepG2). While these models are commonly employed, they may exhibit metabolic and physiological traits distinct from those of normal hepatocytes. Furthermore, although the approaches utilized in this study were robust, they were primarily investigative in nature and, therefore, provide a relatively narrow perspective on specific cellular processes. Future research could benefit from incorporating complementary methodologies, such as molecular assays, to explore broader molecular changes induced by MPs.

Despite these limitations, our study provides valuable contributions to the field of MPs hepatotoxicity by highlighting cellular phenotypic alterations that may be considered elements of adverse outcome pathways (AOPs). These findings can serve as a starting point for further investigations to better understand the effects of MPs on human hepatocytes. In addition to supporting the limited number of studies currently available on MPs toxicity, the specific cellular alterations demonstrated in this study could aid in the development of AOPs for MPs in hepatic cells. This would provide useful tools for assessing the health risks posed by these particles and contribute to building a more reliable and reproducible database for evaluating the potential risks of MPs in humans.

5. CONCLUSION

Our study demonstrates that PS-MPs can be internalized by Huh7 and HepG2 cells, leading to significant phenotypic alterations, particularly at higher concentrations compared to environmental levels. A notable finding was the significant decrease in the number of dead Huh7 and HepG2 cells after exposure to PS-MPs, which may be related to the activation of cell survival pathways—an observation that, to the best of our knowledge, has not been previously reported in the literature. Furthermore, another novel finding was the marked increase in acidic vesicles in Huh7 cells, which resembles what occurs in autophagy and senescence processes. Additionally, supporting previous findings in the literature, HepG2 cells exhibited cell disaggregation, which may be linked to the accumulation of PS-MPs near the plasma membrane in these cells. However, no significant cellular phenotypic alterations were observed at environmentally relevant concentrations associated with human exposure to PS-MPs. While higher concentrations represent extreme scenarios, it is important to consider that human exposure to MPs is cumulative and occurs on a daily basis, and the environmental concentration of MPs is expected to rise over time. Our findings contribute to a deeper understanding of the hepatotoxic potential of PS-MPs in humans and highlight elements of Adverse Outcome Pathways (AOPs) associated with different PS-MP concentrations. These specific cellular alterations could serve as a starting point for future research into the mechanisms underlying the effects of PS-MPs on human hepatocytes and support the development of AOPs for MPs in hepatic cells, providing useful tools for assessing the health risks posed by these particles to humans.

6. REFERENCES

- Adam, A.A.A., van der Mark, V.A., Donkers, J.M., Wildenberg, M.E., Oude Elferink, R.P.J., Chamuleau, R.A.F.M., Hoekstra, R., 2018. A practice-changing culture method relying on shaking substantially increases mitochondrial energy metabolism and functionality of human liver cell lines. *PLoS One* 13, e0193664. <https://doi.org/10.1371/journal.pone.0193664>
- Akhbarizadeh, R., Moore, F., Keshavarzi, B., 2018. Investigating a probable relationship between microplastics and potentially toxic elements in fish muscles from northeast of Persian Gulf. *Environmental Pollution* 232, 154–163. <https://doi.org/10.1016/j.envpol.2017.09.028>
- Alberghini, L., Truant, A., Santonicola, S., Colavita, G., Giaccone, V., 2023. Microplastics in Fish and Fishery Products and Risks for Human Health: A Review. *International Journal of Environmental Research and Public Health* 20, 789. <https://doi.org/10.3390/ijerph20010789>
- Amit, S.K., Iain, G., R., S.O., Christopher, L.S., Ernesto, C., Kirk, R.H., Abdul, E.M., Deepak, K.D., Jae, S.L., Yasuhiro, N., John, P.O., Jason, B., Shawn, P.H., 2005. A Comprehensive Listing of Bioactivation Pathways of Organic Functional Groups. *Current Drug Metabolism* 6, 161–225.
- Anguissola, S., Garry, D., Salvati, A., O'Brien, P.J., Dawson, K.A., 2014. High Content Analysis Provides Mechanistic Insights on the Pathways of Toxicity Induced by Amine-Modified Polystyrene Nanoparticles. *PLoS One* 9, e108025. <https://doi.org/10.1371/journal.pone.0108025>
- Arzumanian, V.A., Kiseleva, O.I., Poverennaya, E.V., 2021. The Curious Case of the HepG2 Cell Line: 40 Years of Expertise. *International Journal of Molecular Sciences* 22, 13135. <https://doi.org/10.3390/ijms222313135>
- Baeza-Martínez, C., Olmos, S., González-Pleiter, M., López-Castellanos, J., García-Pachón, E., Masiá-Canuto, M., Hernández-Blasco, L., Bayo, J., 2022. First evidence of microplastics isolated in European citizens' lower airway. *Journal of Hazardous Materials* 438, 129439. <https://doi.org/10.1016/j.jhazmat.2022.129439>
- Banaei, M., Forouzanfar, M., Jafarinia, M., 2022. Toxic effects of polyethylene microplastics on transcriptional changes, biochemical response, and oxidative stress in common carp (*Cyprinus carpio*). *Comparative Biochemistry and Physiology Part C: Toxicology & Pharmacology* 261, 109423. <https://doi.org/10.1016/j.cbpc.2022.109423>
- Bandi, S., Viswanathan, P., Gupta, S., 2014. Evaluation of Cytotoxicity and DNA Damage Response with Analysis of Intracellular ATM Signaling Pathways. *ASSAY and Drug Development Technologies* 12, 272–281. <https://doi.org/10.1089/adt.2014.571>
- Banerjee, A., Billey, L.O., McGarvey, A.M., Shelper, W.L., 2022. Effects of polystyrene micro/nanoplastics on liver cells based on particle size, surface functionalization, concentration

- and exposure period. *Science of The Total Environment* 836, 155621. <https://doi.org/10.1016/j.scitotenv.2022.155621>
- Barboza, L.G.A., Lopes, C., Oliveira, P., Bessa, F., Otero, V., Henriques, B., Raimundo, J., Caetano, M., Vale, C., Guilhermino, L., 2020. Microplastics in wild fish from North East Atlantic Ocean and its potential for causing neurotoxic effects, lipid oxidative damage, and human health risks associated with ingestion exposure. *Science of The Total Environment* 717, 134625. <https://doi.org/10.1016/j.scitotenv.2019.134625>
- Barrett, J., Chase, Z., Zhang, J., Holl, M.M.B., Willis, K., Williams, A., Hardesty, B.D., Wilcox, C., 2020. Microplastic Pollution in Deep-Sea Sediments From the Great Australian Bight. *Front. Mar. Sci.* 7. <https://doi.org/10.3389/fmars.2020.576170>
- Begrache, K., Massart, J., Robin, M.-A., Borgne-Sanchez, A., Fromenty, B., 2011. Drug-induced toxicity on mitochondria and lipid metabolism: Mechanistic diversity and deleterious consequences for the liver. *Journal of Hepatology* 54, 773–794. <https://doi.org/10.1016/j.jhep.2010.11.006>
- BfR, Shopova, S., Sieg, H., Braeuning, A., 2020. Risk assessment and toxicological research on micro- and nanoplastics after oral exposure via food products. *EFSA Journal* 18, e181102. <https://doi.org/10.2903/j.efsa.2020.e181102>
- Brahney, J., Hallerud, M., Heim, E., Hahnenberger, M., Sukumaran, S., 2020. Plastic rain in protected areas of the United States. *Science* 368, 1257–1260. <https://doi.org/10.1126/science.aaz5819>
- Bratosin, D., Mitrofan, L., Palli, C., Estaquier, J., Montreuil, J., 2005. Novel fluorescence assay using calcein-AM for the determination of human erythrocyte viability and aging. *Cytometry A* 66, 78–84. <https://doi.org/10.1002/cyto.a.20152>
- Bray, M.-A., Singh, S., Han, H., Davis, C.T., Borgeson, B., Hartland, C., Kost-Alimova, M., Gustafsdottir, S.M., Gibson, C.C., Carpenter, A.E., 2016. Cell Painting, a high-content image-based assay for morphological profiling using multiplexed fluorescent dyes. *Nat Protoc* 11, 1757–1774. <https://doi.org/10.1038/nprot.2016.105>
- Broad Institute, 2024. Morpheus [WWW Document]. URL <https://software.broadinstitute.org/morpheus/> (accessed 1.12.25).
- Canha, N., Jafarova, M., Grifoni, L., Gamelas, C.A., Alves, L.C., Almeida, S.M., Loppi, S., 2023. Microplastic contamination of lettuces grown in urban vegetable gardens in Lisbon (Portugal). *Sci Rep* 13, 14278. <https://doi.org/10.1038/s41598-023-40840-z>
- Capó, X., Company, J.J., Alomar, C., Compa, M., Sureda, A., Grau, A., Hansjosten, B., López-Vázquez, J., Quintana, J.B., Rodil, R., Deudero, S., 2021. Long-term exposure to virgin and seawater exposed microplastic enriched-diet causes liver oxidative stress and inflammation in

- gilthead seabream *Sparus aurata*, Linnaeus 1758. *Science of The Total Environment* 767, 144976. <https://doi.org/10.1016/j.scitotenv.2021.144976>
- Carpenter, A.E., Jones, T.R., Lamprecht, M.R., Clarke, C., Kang, I.H., Friman, O., Guertin, D.A., Chang, J.H., Lindquist, R.A., Moffat, J., Golland, P., Sabatini, D.M., 2006. CellProfiler: image analysis software for identifying and quantifying cell phenotypes. *Genome Biology* 7, R100. <https://doi.org/10.1186/gb-2006-7-10-r100>
- Carr, S.A., Liu, J., Tesoro, A.G., 2016. Transport and fate of microplastic particles in wastewater treatment plants. *Water Res* 91, 174–182. <https://doi.org/10.1016/j.watres.2016.01.002>
- Chatterjee, S., Sharma, S., 2019. Microplastics in our oceans and marine health. *Field Actions Science Reports. The journal of field actions* 54–61.
- Chen, L., Qi, M., Zhang, L., Yu, F., Tao, D., Xu, C., Xu, S., n.d. Di(2-ethylhexyl) phthalate and microplastics cause necroptosis and apoptosis in hepatocytes of mice by inducing oxidative stress. *Environmental Toxicology* n/a. <https://doi.org/10.1002/tox.23759>
- Chen, R.-J., Chen, Y.-Y., Liao, M.-Y., Lee, Y.-H., Chen, Z.-Y., Yan, S.-J., Yeh, Y.-L., Yang, L.-X., Lee, Y.-L., Wu, Y.-H., Wang, Y.-J., 2020a. The Current Understanding of Autophagy in Nanomaterial Toxicity and Its Implementation in Safety Assessment-Related Alternative Testing Strategies. *International Journal of Molecular Sciences* 21, 2387. <https://doi.org/10.3390/ijms21072387>
- Cheng, W., Li, X., Zhou, Y., Yu, H., Xie, Y., Guo, H., Wang, H., Li, Y., Feng, Y., Wang, Y., 2022. Polystyrene microplastics induce hepatotoxicity and disrupt lipid metabolism in the liver organoids. *Science of The Total Environment* 806, 150328. <https://doi.org/10.1016/j.scitotenv.2021.150328>
- Choi, Y.J., Park, J.W., Lim, Y., Seo, S., Hwang, D.Y., 2021. *In vivo* impact assessment of orally administered polystyrene nanoplastics: biodistribution, toxicity, and inflammatory response in mice. *Nanotoxicology* 15, 1180–1198. <https://doi.org/10.1080/17435390.2021.1996650>
- Cui, J., Zhang, Y., Liu, L., Zhang, Q., Xu, S., Guo, M., 2023. Polystyrene microplastics induced inflammation with activating the TLR2 signal by excessive accumulation of ROS in hepatopancreas of carp (*Cyprinus carpio*). *Ecotoxicology and Environmental Safety* 251, 114539. <https://doi.org/10.1016/j.ecoenv.2023.114539>
- Ding, Y., Zhang, R., Li, B., Du, Y., Li, J., Tong, X., Wu, Y., Ji, X., Zhang, Y., 2021. Tissue distribution of polystyrene nanoplastics in mice and their entry, transport, and cytotoxicity to GES-1 cells. *Environmental Pollution* 280, 116974. <https://doi.org/10.1016/j.envpol.2021.116974>
- Djouina, M., Waxin, C., Dubuquoy, L., Launay, D., Vignal, C., Body-Malapel, M., 2023. Oral exposure to polyethylene microplastics induces inflammatory and metabolic changes and promotes

- fibrosis in mouse liver. *Ecotoxicology and Environmental Safety* 264, 115417. <https://doi.org/10.1016/j.ecoenv.2023.115417>
- Doan, M., Vorobjev, I., Rees, P., Filby, A., Wolkenhauer, O., Goldfeld, A.E., Lieberman, J., Barteneva, N., Carpenter, A.E., Hennig, H., 2018. Diagnostic Potential of Imaging Flow Cytometry. *Trends in Biotechnology* 36, 649–652. <https://doi.org/10.1016/j.tibtech.2017.12.008>
- Dogra, S., Bandi, S., Viswanathan, P., Gupta, S., 2015. Arsenic trioxide amplifies cisplatin toxicity in human tubular cells transformed by HPV-16 E6/E7 for further therapeutic directions in renal cell carcinoma. *Cancer Letters* 356, 953–961. <https://doi.org/10.1016/j.canlet.2014.11.008>
- Dong, R., Zhou, C., Wang, S., Yan, Y., Jiang, Q., 2022. Probiotics ameliorate polyethylene microplastics-induced liver injury by inhibition of oxidative stress in Nile tilapia (*Oreochromis niloticus*). *Fish & Shellfish Immunology* 130, 261–272. <https://doi.org/10.1016/j.fsi.2022.09.022>
- Dris, R., Gasperi, J., Saad, M., Mirande, C., Tassin, B., 2016. Synthetic fibers in atmospheric fallout: A source of microplastics in the environment? *Marine Pollution Bulletin* 104, 290–293. <https://doi.org/10.1016/j.marpolbul.2016.01.006>
- Dyken, J.A., Will, Y., 2007. The significance of mitochondrial toxicity testing in drug development. *Drug Discovery Today* 12, 777–785. <https://doi.org/10.1016/j.drudis.2007.07.013>
- Ebrahimkhani, M.R., Neiman, J.A.S., Raredon, M.S.B., Hughes, D.J., Griffith, L.G., 2014. Bioreactor technologies to support liver function *in vitro*. *Advanced Drug Delivery Reviews, Innovative tissue models for drug discovery and development* 69–70, 132–157. <https://doi.org/10.1016/j.addr.2014.02.011>
- ECHA, 2023. EU action against microplastics. Publications Office of the European Union. Publications Office of the European Union. URL: <https://data.europa.eu/doi/10.2779/917472> (accessed 1.26.25)
- ECHA's SEAC validates a broad ban on microplastics - European Commission, 2020. URL <https://cosmeticobs.com/en/articles/european-commission-45/echas-seac-validates-a-broad-ban-on-microplastics-5606> (accessed 8.17.21)
- FAO, 2022. Microplastics in food commodities. URL: <https://openknowledge.fao.org/handle/20.500.14283/cc2392en> (accessed 1.26.25)
- Feng, Y., Mitchison, T.J., Bender, A., Young, D.W., Tallarico, J.A., 2009. Multi-parameter phenotypic profiling: using cellular effects to characterize small-molecule compounds. *Nat Rev Drug Discov* 8, 567–578. <https://doi.org/10.1038/nrd2876>
- Fritsche, E., Haarmann-Stemmann, T., Kapr, J., Galanjuk, S., Hartmann, J., Mertens, P.R., Kämpfer, A.A.M., Schins, R.P.F., Tigges, J., Koch, K., 2021. Stem Cells for Next Level Toxicity Testing in the 21st Century. *Small* 17, 2006252. <https://doi.org/10.1002/sml.202006252>

- Gambino, I., Bagordo, F., Grassi, T., Panico, A., De Donno, A., 2022. Occurrence of Microplastics in Tap and Bottled Water: Current Knowledge. *Int J Environ Res Public Health* 19, 5283. <https://doi.org/10.3390/ijerph19095283>
- Garcia-Fossa, F., Cruz, M.C., Haghighi, M., de Jesus, M.B., Singh, S., Carpenter, A.E., Cimini, B.A., 2023. Interpreting Image-based Profiles using Similarity Clustering and Single-Cell Visualization. *Current Protocols* 3, e713. <https://doi.org/10.1002/cpz1.713>
- Garcia-Fossa, F., Moraes-Lacerda, T., Rodrigues-da-Silva, M., Diaz-Rohrer, B., Singh, S., Carpenter, A.E., Cimini, B.A., Jesus, M.B. de, 2024. Live Cell Painting: image-based profiling in live cells using Acridine Orange. <https://doi.org/10.1101/2024.08.28.610144>
- Geyer, R., Jambeck, J.R., Law, K.L., n.d. Production, use, and fate of all plastics ever made. *Science Advances* 3, e1700782. <https://doi.org/10.1126/sciadv.1700782>
- Gigault, J., Halle, A.T., Baudrimont, M., Pascal, P.-Y., Gauffre, F., Phi, T.-L., El Hadri, H., Grassl, B., Reynaud, S., 2018. Current opinion: What is a nanoplastic? *Environ Pollut* 235, 1030–1034. <https://doi.org/10.1016/j.envpol.2018.01.024>
- Giuliano, K.A., Haskins, J.R., Taylor, D.L., 2003. Advances in High Content Screening for Drug Discovery. *ASSAY and Drug Development Technologies* 1, 565–577. <https://doi.org/10.1089/154065803322302826>
- Goodman, A., Carpenter, A.E., 2016. High-Throughput, Automated Image Processing for Large-Scale Fluorescence Microscopy Experiments. *Microscopy and Microanalysis* 22, 538–539. <https://doi.org/10.1017/S1431927616003548>
- Goodman, K.E., Hare, J.T., Khamis, Z.I., Hua, T., Sang, Q.-X.A., 2021. Exposure of Human Lung Cells to Polystyrene Microplastics Significantly Retards Cell Proliferation and Triggers Morphological Changes. *Chem. Res. Toxicol.* 34, 1069–1081. <https://doi.org/10.1021/acs.chemrestox.0c00486>
- Goodman, K.E., Hua, T., Sang, Q.-X.A., 2022. Effects of Polystyrene Microplastics on Human Kidney and Liver Cell Morphology, Cellular Proliferation, and Metabolism. *ACS Omega* 7, 34136–34153. <https://doi.org/10.1021/acsomega.2c03453>
- Grandl, M., Schmitz, G., 2010. Fluorescent high-content imaging allows the discrimination and quantitation of E-LDL-induced lipid droplets and Ox-LDL-generated phospholipidosis in human macrophages. *Cytometry A* 77, 231–242. <https://doi.org/10.1002/cyto.a.20828>
- Guo, L., Dial, S., Shi, L., Branham, W., Liu, J., Fang, J.-L., Green, B., Deng, H., Kaput, J., Ning, B., 2011. Similarities and Differences in the Expression of Drug-Metabolizing Enzymes between Human Hepatic Cell Lines and Primary Human Hepatocytes. *Drug Metabolism and Disposition* 39, 528–538. <https://doi.org/10.1124/dmd.110.035873>

- Halappanavar, S., Nymark, P., Krug, H.F., Clift, M.J.D., Rothen-Rutishauser, B., Vogel, U., 2021. Non-Animal Strategies for Toxicity Assessment of Nanoscale Materials: Role of Adverse Outcome Pathways in the Selection of Endpoints. *Small* 17, 2007628. <https://doi.org/10.1002/smll.202007628>
- Hansjosten, I., Rapp, J., Reiner, L., Vatter, R., Fritsch-Decker, S., Peravali, R., Palosaari, T., Joossens, E., Gerloff, K., Macko, P., Whelan, M., Gilliland, D., Ojea-Jimenez, I., Monopoli, M.P., Rocks, L., Garry, D., Dawson, K., Röttgermann, P.J.F., Murschhauser, A., Rädler, J.O., Tang, S.V.Y., Gooden, P., Belinga-Desaunay, M.-F.A., Khan, A.O., Briffa, S., Guggenheim, E., Papadiamantis, A., Lynch, I., Valsami-Jones, E., Diabaté, S., Weiss, C., 2018. Microscopy-based high-throughput assays enable multi-parametric analysis to assess adverse effects of nanomaterials in various cell lines. *Arch Toxicol* 92, 633–649. <https://doi.org/10.1007/s00204-017-2106-7>
- He, Y., Li, J., Chen, J., Miao, X., Li, G., He, Q., Xu, H., Li, H., Wei, Y., 2020. Cytotoxic effects of polystyrene nanoplastics with different surface functionalization on human HepG2 cells. *Science of The Total Environment* 723, 138180. <https://doi.org/10.1016/j.scitotenv.2020.138180>
- Hernandez, L., Yousefi, N., Tufenkji, N., 2017. Are There Nanoplastics in Your Personal Care Products? *Environmental Science & Technology Letters* 4. <https://doi.org/10.1021/acs.estlett.7b00187>
- Hernandez, L.M., Xu, E.G., Larsson, H.C.E., Tahara, R., Maisuria, V.B., Tufenkji, N., 2019. Plastic Teabags Release Billions of Microparticles and Nanoparticles into Tea. *Environ. Sci. Technol.* 53, 12300–12310. <https://doi.org/10.1021/acs.est.9b02540>
- Holt, M.P., Ju, C., 2006. Mechanisms of drug-induced liver injury. *AAPS J* 8, E48–E54. <https://doi.org/10.1208/aapsj080106>
- Horvatits, T., Tamminga, M., Liu, B., Sebode, M., Carambia, A., Fischer, L., Püschel, K., Huber, S., Fischer, E.K., 2022. Microplastics detected in cirrhotic liver tissue. *EBioMedicine* 82, 104147. <https://doi.org/10.1016/j.ebiom.2022.104147>
- Houle, D., Govindaraju, D.R., Omholt, S., 2010. Phenomics: the next challenge. *Nat Rev Genet* 11, 855–866. <https://doi.org/10.1038/nrg2897>
- Ibrahim, Y.S., Tuan Anuar, S., Azmi, A.A., Wan Mohd Khalik, W.M.A., Lehata, S., Hamzah, S.R., Ismail, D., Ma, Z.F., Dzulkarnaen, A., Zakaria, Z., Mustaffa, N., Tuan Sharif, S.E., Lee, Y.Y., 2020. Detection of microplastics in human colectomy specimens. *JGH Open* 5, 116–121. <https://doi.org/10.1002/jgh3.12457>

- Jouan, E., Le Vée, M., Denizot, C., Parmentier, Y., Fardel, O., 2017. Drug Transporter Expression and Activity in Human Hepatoma HuH-7 Cells. *Pharmaceutics* 9, 3. <https://doi.org/10.3390/pharmaceutics9010003>
- Kedzierski, M., Lechat, B., Sire, O., Le Maguer, G., Le Tilly, V., Bruzard, S., 2020. Microplastic contamination of packaged meat: Occurrence and associated risks. *Food Packaging and Shelf Life* 24, 100489. <https://doi.org/10.1016/j.fpsl.2020.100489>
- Kosuth, M., Mason, S.A., Wattenberg, E.V., 2018. Anthropogenic contamination of tap water, beer, and sea salt. *PLoS One* 13, e0194970. <https://doi.org/10.1371/journal.pone.0194970>
- Koundouros, N., Poulogiannis, G., 2018. Phosphoinositide 3-Kinase/Akt Signaling and Redox Metabolism in Cancer. *Front Oncol* 8, 160. <https://doi.org/10.3389/fonc.2018.00160>
- Kutralam-Muniasamy, G., Pérez-Guevara, F., Elizalde-Martínez, I., Shruti, V.C., 2020. Branded milks – Are they immune from microplastics contamination? *Science of The Total Environment* 714, 136823. <https://doi.org/10.1016/j.scitotenv.2020.136823>
- Laurent, V., Glaise, D., Nübel, T., Gilot, D., Corlu, A., Loyer, P., 2013. Highly efficient SiRNA and gene transfer into hepatocyte-like HepaRG cells and primary human hepatocytes: new means for drug metabolism and toxicity studies. *Methods Mol Biol* 987, 295–314. https://doi.org/10.1007/978-1-62703-321-3_25
- Lehr, C.-M., Poelma, F.G.J., Junginger, H.E., Tukker, J.J., 1991. An estimate of turnover time of intestinal mucus gel layer in the rat in situ loop. *International Journal of Pharmaceutics* 70, 235–240. [https://doi.org/10.1016/0378-5173\(91\)90287-X](https://doi.org/10.1016/0378-5173(91)90287-X)
- Lenz, R., Enders, K., Nielsen, T.G., 2016. Microplastic exposure studies should be environmentally realistic. *PNAS* 113, E4121–E4122. <https://doi.org/10.1073/pnas.1606615113>
- Leonard, S., Liddle, C.R., Atherall, C.A., Chapman, E., Watkins, M., D. J. Calaminus, S., Rotchell, J.M., 2024. Microplastics in human blood: Polymer types, concentrations and characterisation using μ FTIR. *Environment International* 188, 108751. <https://doi.org/10.1016/j.envint.2024.108751>
- Li, J., Yang, D., Li, L., Jabeen, K., Shi, H., 2015. Microplastics in commercial bivalves from China. *Environmental Pollution* 207, 190–195. <https://doi.org/10.1016/j.envpol.2015.09.018>
- Li, L., Xu, M., He, C., Wang, H., Hu, Q., 2022. Polystyrene nanoplastics potentiate the development of hepatic fibrosis in high fat diet fed mice. *Environ Toxicol* 37, 362–372. <https://doi.org/10.1002/tox.23404>
- Li, S., Ma, Y., Ye, S., Tang, S., Liang, N., Liang, Y., Xiao, F., 2021a. Polystyrene microplastics trigger hepatocyte apoptosis and abnormal glycolytic flux via ROS-driven calcium overload. *Journal of Hazardous Materials* 417. <https://doi.org/10.1016/j.jhazmat.2021.126025>

- Li, Siwen, Ma, Y., Ye, S., Tang, S., Liang, N., Liang, Y., Xiao, F., 2021a. Polystyrene microplastics trigger hepatocyte apoptosis and abnormal glycolytic flux via ROS-driven calcium overload. *Journal of Hazardous Materials* 417, 126025. <https://doi.org/10.1016/j.jhazmat.2021.126025>
- Li, S., Shi, M., Wang, Y., Xiao, Y., Cai, D., Xiao, F., 2021b. Keap1-Nrf2 pathway up-regulation via hydrogen sulfide mitigates polystyrene microplastics induced-hepatotoxic effects. *Journal of Hazardous Materials* 402, 123933. <https://doi.org/10.1016/j.jhazmat.2020.123933>
- Li, Y., Peng, L., Fu, J., Dai, X., Wang, G., 2022. A microscopic survey on microplastics in beverages: the case of beer, mineral water and tea. *Analyst* 147, 1099–1105. <https://doi.org/10.1039/D2AN00083K>
- Liebezeit, G., Liebezeit, E., 2013. Non-pollen particulates in honey and sugar. *Food Addit Contam Part A Chem Anal Control Expo Risk Assess* 30, 2136–2140. <https://doi.org/10.1080/19440049.2013.843025>
- Liu, L., Xu, K., Zhang, B., Ye, Y., Zhang, Q., Jiang, W., 2021. Cellular internalization and release of polystyrene microplastics and nanoplastics. *Science of The Total Environment* 779, 146523. <https://doi.org/10.1016/j.scitotenv.2021.146523>
- Lu, T., Yuan, X., Sui, C., Yang, C., Li, D., Liu, H., Zhang, G., Li, G., Li, S., Zhang, J., Zhou, L., Xu, M., 2024. Exposure to Polypropylene Microplastics Causes Cardiomyocyte Apoptosis Through Oxidative Stress and Activation of the MAPK-Nrf2 Signaling Pathway. *Environmental Toxicology* 39, 5371–5381. <https://doi.org/10.1002/tox.24411>
- Lu, Y., Cao, M., Tian, M., Huang, Q., 2023. Internalization and cytotoxicity of polystyrene microplastics in human umbilical vein endothelial cells. *Journal of Applied Toxicology* 43, 262–271. <https://doi.org/10.1002/jat.4378>
- Luo, T., Wang, C., Pan, Z., Jin, C., Fu, Z., Jin, Y., 2019. Maternal Polystyrene Microplastic Exposure during Gestation and Lactation Altered Metabolic Homeostasis in the Dams and Their F1 and F2 Offspring. *Environ. Sci. Technol.* 53, 10978–10992. <https://doi.org/10.1021/acs.est.9b03191>
- MacLeod, M., Arp, H.P.H., Tekman, M.B., Jahnke, A., 2021. The global threat from plastic pollution. *Science* 373, 61–65. <https://doi.org/10.1126/science.abg5433>
- Mandavilli, B.S., Janes, M.S., 2010. Detection of Intracellular Glutathione Using ThiolTracker Violet Stain and Fluorescence Microscopy. *Current Protocols in Cytometry* 53, 9.35.1-9.35.8. <https://doi.org/10.1002/0471142956.cy0935s53>
- Massardo, S., Verzola, D., Alberti, S., Caboni, C., Santostefano, M., Eugenio Verrina, E., Angeletti, A., Lugani, F., Ghiggeri, G.M., Bruschi, M., Candiano, G., Rumeo, N., Gentile, M., Cravedi, P., La Maestra, S., Zaza, G., Stallone, G., Esposito, P., Viazzi, F., Mancianti, N., La Porta, E., Artini, C., 2024. MicroRaman spectroscopy detects the presence of microplastics in human urine and

- kidney tissue. *Environment International* 184, 108444. <https://doi.org/10.1016/j.envint.2024.108444>
- Morris, S.A., 2019. The evolving concept of cell identity in the single cell era. *Development* 146. <https://doi.org/10.1242/dev.169748>
- Mosmann, T., 1983. Rapid colorimetric assay for cellular growth and survival: application to proliferation and cytotoxicity assays. *J Immunol Methods* 65, 55–63. [https://doi.org/10.1016/0022-1759\(83\)90303-4](https://doi.org/10.1016/0022-1759(83)90303-4)
- Napper, I.E., Bakir, A., Rowland, S.J., Thompson, R.C., 2015. Characterisation, quantity and sorptive properties of microplastics extracted from cosmetics. *Marine Pollution Bulletin* 99, 178–185. <https://doi.org/10.1016/j.marpolbul.2015.07.029>
- Nitulescu, G.M., Van De Venter, M., Nitulescu, G., Ungurianu, A., Juzenas, P., Peng, Q., Olaru, O.T., Grădinaru, D., Tsatsakis, A., Tsoukalas, D., Spandidos, D.A., Margina, D., 2018. The Akt pathway in oncology therapy and beyond (Review). *International Journal of Oncology* 53, 2319–2331. <https://doi.org/10.3892/ijo.2018.4597>
- O'Brien, P.J., 2014. High-Content Analysis in Toxicology: Screening Substances for Human Toxicity Potential, Elucidating Subcellular Mechanisms and *In Vivo* Use as Translational Safety Biomarkers. *Basic & Clinical Pharmacology & Toxicology* 115, 4–17. <https://doi.org/10.1111/bcpt.12227>
- O'Brien, P.J., 2009. Discovery Toxicology Screening: Predictive, *In Vitro* Cytotoxicity, in: Hit and Lead Profiling. John Wiley & Sons, Ltd, pp. 323–343. <https://doi.org/10.1002/9783527627448.ch14>
- O'Brien, P.J., Irwin, W., Diaz, D., Howard-Cofield, E., Krejsa, C.M., Slaughter, M.R., Gao, B., Kaludercic, N., Angeline, A., Bernardi, P., Brain, P., Hougham, C., 2006. High concordance of drug-induced human hepatotoxicity with *in vitro* cytotoxicity measured in a novel cell-based model using high content screening. *Arch Toxicol* 80, 580–604. <https://doi.org/10.1007/s00204-006-0091-3>
- Olsavsky, K.M., Page, J.L., Johnson, M.C., Zarbl, H., Strom, S.C., Omiecinski, C.J., 2007. Gene expression profiling and differentiation assessment in primary human hepatocyte cultures, established hepatoma cell lines, and human liver tissues. *Toxicology and Applied Pharmacology* 222, 42–56. <https://doi.org/10.1016/j.taap.2007.03.032>
- Owada, S., Endo, H., Shida, Y., Okada, C., Ito, K., Nezu, T., Tatemichi, M., 2018. Autophagy-mediated adaptation of hepatocellular carcinoma cells to hypoxia-mimicking conditions constitutes an attractive therapeutic target. *Oncol Rep* 39, 1805–1812. <https://doi.org/10.3892/or.2018.6279>

- Palaniappan, S., Sadacharan, C.M., Rostama, B., 2022. Polystyrene and Polyethylene Microplastics Decrease Cell Viability and Dysregulate Inflammatory and Oxidative Stress Markers of MDCK and L929 Cells *In Vitro*. *Expo Health* 14, 75–85. <https://doi.org/10.1007/s12403-021-00419-3>
- Pan, L., Yu, D., Zhang, Y., Zhu, C., Yin, Q., Hu, Y., Zhang, X., Yue, R., Xiong, X., 2021a. Polystyrene microplastics-triggered mitophagy and oxidative burst via activation of PERK pathway. *Science of The Total Environment* 781, 146753. <https://doi.org/10.1016/j.scitotenv.2021.146753>
- Pan, L., Yu, D., Zhang, Y., Zhu, C., Yin, Q., Hu, Y., Zhang, X., Yue, R., Xiong, X., 2021b. Polystyrene microplastics-triggered mitophagy and oxidative burst via activation of PERK pathway. *Science of The Total Environment* 781, 146753. <https://doi.org/10.1016/j.scitotenv.2021.146753>
- Perkins, E.J., Ashauer, R., Burgoon, L., Conolly, R., Landesmann, B., Mackay, C., Murphy, C.A., Pollesch, N., Wheeler, J.R., Zupanec, A., Scholz, S., 2019. Building and Applying Quantitative Adverse Outcome Pathway Models for Chemical Hazard and Risk Assessment. *Environmental Toxicology and Chemistry* 38, 1850–1865. <https://doi.org/10.1002/etc.4505>
- Persson, M., Løye, A.F., Jacquet, M., Mow, N.S., Thougard, A.V., Mow, T., Hornberg, J.J., 2014. High-Content Analysis/Screening for Predictive Toxicology: Application to Hepatotoxicity and Genotoxicity. *Basic & Clinical Pharmacology & Toxicology* 115, 18–23. <https://doi.org/10.1111/bcpt.12200>
- Prata, J.C., 2018. Airborne microplastics: Consequences to human health? *Environmental Pollution* 234, 115–126. <https://doi.org/10.1016/j.envpol.2017.11.043>
- Qian, N., Gao, X., Lang, X., Deng, H., Bratu, T.M., Chen, Q., Stapleton, P., Yan, B., Min, W., 2024. Rapid single-particle chemical imaging of nanoplastics by SRS microscopy. *Proc Natl Acad Sci U S A* 121, e2300582121. <https://doi.org/10.1073/pnas.2300582121>
- Qian, S., Wei, Z., Yang, W., Huang, J., Yang, Y., Wang, J., 2022. The role of BCL-2 family proteins in regulating apoptosis and cancer therapy. *Front. Oncol.* 12. <https://doi.org/10.3389/fonc.2022.985363>
- Rafazi, P., Haghi-Aminjan, H., Bagheri, Z., Rahimifard, M., 2024. Microplásticos e progressão do câncer: Um estudo comparativo de modelos de câncer gástrico 2D e 3D usando protocolos compatíveis com ISO. *Results in Engineering* 24, 103329. <https://doi.org/10.1016/j.rineng.2024.103329>
- Ragusa, A., Svelato, A., Santacroce, C., Catalano, P., Notarstefano, V., Carnevali, O., Papa, F., Rongioletti, M.C.A., Baiocco, F., Draghi, S., D'Amore, E., Rinaldo, D., Matta, M., Giorgini, E., 2021. Plasticenta: First evidence of microplastics in human placenta. *Environment International* 146, 106274. <https://doi.org/10.1016/j.envint.2020.106274>

- Renzi, M., Blašković, A., 2018. Litter & microplastics features in table salts from marine origin: Italian versus Croatian brands. *Marine Pollution Bulletin* 135, 62–68. <https://doi.org/10.1016/j.marpolbul.2018.06.065>
- Rochman, C.M., Kross, S.M., Armstrong, J.B., Bogan, M.T., Darling, E.S., Green, S.J., Smyth, A.R., Veríssimo, D., 2015. Scientific Evidence Supports a Ban on Microbeads. *Environ. Sci. Technol.* 49, 10759–10761. <https://doi.org/10.1021/acs.est.5b03909>
- Russell, W.M.S., Burch, R.L., 1959. The principles of humane experimental technique. The principles of humane experimental technique.
- Salvati, A., Åberg, C., dos Santos, T., Varela, J., Pinto, P., Lynch, I., Dawson, K.A., 2011. Experimental and theoretical comparison of intracellular import of polymeric nanoparticles and small molecules: toward models of uptake kinetics. *Nanomedicine: Nanotechnology, Biology and Medicine* 7, 818–826. <https://doi.org/10.1016/j.nano.2011.03.005>
- Saran, C., Fu, D., Ho, H., Klein, A., Fallon, J.K., Honkakoski, P., Brouwer, K.L.R., 2022. A novel differentiated HuH-7 cell model to examine bile acid metabolism, transport and cholestatic hepatotoxicity. *Sci Rep* 12, 14333. <https://doi.org/10.1038/s41598-022-18174-z>
- Schindelin, J., Arganda-Carreras, I., Frise, E., Kaynig, V., Longair, M., Pietzsch, T., Preibisch, S., Rueden, C., Saalfeld, S., Schmid, B., Tinevez, J.-Y., White, D.J., Hartenstein, V., Eliceiri, K., Tomancak, P., Cardona, A., 2012. Fiji: an open-source platform for biological-image analysis. *Nat Methods* 9, 676–682. <https://doi.org/10.1038/nmeth.2019>
- Senathirajah, K., Attwood, S., Bhagwat, G., Carbery, M., Wilson, S., Palanisami, T., 2021. Estimation of the mass of microplastics ingested – A pivotal first step towards human health risk assessment. *Journal of Hazardous Materials* 404, 124004. <https://doi.org/10.1016/j.jhazmat.2020.124004>
- Serrano, E., Chandrasekaran, S.N., Buntin, D., Brewer, K.I., Tomkinson, J., Kern, R., Bornholdt, M., Fleming, S., Pei, R., Arevalo, J., Tsang, H., Rubinetti, V., Tromans-Coia, C., Becker, T., Weisbart, E., Bunne, C., Kalinin, A.A., Senft, R., Taylor, S.J., Jamali, N., Adeboye, A., Abbasi, H.S., Goodman, A., Caicedo, J.C., Carpenter, A.E., Cimini, B.A., Singh, S., Way, G.P., 2024. Reproducible image-based profiling with Pycytominer. *ArXiv arXiv:2311.13417v2*.
- Shaw, S.Y., Westly, E.C., Pittet, M.J., Subramanian, A., Schreiber, S.L., Weissleder, R., 2008. Perturbational profiling of nanomaterial biologic activity. *PNAS* 105, 7387–7392. <https://doi.org/10.1073/pnas.0802878105>
- Simm, J., Klambauer, G., Arany, A., Steijaert, M., Wegner, J.K., Gustin, E., Chupakhin, V., Chong, Y.T., Vialard, J., Buijnsters, P., Velter, I., Vapirev, A., Singh, S., Carpenter, A.E., Wuyts, R., Hochreiter, S., Moreau, Y., Ceulemans, H., 2018. Repurposing High-Throughput Image Assays

- Enables Biological Activity Prediction for Drug Discovery. *Cell Chemical Biology* 25, 611-618.e3. <https://doi.org/10.1016/j.chembiol.2018.01.015>
- Sivertsson, L., Edebert, I., Palmertz, M.P., Ingelman-Sundberg, M., Neve, E.P.A., 2013. Induced CYP3A4 Expression in Confluent Huh7 Hepatoma Cells as a Result of Decreased Cell Proliferation and Subsequent Pregnane X Receptor Activation. *Molecular Pharmacology* 83, 659–670. <https://doi.org/10.1124/mol.112.082305>
- Smith, K., Piccinini, F., Balassa, T., Koos, K., Danka, T., Azizpour, H., Horvath, P., 2018. Phenotypic Image Analysis Software Tools for Exploring and Understanding Big Image Data from Cell-Based Assays. *Cell Syst* 6, 636–653. <https://doi.org/10.1016/j.cels.2018.06.001>
- Stirling, D.R., Swain-Bowden, M.J., Lucas, A.M., Carpenter, A.E., Cimini, B.A., Goodman, A., 2021. CellProfiler 4: improvements in speed, utility and usability. *BMC Bioinformatics* 22, 433. <https://doi.org/10.1186/s12859-021-04344-9>
- Stringer, C., Wang, T., Michaelos, M., Pachitariu, M., 2021. Cellpose: a generalist algorithm for cellular segmentation. *Nat Methods* 18, 100–106. <https://doi.org/10.1038/s41592-020-01018-x>
- Tanaka, Y., Takahashi, A., 2021. Senescence-associated extracellular vesicle release plays a role in senescence-associated secretory phenotype (SASP) in age-associated diseases. *The Journal of Biochemistry* 169, 147–153. <https://doi.org/10.1093/jb/mvaa109>
- Umamaheswari, S., Priyadarshinee, S., Bhattacharjee, M., Kadirvelu, K., Ramesh, M., 2021. Exposure to polystyrene microplastics induced gene modulated biological responses in zebrafish (*Danio rerio*). *Chemosphere* 281, 128592. <https://doi.org/10.1016/j.chemosphere.2020.128592>
- Van Cauwenberghe, L., Vanreusel, A., Mees, J., Janssen, C.R., 2013. Microplastic pollution in deep-sea sediments. *Environ Pollut* 182, 495–499. <https://doi.org/10.1016/j.envpol.2013.08.013>
- Visalli, G., Facciola, A., Pruiti Ciarello, M., De Marco, G., Maisano, M., Di Pietro, A., 2021. Acute and Sub-Chronic Effects of Microplastics (3 and 10 μm) on the Human Intestinal Cells HT-29. *International Journal of Environmental Research and Public Health* 18, 5833. <https://doi.org/10.3390/ijerph18115833>
- Volpe, A.R., Carmignani, M., Cesare, P., 2023. Hydroalcoholic extract of *Buxus sempervirens* shows antiproliferative effect on melanoma, colorectal carcinoma and prostate cancer cells by affecting the autophagic flow. *Front Pharmacol* 14, 1073338. <https://doi.org/10.3389/fphar.2023.1073338>
- Wan, S., Wang, X., Chen, W., Wang, M., Zhao, J., Xu, Z., Wang, R., Mi, C., Zheng, Z., Zhang, H., 2024. Exposure to high dose of polystyrene nanoplastics causes trophoblast cell apoptosis and induces miscarriage. *Particle and Fibre Toxicology* 21. <https://doi.org/10.1186/s12989-024-00574-w>

- Weaver, R.J., Betts, C., Blomme, E.A.G., Gerets, H.H.J., Gjervig Jensen, K., Hewitt, P.G., Juhila, S., Labbe, G., Liguori, M.J., Mesens, N., Ogeese, M.O., Persson, M., Snoeys, J., Stevens, J.L., Walker, T., Park, B.K., 2017. Test systems in drug discovery for hazard identification and risk assessment of human drug-induced liver injury. *Expert Opin Drug Metab Toxicol* 13, 767–782. <https://doi.org/10.1080/17425255.2017.1341489>
- Weaver, R.J., Blomme, E.A., Chadwick, A.E., Copple, I.M., Gerets, H.H.J., Goldring, C.E., Guillouzo, A., Hewitt, P.G., Ingelman-Sundberg, M., Jensen, K.G., Juhila, S., Klingmüller, U., Labbe, G., Liguori, M.J., Lovatt, C.A., Morgan, P., Naisbitt, D.J., Pieters, R.H.H., Snoeys, J., van de Water, B., Williams, D.P., Park, B.K., 2020. Managing the challenge of drug-induced liver injury: a roadmap for the development and deployment of preclinical predictive models. *Nat Rev Drug Discov* 19, 131–148. <https://doi.org/10.1038/s41573-019-0048-x>
- Weir, A., Westerhoff, P., Fabricius, L., Hristovski, K., von Goetz, N., 2012. Titanium dioxide nanoparticles in food and personal care products. *Environ Sci Technol* 46, 2242–2250. <https://doi.org/10.1021/es204168d>
- Weisbart, E., Tromans-Coia, C., Diaz-Rohrer, B., Stirling, D.R., Garcia-Fossa, F., Senft, R.A., Hiner, M.C., de Jesus, M.B., Eliceiri, K.W., Cimini, B.A., 2023. CellProfiler plugins - an easy image analysis platform integration for containers and Python tools. *ArXiv arXiv:2306.01915v2*.
- Xu, J.J., Diaz, D., O'Brien, P.J., 2004. Applications of cytotoxicity assays and pre-lethal mechanistic assays for assessment of human hepatotoxicity potential. *Chemico-Biological Interactions, Accurate Prediction of Human Drug Toxicity* 150, 115–128. <https://doi.org/10.1016/j.cbi.2004.09.011>
- Xu, J.J., Henstock, P.V., Dunn, M.C., Smith, A.R., Chabot, J.R., de Graaf, D., 2008. Cellular Imaging Predictions of Clinical Drug-Induced Liver Injury. *Toxicological Sciences* 105, 97–105. <https://doi.org/10.1093/toxsci/kfn109>
- Yan, L., Yu, Z., Lin, P., Qiu, S., He, Liuying, Wu, Z., Ma, L., Gu, Y., He, Lei, Dai, Z., Zhou, C., Hong, P., Li, C., 2023. Polystyrene nanoplastics promote the apoptosis in Caco-2 cells induced by okadaic acid more than microplastics. *Ecotoxicology and Environmental Safety* 249, 114375. <https://doi.org/10.1016/j.ecoenv.2022.114375>
- Yang, Y., Xie, E., Du, Z., Peng, Z., Han, Z., Li, L., Zhao, R., Qin, Y., Xue, M., Li, F., Hua, K., Yang, X., 2023. Detection of Various Microplastics in Patients Undergoing Cardiac Surgery. *Environ. Sci. Technol.* 57, 10911–10918. <https://doi.org/10.1021/acs.est.2c07179>
- Yu, Y.-L., Yiang, G.-T., Chou, P.-L., Tseng, H.-H., Wu, T.-K., Hung, Y.-T., Lin, P.-S., Lin, S.-Y., Liu, H.-C., Chang, W.-J., Wei, C.-W., 2014. Dual role of acetaminophen in promoting hepatoma cell

- apoptosis and kidney fibroblast proliferation. *Mol Med Rep* 9, 2077–2084. <https://doi.org/10.3892/mmr.2014.2085>
- Zhao, F., Zhao, Ying, Liu, Y., Chang, X., Chen, C., Zhao, Yuliang, 2011. Cellular Uptake, Intracellular Trafficking, and Cytotoxicity of Nanomaterials. *Small* 7, 1322–1337. <https://doi.org/10.1002/smll.201100001>
- Zhao, Q., Zhu, L., Weng, J., Jin, Z., Cao, Y., Jiang, H., Zhang, Z., 2023. Detection and characterization of microplastics in the human testis and semen. *Science of The Total Environment* 877, 162713. <https://doi.org/10.1016/j.scitotenv.2023.162713>
- Zheng, H., Wang, J., Wei, X., Chang, L., Liu, S., 2021. Proinflammatory properties and lipid disturbance of polystyrene microplastics in the livers of mice with acute colitis. *Science of The Total Environment* 750, 143085. <https://doi.org/10.1016/j.scitotenv.2020.143085>
- Zheng, T., Yuan, D., Liu, C., 2019. Molecular toxicity of nanoplastics involving in oxidative stress and desoxyribonucleic acid damage. *Journal of Molecular Recognition* 32, e2804. <https://doi.org/10.1002/jmr.2804>
- Zhitomirsky, B., Yunaev, A., Kreiserman, R., Kaplan, A., Stark, M., Assaraf, Y.G., 2018. Lysosomotropic drugs activate TFEB via lysosomal membrane fluidization and consequent inhibition of mTORC1 activity. *Cell Death Dis* 9, 1–15. <https://doi.org/10.1038/s41419-018-1227-0>

7. APPENDICES

7.1. **APPENDIX 1: Preliminary Expression Assays of BAX- α and Akt Proteins in Huh7 and HepG2 cells (after PS-MPs exposure) via Western Blot**

7.1.1. **Materials and Method**

7.1.1.1. ***Cell Plating and Exposure***

HepG2 and Huh7 were plated in T25 cell culture flasks at respective concentrations of 660,000 and 225,000 cells per flask in DMEM medium supplemented with 10% FBS and 1% Pen/Strep and were incubated at 37°C with 95% humidity in a Panasonic incubator. After 24 hours, the cells were exposed for 24 hours in triplicate with PS MPs (3 mL) at concentrations of 1 mg, 100 mg, and 1 g/L in serum-free culture medium with 0.0025% (v/v) Tween 20. As negative control, cells were exposed with DMEM serum-free (3 mL) with 0.0025% (v/v) Tween 20.

7.1.1.2. ***Protein Extraction from HepG2 and Huh7 Cells***

For the protein extraction from HepG2 and Huh7 cells, the RIPA (Radio-Immunoprecipitation Assay) Lysis Buffer System kit (Santa Cruz Biotechnology, ChemCruz #sc-24948A, USA) was used after the cells exposure to PS-MPs and negative control. Immediately before cell lysis, the lysis solution was prepared containing RIPA, PMSF (Phenylmethylsulfonyl fluoride), sodium orthovanadate, and protease inhibitor cocktail in the respective proportion of 1000:10:10:15, as per the manufacturer's instructions. Then, the cells in the flasks were placed on an ice pack, and the PS-MPs and culture medium were removed. The cells were washed three times with cold PBS 1 \times (3 mL). Next, the lysis solution was added to each flask (500 μ L) and cells were resuspended until no cells were adhered to the bottom of the flask. The lysis solutions with the lysed cells were transferred to microcentrifuge tubes, which were placed on ice. Subsequently, using a 1 mL syringe with a 0.45 x 13 mm needle, the solutions with the lysed cells were resuspended five times to extract the cellular proteins. The solution was then centrifuged at 13,000 x g for 20 minutes at 4°C, and the supernatants containing the soluble proteins were transferred to new microcentrifuge tubes and stored in a -80°C biofreezer.

7.1.1.3. ***Quantification of Proteins Extracted from HepG2 and Huh7 Cells***

For the quantification of proteins extracted from HepG2 and Huh7 cells in the previous step, the Bicinchoninic Acid (BCA) Protein Assay Kit (Santa Cruz Biotechnology, ChemCruz #sc-

202389, USA) was used. The soluble proteins extracted from the cells were thawed at room temperature. BSA solutions were prepared at concentrations of 2000, 1500, 1000, 750, 500, 250, 125, 25, and 0 µg/ml, diluted in RIPA to create the standard curve. Then, each of the nine BSA solutions (10 µL) were added separately in triplicate (three wells) in a 96-well plate, as well as each protein solution (10 µL) extracted from Huh7 and HepG2 cells treated with negative control and PS MPs at concentrations of 1 mg, 100 mg, and 1 g/L. Immediately before use, the AB Reagent was prepared by mixing Reagent A and Reagent B from the kit in the proportion of 50:1, as directed by the manufacturer. Then, the AB Reagent (200 µL) were added to all wells containing the previously added samples. The plate was incubated for 30 minutes at 37°C. After incubation, the plate was allowed to cool for 5 minutes at room temperature, and the absorbance of each well was read at 562 nm using the Cytation 5.

The results were extracted into spreadsheets, and the absorbance values of the standard BSA dilutions were used along with their respective known concentrations to plot a standard curve (absorbance on the y-axis and concentrations on the x-axis). From the linear equation of the curve, and using the absorbance values of the protein solutions extracted from Huh7 and HepG2 cells, the concentrations of the extracted proteins were determined. Based on these determined concentrations, the extracted protein samples were diluted in milliQ H₂O so that all had a concentration of 30 µg/20 µL for performing the Western Blot.

7.1.1.4. Western Blot of BAX and Akt Proteins

7.1.1.4.1. Western Blot

In microcentrifuge tubes, 50 µL of each soluble protein solution extracted from HepG2 and Huh7 cells (quantified and prepared in the previous step) were added, along with 15 µL of Laemmli sample buffer (Sigma-Aldrich, USA), 2 µL of β-mercaptoethanol (Bio-Rad Laboratories, USA), and 1 µL of Sodium Dodecyl Sulfate (SDS) (Sigma-Aldrich, USA) at 10% (w/v). The tubes were then placed in a dry bath at 100°C for 5 minutes, and the samples were stored at -20°C until further use. A solution for the polyacrylamide running gel (12%) was prepared using 50 mL of 30% acrylamide solution (w/v) with 0.8% bisacrylamide (w/v) (Bio-Rad Laboratories, USA), 37.5 mL of Tris-HCl (Amresco, USA) pH 8.8 at 1 M, 1 mL of SDS at 10%, and 11.5 mL of milliQ water. Subsequently, 9 mL of this solution was added to 40 µL of Ammonium Persulfate (APS) solution at 25% (v/v) and 10 µL of Tetramethylethylenediamine (TEMED) (all from Bio-Rad Laboratories, USA). This mixture was immediately added to the glass plates of the Mini Trans-Blot® (Bio-Rad Laboratories, USA), which were then filled with distilled water. After gel polymerization (30 minutes), the water was removed. Next, a stacking gel solution (3,5%) was

prepared using 20 mL of 30% acrylamide solution (w/v) with 0.8% bisacrylamide (w/v), 12.5 mL of Tris-HCl pH 6.8 at 1 M, 1 mL of SDS at 10%, and 66.5 mL of milliQ water. Subsequently, 3.5 mL of this solution was added to 20 μ L of APS solution at 25% (v/v) and 5 μ L of TEMED. This mixture was immediately added to the glass plate. The comb of the Western Blot system was then inserted, and the running buffer solution (100 mL of 10 \times Tris-Glycine (Amresco, USA), 10 mL of SDS at 10%, and 890 mL of milliQ water) was added to cover the entire gel. The comb was removed, and 20 μ L of protein samples (in triplicate) and 3 μ L of Recombinant Protein Molecular Weight Marker were added. The run was initiated at 80 Volts for 10 minutes and at 120 Volts for 2 hours (until the run was completed). At the end of the run, a “sandwich” was assembled for the Mini Trans-Blot® in the following order: sponge + filter paper + Nitrocellulose Membrane, 0.45 μ m (Bio-Rad Laboratories, USA) + running gel (with the stacking gel removed) + filter paper + sponge. This “sandwich” was placed in the Mini Trans-Blot®, and an ice pack was added to the device’s chamber to prevent protein denaturation. The device was turned on, and the transfer was carried out at 100 Volts for 1 hour in the refrigerator. After the transfer, the membrane was removed from the “sandwich” and placed in 1 \times TBS solution (made with Tris base and sodium chloride, both from Fisher Chemical, USA).

7.1.1.4.2. *Antibodies and Detection*

The membrane was removed from the 1 \times TBS solution and placed in a blocking solution of 3% BSA in 0.1% Tween 20 TBS (TBS-T) for 1 hour on a shaker. After 1 hour, the membrane was covered with 5 mL of the primary antibody solution anti-BAX (mouse) (Santa Cruz Biotechnology #sc-7480, USA) or anti-Akt (rabbit) (Cell Signaling #9272S, USA) at a concentration of 2 μ L/mL in 5% BSA in TBS-T, overnight, on a shaker at room temperature. The membrane was then washed 3 times for 10 minutes with 10 mL of 1 \times TBS.

Next, 5 mL of a solution of 1 μ L/mL of the secondary antibody (either goat anti-mouse or anti-rabbit IgG-HRP) in blocking solution was added to the membrane for 1 hour on a shaker. After 1 hour, the membrane was washed 3 times for 10 minutes with 10 mL of 1 \times TBS. The membrane was gently blotted with paper towels, and an ECL solution (2 mL of Tris-HCl pH 8.8 at 100 mM, 11 μ L of p-coumaric acid (Sigma-Aldrich, USA) at 50 mM, 50 μ L of luminol (Sigma-Aldrich, USA) at 50 mM, and 5 μ L of H₂O₂ (Amresco, USA) at 3.8% (v/v)) was added for 1 minute. The membrane was then placed in the Alliance 2.7 photodocumenter (UVITEC Cambridge, UK) for image capture.

7.1.1.4.3. *Endogenous Control*

The membranes for the BAX and Akt antibodies were washed 3 times for 10 minutes with 10 mL of TBS-T. The membranes were then covered with 5 mL of the primary antibody solution anti- β -actin (rabbit and mouse) (Cell Signaling #13E5, USA) at a concentration of 2 μ L/mL in 5% BSA in TBS-T for 1 hour on a shaker at room temperature. The membranes were subsequently washed 3 times for 10 minutes with 10 mL of TBS-T. Then, 5 mL of a 1 μ L/mL solution of the secondary antibody (anti-rabbit #DATA) in blocking solution was added to the membranes for 1 hour on a shaker. After 1 hour, the membranes were washed twice with 10 mL of TBS-T and once with 10 mL of 1 \times TBS, each for 10 minutes. The membranes were then developed with ECL in the Alliance 2.7 photodocumenter (UVITEC Cambridge, UK) as described above.

7.1.1.4.4. *Analysis of Western Blot Bands and Statistics*

For the analysis of Western Blot bands, we used the Fiji software. The first band of interest was selected using the 'Rectangle Tool,' followed by Analyze > Gels > Select First Lane. The rectangle was then moved to the next band, followed by Analyze > Gels > Select Next Lane. This step was repeated for each band. After selecting all the bands, a density plot was generated for each band using Analyze > Gels > Plot Lanes. To measure the intensity of each band, the 'Wand (tracing)' tool was used to click and select the peak corresponding to each band in the generated plot, and then we used Analyze > Measure. The area under the curve values, corresponding to the band intensities, were displayed in the 'Results' window. The band intensities were extracted to a spreadsheet and then normalized against the endogenous control (β -actin), i.e., the intensity of each band was divided by the intensity of the corresponding control band. Subsequently, the values were normalized again relative to the average values from the proteins of cells treated with the negative control, which was set to 100%. With these normalized intensity values at the respective concentrations of PS MPs, a graph was plotted using GraphPad Prism 8.0.2 software. Statistical analysis of both assay was conducted using GraphPad Prism software, employing Kruskal-Wallis followed by Dunn's multiple comparisons test, to compare the negative control with all concentrations of PS MPs; $p \leq 0.05$ indicates statistical significance compared to the non-treated group and were presented as '**'.

7.1.2. Results and Conclusions

As showed in this (Calcein-PI-Hoechst assay; Section 3.2.2.), we observed a trend toward a reduction in the number of dead cells. To specifically investigate the pronounced reduction in dead cells following PS-MPs treatment in both cell lines, a preliminary study was conducted to assess the expression of BAX- α and Akt proteins via Western blot analysis. This investigation was based on reports suggesting that hepatocyte and other cell types' death induced by PS-MPs may occur through apoptosis (Lu et al., 2024; Wan et al., 2024; Chen et al., 2023; Yan et al., 2023). BAX- α is a pro-apoptotic protein that collaborates with other BCL-2 family proteins to regulate apoptotic pathways critical for cellular homeostasis (Qian et al., 2022). Conversely, Akt is a key protein in cell survival pathways, regulating processes such as inhibiting pro-apoptotic factors and promoting cell survival via the PI3K/Akt/mTOR signaling axis (Nitulescu et al., 2018). Thus, both proteins are closely associated with apoptosis.

Given the observed reduction in cell death following treatment with high concentrations of PS-MPs, we hypothesized that these conditions might modulate the expression of these proteins, potentially decreasing BAX- α expression to reduce apoptosis or increasing Akt expression to enhance survival. However, our preliminary study, which was conducted in only one independent assay with triplicates per sample, revealed no significant changes in BAX- α or Akt expression in Huh7 cells treated with PS-MPs (Fig. AP1, items A–H). In HepG2 cells, a trend toward decreased expression of both proteins was observed at PS-MPs concentrations; however, this difference was not statistically significant. To confirm whether this trend in reduced protein expression is consistent, a minimum of three independent assays will be required.

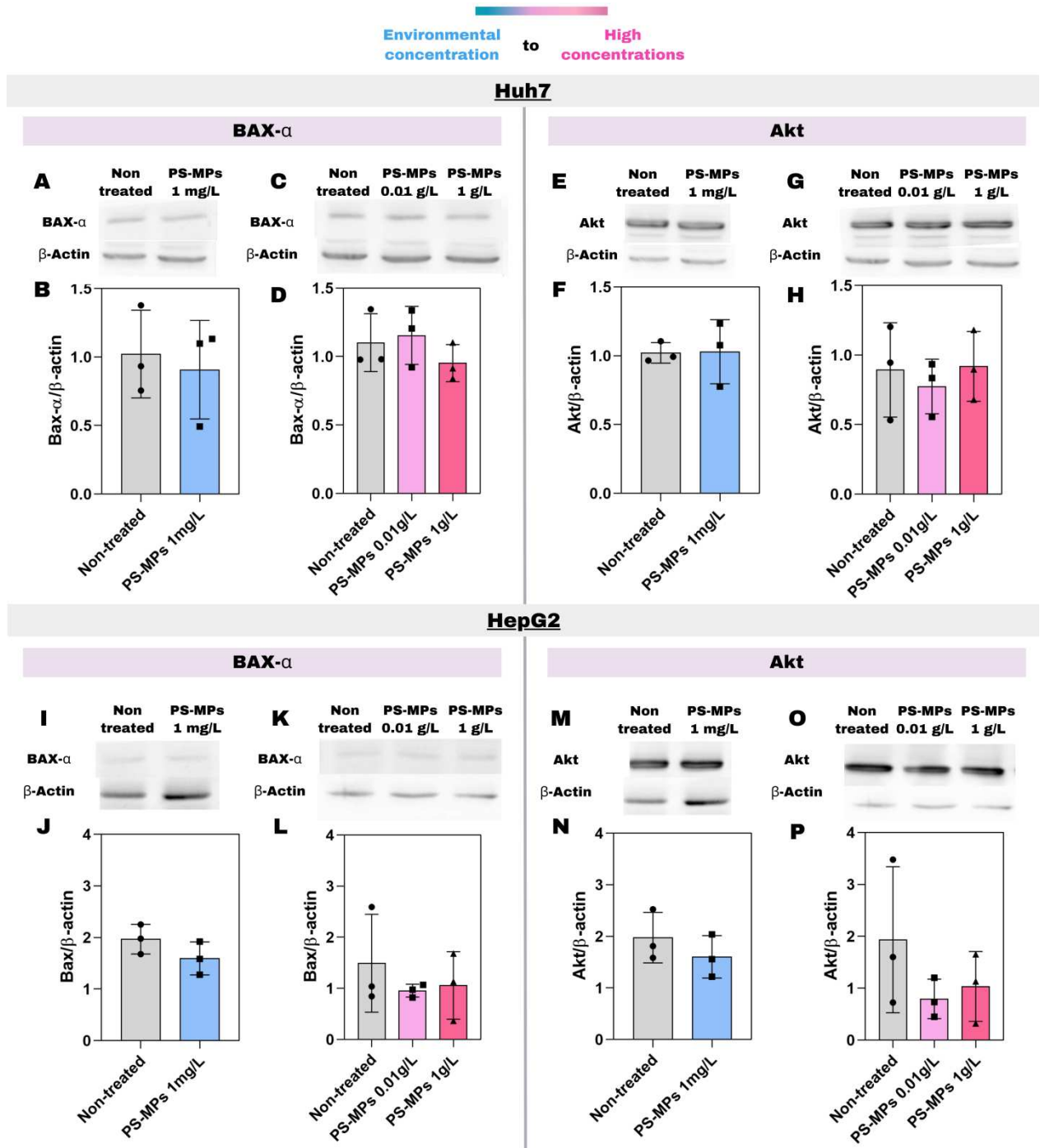


Fig. AP1 - Expression Levels of BAX-α and Akt Proteins in Huh7 and HepG2 Cells Following PS-MPs Exposure via Western Blot. Huh7 and HepG2 cells were treated with PS-MPs (1 mg/L, 0.01 g/L, and 1 g/L) for 24 hours, after which their proteins were extracted and analyzed by Western Blot using antibodies against BAX-α, Akt, and the endogenous control β-actin. **(A, C, E, G)** Western Blot bands showing the expression levels of BAX-α and Akt in Huh7 cells following PS-MPs exposure. **(B, D, F, H)** The ratio of the intensity of BAX-α or Akt protein

bands to β -actin bands, representing the expression levels of BAX- α (B and D) or Akt (F and H) in Huh7 cells after treatment with PS-MPs. **(I, K, M, O)** Western Blot bands showing the expression levels of BAX- α and Akt in HepG2 cells following PS-MPs exposure. **(J, L, N, P)** The ratio of the intensity of BAX- α or Akt protein bands to β -actin bands, representing the expression levels of BAX- α (J and L) or Akt (N and P) in HepG2 cells after treatment with PS-MPs. These data are derived from a single independent assay, with triplicate samples for each cell exposure condition. Statistical analysis was performed using the Kruskal-Wallis test followed by Dunn's multiple comparisons test in GraphPad Prism: * $p \leq 0.05$ indicates statistical significance compared to the non-treated group.

7.2. ***APPENDIX 2: Investigation of Autophagic Processes in Huh7 and HepG2 Cells Exposed to PS-MPs using MTT Assay***

7.2.1. **Materials and Method**

To evaluate the contribution of autophagy to the effects of PS-MPs, Huh7 and HepG2 cells were plated in 96-well plates at 7,500 and 22,000 cells per well, respectively, and incubated for 24 hours. Next, cells were pre-treated with the autophagy inhibitor Bafilomycin A1 (2 μ M; inhibits lysosomal acidification via V-ATPase) or 3-Methyladenine (3-MA; 5 mM; inhibits class III PI3K, blocking autophagosome formation) for 1 hour. Next, cells were exposed to PS-MPs (0.01, 0.1 and 1 g/L) in the presence of Bafilomycin A1 (2 μ M) or 3-MA (5 mM) for 24 hours. Control treatments included cells exposed to PS-MPs alone (0.01, 0.1 and 1 g/L), to Bafilomycin A1 alone (2 μ M), and to 3-MA alone (5 mM). All exposures were performed in triplicate, and each experimental replicate was conducted on at least three different days with a randomized plate layout to vary the treatment positions. After 24-hours exposure, cell viability was assessed using the MTT assay (as described in Section 3.1.3.2.).

7.2.2. **Results and Conclusions**

In addition to associating the increase in acidic vesicles with PS-MPs internalization, observed especially in Huh7 cells treated with PS-MPs at high concentrations (0.5 and 1 g/L), we hypothesized that the increase in acidic vesicles could be caused by cellular autophagy, as this vesicle pattern is characteristic of cells undergoing autophagic processes (Volpe et al., 2023). Autophagy could serve as a mechanism for cells to manage internalized PS-MPs, potentially offering temporary protection and delaying cell death. This could explain the reduction in dead cells observed in the Calcein-PI-Hoechst assay for Huh7 and HepG2 cells treated with PS-MPs at 0.5 and 1 g/L. To investigate this hypothesis, we conducted MTT assays using autophagy inhibitors (3-MA (5 mM) and Bafilomycin A1 (2 μ M)) in the presence of PS-MPs.

If this hypothesis were correct, the presence of autophagy inhibitors would prevent the cells from using autophagy as a mechanism to cope with the presence of PS-MPs at high concentrations, thereby evading cell death. Consequently, the cells would die, and cell viability at these PS-MPs concentrations would decrease. However, no significant reduction in cell viability was observed in the presence of autophagy inhibitors and PS-MPs (Fig. AD2). Nevertheless, due to the large standard deviation observed across the three independent assays, the data become inconclusive. **Therefore, we cannot suggest that autophagy is not associated with the reduction in cell death.**

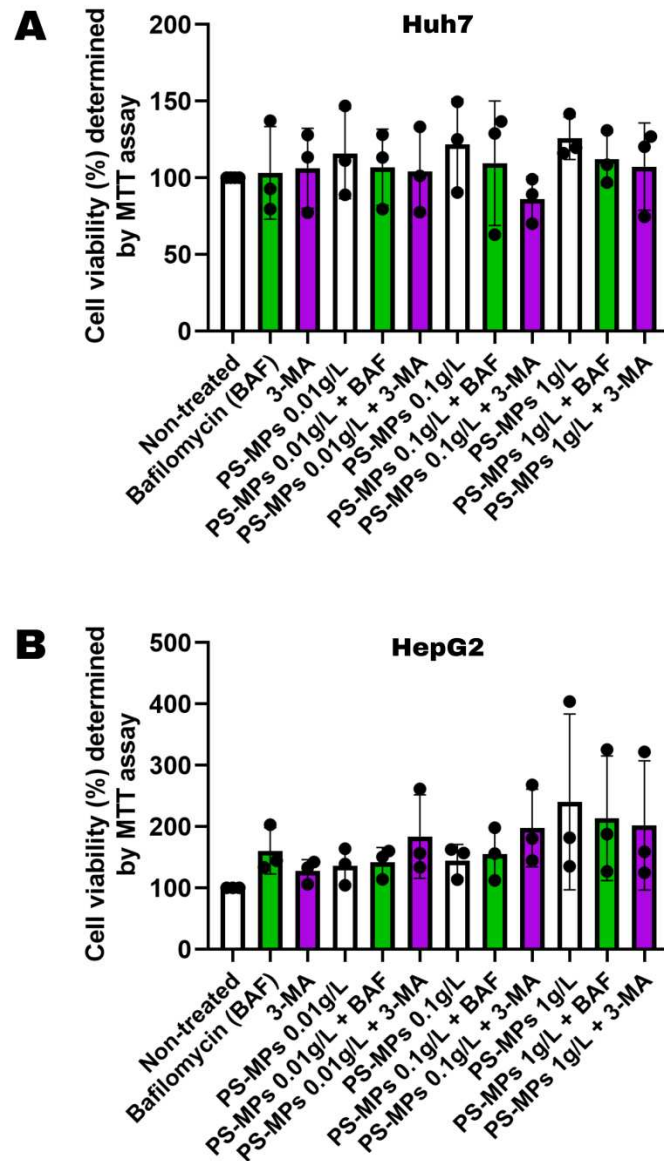


Fig. AP2 – Cell Viability of Huh7 and HepG2 Cells After Exposure to Autophagy Inhibitors (Bafilomycin 2 μ M and 3-MA 5 mM) and PS-MPs. Huh7 and HepG2 cells were plated at a density of 7,500 and 22,000 cells/well, respectively, in 96-well plates. Cells were pre-treated with the autophagy inhibitor Bafilomycin A1 (2 μ M) or 3-Methyladenine (5 mM) for 1 hour. Next, cells were exposed to PS-MPs (0.01, 0.1 and 1 g/L) in the presence of Bafilomycin A1 (2 μ M) or 3-Methyladenine (5 mM; 3-MA) for 24 hours. Control treatments included cells exposed to PS-MPs alone (0.01, 0.1 and 1 g/L), Bafilomycin A1 alone (2 μ M), 3-MA alone (5 mM). Viability was then assessed by MTT assays. Cell viabilities were calculated relative to the non-treated group, which

was considered 100%. **(A)** Huh7 cells viability obtained by the MTT assay. **(B)** Huh7 cells viability obtained by the MTT assay. Data were aggregated by independent replicate (plate). This assay were performed at least three independent replicates. Statistical analysis was performed using the Kruskal-Wallis test followed by Dunn's multiple comparisons test using GraphPad Prism software: * $p \leq 0.05$ indicates statistical significance compared to the non-treated group.

7.3. APPENDIX 3: Attempted Co-localization Assay of Autophagolysosome Proteins LC3 and LAMP-1

7.3.1. Materials and Method

Huh7 and HepG2 cells were plated in 96-well plates at 7,500 and 22,000 cells per well, respectively, and incubated for 24 hours. Next, the cells were exposed in triplicate to PS-MPs at concentrations of 1 mg/L, 0.01 g/L, and 1 g/L, and with CoCl₂ (300 µM; autophagy positive control; Owada et al., 2018). After 24 hours of treatment, cells were fixed with PFA (4% w/v) for 20 minutes. Then, cells were washed with PBS 1×, and Blocking Buffer (PBS 1× with 5% goat serum and 0.3% Triton X-100) was added. After 1 hour, the cells were washed with PBS 1× and were incubated at 27°C with the primary antibody solution (25 µL) containing LAMP1 Mouse mAb (Cell Signaling #15665S, USA) and Anti LC3 B Rabbit mAb (Sigma Aldrich, L7543-200UL, USA) both at 5 µL/mL in PBS 1× for 1 hour. Next, the cells were washed with PBS 1×, and the secondaries antibodies solutions (25 µL) containing Alexa Fluor 647 goat anti-mouse IgG (Life Technologies, USA) and Alexa Fluor 488 goat anti-rabbit IgG (Life Technologies, USA) both at 1 µL/mL in PBS 1× was added. After 1 hour at room temperature, the wells were washed with PBS 1× and Hoechst (1.6 µM; 50 µL) in PBS 1× was added to each well. After 30 minutes of incubation at 37°C, the Hoechst solution was removed and PBS 1× with 0.05% (w/v) sodium azide (100 µL) was added to the wells. Fluorescence images were acquired using a 40× objective (EC Plan-Neofluar 40×/1.3 Oil DIC M27) on the Airyscan Confocal Microscope using a 405 nm laser line (blue) for excitation of Hoechst, and a 633 nm laser line (deep red) for excitation of Alexa Fluor 647 goat anti-mouse IgG, and a 488 nm laser line (green) for excitation of and Alexa Fluor 488 goat anti-rabbit IgG, both with the pinhole set to 1 AU.

7.3.2. Results and Conclusions

As a confirmation step regarding the occurrence of autophagy triggered by PS-MPs in Huh7 cells, we performed immunofluorescence assays for Lysosome-Associated Membrane Protein 1 (LAMP-1) and LC3 (Autophagosome Membrane Protein) using confocal microscopy to investigate whether there was colocalization between these proteins, which would indicate the presence of autophagolysosomes. However, the LC3 antibody showed non-specific cytoplasmic distribution and was therefore unsuitable for colocalization analysis (Fig. AP3.1). In contrast, the LAMP-1 antibody performed as expected, marking lysosomes and revealing an increase in their number at a 1 g/L PS-MPs concentration (Fig. AP3.2). This finding corroborates the results observed in the Live Cell Painting assay, which indicated an increase in acidic vesicles, and lysosomal stress.

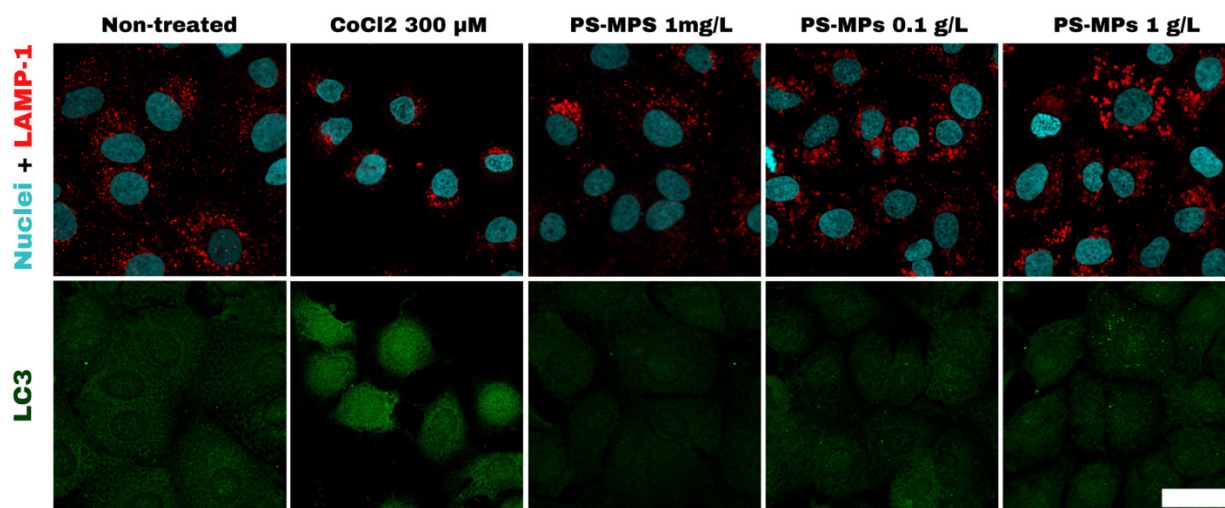


Fig. AP3.1 – Immunofluorescence Assay with Confocal Microscopy of Lysosome-Associated Membrane Protein 1 (LAMP-1) and LC3 (Autophagosome Membrane Protein) in Huh7 Cells after PS-MPs exposure. Huh7 cells were plated at densities of 7,500 cells per well, in 96-well plates. The cells were exposed in triplicate to PS-MPs at concentrations of 1 mg/L, 0.01 g/L, and 1 g/L, as well as to CoCl₂ (300 μM; positive control for autophagy), for 24 hours. After exposure, the cells were fixed, and the immunofluorescence assay was performed for LAMP-1 and LC3. Fluorescent labeling was achieved using Alexa Fluor 647 goat anti-mouse IgG (deep red) for LAMP-1 and Alexa Fluor 488 goat anti-rabbit IgG (green) for LC3, while nuclei were stained with Hoechst (blue, but represented in cyan in the images). Images were acquired using a Zeiss LSM880 Airyscan Inverted Confocal Microscope with a 40× objective. The white scale bar represents a scale of 40 μm. This assay was performed in two independent experiments. **Note: the LC3 antibody displayed non-specific cytoplasmic distribution.**

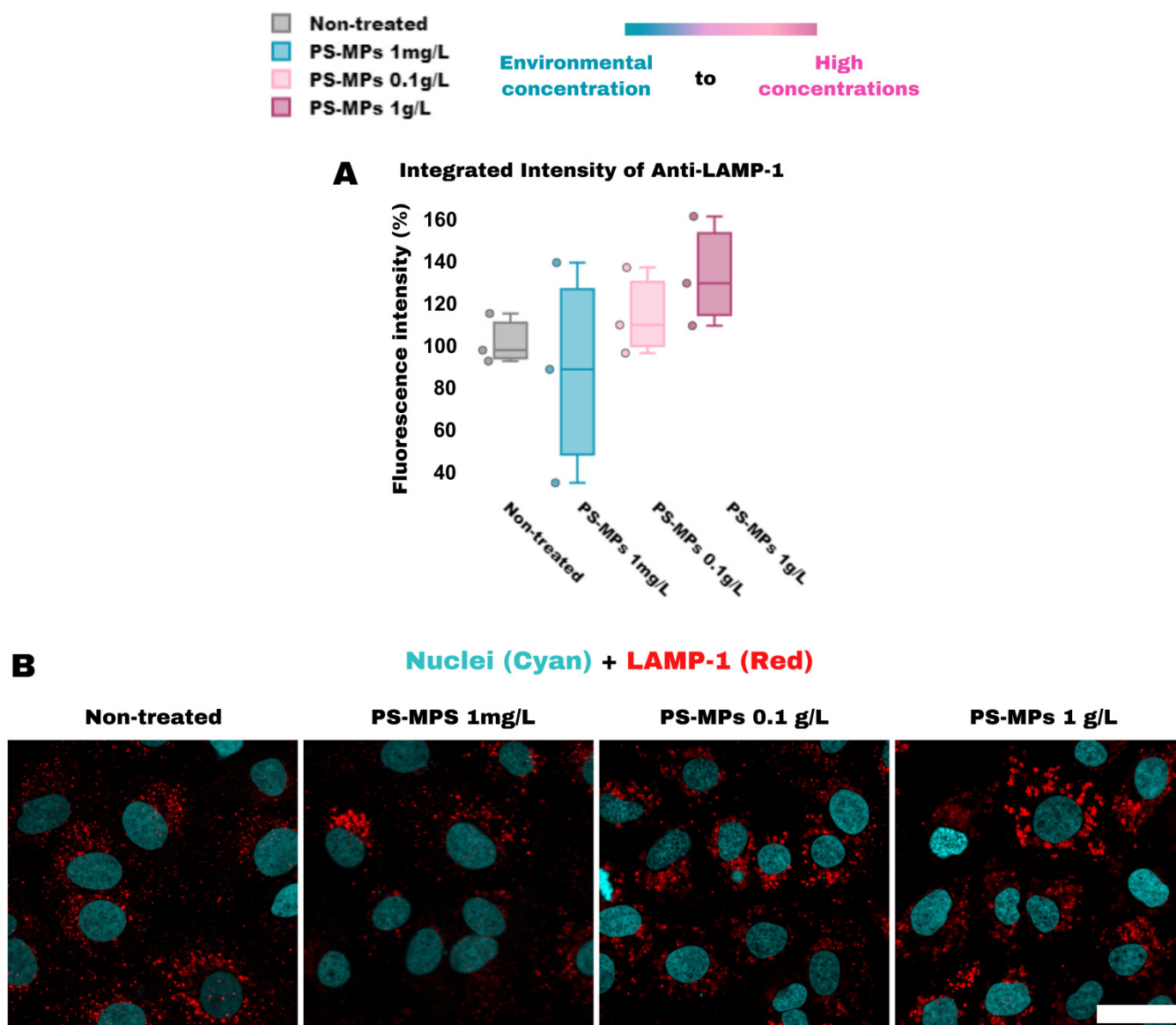


Fig. AP3.2 – Features and Confocal Fluorescence Microscopy Images from the Immunofluorescence Assay of LAMP-1 in Huh7 Cells Exposed to PS-MPs. Huh7 cells were plated at densities of 7,500 cells per well, in 96-well plates. The cells were exposed in triplicate to PS-MPs at concentrations of 1 mg/L, 0.01 g/L, and 1 g/L, for 24 hours. After exposure, the cells were fixed, and the immunofluorescence assay was performed for LAMP-1. Fluorescent labeling was achieved using Alexa Fluor 647 goat anti-mouse IgG (deep red) for LAMP-1, while nuclei were stained with Hoechst (blue, but represented in cyan in the images). Images were acquired using a Zeiss LSM880 Airyscan Inverted Confocal Microscope with a 40× objective. The acquired images were analyzed in CellProfiler, where objects (cells, nuclei, and cytoplasm) were segmented, and their features extracted. These features were subsequently aggregated by

well and normalized relative to the non-treated group, which was set at 100%. **(A)** Plot of fluorescence intensity of LAMP-1 label with Alexa Fluor 647. **(B)** Representative fluorescence confocal microscopy images of Huh7 cells. The white scale bar represents a scale of 40 μm . This assay was performed in a single independent experiments, and each point in the plots represents well-aggregated data. Statistical analysis was performed using the Kruskal-Wallis test followed by Bonferroni post hoc testing in Jupyter Notebook, utilizing the scipy and statsmodels libraries: * $p \leq 0.05$ indicates statistical significance compared to the non-treated group.

7.4. **APPENDIX 4: Preliminary Expression Assays of Cell-Cell Junction Proteins β -Catenin and ZO-1 in HepG2 Cells**

7.4.1. **Materials and Method**

7.4.1.1. ***Detection of β -catenin and ZO-1 Proteins Expression via Western Blot***

The Western Blot protocol for β -catenin and ZO-1 proteins of HepG2 cells was the same as described in **Appendix 1** (Section 7.1.) and the primary antibodies used were: anti-Beta-catenin- Rabbit mAb (Cell Signaling #D10A8, USA) and Anti-ZO-1 (rabbit polyclonal) (Merck #AB2272, USA).

7.4.1.2. ***Detection of β -catenin and ZO-1 Proteins Expression via Immunofluorescence***

HepG2 cells were plated in 96-well plates at 22,000 cells per well, and incubated for 24 hours. Next, cells were exposed in triplicate to PS-MPs at concentrations of 1 mg/L, 0.01 g/L, 0.1 g/L, and 1 g/L. After 24 hours, cells were fixed with PFA 4%. After 20 minutes, the cells were washed with PBS 1 \times . Next, 100 μ L of Blocking Buffer (1 \times PBS with 5% (v/v) goat serum and 0.3% (v/v) Triton X-100) was added. After 1 hour, the cells were washed with PBS 1 \times , and the were incubated at 37°C with the primary antibody solution (25 μ L) containing Rabbit anti-ZO-1 (Invitrogen #617300, USA) at 5 μ L/mL in PBS 1 \times or Rabbit anti- β -catenin mAb (Cell Signaling #8480S, USA) at 5 μ L/mL in PBS 1 \times for 1 hour. Then, the cells were washed with PBS 1 \times , and the secondary antibody solution (25 μ L) containing Alexa Fluor 488 goat anti-rabbit IgG (Life Technologies, USA) at 1 μ L/mL in PBS 1 \times was added in the ZO-1 assay, and the secondary antibody solution (25 μ L) containing Alexa Fluor 647 goat anti-rabbit IgG (Life Technologies, USA) at 1 μ L/mL in PBS 1 \times was added in the β -catenin assay. After 1 hour at room temperature, the cells were washed with PBS 1 \times , and stained with Hoechst (1.6 μ M; 50 μ L). Fluorescence images were acquired using a 40 \times objective (EC Plan-Neofluar 40 \times /1.3 Oil DIC M27) on the Airyscan Confocal Microscope using a 405 nm laser line (blue) for excitation of Hoechst, and a 633 nm laser line (deep red) for excitation of Alexa Fluor 647 goat anti-mouse IgG (indicating β -catenin expression), and a 488 nm laser line (green) for excitation of and Alexa Fluor 488 goat anti-rabbit IgG (indicating ZO-1 expression), both with the pinhole set to 1 AU.

7.4.2. **Results and Conclusions**

This preliminary investigations into the expression of two cell–cell junction proteins, β -Catenin and ZO-1, expressed in HepG2 cells (Arzumanian et al., 2021), were conducted using Western Blot (Fig. AP4.1) and Immunofluorescence assays (Fig. AP4.2). These preliminary

investigations revealed no statistically significant changes in the expression of these proteins in cells treated with PS-MPs at a concentration of 1 g/L, although ZO-1 showed a slight trend toward reduced expression in the Western Blot assay.

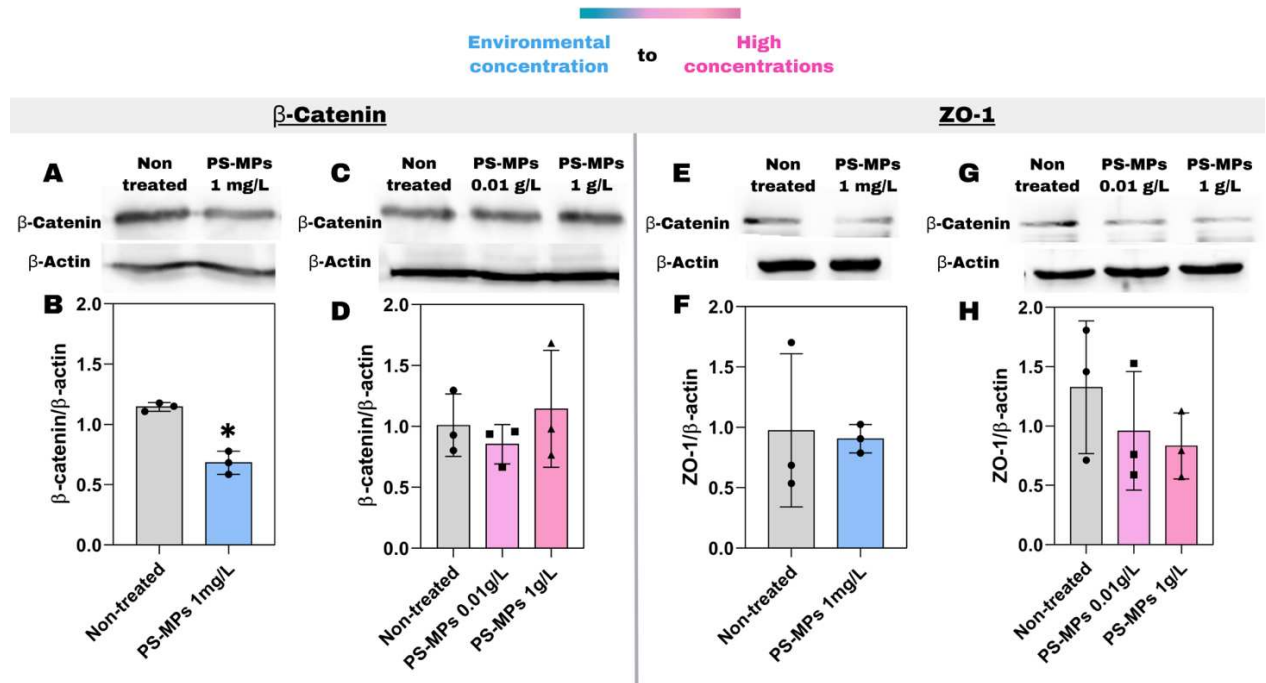


Fig. AP4.1 - Expression Levels of β -Catenin and ZO-1 Proteins via Western Blot in HepG2 Cells Exposed to PS-MPs. HepG2 cells were treated with PS-MPs (1 mg/L, 0.01 g/L, and 1 g/L) for 24 hours, after which their proteins were extracted and analyzed by Western Blot using antibodies against β -Catenin, ZO-1 and the endogenous control β -actin. **(A, C, E, G)** Western Blot bands showing the expression levels of β -Catenin and ZO-1 in HepG2 cells following PS-MPs exposure. **(B, D, F, H)** The ratio of the intensity of β -Catenin or ZO-1 protein bands to β -actin bands, representing the expression levels of β -Catenin (B and D) or ZO-1 (F and H) in HepG2 cells after treatment with PS-MPs. These data are derived from a single independent assay, with triplicate samples for each cell exposure condition. Statistical analysis was performed using the Kruskal-Wallis test followed by Dunn's multiple comparisons test in GraphPad Prism: *p ≤ 0.05 indicates statistical significance compared to the non-treated group.

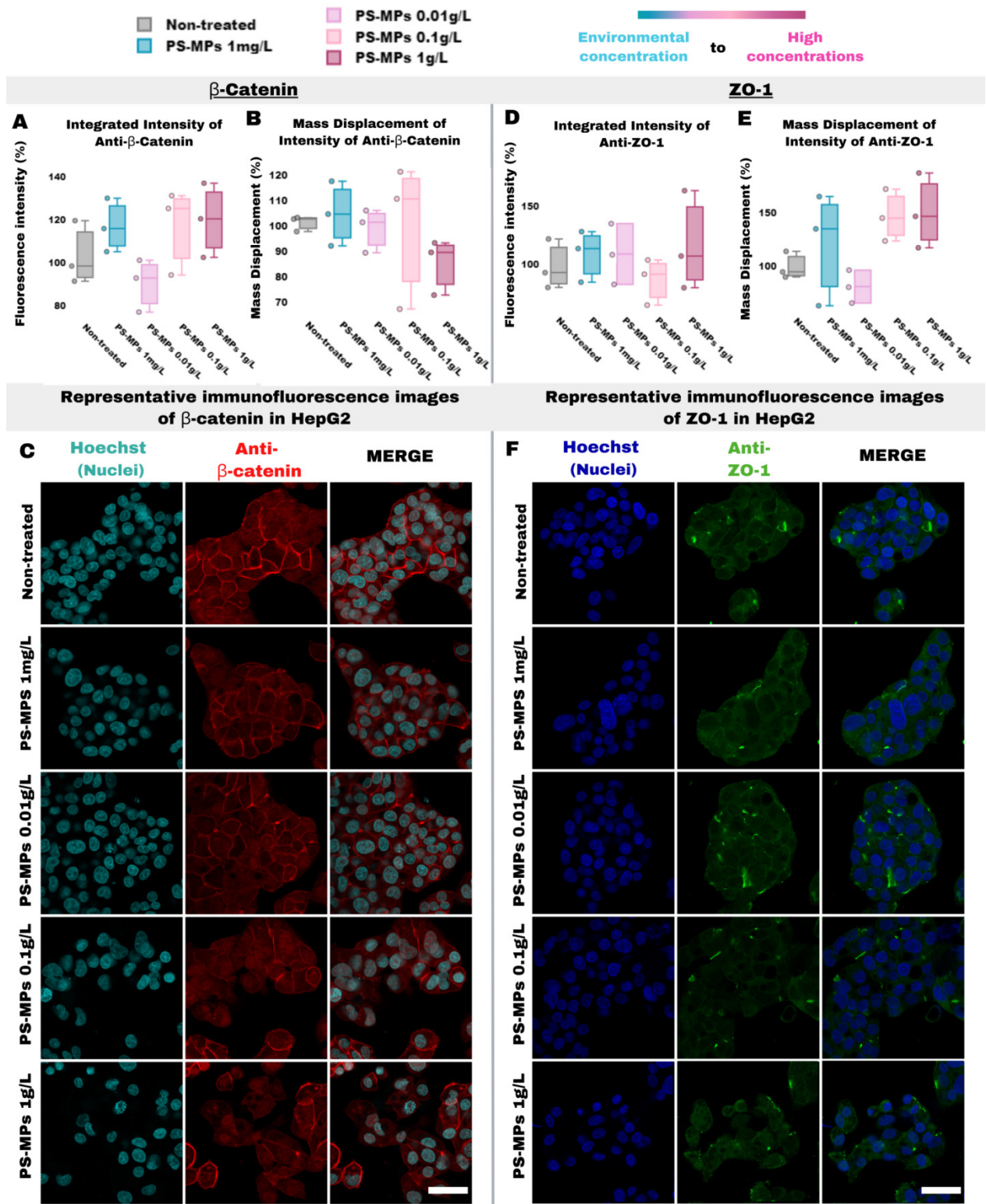


Fig. AP4.2 – Features and Confocal Fluorescence Microscopy Images from the Immunofluorescence Assay of β-Catenin and ZO-1 in HepG2 Cells Exposed to PS-MPs. HepG2 cells were plated at density of 22,000 cells per well, in 96-well plates. The cells were

exposed in triplicate to PS-MPs at concentrations of 1 mg/L, 0.01 g/L, and 1 g/L, for 24 hours. After exposure, the cells were fixed, and the immunofluorescence assay was performed for β -Catenin and ZO-1. Fluorescent labeling was achieved using Alexa Fluor 647 goat anti-mouse IgG (deep red) for β -Catenin, and using Alexa Fluor 488 goat anti-rabbit IgG (green) for ZO-1. While nuclei were stained with Hoechst (blue, but represented in cyan in the β -Catenin assay images). Images were acquired using a Zeiss LSM880 Airyscan Inverted Confocal Microscope with a 40 \times objective. The acquired images were analyzed in CellProfiler, where objects (cells, nuclei, and cytoplasm) were segmented, and their features extracted. These features were subsequently aggregated by well and normalized relative to the non-treated group, which was set at 100%. **(A,B)** Plots of fluorescence intensity and its mass displacement of β -Catenin label with Alexa Fluor 647. **(C)** Representative fluorescence confocal microscopy images of HepG2 cells after β -Catenin immunofluorescence assay. **(D,E)** Plots of fluorescence intensity and its mass displacement of ZO-1 label with Alexa Fluor 488. **(F)** Representative fluorescence confocal microscopy images of HepG2 cells after ZO-1 immunofluorescence assay. The white scale bar represents a scale of 40 μ m. This assay was performed in a single independent experiments, and each point in the plots represents well-aggregated data. Statistical analysis was performed using the Kruskal-Wallis test followed by Bonferroni post hoc testing in Jupyter Notebook, utilizing the scipy and statsmodels libraries: * $p \leq 0.05$ indicates statistical significance compared to the non-treated group.

7.5. **APPENDIX 5: HepatotoxPath Assay**

7.5.1. **Materials and Method**

7.5.1.1. ***Cell Exposure***

After 24 hours of plating, cells were exposed in triplicate to PS-MPs (100 μ L) at concentrations ranging from 1 μ g/L to 1 g/L (that includes environmental and relevant human exposure concentrations (1 μ g/L and 1 mg/L) and higher concentrations (0.01, 0.1 and 1 g/L)) for 24 hours at 37 °C. As a negative control, antibiotic-and-serum-free DMEM containing 0.0025% (v/v) Tween 20 (100 μ L) and Lactose (100 μ L; 1 μ M; Merck, USA) were used. Bafilomycin A (100 μ L; 2 μ M) and Amiodarone (100 μ L; 10 μ M; Chem-Impex, USA) served as positive controls for cell damage and hepatotoxicity, respectively. Each experiment was conducted on at least three independent days, with a different plate layout used for each experimental run.

7.5.1.2. ***HepatotoxPath Imaging Protocol***

After cell exposure, the treatment medium was replaced with a staining solution (30 μ L) prepared in FluoroBrite DMEM containing Fluo-4 AM (5 μ M), Tetramethylrhodamine (100 nM; TMRM), LysoTracker™ Deep Red (75 nM), and Hoechst (1.6 μ M) (all reagents from Invitrogen, USA). Cells were incubated for 35 minutes at 37 °C. After incubation, cells were washed twice with Phosphate Buffered Saline 1 \times (100 μ L; PBS 1 \times) (Sigma-Aldrich, USA), and wells were filled with FluoroBrite DMEM (100 μ L). Subsequently, fluorescence images were acquired at 12 sites per well using a 20 \times objective on the Cytation 5 with the following filter cubes: GFP (green; excitation/emission = 445/510 nm) for Fluo-4, RFP (orange; excitation/emission = 531/593 nm) for TMRM, CY5 (deep red; excitation/emission = 628/685 nm) for LysoTracker, and DAPI (blue; excitation/emission = 377/447 nm) for Hoechst.

Note: HepatotoxPath assay was originally designed to include ThiolTracker™ Violet (a glutathione detection reagent) (Invitrogen, USA) to assess intracellular glutathione levels. However, due to its broad spectral range (excitation/emission = 405/526 nm) and significant overlap with both the DAPI and GFP channels (Fig. AP5.1)—particularly interfering with the Fluo-4 signal—this dye was removed from the protocol to accommodate the specifications of the Cytation 5 equipment.

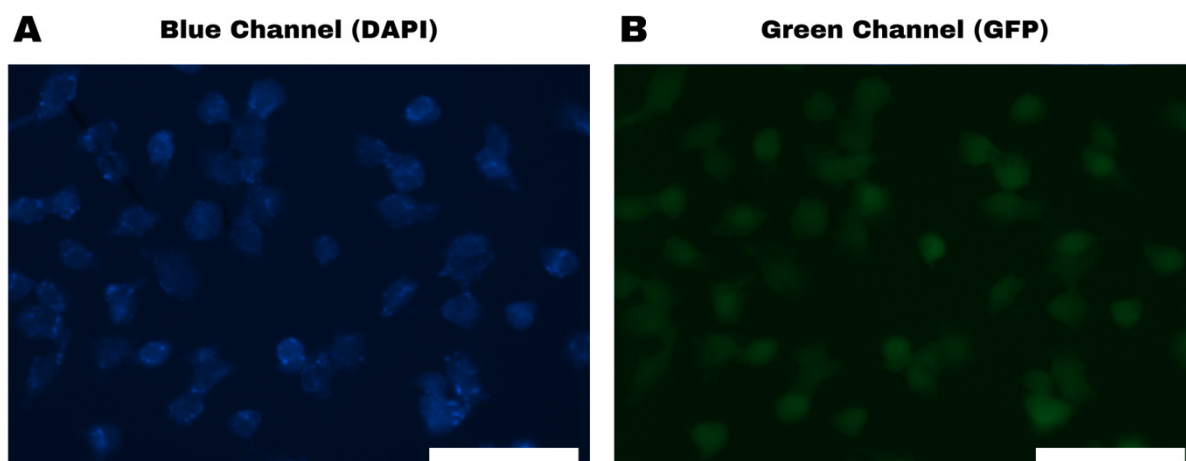


Fig. AP5.1 – Huh7 Cells Stained with ThiolTracker, which is detected in both the blue and green channels. The white scale bar in the lower right corner of the images represents 100 μm .

7.5.1.3. *HepatotoxPath Image Analysis*

To perform cell segmentation for HepatotoxPath assay, stacks combining nuclear images (Hoechst, blue channel) and mitochondrial images (TMRM, orange channel), which delineate the cell shape, were created following the same protocol described in section 3.1.3.5. For each cell line, a pipeline was developed in CellProfiler to segment nuclei (Hoechst, blue channel), cells (TMRM, orange channel; using the previously trained cell segmentation model loaded into the 'RunCellpose' plugin for both cell lines), and cytoplasm (TMRM, orange channel). After segmenting each object (nucleus, cell, and cytoplasm), single-cell object features were extracted into a database using CellProfiler modules. These features included the size and shape of objects, pixel intensity, and texture. The numerical values for each feature were then exported as '.csv' files for further analysis.

7.5.1.3.1. *Phenotypic Profiling*

Cell profiling using the feature data extracted ('.csv') from the HepatotoxPath assay was performed as described in section 3.1.5.3.

7.5.2. Results and Conclusions

After the investigations conducted in this study to obtain a broader understanding of the cellular phenotypic alterations triggered by PS-MPs, we decided to perform a mechanistic assay focused on detecting cellular changes associated with *in vitro* hepatotoxicity. We utilized a combination of fluorescent cellular dyes that allow the visualization of parameters commonly affected in hepatotoxicity *in vitro* studies. These parameters included intracellular calcium ion levels (Holt et al., 2006; O'Brien et al., 2004), mitochondrial membrane potential (MMP)—considered the most sensitive parameter for predicting human liver damage induced by xenobiotics (Persson et al., 2014; Dykens & Will, 2007)—and lysosomal integrity (Begrache et al., 2011), especially since PS-MPs can enter cells via endocytosis (Ding et al., 2021; Liu et al., 2021).

Cells were treated with PS-MPs at concentrations ranging from 1 µg/L to 1 g/L (environmental to higher concentrations), with Amiodarone (10 µM) as a positive control for hepatotoxicity, Bafilomycin A1 (2 µM) as a positive control for cellular damage (expected to drastically alter all fluorescent dyes used), and Lactose (1 µM) as a negative control for hepatotoxicity. The exposure time was 24 hours. After exposure, cells were stained with Hoechst (to visualize the nucleus), Fluo-4 (to detect intracellular calcium ions), TMRM (to assess mitochondria with established membrane potential), and LysoTracker (to label lysosomes, late endosomes, and other acidic vesicles). Although LysoTracker stains acidic vesicles similarly to AO used in the Live Cell Painting assay, we included it in the HepatotoxPath assay because repeating the vesicle patterns observed with AO using LysoTracker would reinforce the robustness of the results, demonstrating consistency across different dyes and methodologies. After staining, fluorescence images were acquired using a 20× objective on Cytation 5. Representative images from the HepatotoxPath assay after treatment of Huh7 and HepG2 cells with all PS-MPs concentrations (1 µg/L, 1 mg/L, 0.01 g/L, 0.1 g/L, and 1 g/L) and presented in larger size can be found in **Section 7.5.3. of this Appendix (Figs. AP5.6 and AP5.7).**

In these images, CellProfiler was used to extract morphological features of single cells, such as fluorescence signal intensity, staining texture, object size, and shape. The phenotypic profiling of the HepatotoxPath assay was conducted as described for the Live Cell Painting assay (Sections 3.1.5.3. and 3.2.4). Briefly, we followed the steps outlined in Basic Protocol I (Garcia-Fossa et al., 2023), applied LDA for dimensionality reduction and data visualization, and identified the top 10 features contributing to data clustering, represented as ten vectors (Fig. AP5.2 and Fig. AP5.4, items A). The top ten features representing these vectors are plotted in **Section 7.5.3. of this Appendix. (Figs. AP5.8 and AP5.9).** We then performed K-means

clustering to group treatments and used LDA and the online software Morpheus to identify biologically interpretable features that varied significantly compared to the non-treated group.

For Huh7 cells, three cellular phenotypic profiles were identified (Fig. AP5.2, items A and B). Cluster 0 grouped non-treated cells (0 g/L PS-MPs) with cells treated with PS-MPs at 1 μ g/L and 1 mg/L, indicating no significant morphological changes at these concentrations. Cluster 1 included cells treated with PS-MPs at 1 g/L, while Cluster 2 grouped cells treated with PS-MPs at 0.01 and 0.1 g/L, indicating distinct phenotypic alterations between these clusters. The primary change observed in Clusters 1 and 2, also seen in Amiodarone-treated cells (10 μ M), was a significant increase in the number and size of acidic vesicles, evident in Fig. AP5.2, item E. This increase was accompanied by elevated integrated LysoTracker fluorescence intensity (Fig. AP5.3, item D), reinforcing results from the Live Cell Painting assay (Section 3.2.4). Additionally, the increased LysoTracker intensity in Huh7 cells treated with PS-MPs (0.1 and 1 g/L) was accompanied by a decrease in Minimum Intensity (MinIntensity) of LysoTracker fluorescence in the cytoplasm. A lower MinIntensity suggests that certain cytoplasmic regions contain vesicles with reduced intensity or "empty" areas without LysoTracker signal, reflecting a heterogeneous distribution of acidic vesicles. This indeed occurs, as we can observe a predominant concentration of lysosomes in the perinuclear region (Fig. AP5.6).

For the other hepatotoxicity-related parameters, no significant changes were observed in Huh7's Clusters 1 and 2 (treated with PS-MPs at 0.1 and 1 g/L) regarding the intensity of Fluo-4 and TMRM fluorescence (Fig. AP5.3, items B and C), which remained similar to those of Cluster 0 (PS-MPs at 0–1 mg/L). However, Clusters 1 and 2 exhibited a significant increase in a Fluo-4 texture feature, which was also observed in Amiodarone-treated cells (Fig. AP5.3, item F). The increase in this feature indicates a more uniform distribution of intracellular calcium, and it may reflect disruptions in calcium homeostasis caused by PS-MPs-induced cellular stress.

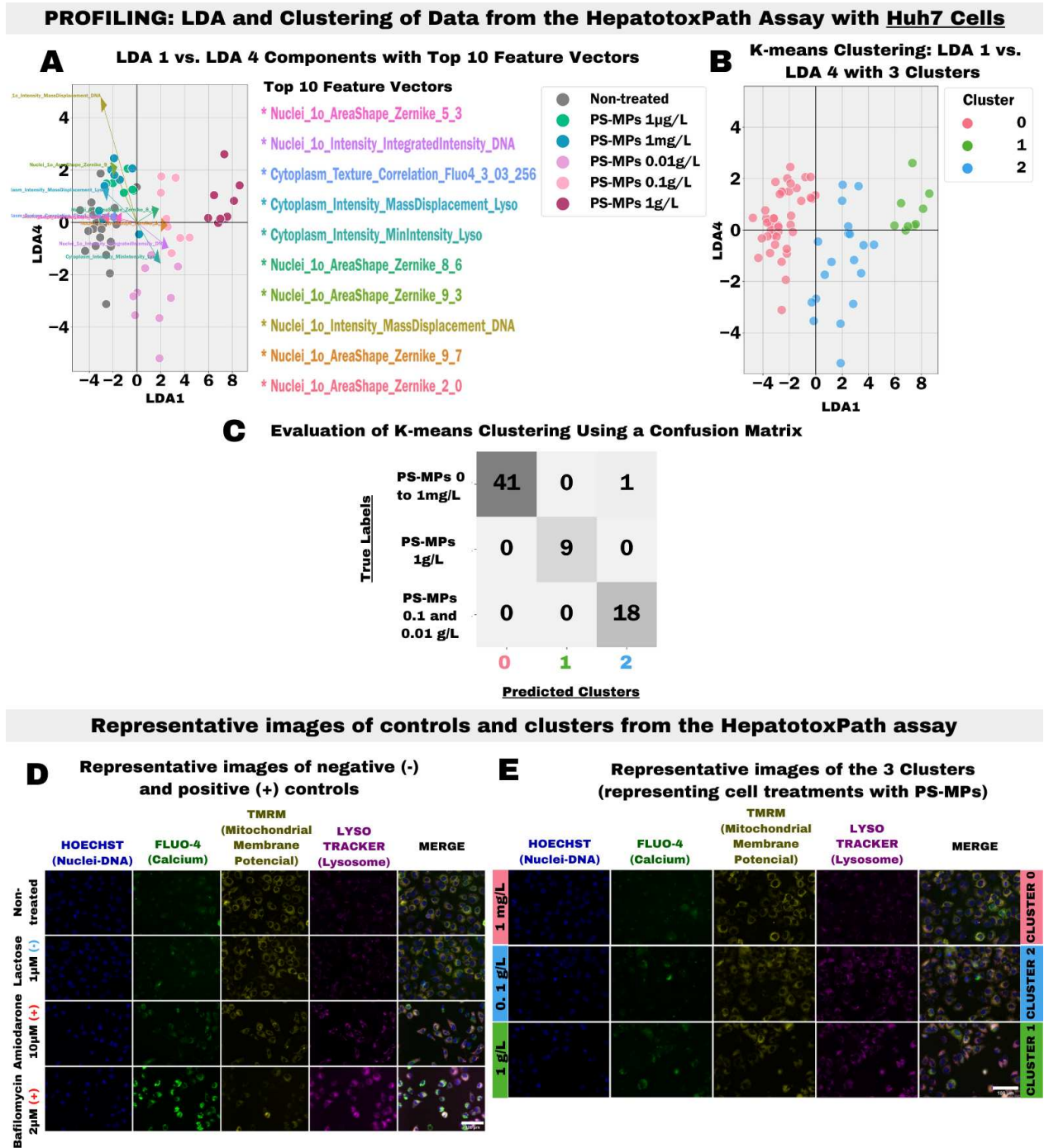


Fig. AP5.2 – Phenotypic Profiling of Huh7 cells after treatment with PS-MPs using the HepatotoxPath assay. Huh7 cells were plated at a density of 7,500 cells per well in 96-well plates. After 24 hours, cells were treated in triplicate with PS-MPs (1 µg/L, 1 mg/L, 0.01 g/L, 0.1 g/L, and 1 g/L), with Amiodarone (10 µM) as a positive control for hepatotoxicity, Bafilomycin A1 (2 µM) as a positive control for cellular damage (expected to drastically alter all fluorescent dyes

used), and Lactose (1 μ M) as a negative control for hepatotoxicity. The exposure time was 24 hours. After exposure, cells were stained with Hoechst (to visualize the nucleus), Fluo-4 (to detect intracellular calcium ions), TMRM (to assess mitochondria with established membrane potential), and LysoTracker (to label lysosomes, late endosomes, and other acidic vesicles). Images were acquired using a Cytation 5 (20 \times objective), and the images were analyzed using CellProfiler, where objects (cells, nuclei, and cytoplasm) were segmented, and their features extracted. These features were subsequently aggregated by well, normalized relative to the non-treated group, and selected using PyCytominer. **(A)** LDA was applied for dimensionality reduction and visualization, with vectors representing the 10 features contributing most to group separation plotted. **(B)** K-means clustering grouped treatments based on similar feature variances. **(C)** A confusion matrix validated the clusters obtained by K-means. **(D)** Representative fluorescence microscopy images of Huh7 cells that were non-treated (negative control), treated with the positive controls (Amiodarone (10 μ M) and Bafilomycin (2 μ M)), and treated with the negative control (Lactose (1 μ M)). **(E)** Representative fluorescence microscopy images of each cluster obtained from the Huh7 phenotypic profiling, represented by treatments with PS-MPs at 1 mg/L, 0.1 g/L, and 1 g/L. The white scale bar in the lower right corner of the (D) and (E) images in the fifth column indicates a scale of 100 μ m. Experiments were performed in three independent replicates, and each point in the plots represents well-aggregated data.

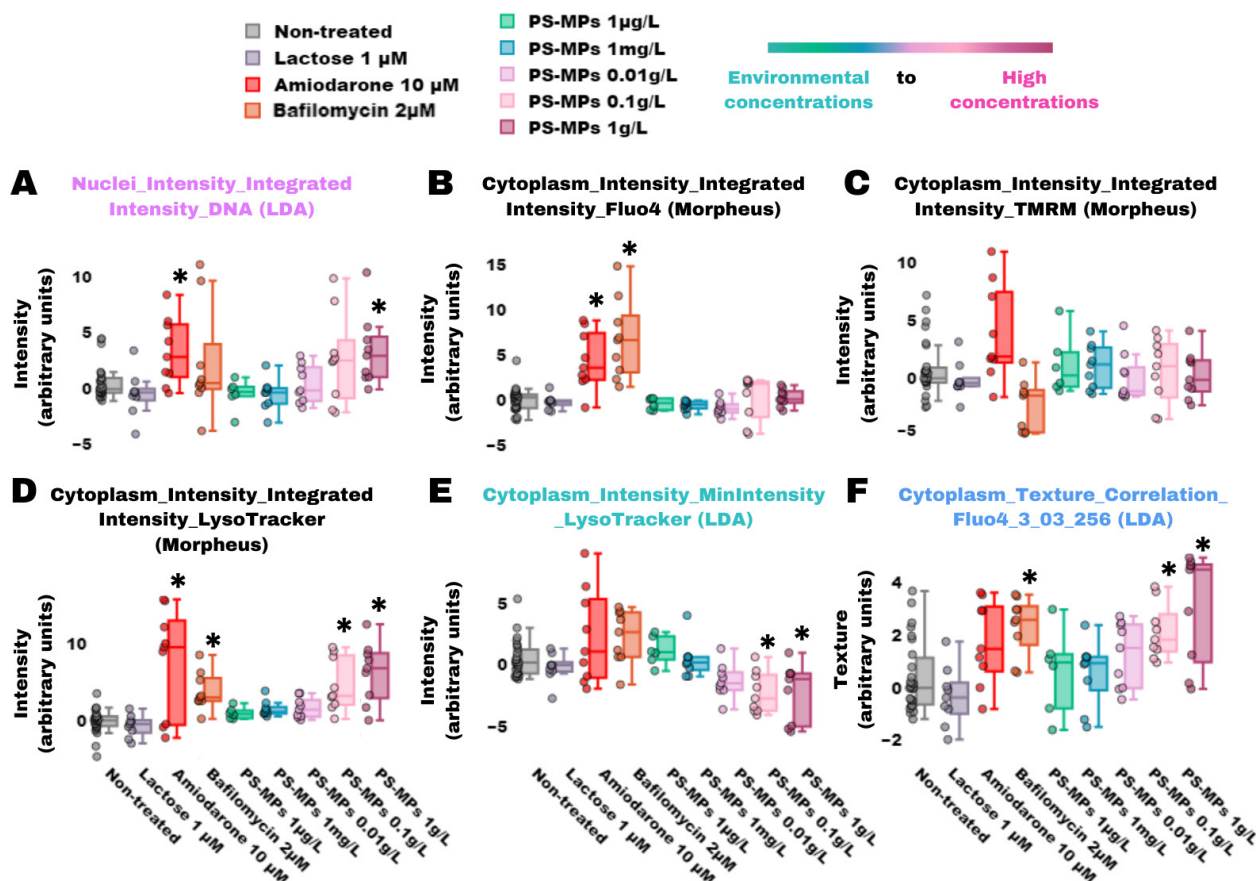


Fig. AP5.3 – Biologically Interpretable Huh7 Cells Features from HepatotoxPath Assay Selected after LDA and Morpheus feature selection. Huh7 cells were plated at a density of 7,500 cells per well in 96-well plates. After 24 hours, cells were treated in triplicate with PS-MPs (1 µg/L, 1 mg/L, 0.01 g/L, 0.1 g/L, and 1 g/L), with Amiodarone (10 µM) as a positive control for hepatotoxicity, Bafilomycin A1 (2 µM) as a positive control for cellular damage (expected to drastically alter all fluorescent dyes used), and Lactose (1 µM) as a negative control for hepatotoxicity. The exposure time was 24 hours. After exposure, cells were stained with Hoechst (to visualize the nucleus), Fluo-4 (to detect intracellular calcium ions), TMRM (to assess mitochondria with established membrane potential), and LysoTracker (to label lysosomes, late endosomes, and other acidic vesicles). Images were acquired using a Cytation 5 (20× objective), and the images were analyzed using CellProfiler, where objects (cells, nuclei, and cytoplasm) were segmented, and their features extracted. These features were subsequently aggregated by well, normalized relative to the non-treated group, and selected using PyCytominer. LDA analysis was used to list important features for each of the five components, enabling the selection of biologically interpretable features. Morpheus software was also used

for this purpose, performing marker selection (t-test) between the non-treated group and groups treated with the highest concentrations of PS-MPs (0.1 and 1 g/L). **(A-F)** Plots of the features of Huh7 cells selected by LDA and Morpheus analysis that were considered clearly biologically interpretable: fluorescence intensity, and texture patterns of cell dyes. Experiments were performed in three independent replicates, and each point in the plots represents well-aggregated data. Statistical analysis was performed using the Kruskal-Wallis test followed by Bonferroni post hoc testing in Jupyter Notebook, utilizing the `scipy` and `statsmodels` libraries: * $p \leq 0.05$ indicates statistical significance compared to the non-treated group.

For HepG2 cells, three phenotypic profiles were also identified (Fig. AP5.4, items A and B). Cluster 0 grouped non-treated cells (0 g/L PS-MPs) with cells treated at 1 μ g/L, 1 mg/L, and 0.01 g/L, indicating no significant changes at these concentrations. Cluster 1 grouped cells treated with PS-MPs at 1 g/L, while Cluster 2 included cells treated at 0.1 g/L. The primary changes observed in Clusters 1 and 2, also seen in Amiodarone-treated cells, were: an increase in TMRM (MMP stain) fluorescence intensity (Fig. AP5.5, item C); a significant increase in a TMRM texture feature, indicating more homogeneous fluorescence signals within the cytoplasm (Fig. AP5.5, item E); and an increase in the TMRM mass displacement feature (Fig. AP5.5, item F), suggesting a spatial redistribution of mitochondria, with fluorescence concentrated in specific areas of the cytoplasm.

However, some precipitates were observed in the fluorescence microscopy images of HepG2 cells treated with PS-MPs at 1 g/L in the RFP channel, where TMRM is detected. These may represent PS-MPs aggregates emitting fluorescence at the same wavelength as TMRM (orange). Consequently, we cannot confirm that HepG2 cells treated with the highest PS-MPs concentration (1 g/L) underwent alterations in MMP, as these changes may result from artifacts. Importantly, such precipitates were not observed in images of HepG2 cells treated with concentrations lower than 1 g/L, nor in those of Huh7 cells treated with PS-MPs at 1 g/L or other concentrations. For the other hepatotoxicity-related parameters, no significant changes were observed in HepG2 cells treated with PS-MPs at 0.1 and 1 g/L (Clusters 1 and 2) compared to Cluster 0 (PS-MPs at 0–0.01 g/L). Overall, due to potential artifacts, we cannot conclusively state that PS-MPs induce alterations in mechanistic parameters of *in vitro* hepatotoxicity in HepG2 cells. However, we can confirm that environmental concentrations of PS-MPs did not trigger alterations in mechanistic parameters of hepatotoxicity in HepG2 cells.

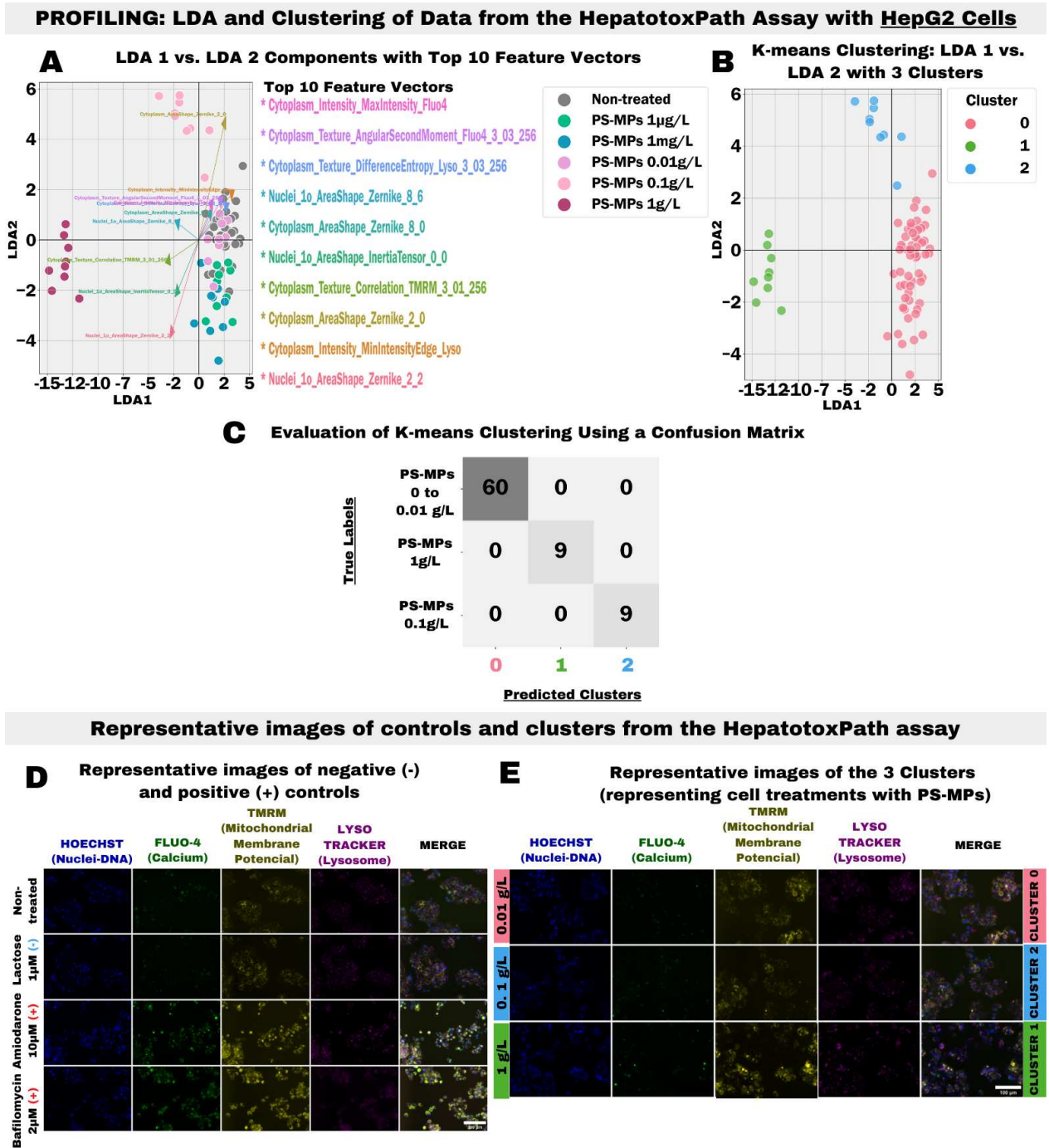


Fig. AP5.4 – Phenotypic Profiling of HepG2 cells after treatment with PS-MPs using the HepatotoxPath assay. HepG2 cells were plated at a density of 22,000 cells per well in 96-well plates. After 24 hours, cells were treated in triplicate with PS-MPs (1 µg/L, 1 mg/L, 0.01 g/L, 0.1 g/L, and 1 g/L), with Amiodarone (10 µM) as a positive control for hepatotoxicity, Bafilomycin A1 (2 µM) as a positive control for cellular damage (expected to drastically alter all fluorescent dyes used), and Lactose (1 µM) as a negative control for hepatotoxicity. The exposure time was

24 hours. After exposure, cells were stained with Hoechst (to visualize the nucleus), Fluo-4 (to detect intracellular calcium ions), TMRM (to assess mitochondria with established membrane potential), and LysoTracker (to label lysosomes, late endosomes, and other acidic vesicles). Images were acquired using a Cytation 5 (20× objective), and the images were analyzed using CellProfiler, where objects (cells, nuclei, and cytoplasm) were segmented, and their features extracted. These features were subsequently aggregated by well, normalized relative to the non-treated group, and selected using PyCytominer. **(A)** LDA was applied for dimensionality reduction and visualization, with vectors representing the 10 features contributing most to group separation plotted. **(B)** K-means clustering grouped treatments based on similar feature variances. **(C)** A confusion matrix validated the clusters obtained by K-means. **(D)** Representative fluorescence microscopy images of HepG2 cells that were non-treated (negative control), treated with the positive controls (Amiodarone (10 μ M) and Bafilomycin (2 μ M)), and treated with the negative control (Lactose (1 μ M)). **(E)** Representative fluorescence microscopy images of each cluster obtained from the HepG2 phenotypic profiling, represented by treatments with PS-MPs at 0.01 g/L, 0.1 g/L, and 1 g/L. The white scale bar in the lower right corner of the (D) and (E) images in the fifth column indicates a scale of 100 μ m. Experiments were performed in three independent replicates, and each point in the plots represents well-aggregated data.

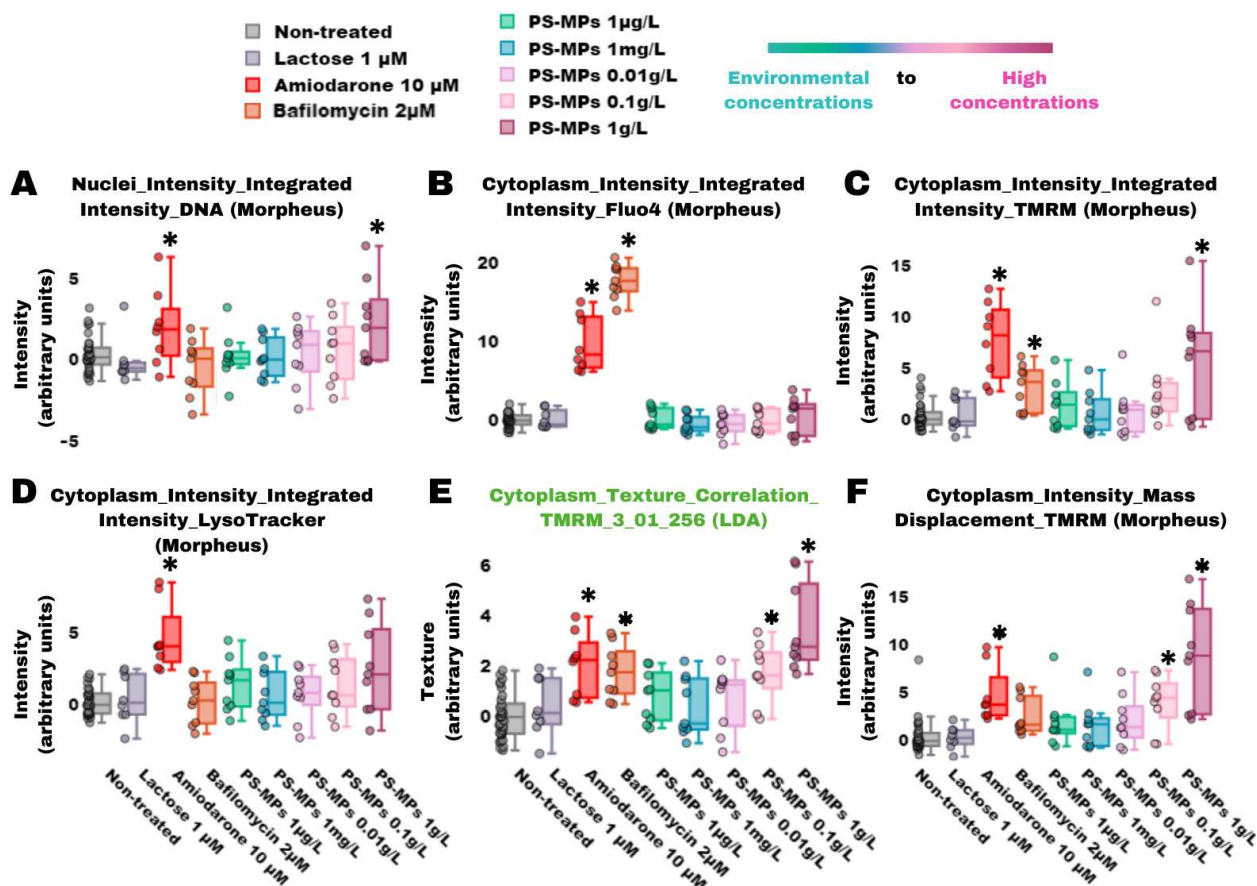


Fig. AP5.5 – Biologically Interpretable HepG2 Cells Features from HepatotoxPath Assay Selected after LDA and Morpheus feature selection. HepG2 cells were plated at a density of 22,000 cells per well in 96-well plates. After 24 hours, cells were treated in triplicate with PS-MPs (1 µg/L, 1 mg/L, 0.01 g/L, 0.1 g/L, and 1 g/L), with Amiodarone (10 µM) as a positive control for hepatotoxicity, Bafilomycin A1 (2 µM) as a positive control for cellular damage (expected to drastically alter all fluorescent dyes used), and Lactose (1 µM) as a negative control for hepatotoxicity. The exposure time was 24 hours. After exposure, cells were stained with Hoechst (to visualize the nucleus), Fluo-4 (to detect intracellular calcium ions), TMRM (to assess mitochondria with established membrane potential), and LysoTracker (to label lysosomes, late endosomes, and other acidic vesicles). Images were acquired using a Cytation 5 (20× objective), and the images were analyzed using CellProfiler, where objects (cells, nuclei, and cytoplasm) were segmented, and their features extracted. These features were subsequently aggregated by well, normalized relative to the non-treated group, and selected using PyCytominer. LDA analysis was used to list important features for each of the five components, enabling the selection of biologically interpretable features. Morpheus software was also used

for this purpose, performing marker selection (t-test) between the non-treated group and groups treated with the highest concentrations of PS-MPs (0.1 and 1 g/L). **(A-F)** Plots of the features of HepG2 cells selected by LDA and Morpheus analysis that were considered clearly biologically interpretable: fluorescence intensity, and texture patterns of cell dyes. Experiments were performed in three independent replicates, and each point in the plots represents well-aggregated data. Statistical analysis was performed using the Kruskal-Wallis test followed by Bonferroni post hoc testing in Jupyter Notebook, utilizing the scipy and statsmodels libraries: * $p \leq 0.05$ indicates statistical significance compared to the non-treated group.

7.5.3. Additional Representative Fluorescence Microscopy Images and Graphs from the HepatotoxPath Assay with Huh7 and HepG2 Cells

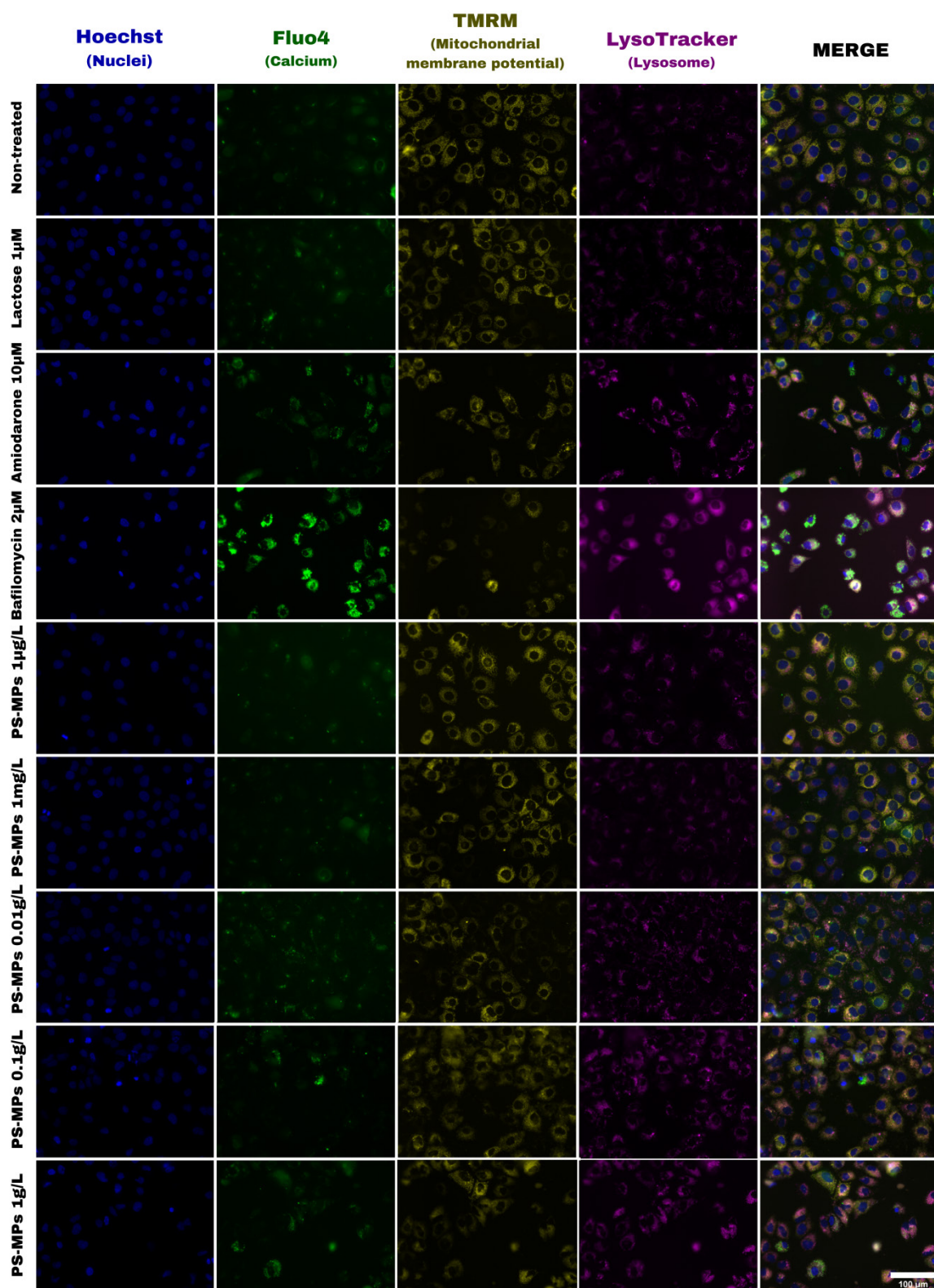


Fig. AP5.6 – Representative Fluorescence Microscopy Images from the HepatotoxPath Assay of Huh7 Cells Exposed to PS-MPs.

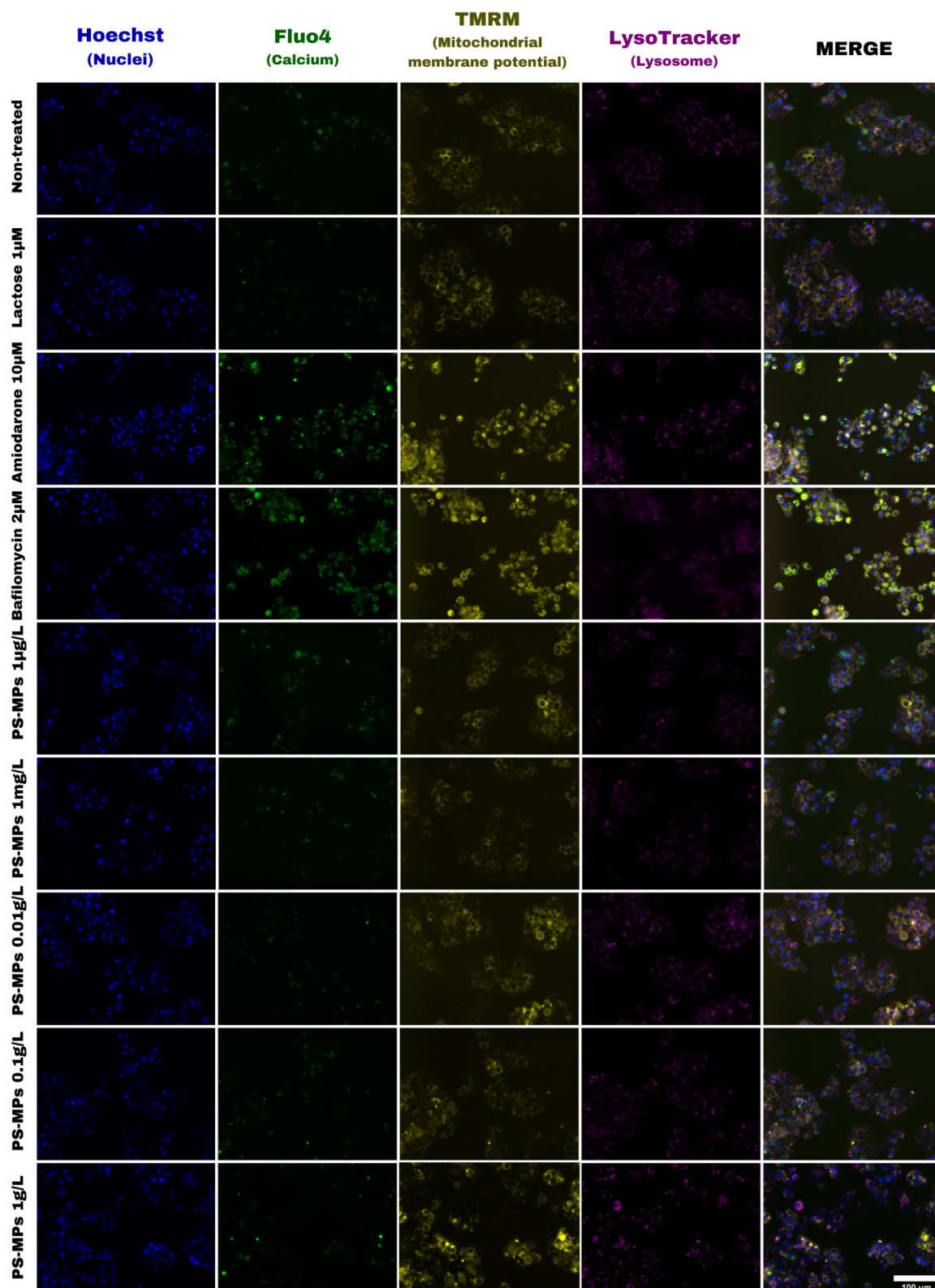


Fig. AP5.7 – Representative Fluorescence Microscopy Images from the HepatotoxPath Assay of HepG2 Cells Exposed to PS-MPs.

Figs. AP5.6 and AP5.7 description: Huh7 cells were plated at a density of 7,500 cells per well in 96-well plates. After 24 hours, cells were treated in triplicate with PS-MPs (1 µg/L, 1 mg/L, 0.01 g/L, 0.1 g/L, and 1 g/L), with Amiodarone (10 µM) as a positive control for hepatotoxicity, Bafilomycin A1 (2 µM) as a positive control for cellular damage (expected to drastically alter all fluorescent dyes used), and Lactose (1 µM) as a negative control for hepatotoxicity. The exposure time was 24 hours. After exposure, cells were stained with Hoechst (to visualize the nucleus), Fluo-4 (to detect intracellular calcium ions), TMRM (to assess mitochondria with established membrane potential), and LysoTracker (to label lysosomes, late endosomes, and other acidic vesicles). Images were acquired using a Cytation 5 (20× objective), **(AP5.6)** Representative fluorescence microscopy images of **Huh7 cells** that were non-treated, treated with the negative and positive control, and treated with PS-MPs (1 µg/L, 1 mg/L, 0.01 g/L, 0.1 g/L, and 1 g/L). **(AP5.7)** Representative fluorescence microscopy images of **HepG2 cells** that were non-treated, treated with the negative and positive control, and treated with PS-MPs (1 µg/L, 1 mg/L, 0.01 g/L, 0.1 g/L, and 1 g/L). The white scale bar in the lower right corner of the images in the fourth column indicates a scale of 100 µm. Experiments were conducted in three independent replicates.

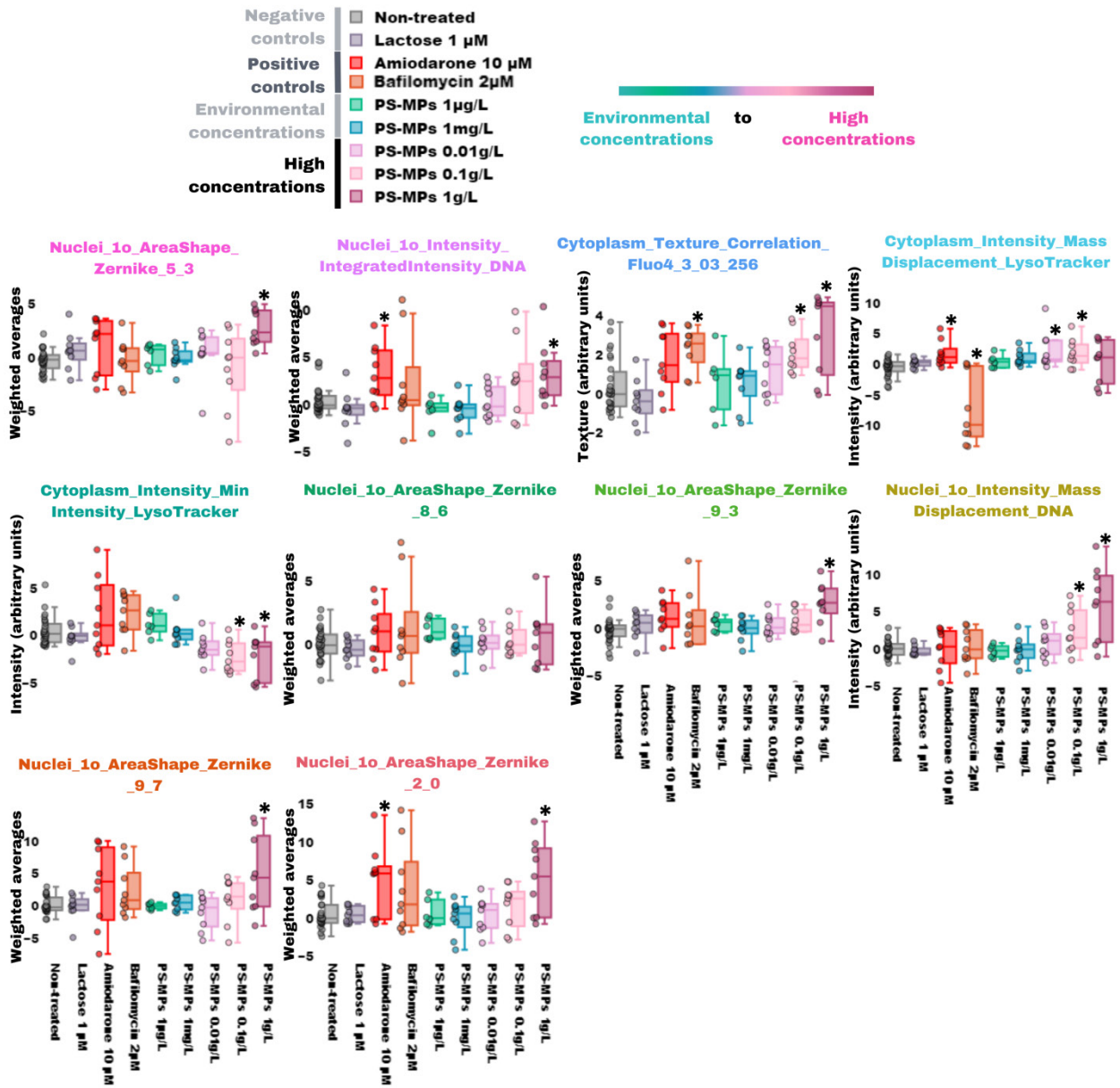


Fig. AP5.8 – Top 10 Feature Vectors from LDA Analysis of Data from the HepatotoxPath Assay with Huh7 Cells.

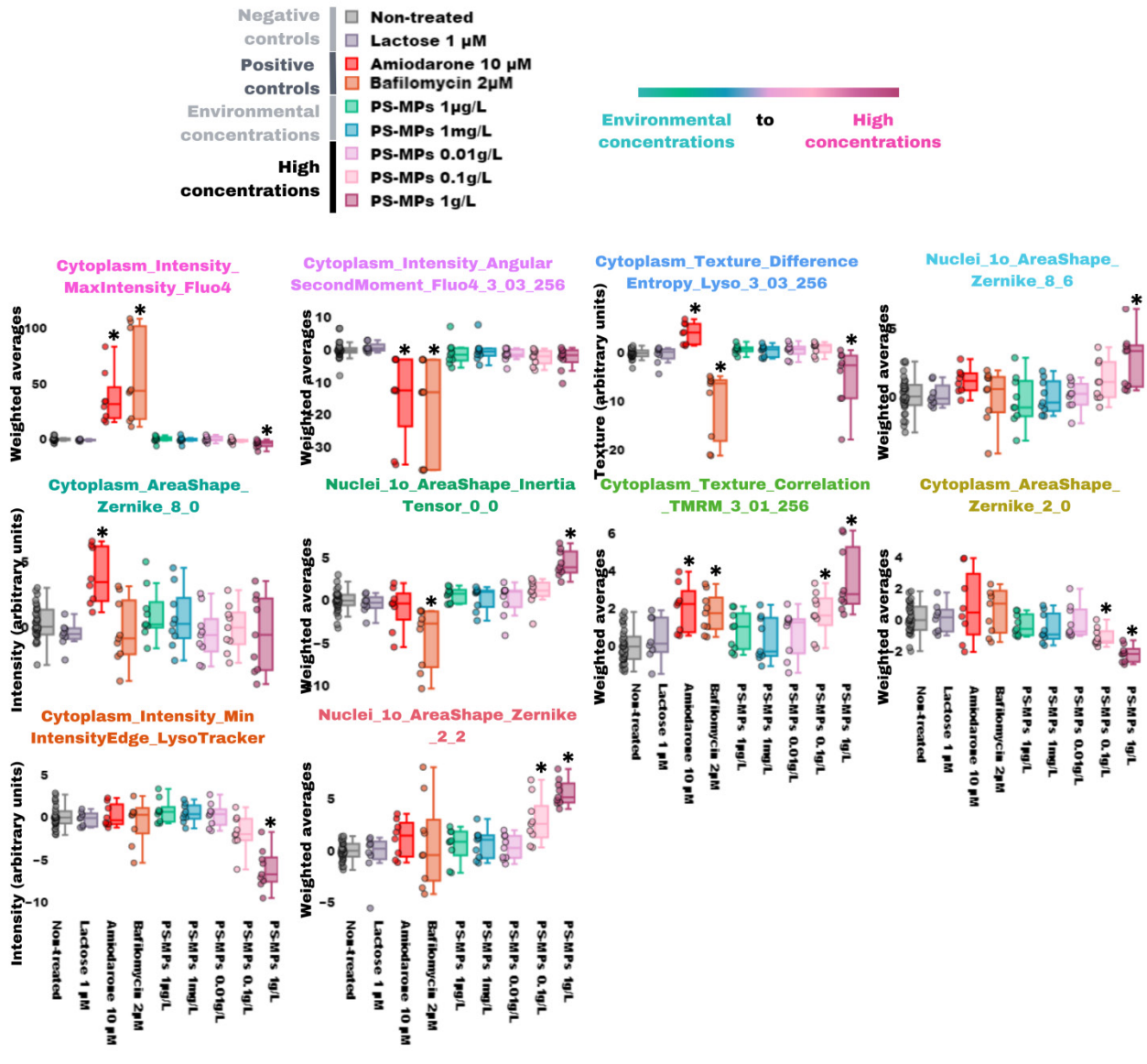


Fig. AP5.9 – Top 10 Feature Vectors from LDA Analysis of Data from the HepatotoxPath Assay with HepG2 Cells.

Figs. AP5.8 and AP5.9 description: The acquired images from the HepatotoxPath Assay were analyzed using CellProfiler, where objects (cells, nuclei, and cytoplasm) were segmented, and their features extracted. These features were subsequently aggregated by well, normalized relative to the non-treated group, and selected using PyCytominer. LDA was applied for dimensionality reduction and visualization, with vectors representing the 10 features contributing the most to group separation and cell phenotypic profiling. These top 10 features are plotted in the images **(AP5.8) for Huh7** and **(AP5.9) for HepG2**. Experiments were performed in three independent replicates, and each point in the plots represents well-aggregated data. Statistical analysis was performed using the Kruskal-Wallis test followed by Bonferroni post hoc testing in Jupyter Notebook, utilizing the scipy and statsmodels libraries: * $p \leq 0.05$ indicates statistical significance compared to the non-treated group.

7.6. **APPENDIX 6: Steatosis Assay**

7.6.1. **Materials and Method**

7.6.1.1. ***Cell Exposure***

After 24 hours of plating, cells were exposed in triplicate to PS-MPs (100 μ L) at concentrations ranging from 1 μ g/L to 1 g/L (that includes environmental and relevant human exposure concentrations (1 μ g/L and 1 mg/L) and higher concentrations (0.01, 0.1 and 1 g/L)) for 24 hours at 37 °C. As a negative control, antibiotic-and-serum-free DMEM containing 0.0025% (v/v) Tween 20 (100 μ L) and Lactose (100 μ L; 1 μ M; Merck, USA) were used. Cyclosporine A (100 μ L; 30 μ M; Invitrogen, USA) was used as a positive control for hepatic steatosis. Each experiment was conducted on at least three independent days, with a different plate layout used for each experimental run.

7.6.1.2. ***Steatosis Imaging Protocol***

After 24 hours, cells were fixed with 4% (w/v) paraformaldehyde (PFA; Sigma-Aldrich, USA) (100 μ L) for 20 minutes at room temperature, followed by two washes with 1 \times PBS (100 μ L). Next, a staining solution (100 μ L) prepared in a permeabilization solution (1% (w/v) Bovine Serum Albumin (BSA) (Sigma-Aldrich, USA) and 0.1% (v/v) Triton X-100 in 1 \times PBS) containing HCS LipidTOX™ Green Neutral Lipid Stain 1 \times , HCS CellMask™ Blue (60 μ M), and Hoechst (1.6 μ M) (all from Invitrogen, USA) were added. After 30 minutes of incubation at 37 °C, fluorescence images were acquired at 12 sites per well using a 20 \times objective on the Cytation 5 with the following filter cubes: GFP (green; excitation/emission = 445/510 nm) for HCS LipidTOX™ Green Neutral and DAPI (blue; excitation/emission = 377/447 nm) for Hoechst and CellMask.

7.6.1.2.1. ***Steatosis Image Analysis***

To perform cell segmentation for the Steatosis assay, only images from the blue channel (Hoechst + CellMask dyes) were used, as they provide both nuclear and cellular delineation within the same image. After cell segmentation, single-cell features were extracted into a database using CellProfiler modules. In summary, features related to pixel intensity in the GFP channel (associated with HCS LipidTOX™ Green Neutral dye) within the cellular area defined by segmentation were obtained. The numerical values of these features were exported as '.csv' files and analyzed in Jupyter Notebooks.

7.6.2. Results and Conclusions

To complement the HepatotoxPath mechanistic assay (Appendix 5; Section 7.5.), and considering studies that have reported changes in hepatic lipid metabolism induced by microplastics *in vivo* and *in vitro*, leading to hepatic steatosis (Djouina et al., 2023; Cheng et al., 2022; Zheng et al., 2021; Luo et al., 2019), we sought to investigate whether PS-MPs at environmental or higher concentrations could alter intracellular lipid droplets in Huh7 and HepG2 cells. In this steatosis assay, cells were treated with PS-MPs at concentrations ranging from 1 µg/L to 1 g/L, with Cyclosporine A (30 µM) as a positive control for hepatic steatosis and Lactose (1 µM) as a negative control for hepatic steatosis. The exposure time was 24 hours.

After exposure, cells were fixed and stained with Hoechst (to visualize the nucleus), CellMask Blue (to visualize the plasma membrane), and LipidTOX Stain (to label neutral lipid deposits, such as those found in lipid droplets in the cytoplasm). After staining, fluorescence images were acquired using a 20× objective on Cytation 5. Representative images from the steatosis assay after treatment of Huh7 and HepG2 cells with all PS-MPs concentrations (1 µg/L, 1 mg/L, 0.01 g/L, 0.1 g/L, and 1 g/L) and in larger size can be found in **Section 7.6.3. of this Appendix (Figs. AP6.2 and AP6.3)**. CellProfiler was utilized to extract single-cell features, including fluorescence signal intensity, texture, and granularity patterns, from the acquired images. From these data, we identified features that varied between PS-MPs-treated cells and non-treated cells and were biologically interpretable. These features included integrated fluorescence intensity, mass displacement, and granularity of LipidTOX (Fig. AP6.1).

The data revealed very similar responses between the two hepatocyte models. Huh7 and HepG2 cells treated with PS-MPs at higher concentrations, such as 0.1 and 1 g/L, showed a significant increase in LipidTOX integrated fluorescence intensity compared to the negative control. Furthermore, this increase in LipidTOX intensity in PS-MPs-treated cells was considerably more pronounced than in cells treated with Cyclosporine A (30 µM, positive control for steatosis). There was also an increase in the Intensity Mass Displacement feature of LipidTOX in cells treated with the two highest PS-MPs concentrations (0.1 and 1 g/L), as well as in cells treated with Cyclosporine. This increase suggests that lipid droplets are distributed more heterogeneously in the cytoplasm compared to the negative control. In the negative control, lipid droplets were visibly smaller, closer together, and predominantly located in the perinuclear region, whereas in the Cyclosporine, the lipid droplets were larger, more rounded, and more spaced apart. In contrast, in PS-MP-treated cells (0.1 and 1 g/L), lipid droplets appeared very small, spread throughout the cytoplasm, and were often difficult to delineate. This observation

suggests that, due to the physical presence of PS-MPs in the cells, they may be affecting the fluorescence pattern or interfering with the organization of these structures.

The granularity patterns, measured by Granularity 2 (Fig. AP6.1, item C and G) and Granularity 8 (Fig. AP6.1, D and H), also showed marked differences between treatments with Cyclosporine and PS-MPs (0.1 and 1 g/L). Granularity 2, which is associated with smaller structures, significantly increased in Cyclosporine-treated cells, suggesting a pattern of more fragmented or dispersed droplets. In contrast, this feature decreased in PS-MP-treated cells (0.1 and 1 g/L), indicating less fragmented or more diffuse structures. Conversely, Granularity 8, which measures larger structures, decreased in Cyclosporine-treated cells, while it increased in PS-MP-treated cells (0.1 and 1 g/L), suggesting a redistribution of lipid droplets or alterations in cytoplasmic organization.

These differences from the negative control indicate alterations in lipid droplets; however, the discrepancies observed in relation to the positive control for steatosis suggest that these changes do not exhibit typical characteristics of hepatic steatosis. Instead, they may be related to the physical interaction of PS-MPs with cells, leading to a redistribution of lipid droplets or even interference with fluorescence patterns. **Furthermore, as observed in the HepatotoxPath assay, precipitates were present in the background of fluorescence microscopy images of cells treated with PS-MPs at highest concentration (1 g/L), emitting the same fluorescence color as LipidTOX. These precipitates may correspond to unstable PS-MP aggregates in the medium, reinforcing the need for caution in data interpretation. While PS-MPs cause changes in LipidTOX staining patterns, it cannot be concluded that they induce steatosis in Huh7 and HepG2 cells.** However, it can be stated that PS-MPs at environmental concentrations do not lead to hepatic steatosis in the Huh7 and HepG2 models, as cells treated with concentrations ranging from 1 µg/L to 0.01 g/L did not show significant differences in lipid droplets compared to the negative control. Furthermore, the precipitates observed at higher concentrations were absent in the environmental concentration group, further supporting this conclusion.

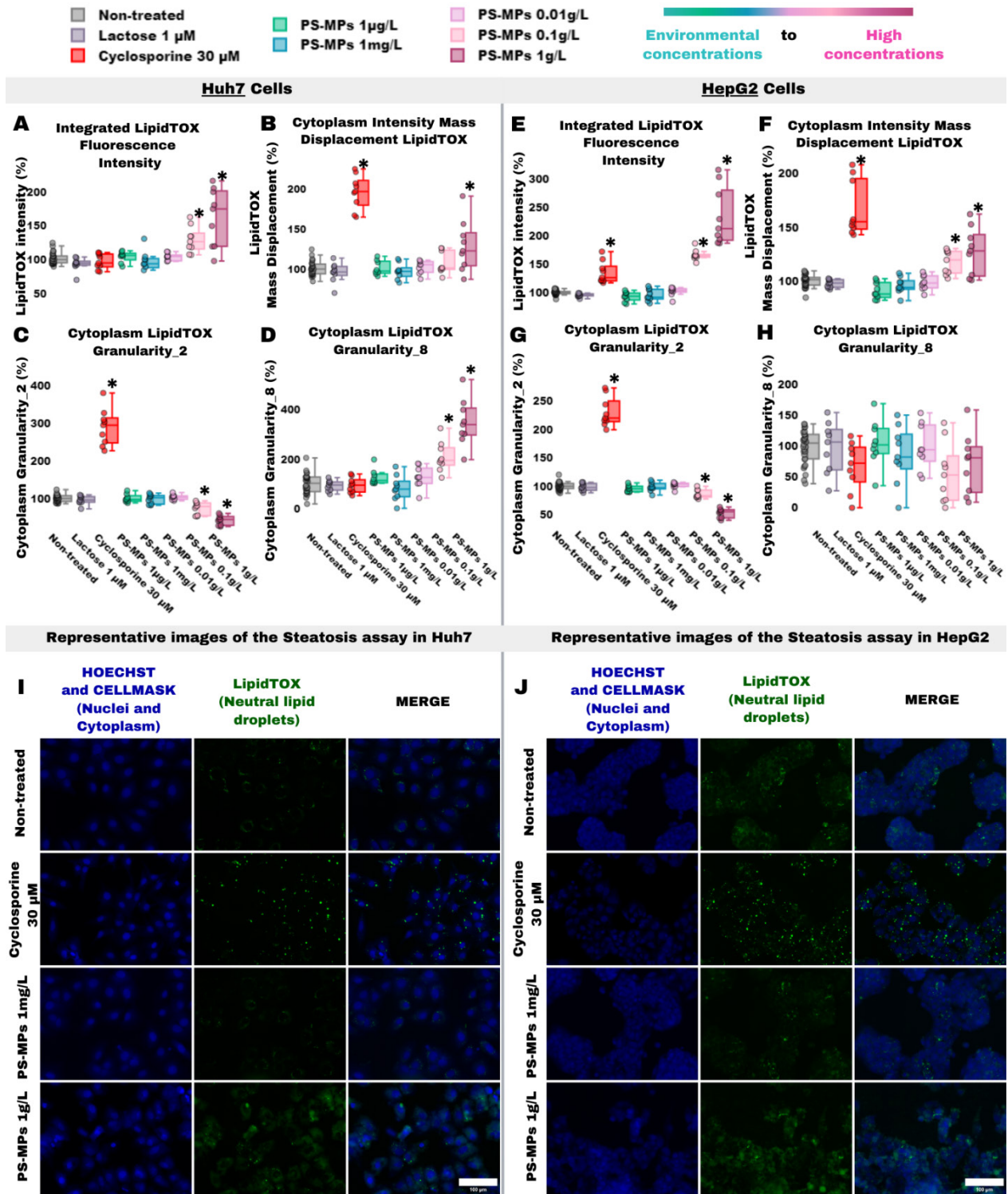


Fig. AP6.1 – Features and fluorescence microscopy images from the Steatosis assay of Huh7 and HepG2 cells exposed to PS-MPs. Huh7 and HepG2 cells were plated at densities of

7,500 and 22,000 cells per well, respectively, in 96-well plates. After 24 hours, cells were treated in triplicate with PS-MPs (1 μ g/L, 1 mg/L, 0.01 g/L, 0.1 g/L, and 1 g/L), Cyclosporine A (30 μ M; positive control for hepatic steatosis), and Lactose (1 μ M; negative control for steatosis) for 24 hours. Images were acquired after cell fixation with PFA and staining with Hoechst (to visualize the nucleus), CellMask Blue (to visualize the plasma membrane), and LipidTOX (to visualize neutral lipid droplets in the cytoplasm) (Cytation 5, 20 \times objective). The acquired images were analyzed in CellProfiler, where objects (cells, nuclei, and cytoplasm) were segmented, and their features extracted. These features were subsequently aggregated by well and normalized relative to the non-treated group, which was set at 100%. **(A–D)** Plots of integrated fluorescence intensity, intensity mass displacement, and granularity of LipidTOX stain extracted from the cytoplasm of Huh7 cells. **(E–H)** Plots of integrated fluorescence intensity, intensity mass displacement, and granularity of LipidTOX stain extracted from the cytoplasm of HepG2 cells. **(I)** Representative fluorescence microscopy images of Huh7 cells that were non-treated, treated with the positive and negative controls, and treated with PS-MPs at concentrations of 1 mg/L and 1 g/L. **(J)** Representative fluorescence microscopy images of HepG2 cells that were non-treated, treated with the positive and negative controls, and treated with PS-MPs at concentrations of 1 mg/L and 1 g/L. The white scale bar in the lower right corner of the (I) and (J) images in the third column indicates a scale of 100 μ m. Experiments were performed in three independent replicates, and each point in the plots represents well-aggregated data. Statistical analysis was performed using the Kruskal-Wallis test followed by Bonferroni post hoc testing in Jupyter Notebook, utilizing the scipy and statsmodels libraries: * $p \leq 0.05$ indicates statistical significance compared to the non-treated group.

7.6.3. Full representative fluorescence microscopy images of Steatosis assay with Huh7 and HepG2 cells

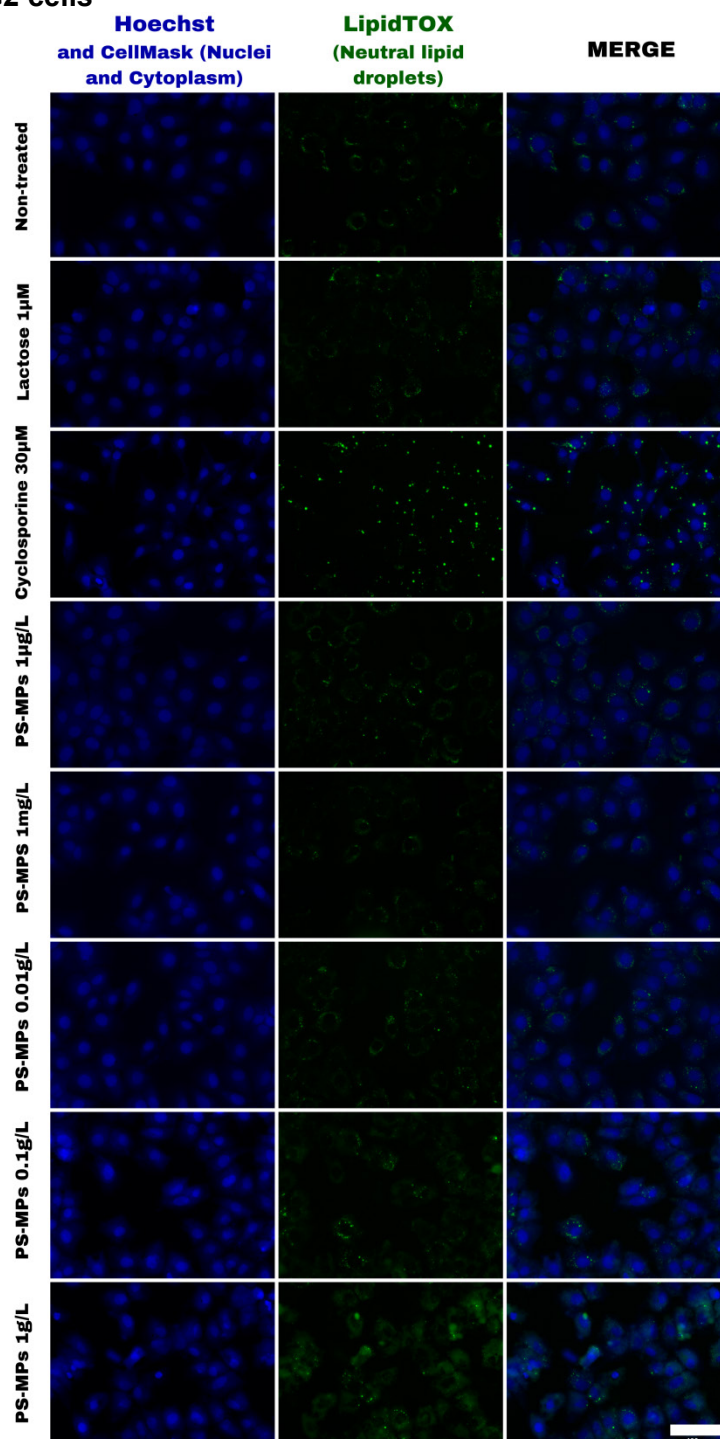


Fig. AP6.2 – Representative Fluorescence Microscopy Images from the Steatosis Assay of Huh7 Cells Exposed to PS-MPs.

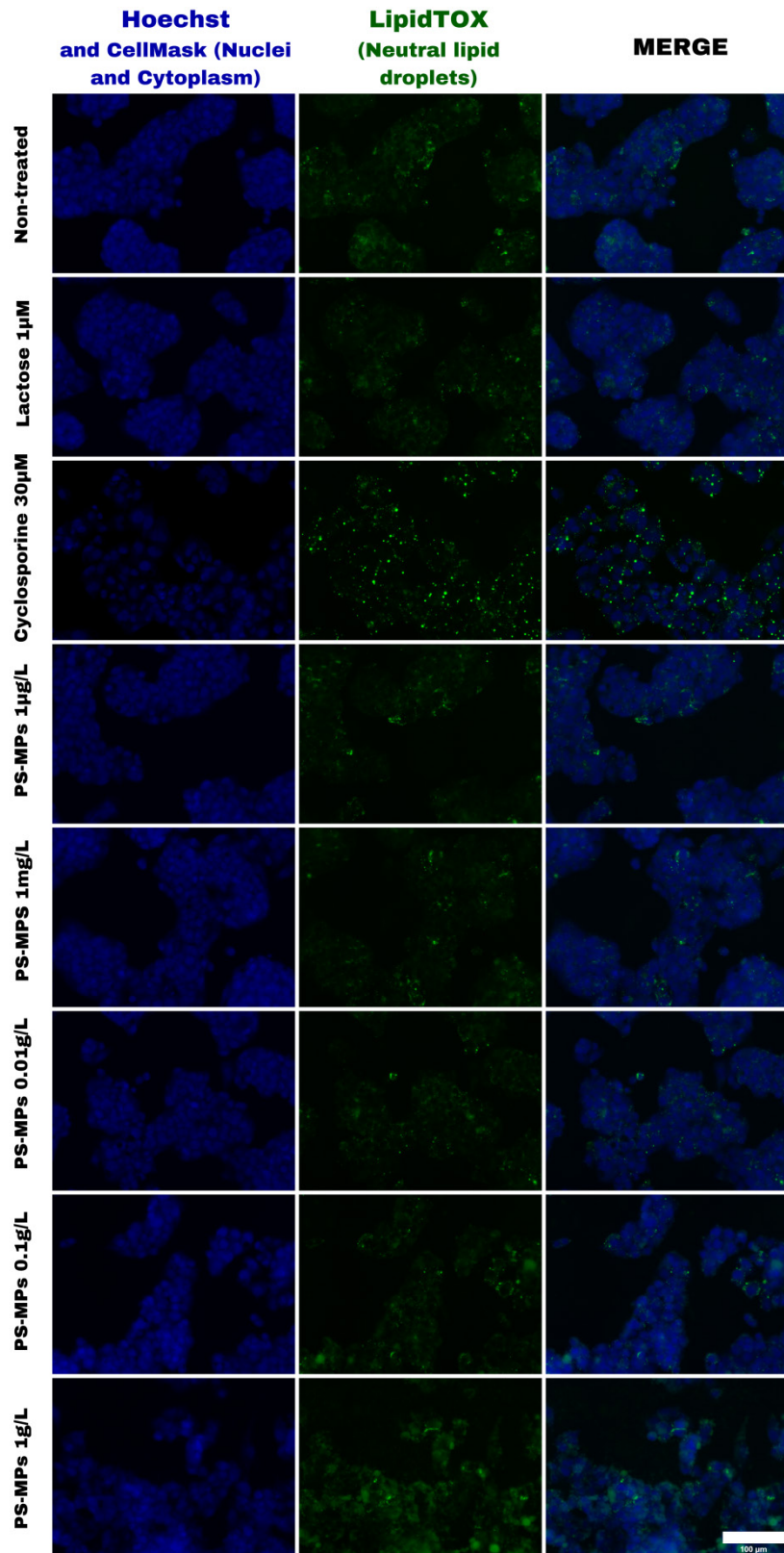


Fig. AP6.3 – Representative Fluorescence Microscopy Images from the Steatosis Assay of HepG2 Cells Exposed to PS-MPs.

Figs. AP6.2 and AP6.3 description: . Huh7 and HepG2 cells were plated at densities of 7,500 and 22,000 cells per well, respectively, in 96-well plates. After 24 hours, cells were treated in triplicate with PS-MPs (1 µg/L, 1 mg/L, 0.01 g/L, 0.1 g/L, and 1 g/L), Cyclosporine A (30 µM; positive control for hepatic steatosis), and Lactose (1 µM; negative control for steatosis) for 24 hours. Images were acquired after cell fixation with paraformaldehyde and staining with Hoechst (to visualize the nucleus), CellMask Blue (to visualize the plasma membrane), and LipidTOX (to visualize neutral lipid droplets in the cytoplasm) (Cytation 5, 20× objective). **(AP6.2)** Representative fluorescence microscopy images of **Huh7 cells** that were non-treated, treated with the negative and positive control, and treated with PS-MPs (1 µg/L, 1 mg/L, 0.01 g/L, 0.1 g/L, and 1 g/L). **(AP6.3)** Representative fluorescence microscopy images of **HepG2 cells** that were non-treated, treated with the negative and positive control, and treated with PS-MPs (1 µg/L, 1 mg/L, 0.01 g/L, 0.1 g/L, and 1 g/L). The white scale bar in the lower right corner of the images in the fourth column indicates a scale of 100 µm. Experiments were conducted in three independent replicates.

8. ANNEX 1



COORDENADORIA DE PÓS-GRADUAÇÃO INSTITUTO DE
BIOLOGIA
Universidade Estadual de Campinas
Caixa Postal 6109. 13083-970, Campinas, SP, Brasil Fone (19)
3521-6378. email: cpgib@unicamp.br



DECLARAÇÃO

Em observância ao **§5º do Artigo 1º da Informação CCPG-UNICAMP/001/15**, referente a Bioética e Biossegurança, declaro que o conteúdo de minha Dissertação de Mestrado, intitulada **“DETERMINAÇÃO DE ALTERAÇÕES FENOTÍPICAS SUBLETAIS DESENCADEADAS POR MICROPLÁSTICOS EM DOIS MODELOS DE HEPATÓCITOS HUMANOS ATRAVÉS DE TRIAGEM CELULAR MULTIPARAMÉTRICA DE ALTO CONTEÚDO”**, desenvolvida no

Programa de Pós-Graduação em Biologia Molecular e Morfofuncional do Instituto de Biologia da Unicamp, não versa sobre pesquisa envolvendo seres humanos, animais ou temas afetos a Biossegurança.

Assinatura: _____

Nome do(a) aluno(a): Mariana Rodrigues da Silva

Documento assinado digitalmente



MARCELO BISPO DE JESUS
Data: 12/05/2025 09:19:18-0300
Verifique em <https://validar.iti.gov.br>

Assinatura: _____

Nome do(a) orientador(a): Prof. Dr. Marcelo Bispo de Jesus

Data: 12/05/2025

9. ANNEX 2**DECLARAÇÃO**


As cópias de artigos de minha autoria ou de minha co-autoria, já publicados ou submetidos para publicação em revistas científicas ou anais de congressos sujeitos a arbitragem, que constam da minha Dissertação/Tese de Mestrado/Doutorado, intitulada **DETERMINAÇÃO DE ALTERAÇÕES FENOTÍPICAS SUBLETAIS DESENCADEADAS POR MICROPLÁSTICOS EM DOIS MODELOS DE HEPATÓCITOS HUMANOS ATRAVÉS DE TRIAGEM CELULAR MULTIPARAMÉTRICA DE ALTO CONTEÚDO**, não infringem os dispositivos da Lei n.º 9.610/98, nem o direito autoral de qualquer editora.

Campinas, 12 de Maio de 2025

Assinatura : Mariana R. da Silva

Nome do(a) autor(a): **Mariana Rodrigues da Silva**

RG n.º 54.404.963-9

Documento assinado digitalmente
 **MARCELO BISPO DE JESUS**
Data: 12/05/2025 09:20:42-0300
Verifique em <https://validar.iti.gov.br>

Assinatura : _____

Nome do(a) orientador(a): **Prof. Dr. Marcelo Bispo de Jesus**

RG n.º 32.591.974-4